Structure-property-function Relationships for Segmented Ionenes

by

Jae Sang Lee

A Dissertation Presented in Partial Fulfillment
of the Requirements for the Degree
Doctor of Philosophy

Approved April 2023 by the
Graduate Supervisory Committee:

Matthew D. Green, Chair
Timothy E. Long
Julianne L. Holloway
Kailong Jin
S. Eileen Seo

ARIZONA STATE UNIVERSITY

May 2023

ABSTRACT

There are limited analyses of the properties of segmented ionenes on the influence of the type, structure, content of soft/hard segments, and type of counterions through direct comparisons, which are needed for a diverse set of applications. This dissertation research focuses on resolving the gaps in the structure-property-function relationship of segmented ionenes. First, the synthesis of novel segmented ionenes using step-growth polymerization via the Menshutkin reaction of ditertiary amines and alkyl dihalides was performed with PEG soft segment with three different content of soft/hard segments, 25, 50, and 75 wt%, and two different hard segments, linear aliphatic and heterocyclic aliphatic hard segments. The content of the soft segment influenced the degree of phase separation and ionic aggregation which affected the thermomechanical properties of segmented ionenes. In addition, the crystallization of the soft segment influenced the mechanical properties of the ionenes. Second, the effect of the type of the soft segment was investigated by analyzing the novel PTMO-based segmented ionenes possessing three different content of soft/hard segments, as well as two different hard segments. The heterocyclic aliphatic hard segment provided a better degree of phase separation compared to the linear aliphatic hard segment irrespective of the type of soft segment, PEG, or PTMO. Moreover, the type and content of hard segments not only affected the thermal and mechanical properties but also the morphology of the segmented ionenes significantly that even inducing an ordered morphology. Third, the counter-anion metathesis was performed with PEG- and PTMO-based segmented ionenes possessing two structurally different hard segments to investigate the effect of the type of counter-

anions with a direct comparison of the type of soft and hard segments. The type of counterion significantly influenced the thermomechanical properties of the segmented ionenes, and the degree of phase separation of different types of counter-anions was dependent on the type of soft and hard segments. The results of this dissertation provide fundamental insights into the correlations between each factor that influences the properties of the segmented ionenes and enable the design of segmented ionenes for a diverse range of applications.

DEDICATION

I would like to dedicate this achievement to my parents and brother for their endless love, unwavering support, and encouragement throughout my doctoral education.

ACKNOWLEDGEMENTS

I am incredibly grateful to the individuals who have supported and encouraged me throughout my PhD journey. First and foremost, I would like to express my heartfelt gratitude to my advisor, Dr. Matthew D. Green, for his unwavering support and guidance. His mentorship and inspiration have been instrumental in shaping me into the scientist and person I am today. Without his understanding, encouragement, and generosity, I would not have been able to overcome the challenges I faced during my graduate studies.

I would also like to extend my sincere appreciation to my committee members, Dr. Timothy Long, Dr. Julianne Holloway, Dr. Kailong Jin, and Dr. Eileen Seo, for their invaluable insights and contributions to my research. Their feedback and suggestions have helped me to advance my work and broaden my perspective on various topics. I am grateful for their willingness to offer their time and expertise to help me succeed. I would like to thank our collaborators, Dr. Reza Montazami and Mehrnoosh Taghavimehr of Iowa State University, and Dr. Lisa Hall and Nick Liesen of Ohio State University, for their enthusiastic collaborations and creative ideas. Their contributions have been essential to the success of my research. I would like to extend my sincere appreciation to Dr. Klaus Lackner, Dr. Frederick Beyer, John Cirucci, Travis Johnson, Jason Kmon, and Thiago Barbosa for their invaluable contributions to my PhD studies. Furthermore, I would like to express my gratitude to the staff at ASU, Fred Pena, Emmanuel Soignard, Diana Convey, and David Wright, for their support and exceptional assistance throughout this endeavor.

My appreciation also goes out to the members of the Green group, including Ani, Hoda, Husain, Brad, Mani, Kacie, Taysha, Deepak, Alexis, Emmie, Jasmine, Kyle, Salma, Dr.

Marlene, and Dr. Zahra. I am fortunate to have had the chance to work with such a supportive and collaborative group. You have been incredible co-workers, always ready to help and discuss experimental issues in the lab, and great friends, willing to lend an ear and offer advice on life issues. I would like to acknowledge our previous lab members, Dr. Yang and Dr. Wang, for helping me to learn the experiments when I first joined the lab.

I want to extend my sincere appreciation to my dear friends Josh, Erik, and YoonSoo, who have provided me with invaluable support and encouragement in my studies. I am also indebted to JuYoung, SangHee, KyuYeon, Hyunji, Grace, Jessica, and Tracy, whose delightful friendships have enriched my life and brightened my days. My heartfelt thanks go to Keun Chan, Keun Young, and their parents whom I fondly call US mom and dad, for being my constant source of support and encouragement throughout my PhD studies. I would also like to express my deep appreciation to my friends in South Korea, including Jaeyeon, Hyeonku, JaeSung, MinSeok, Yohan, MinWoo, Jeonghun, SeungBae, Seondae and DuckWang, for their remarkable friendship and unwavering support. I find myself missing the camaraderie and friendship we shared.

I am grateful to my family, Jaehyun, Jungyoon, Haeyun, as well as my uncle and aunt, for their support, prayers, and encouragement. And finally, I want to acknowledge my mom, dad, and my brother, Jae Won, for always believing in me and supporting my dreams. You have been my rock and my constant source of strength and motivation. I cannot thank you enough for the countless sacrifices you have made for me and for your unwavering love and support. I love you all from the bottom of my heart.

TABLE OF CONTENTS

Page

CHAPTER Page

CHAPTER Page

Page

APPENDIX

LIST OF TABLES

Table Page

Table Page

LIST OF FIGURES

Figure Page

Figure Page

Figure Page

Figure Page

Figure Page

Figure Page

Figure Page

Figure Page

Figure Page

Figure Page

LIST OF SCHEMES

Scheme Page

CHAPTER 1

INTRODUCTION

1.1 Dissertation Overview

This dissertation investigates the structure-property-function relationship of ionenes by examining the effects of the structure of the hard segment, the type of soft segment, and the type of counterions. Chapter two reviewed a comprehensive analysis of the trends in the use of non-segmented ionenes and the relationship between structure and function in segmented ionenes. Chapter three describes the synthesis of poly(ethylene glycol) (PEG)-based segmented ionenes with two structurally different hard segments, linear aliphatic and heterocyclic aliphatic, with three different weight fractions of the soft segments. The thermomechanical properties and morphology of segmented ionenes were investigated. Chapter four focuses on the synthesis and structure-property relationship of poly(tetramethylene oxide) (PTMO)-based segmented ionenes. Two structurally different hard segments, linear aliphatic and heterocyclic aliphatic, were used with three different weight fractions of the soft segment, PTMO, and their thermomechanical properties were evaluated as a function of the type and content of the hard segment. The morphology and microphase separation of PTMO-based segmented ionene were also studied. In chapter five, the structure-property relationship in PEG- and PTMO-based segmented ionenes with three different counter-anion species as well as two structurally different hard segments were examined. The effect of counter-anion species accompanied by the effect of the type of soft and hard segments on thermal, mechanical, and viscoelastic properties of segmented ionenes was investigated. Furthermore, the morphological difference between ionenes with

different counter-anion species was further explored. In chapter six, the effect of mixing two hard segment types in one polymer chain on the thermal and mechanical properties, as well as morphology was studied. The finding and accomplishments of the dissertation are summarized in chapter seven, which also outlines future research directions. Based on the results obtained, the structure-property-function relationship between the molecular weight of the soft segment and the content of the soft segment, and applying the segmented ionenes in biological studies and carbon dioxide capture was suggested.

CHAPTER 2

ADVANCES IN THE MOLECULAR DESIGN OF IONENES FOR A DIVERSE RANGE OF APPLICATIONS

Reproduced with permission from: Lee, J.; Hocken, A.; Green, M. D., *Molecular Systems Design & Engineering*, 6, 334-354, 2021. Copyright 2023. Royal Society of Chemistry

2.1 Abstract

Ionenes are polymers that have charges in their backbone rather than on pendant sites. They can be divided into two overarching categories whether the charge is cationic or anionic, and into two subcategories whether they are segmented or non-segmented polymers. Generally, segmented ionenes exhibit thermoplastic elastomer properties due to their low charge density and phase separation compared to non-segmented ionenes. Non-segmented ionenes have been widely used for the various applications ranging from membrane-based separations to biomedical materials; whereas, segmented ionenes have been mostly studied on a fundamental level. This review focuses on trends in the use of non-segmented ionenes in the above applications and more. Furthermore, it describes the properties of segmented ionenes, with attention to the relationships between the structure and function of the segmented ionenes. Together, this review offers insight into the design of ionenes for use in a diverse set of applications.

2.2 General Information about Ionenes

Ionenes are ion-containing polymers that have charges in the polymer backbone while traditional ionomers and polyelectrolytes have charges pendant to the polymer backbone. Ionenes have received a great deal of attention due to the ability to control the charge density with careful monomer selection and the precise, well-defined spacing of charges in the repeating units. In contrast, ionomers are highly dependent on polymer composition, which presents unequal distributions of ionic groups within a polymer chain, making it challenging to accurately model their behavior.[1] The random distribution of ionic groups in the polymer often complicates the analysis of ionic aggregation effects.[2] Both ionenes and ionomers can be a subset of poly(ionic liquids) (polyILs) that are commonly known as IL-derived polyelectrolytes, but ionenes are typically the product of two neutral monomers that do not show IL formations at any point during the synthesis.[3] In many cases, ionenes are referred to as poly(ILs) or polymeric ILs, which in most cases is incorrect and potentially misleading. Ionenes are also referred to as polyelectrolytes, main-chain polycations, and polyionenes in the scientific literature.[3] Gibbs et al. first synthesized ammonium ionenes via step-growth polymerization of dimethylamino-n-alkyl halides in 1933[4] and Rembaum et al. adopted the name "ionenes" for polymers that contain ionic groups derived from amine-containing monomers in 1968.[5] Most ionenes in the literature are prepared by step-growth polymerization via the Menshutkin reaction of aliphatic or aromatic ditertiary amines with dihalides.

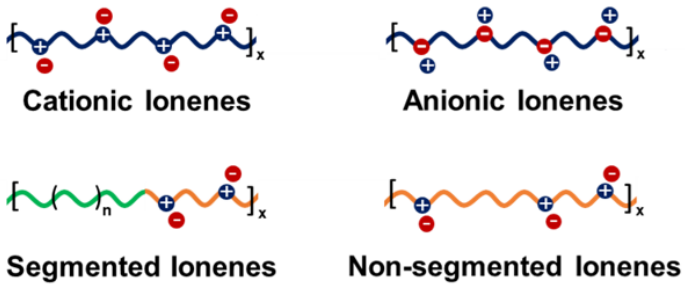

Figure 2.1: Schematic illustration of cationic and anionic ionenes, and segmented and non-segmented ionenes. Green and orange lines refer to soft and hard segments, respectively.

Most of the ionenes that have been reported are cationic, because synthesizing anionic ionenes has proven to be more challenging.[3] Cationic ionenes containing ammonium, pyridinium, phosphonium, imidazolium, and DABCO-based ions have been synthesized. Polyamide, polyimide, polyester, and polyurethane ionenes can also be synthesized using functional monomers in conventional condensation polymers.[3] Recent reports have shown the successful development of poly(arylsulfonimide) ionenes[6] and poly(perfluoroalkylsulfonyl)imide (PFSI) ionenes[7] from anionic ionenes. They show promise due to their improved thermal stability and unique capabilities, such as having a cationic counterion for Li^+ ion batteries, which are unavailable to cationic ionenes.[3]

Ionenes can be divided into two categories: segmented and non-segmented ionenes, and these can be further classified as either cationic or anionic (Figure 2.1). Segmented polymers have alternating hard and soft segments along the backbone, created by the polymerization of oligomeric spacers. This configuration produces polymers with excellent mechanical, thermal, and morphological properties.[8] Segmented ionenes are structurally similar, wherein the oligomeric hard segments typically contain the charged domains, which creates interesting design features because of the mechanical and morphological

characteristics. Some of the soft segments used to make segmented ionenes include poly(tetramethylene oxide) (PTMO), poly(ethylene glycol) (PEG), and poly(propylene glycol) (PPG) and some of the hard segments used to synthesize segmented ionenes include 1,12-dibromododecane, 4,4'-bipyridine, 1,2-bis(4-pyridium)ethylene, N,N,N',N'-tetramethyl-1,6-hexanediamine, 1,4-diazabicyclo[2,2,2]octane (DABCO), and 1,4-dibromo-*p*-xylene. The soft segments have glass transition temperatures (T_g) below ambient temperature (or below the application temperature) which provides flexibility and ductility.[9] Kohjita et al. first reported segmented ammonium cationic ionenes with a PTMO soft segment in 1981.[10] Segmented ionenes typically undergo microphase separation, and, due to the low volume fraction of hard segments relative to soft segments, a continuous soft segment matrix with randomly dispersed and isolated hard segments are formed.[9] This microphase separation is attributed to a combination of Coulombic interactions and segment-segment incompatibility, the latter drives microphase separation in block polymers and segmented polymers (e.g., segmented urethanes).[11] Additionally, crystallization contributes to this separation, which is a function of soft segment molecular weight, volume fraction (relative to the hard segment), and the propensity of the hard and soft segment to crystallize.[12] The mechanical properties of segmented ionenes were found to be dependent on both the nature and the amount of the hard segment.[13] Hard segment contents over 25 wt% incurs connectivity between the hard domains, which can become percolated throughout the matrix.[9] Segmented ionenes have been compared with polyurethanes (PU) because segmented ionenes show high tensile strength and high elongation which mechanically resemble segmented PU.[14] However, segmented PUs are

prepared with toxic isocyanates using a two-step process. In contrast, segmented ionenes are potentially more environmentally friendly, use safer precursors, and are synthesized in a single step process. Segmented PUs need more than one hard segment moiety within a hard segment microdomain to have sufficient microphase separation to enhance the physical properties, whereas segmented ionenes can obtain decent phase separation with a single unit of the ionene hard segment.[11]

The most common type of non-segmented ionenes is an aliphatic ammonium ionene, and it is usually synthesized via the Menshutkin reaction. Aliphatic, non-segmented ammonium ionenes use the following nomenclature: x,y-ionenes, where x and y indicate the number of methylene units in the diamine and dihalide monomers, respectively.[15] The varying charge density can result in different properties of ionenes which can be tuned by varying x and y. For example, non-segmented ionenes are usually brittle materials that show poor mechanical properties due to the high charge density, but the polymer solubility and stability in water-salt media can be tailored with the value of x and y.[16,17] Rembaum and Noguchi revealed that monomers with a low number of methylene spacers (i.e., x,y- equal to 2,1-, 2,2-, 2,3-, or 3,2-) can produce low molecular weight cyclic ionenes.[15] The choice of solvent, reaction temperature, reaction time, and the concentration of the monomer during the polymerization of the non-segmented ionenes all impact the polymerization.[1]

The type of counterions, charge distribution, molecular weight, structural flexibility, and H-bonding capability are critical aspects that may affect the dynamics of the ionic chains that govern ionene properties.[18] The majority of ionenes that have been studied are cationic

with varying halide anions (e.g., fluoride (F^-), chloride (Cl^-), bromide (Br^-) and iodide (I^-)[19]). Other counterions, such as hexafluorophosphate (PF_6^-), tetracyanoquinodimethane ($TCNQ^-$), tetrafluoroborate (BF_4^-), trifluoromethanesulfonate ($CF_3SO_3^-$), and bis(trifluoromethanesulfonyl)imide (Tf_2N^-), have been studied as well.[20,21] Meanwhile, there are only a few anionic ionenes with a cationic counterion; for example, lithium (Li^+), that have been reported.[22,23] Generally, smaller anions attract more water molecules, resulting in a tight hydration shell close to the quaternary nitrogen. Whereas, the larger counterions do not create such a tight shell, resulting in ions that are closer to the ionene chain according to molecular dynamics simulations of non-segmented ammonium 3,3-ionenes.[24] Peter et al. studied the influence of counterions on ion-binding with 3,3-, 6,6-, and 6,9-ionenes, which are aliphatic, cationic, ammonium, and non-segmented ionene.[25] The association of the counterions to the ionene backbone, cationic or anionic, strongly depends on the charge density of the ionene and the chemical nature of the counterions. The strongest effect of charge density and counterion effects is demonstrated in ionene solutions when the counterion is changed from Br^- to F^-. Miha et al. estimated the self-diffusion coefficients of the Br^- and F^- counterions associated with 3,3-, 4,5-, 6,6- and 6,9-ionenes in water.[26,27] The F^- and Br^- counterions preferred longitudinal and transverse fluctuation, respectively, with respect to the polyelectrolyte backbone. This means that F^- counterions prefer to move along the shorter segment of the chain backbone, while Br^- counterions prefer to fluctuate radially to the backbone. The F^- counterions keep their hydration shell intact when approaching the ionene and behave like a charged hard-sphere with a hydrated radius, whereas Br^- counterions give away the hydrated water in order to

interact with the ionene. Thus, the water associated with the Br- counterion is loosely bound due to the chaotropic nature of Br^- ions. The T_g of ionenes is dependent on molecular weight and the chemical structure but also the size and shape of the counterions.[28] Small spherical anions such as BF_4^- decreased T_g, while large counterions, tetraphenylborate (BPh_4), or ethyl-orange sulfonate (EO) led to higher T_gs.[29]

The Hofmann elimination reaction is the most common degradation mechanism for ionenes. It depends on the basicity of the counterions; ionenes with less basic counterions degrade at higher temperatures compared to stronger base counterions.[28] Although decomposition reactions of polymeric ammonium salts are more complicated due to many competing mechanisms occurring in the polymer chain,[30] several ionene degradation processes have been known such as the reverse Menshutkin reaction, nucleophilic substitution reaction, and Hofmann elimination reaction that eliminate alkyl substituents from quaternary salts. Charlier et al. revealed that quaternized ammoniums can have a better thermal stability than tertiary amines.[31] Specifically, the amines degraded at 180 °C, but high charge density aliphatic ionenes are stable to ~250 °C.[32] Ionenes undergo Hofmann elimination and reverse Menshutkin reactions at elevated temperature via anion attack on the ammonium cation. The effect of other factors on the ionenes' properties will be further discussed below in the context of different types of ionenes.

Bara and O'Harra reviewed the current state of the art for ionenes in 2019,[3] which established a clear definition of ionenes (among polyelectrolytes) and provided key lessons for designing anionic and cationic ionenes. However, there is still a gap in the establishment of structure-property-function relationships for ionenes at the interface of various

applications. Specifically, limited analysis of the properties of segmented ionenes exists, which currently limits their implementation in diverse applications. This review will summarize the use of non-segmented ionenes in several widely reported applications and provide the properties of the non-segmented ionene hydrogels. Furthermore, it will create design rules for structure-property-function relationships for segmented ionene elastomers.

2.3 Non-segmented Ionenes

Here, a review of non-segmented ionenes is provided to study structural differences that introduce properties for membrane separations, biomedical therapeutics, and energy storage. This review will provide context for the discussion of segmented ionenes later.

2.3.1 Applications

2.3.1.1 Membrane-based Separations

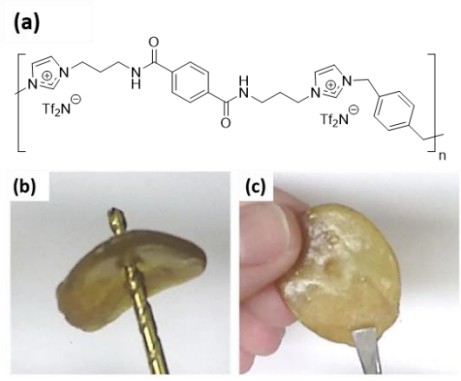

Figure 2.2: (a) Structure of imidazolium-based polyamide ionenes with both amide and xylyl linkages in *para*- positions and illustration of (b) before and (c) after self-healing characteristic of ionene film.[33]

Non-segmented ionenes have been implemented as membranes for gas separations, CO_2 capture, and humidity sensing. Kammakakam et al. introduced imidazolium-based

polyamide ionenes containing Tf_2N^- counterions and revealed that both amide and xylyl linkages attached at *para*- or *meta*- positions resulted in higher perm-selectivity for CO_2/-CH_4 and CO_2/N_2 gas pairs owing to the high CO_2 solubility.[33] However, the permeability of all structural combinations was low relative to controls. When both the amide and xylyl groups were attached in the *para*- position (Figure 2.2a) the membranes showed the highest permeability, possibly due to the lower T_g and looser inter-chain packing. This polymer also showed a self-healing property due to the ionic interactions between imidazolium cations and counteranions as well as hydrogen bonding between amide groups (Figure 2.2b and c). They also described imidazolium-based polyimide ionenes that contained the N,N′-bis(3-imidazol-1-yl-propyl)pyromellitic diimide and *p*-dichloroxylene with Tf_2N^- counterions that were soaked with an IL, [C_4mim][Tf_2N], for gas separation.[34] The ionic polyimides absorbed IL into their structures at ambient temperature, which increased the permeability of CO_2, N_2, and CH_4 by 1800-2700% due to increased gas diffusivity while the gas solubility remained unchanged with the IL present. It is noteworthy that Tf_2N^- counterions have been widely used for gas separation due to their ability to solubilize CO_2.[35]

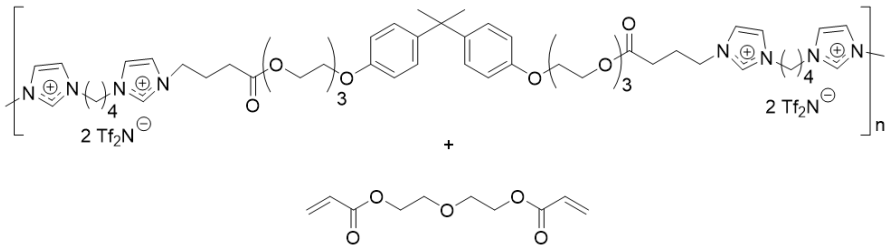

Figure 2.3: Structure of the imidazolium-based ionenes made from bromine-terminated bisphenol poly(ethylene glycol) (PEG) and 1,4-di(1H-imidazol-1-yl)butane that are then crosslinked within a di(ethylene glycol)diacrylate to form a composite network.[35]

Ionenes have also been incorporated into networks and thermosets. For example, an ionene prepared by reacting 1,4-di(1H-imidazol-1-yl)butane and bromine-terminated bisphenol poly(ethylene glycol) was loaded into a composite blend network by crosslinking di(ethylene glycol)diacrylate (DEGDA) around the ionene (Figure 2.3).[35] The low molecular weight DEGDA matrix provided mechanical stability and CO_2 affinity to the membrane. A 2:1 ratio of ionene:DEGDA showed the highest permeability to all gases including CO_2, O_2, and N_2, and a 3:1 ratio yielded the highest CO_2/N_2 perm-selectivity. However, all of the networks exhibited a low gas permeability, and it was suggested that a longer PEG linker in the ionene and/or the crosslinker could improve the gas permeability.

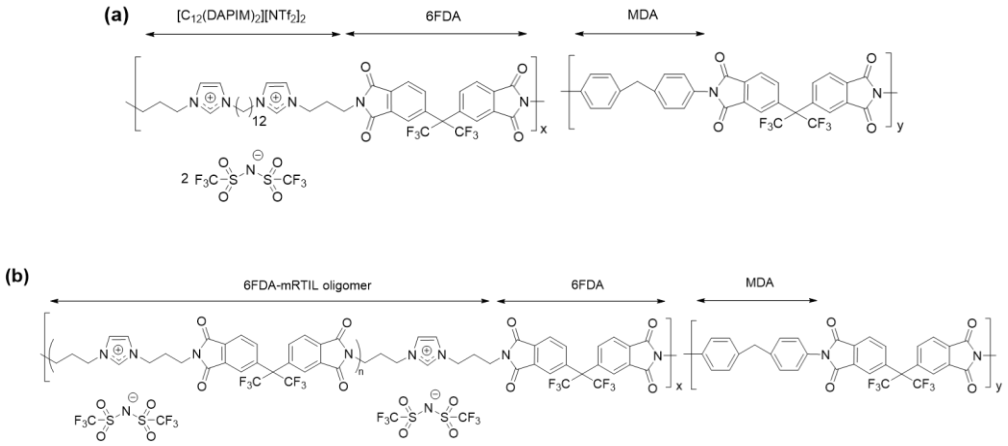

Figure 2.4: Structures of the imidazolium-based copolyimide ionenes having (a) two and (b) one imidazolium ring.[36,37]

Li et al. reported imidazolium-based copolyimide ionenes made from 2,2-bis(3,4-carboxylyphenyl)hexafluoropropane dianhydride (6FDA), *m*-phenylenediamine (MDA), and 6FDA-1,12-di[3-(3-aminopropyl) imidazolium] dodecane bis[(trifluoromethyl)sulfonyl]imide ($[C_{12}(DAPIM)_2][Tf_2N]_2$) (diRTIL), which produced a random copolyimide with two imidazolium rings in the backbone (Figure 2.4a) and Tf_2N

counterions.[36] Whereas, reacting 6FDA, MDA, and 6FDA-[DAPIM][NTf_2] (6FDA-mRTIL) oligomer produced a copolyimide with one imidazolium ring in the backbone (Figure 2.4b).[37] The thermal stability, T_g, d-spacing, and fractional free volume (FFV) decreased upon increasing the concentration of 6FDA-mRTIL oligomer, whereas the polymer density increased gradually. Furthermore, gas permeability, solubility, and diffusivity decreased and perm-selectivity of CO_2/CH_4, H_2/CH_4, and O_2/N_2 gas pairs increased by the incorporation of diRTIL within the 6FDA–MDA backbone. The diRTIL copolymer exhibited a lower perm-selectivity than the mRTIL copolymer, however, both copolyimide ionenes showed a higher ideal CO_2/CH_4 perm-selectivity when compared to 6FDA-MDA. O'Harra et al. incorporated 6FDA into imidazolium-based polyimide ionenes with different structural isomers of xylene and the imidazolium monomer.[38] The -CF_3 groups in 6FDA were able to prevent large chain packing, thus producing a high FFV that enhanced the gas permeability. Interestingly, ionenes made from monomers with para-linkages on both xylene and the imidazolium monomer (Figure 2.5) displayed the highest value of M_n, which the authors attribute to less steric hindrance when compared to ionenes synthesized from monomers with ortho- and meta- linkages. The para-linked polymers also showed the highest d-spacing, which gives insight into the packing efficiency and thus predicts the permeability.

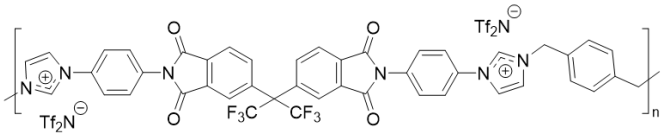

Figure 2.5: Structure of imidazolium-based polyimide ionenes with both imidazolium moiety and xylyl linkages in *para*- positions.[38]

Phosphonium salts typically exhibit enhanced thermal stability relative to quaternary nitrogen-based salts such as imidazolium, ammonium, and pyridinium due to the phosphonium cation's resistance to the reverse Menshutkin degradation and Hofmann elimination.[39] The Hofmann elimination generates an unsaturated alkane and a tertiary amine when the basic counterion attacks the β-carbon (relative to the ammonium ion). However, the phosphonium cation degrades into a tertiary phosphine oxide and alkane under alkaline conditions.[40] Yang et al. prepared phosphonium-based ionenes for CO_2 capture membranes as well as alkaline fuel cell (AFC) membranes.[41] They formed a polymer network using (4-acetylphenyl)diphenyl phosphonium bromide (M1) and 1,4-diacetylbenzene (M2) with Tf_2N^- counterions (Figure 2.6), which displayed an improved thermal and alkaline stability when compared to linear analogs. Furthermore, the ratio of charged (M1) and uncharged (M2) moieties affected the porosity and surface area of the material, a 1:2 ratio exhibited enhanced CO_2 uptake affinity and the values were comparable to analogous non-network and non-phosphonium materials.

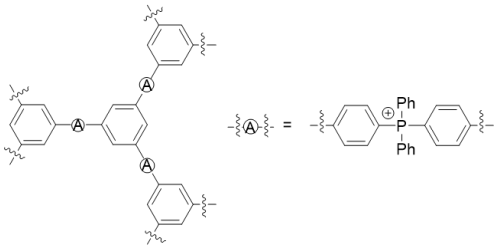

Figure 2.6: The structure of a phosphonium ionene polymer network.[41]

Williams et al. introduced the potential of using 12,12-ammonium-based ionenes as membranes with tunable mechanical properties (Figure 2.7a); the introduction of a cinnamate end group allowed for a UV light-mediated crosslinking reaction (final product

shown in Figure 2.7b).[42] Jeon and Gong reported ammonium-based ionenes for humidity sensing membranes by incorporating 3-(trimethoxysilyl)propyl methacrylate into 4,6-ammonium ionenes to introduce methacrylate end groups (Figure 2.7c).[43] Coating the synthesized ammonium ionenes on the surface of a sensor electrode through the photo-initiated radical polymerization exhibited an improved sensor durability and stability of the humidity sensitive membrane at elevated temperature and humidity. Gong developed ammonium-based ionenes containing a photocurable polyester and aromatic benzyl group as shown in Figure 2.8.[44] The 2,2-ionenes functionalized with a hydroxybenzyl end group and Br^- counterions were copolymerized with 4,4'-dihydroxy chalcone and terephthaloyl chloride to form ammonium-based polyester ionenes. The ionenes functionalized with hydroxybenzyl group were hygroscopic, and the chalcone group could successfully be crosslinked by UV irradiation.

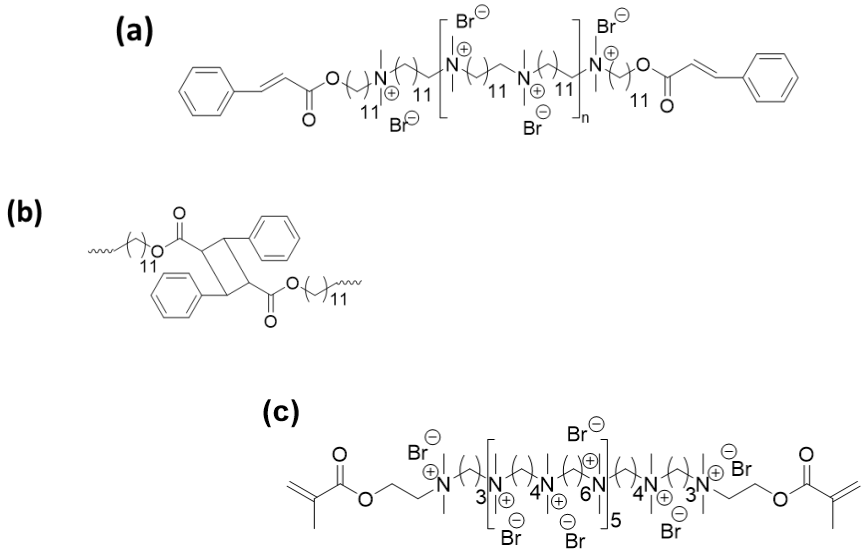

Figure 2.7: Structures of (a) cinnamate-functionalized 12,12-ammonium ionenes, (b) light-mediated crosslinked ammonium ionene network by Williams et al.,[42] and (c) 4,6-ammonium ionenes with methacrylate end groups.[43]

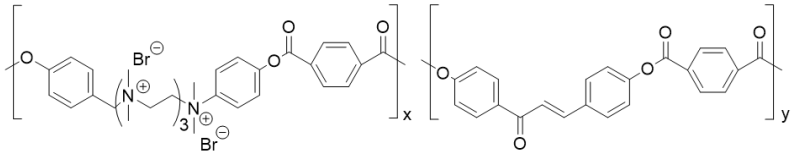

Figure 2.8: Structure of the photo-curable copolymerized ammonium-based copolyester ionenes.[44]

2.3.1.2 Biomedical Materials and Devices

Non-segmented ammonium-based ionenes have been reported in various biomedical applications. The polyelectrolyte complex (PEC) of DNA and ionenes or ionomers is promising for the delivery of genetic material (i.e., gene delivery) due to a lack of immunogenicity, the ability to tailor the complex's properties, and electrostatic attraction of the complex with the slightly negatively charged cellular membranes.[45] An important consideration in designing ionenes to form PECs is the biocompatibility or cytotoxicity of the polymer. Ionenes with a lower charge density and longer hydrophobic segment have been shown to destroy the cell regardless of the amount of polymer bound to the cell membrane. The hydrophobicity of the polymer plays a more critical role in cell disruption when compared to the polymer's charge density, as revealed by cytotoxicity studies performed using a series of x,y-ionenes (x=3, 6 or 12; y=3, 4, 6, or 12) and x,X-ionenes (x=3, 6 or 12, X=xylylene), all of which contained Br^- counterions.[46] The higher polymer charge density proved to promote cell binding but does not destroy the cell.

The stability of the PEC in various relevant conditions (e.g., high salt concentrations, presence of multivalent salts, and varying protein concentrations) is dependent on the type

of charge contained in the ionene as well as the number of methylene units, the polymer chain length, and the charge density.[47–50] Zelikin et al. reported that although it is not universally true that charge density in linear ionenes is a factor in controlling the stability of PEC, they did show that the stability of the PEC increased when charge density increased and the chain shortened.[45] Wahlund et al. compared phase separation of PECs containing either DNA or RNA with 2,5-ionenes containing Br^- counterions.[51] The strong binding of Br^- counterions and relatively low molecular weight (average DP is 40) caused the PEC to precipitate.

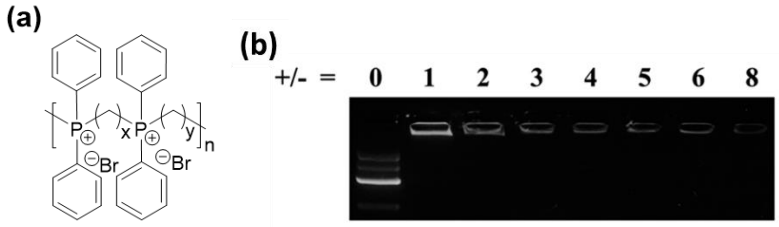

Figure 2.9: (a) Structure of phosphonium-based ionenes synthesized with bis(diphenyl)phosphines and dibromides and (b) DNA binding efficiency of 6P,6-ionene.[39]

Hemp et al. synthesized phosphonium-based ionenes with Br^- counterions from bis(diphenyl)phosphines and dibromides (Figure 2.9a), which exhibited poor water solubility due to the presence of the phenyl group attached to the phosphonium cation.[39] However, it dissolved in water at 100 °C and remained soluble at room temperature, and thus it could be easily applied to DNA binding studies. The 6P,6-ionene (in xP,y-ionene the x and y indicate the length of the methylene space in the ditertiary phosphine and dihaloalkane, respectively) effectively bound plasmid DNA at a phosphonium:phosphate ratio of 1:1 as shown in Figure 2.9b.

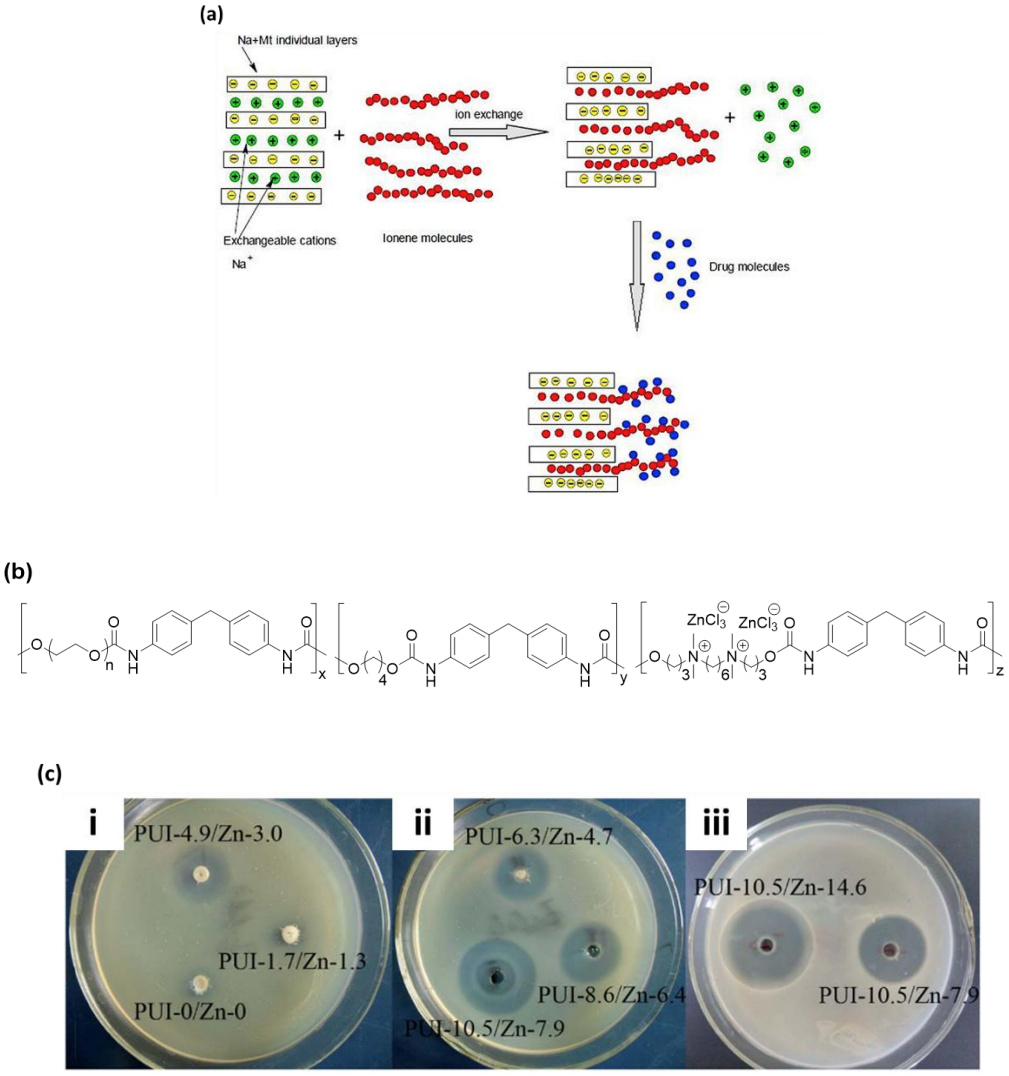

Figure 2.10: (a) Scheme of a drug release system using ammonium ionenes. Montmorillonite (Mt) works as a drug carrier by forming a nanocomposite with ionenes.[52] (b) Structure of the polyurethane ionenes with 1,4-butanediol, 4,4'-diphenylmethane diisocyanate and PEG 4K, and (c) images of the inhibition zones against E. coli growth (i, ii = 48 h and iii = 72 h).[55]

Ionenes have also been studied for use in controlled release systems with applications including drug release for biomedical therapies as well as pesticide release for agricultural purposes. For example, the anti-inflammatory drug, diclofenac sodium, was immobilized onto the ammonium-based ionenes as shown in Figure 2.10a.[52] The ionene-drug complex

exhibited a slower drug release profile compared to a simple quaternary ammonium salt owing to the entrapment of the drug molecules in the entangled ionene chains that slowed down the diffusion. Ionenes have also been studied as antimicrobials; the strong electrostatic interaction between the ionene and bacteria as well as the hydrophobic alkyl chains that make up the backbones of many ionenes, specifically those alkyl spacers with eight or more carbon atoms, facilitate the diffusion of cationic ionenes into bacterial cell membranes.[53–55] As an example, Ding et al. prepared segmented polyurethane ionenes (PUIs) with ammonium-based ionene segments containing $ZnCl_3^-$ counterions (which may exist in a dimeric form $Zn_2Cl_6^{2-}$) and used them as antimicrobial application (Figure 2.10b).[55] The $ZnCl_3^-$ ionenes produced an inhibition zone for both gram-positive and gram-negative bacteria, which increased with an increase in $ZnCl_3^-$ content as shown in Figure 2.10c. However, Cakmak et al. used simple ammonium-based ionenes with Cl^- counterions that exhibited a higher inhibition zone for gram-positive bacteria compared to gram-negative bacteria.[56] An increase in ionene concentration ultimately inhibited all bacterial growth. The linker chemistry also affected the antimicrobial properties and as ionenes with amide bonds were more lethal (>99.9%) at a lower concentration than when ester bonds were incorporated.[57] Geng and Finn revealed a new class of antimicrobial ionenes by introducing thiabicyclo[3.3.1]nonane in pyridinium-based ionenes.[58] Furthermore, Strassburg et al. utilized 3,4-ammonium ionenes with Br^- counterions as an antimicrobial functional structure within an interpenetrating hydrogel for the suppression of bacterial growth in wound healing (Figure 2.11).[59] Even a low concentration of ionenes successfully killed all adhered bacterial cells on the hydrogel for a period of up to 4 weeks. Also,

hydrogels using acrylamide and chloromethylstyrene-functionalized 2,4-ionenes with Br^- counterions showed promise for cell binding, drug delivery, and antimicrobial applications due to the high charge density and hydrophobicity as well as the improved mechanical properties compared to nonionic copolymers.[60] Ionenes showed outstanding skin compatibility with low *in vivo* toxicity,[61] suggesting that ionenes could be used as non-alcohol based and non-dehydrating surgical scrubs and hand sanitizers.

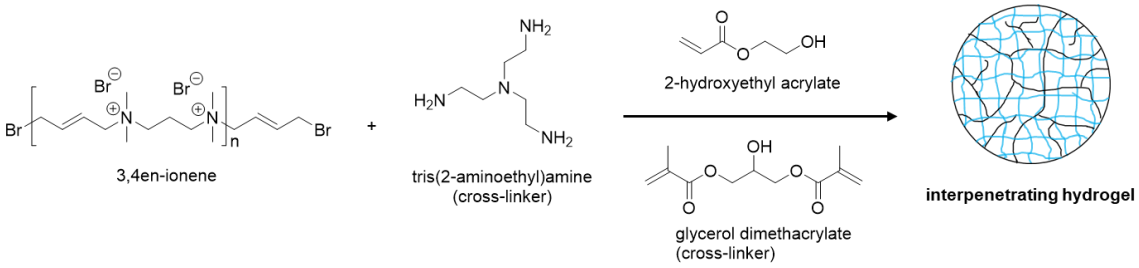

Figure 2.11: Schematic showing the fabrication of an interpenetrating hydrogel with 3,4en-ionenes.[59]

2.3.1.3 Materials for Solar Cells and Batteries

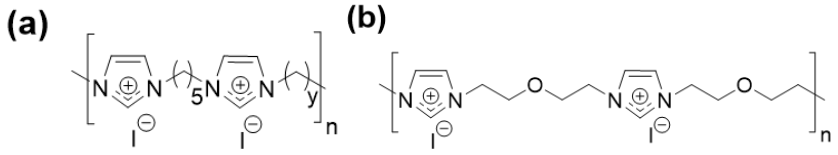

Figure 2.12: (a) Imidazolium-based ionenes synthesized with 1,1'-(1,5-pentamethylene)bis(imidazole) and diiodobutane (y = 4 or 6).[19] and (b) structure of the alkyloxy imidazolium ionene.[65]

Imidazolium-based ionenes have been used as polymer electrolytes in dye-sensitized solar cells (DSCs) and Li-ion batteries.[62–64] For example, Suzuki et al. achieved a 1.3% photon to electron conversion efficiency in the cells containing ionenes.[19] Since solidifying liquid electrolytes can reduce electrolyte leakage and evaporation, they synthesized

imidazolium-based ionenes with I^- counterions (xI,y-ionenes, where x and y indicate the length of the methylene space in the imidazolium and dihaloalkane, respectively). It was regarded as a molten salt type polymer that was suitable for quasi-solidification of IL electrolytes of DSCs by combining 1,1'-(1,5-pentamethylene)bis(imidazole) with 1,4-diiodobutane or 1,6-diiodohexane as shown in Figure 2.12a. Moreover, Li et al. used alkyloxy imidazolium-based ionenes containing I^- counterions (Figure 2.12b) that mixed two monomers, 1,1'-(2,2'-oxybis(ethane-2,1-diyl))bis(imidazole) and diethylene glycol diiodide, and encapsulated ILs, 1-methyl-3-propylimidazolium iodide (MPII) or 1,2-dimethyl-3-propylimidazolium iodide (DMPII), as a quasi-solid electrolyte for DSCs.[65] The MPII encapsulated ionenes exhibited better light-to-electricity conversion efficiency than DMPII. The addition of MPII provided better conversion efficiency, stability, and conductivity on DSCs.[66] Ionenes satisfy the need for a high ionic conductivity and good mechanical strength in DSCs, and the ability to fabricate them with liquid electrolytes, including ILs, has attracted attention to this promising material class.

The use of ionenes improved the performance of lithium-ion batteries (LIBs) by improving the electronic and ionic conductivity of the cathodes. PFSI ionenes (Figure 2.13a, ammonium-based polyimide ionenes) have been used in several ways to improve the battery performance as its backbone provides a low lithium dissociation energy and high cationic exchange capacity.[67] The anionic aliphatic PFSI ionenes with Li^+ counterions mixed with poly(vinylidene difluoride) (PVDF) exhibited a higher energy density and better reversibility than when only PVDF was used.[7] Shi et al. prepared PFSI ionenes with Li^+ counterions mixed with PEG as shown in Figure 2.13b; the perfluoroether connector, -

$CF_2CF_2OCF_2CF_2$-, sustained a high ionic conductivity and lithium-ion transport number.[67] Also, perfluoroether connector gave a better compatibility between flexible ionene and PEG segments that enhanced long-term electrochemical stability.

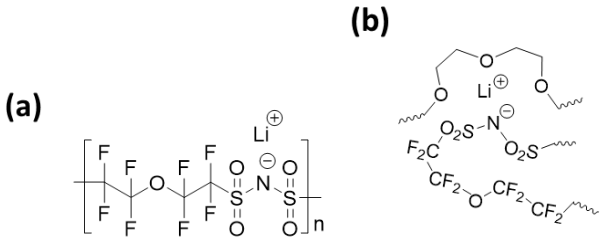

Figure 2.13: Structure of (a) PFSI ionenes with Li^+ counterions and (b) illustration of the interaction between PFSI ionenes and PEG segments with mobile Li^+ ions.[67]

2.3.1.4 Nanoparticle Synthesis Applications

Several works noted that ionenes can be used as a polycationic stabilizer for synthesizing nanoparticles.[68–71] The aggregation of nanoparticles can be detected by changes in color, for instance, orange-brown to gray-blue for silver nanoparticles (AgNPs) and ruby to blue for gold nanoparticles (AuNPs).[69,70] As such, colorimetric techniques using these nanoparticles to sense anions have been suggested. Terenteva et al. stabilized AgNPs using the non-segmented cationic 6,6-ionenes with Br^- counterions to detect the presence of sulfates or pyrophosphate in water.[68,69] The 6,6-ionenes with Br^- counterions also stabilized AuNPs due to the electrostatic repulsion between ionenes and AuNPs and steric stabilization that hindered the aggregation of nanoparticles in order to detect the sulfates in water as shown in Figure 2.14.[71] It was noted that Br^- counterions adsorbed on the surface of AuNPs and recruited ionene adsorption to the surface; the ionene-modified AuNPs were stable in solution for more than 4 months.

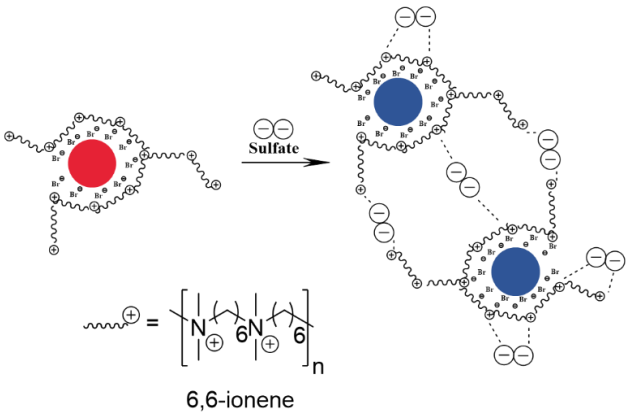

Figure 2.14: Schematic of a colorimetric technique that uses nanoparticles stabilized by 6,6-ionenes to sense sulfate ions.[71]

2.3.1.5 Absorbent Materials

Ionenes have been applied as absorbents for the removal of anionic dyes or to separate oil from water. In either case, the adsorptive property is driven by the interaction between the positive charges on the cationic ionene and the negative charges on the dye or oil. A sulfonate dye molecule remains in water longer and demonstrates lower adsorption on common adsorbents when compared to cationic dyes.[72] As an example, silica nanofibers were modified with an aliphatic non-segmented 2,3-ionene (Figure 2.15), which exhibited improved adsorption of a sulfonate-based Acid yellow dye when compared to unmodified nanofibers.[72]

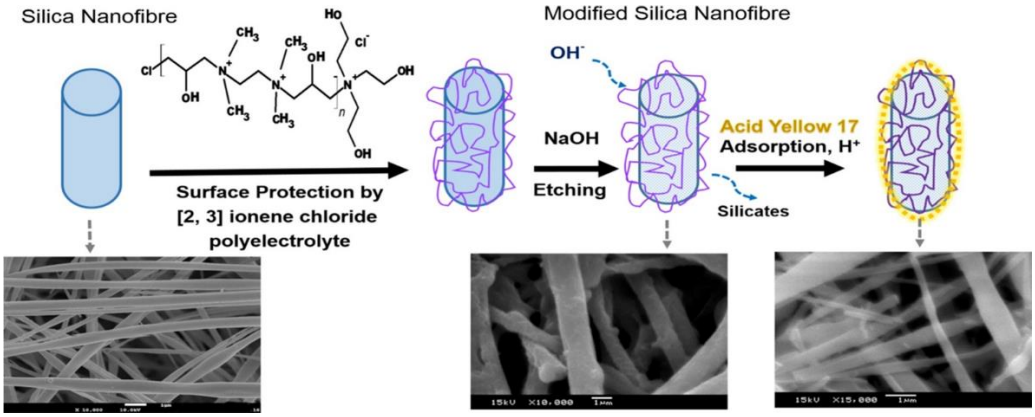

Figure 2.15: Schematic showing the modification of electrospun silica nanofibers with 2,3-ionenes.[72]

Dragan et al. introduced DABCO-based polyamide ionenes containing Cl^- counterions for the removal of 3 different azo dyes, Methyl Orange (MO), Ponceau SS (PSS), and Chicago Sky Blue 6B (DB1).[73] The MO, PSS, and DB1 dyes have 1, 2, and 4 sulfonate groups, respectively. Three different DABCO-based polyamide ionenes with different structural isomers of phenylenediamine, *ortho*- (Figure 2.16a), *meta*- (Figure 2.16b) and *para*- (Figure 2.16c), induced adsorption of the dyes onto the ionenes that was dependent on the dye structure and the topology of the ionenes. MO preferably bound onto all of the *meta*-, *ortho*- and *para*-linked isomers of the DABCO-based polyamide ionenes, PSS bound onto the *meta*- and *ortho*-linked isomers of the ionenes, and DB1 bound only onto the *para*-linked isomer of the ionenes. Pirogov et al. demonstrated that using rigid aromatic ionenes, such as 3,X-ionene, as sorbents for aromatic acids was favorable over aliphatic analogs (e.g., 3,8-ionenes) due to π-π interactions between the sorbent and sorbate.[74] Furthermore, Mansur et al. prepared nanocomposites consisting of 2,y-ionenes (y = 4, 6, 10, and 12) and bentonite to remove oil from oily water.[75] Adding the ionenes improved the removal efficiency by up to ~90% compared to the only bentonite without ionenes. The

ionenes intercalated into the bentonite and increased the clay basal space result from the increase of adsorption; however, despite a systematic increase in basal space with an increase in y, the oil removal efficiency was not dependent on y.

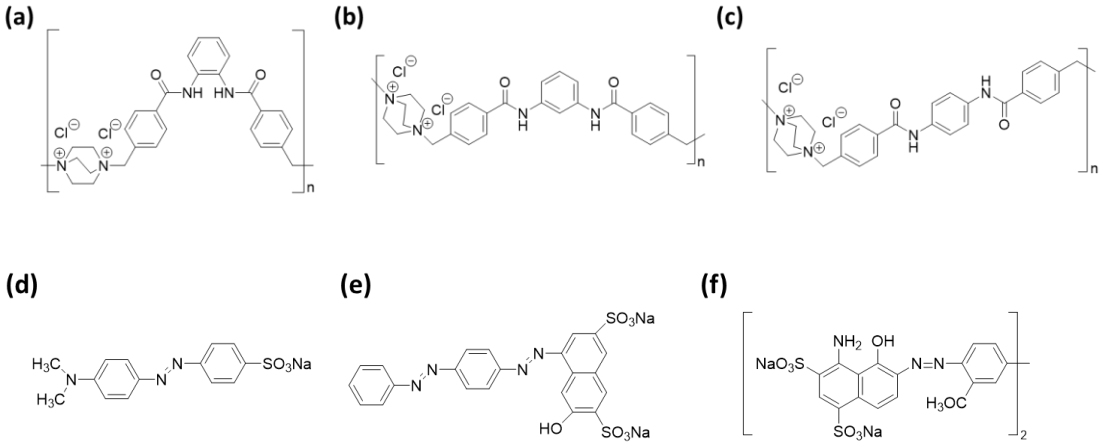

Figure 2.16: DABCO-based polyamide ionenes having different structural isomers of phenylenediamine (a) *ortho*-, (b) *meta*-, and (c) *para*- position.[73] and (d), (e), and (f) represent structures of MO, PSS, and DB1 dyes, respectively.

2.3.1.6 Other Applications

The previously mentioned *meta*-positioned cationic DABCO-based polyamide ionenes (Figure 2.16b) that was used as a dye adsorbent was also used as an n-doping agent in poly(3,4-ethylenedioxythiophene) (PEDOT) for electrochemical devices.[76] The film that was n-doped with ionenes exhibited better thermal stability and was more hydrophilic than the film n-doped with tetramethylammonium owing to the presence of polar amide groups in the ionene. Later, an imidazolium ionic liquid (1-ethyl-3-methylimidazolium with Tf_2N^- counterions) better stabilized the negative charge of the n-doped PEDOT, showing a higher n-doping concentration than an ammonium cation.[77] This suggests that using imidazolium-

based ionenes instead of ammonium-based ionenes could improve the performance of electrochemical devices.

2.3.2 Hydrogels

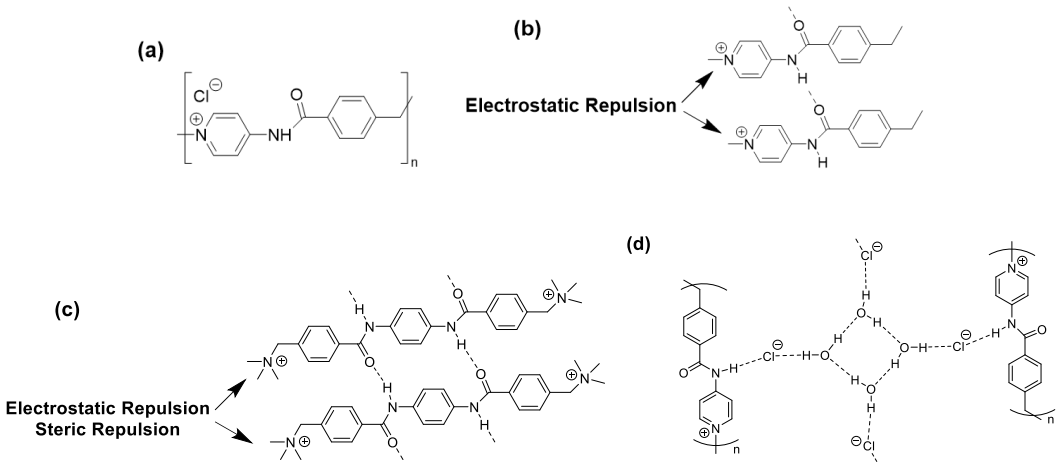

Figure 2.17: (a) Structure of the pyridinium-based polyamide ionene and illustration of the possible hydrogen bonding (b, c) between amide groups, and (d) mediated by the Cl^- counterions.[82]

Solvent-swollen gels can be categorized as either hydrogels or organogels depending on the solvents (i.e., water or an organic solvent). Hydrogels are promising candidates for biomaterials due to their favorable swelling behavior that mimic biological tissue and they have also been used in fuel cells and batteries.[78–80] For the physically crosslinked hydrogel using the cationic ionenes, the driving force of the gelation is weak and non-covalent interactions such as hydrogen bonding, van der Waals, π-π stacking, and electrostatic forces between the gelator molecules and a reversible thermal-phase transition between gel and sol sates is their main feature.[81] The Yoshida group created pyridinium-based ionene hydrogels containing a benzamide group and Cl^- counterions (Figure 2.17a) and hydrogen bonds between the amide groups (Figure 2.17b and 2.17c), and the amide group the Cl^-

counterions and water (Figure 2.17d) caused the gel to form.[82] At higher concentrations (30 g/L) the ionene hydrogel started to collapse at 10% strain, but it recovered rapidly, which is a common property for ionene-based hydrogels. Moreover, the incorporation of single-walled carbon nanotubes (0.1 g/L) decreased the T_{gel} of the hydrogel (20 g/L) from ca. 80 ℃ to ca. 56 ℃. The addition of inorganic salts increased the T_{gel} gradually due to the salt-in behavior.[83] The brittleness of the hydrogel increased with an increasing salt concentration because the hydrogel became more tightly packed and formed a stronger network. The hydrogel began precipitating at a certain salt concentration (i.e., 0.07 mM for NaCl and 0.04 mM for NaBr) owing to the excessive network formation which collapses the network structure, and the presence of salt also reduced the recovery process. The ionenes with Cl^- counterions formed a gel even in acid, pH 1, in contrast to natural gelators. The Yoshida group exchanged the counterions by a simple anion exchange reaction to examine the ionene solubility in various solvents (summarized in Table 2.1).[84] Overall, by simply exchanging anionic counterions on the pyridinium-based polyamide ionenes, they dramatically changed the solubility in organic solvents. Misawa et al. synthesized DABCO-based polyamide ionenes and ammonium-based polyamide ionene hydrogels containing with Cl^- counterions as shown in Figure 2.18ai.[85] The intermolecular hydrogen bonding between amide groups induced a gel network as confirmed by the vial inversion method (Figure 2.18aii). DABCO-based ionenes at 50 g/L took 3 days to produce hydrogels in water with heat, whereas aliphatic ammonium ionenes at 30 g/L took only 5 h due to the flexible ethylene linker. Although the higher concentration of the ionenes caused the gel to be brittle, the gelation time decreased with an increase in the concentration.

The length of the alkylene spacer between ionic groups affected the gelation time; a spacer with six methylene units formed a gel after 3 h at 10 g/L whereas two and three methylene units formed a gel after 5 h and 3-4 d at 30 g/L, respectively. Diaz and coworkers examined DABCO-based polyamide ionenes with Cl^- counterions (Figure 2.16), but compared *para*-linked phenylenediamine with *ortho*- and *meta*-linked analogs.[86] The computational studies predicted that the *ortho*-linker was the most suitable to form a stable hydrogel due to the complex and dense hydrogen bonding and π-π stacking interaction network, although the *meta*-positioned linker had more abundant interactions (Figure 2.18b). The difference in the molecular structure influenced the gelation kinetics and critical gelation concentration (CGC). The *ortho*-linker had a four and two-fold lower CGC than *meta*- and *para*-linkers, respectively as well as the fastest gelation time at a consistent concentration, but also the gel-to-sol transition occurred by sonication rather than heating. Moreover, *ortho*-linked DABCO-based polyamide ionenes containing Cl^- counterions formed better gels in solutions of varying pH and ionic strength when compared to *meta*- and *para*-linked ionenes due to the synergistic effect of polymer-polymer interactions and polymer-counterion interactions, while *meta*- and *para*-linked ionenes showed only singular trends.[18] Separately, the authors demonstrated that *ortho*-linked hydrogels exhibited self-healing properties and that they could be injected through a 21-gauge needle into various shapes for biomedical applications (Figure 2.18c).[87]

Table 2.1: Solubility and gelation ability based on the type of counterions (No: insoluble; Yes: soluble; Gel: formed a gel at 1 wt% concentration).[84]

Solvent	Cl^-	BF_4^-	PF_6^-	Tf_2N^-	BPh_4^-	I^-	SCN^-	DCA^-	ClO_4^-	$CF_3SO_3^-$
DMA	No	Yes	Yes	Yes	Yes	Gel	Yes	No	Yes	Yes
DMSO	No	Yes	Yes	Yes	Yes	Yes	Yes	Yes	Yes	Yes
DMF	No	Yes	Yes	Yes	Yes	Gel	Yes	Yes	Yes	Yes

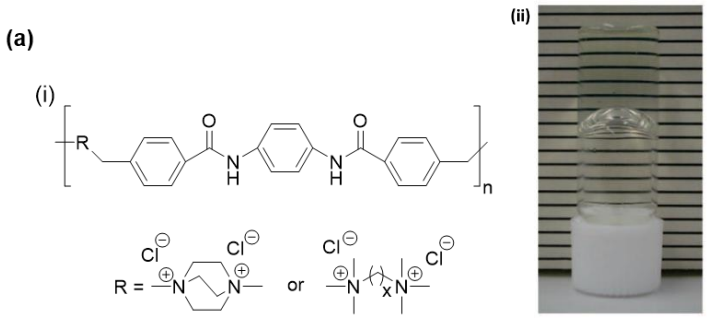

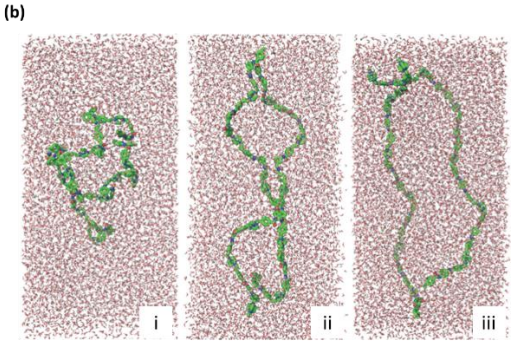

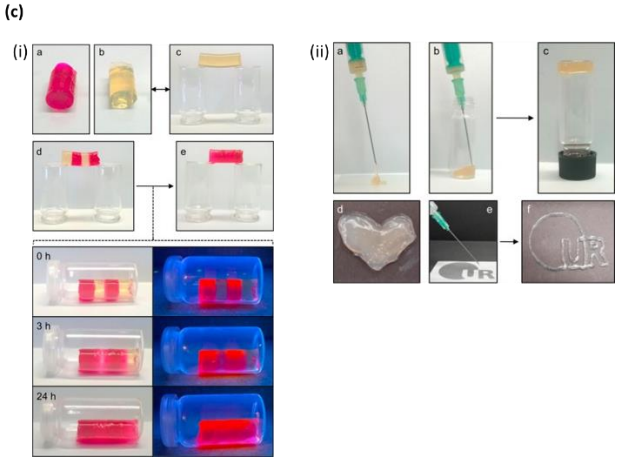

Figure 2.18: (a) Structure of the DABCO-based polyamide ionenes and aromatic polyamide ammonium ionene (i) and DABCO-based polyamide ionenes with Cl^- counterion hydrogel (ii).[85] (b) computer simulated DABCO-based polyamide ionenes with three different structure. (i : *ortho*-, ii : *meta*-, and iii : *para*-).[86] (c) illustration of the *ortho*-linked DABCO-based polyamide ionene hydrogel. The fusion of dye doped and undoped gel became a gel bridge after 24 h showing dye diffusion through self-healed gel (i), and showed injectability property (injectable hydrogel) (ii).[87]

2.4 Segmented Ionenes

Unlike non-segmented ionenes, most segmented ionenes show elastomeric behavior due to the presence of soft and hard repeating segment. Typically, segmented ionenes demonstrate superior mechanical performance and elastic behavior, related to the microphase separation, when compared to non-segmented ionenes. Williams and Long reviewed the state of ionenes in 2009 including a description of segmented ionenes and the varying types of soft segments.[1] However, various segmented ionenes have been reported during the past decade composed of more diverse soft segments that have not been reviewed. Several oligomeric monomers including PTMO, PEG, and PPG have been used to make ionenes with ammonium, imidazolium, DABCO, or pyridinium ionic groups.[88–90] The elastic nature of the ionenes arises from the ionic clustering induced by electrostatic interactions between the backbone ions and counterions, which produce physical crosslinking points.[91] In surveying the literature, we categorized the segmented ionenes into three types: aliphatic ionenes, aromatic ionenes, and heterocyclic ionenes (e.g., pyridinium, imidazolium, or DABCO charged groups) as shown in Figure 2.19. The soft segment is shown as PTMO in each case for direct comparison, also the charged sites for the aliphatic and aromatic ionenes are shown as ammonium. In this way, it will decouple

the role of hard and soft segments and give insights to design future segmented ionenes for various applications.

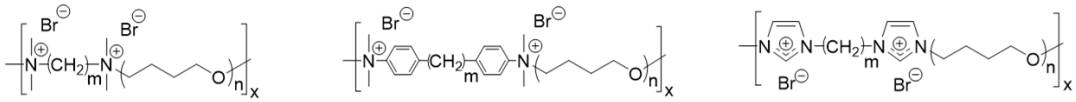

Figure 2.19: Schematic showing the three types of hard segments in segmented ionenes.

2.4.1 Elastomer

2.4.1.1 Aliphatic and Aromatic Ammonium Ionenes

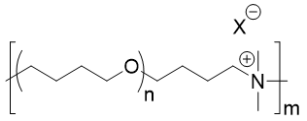

Figure 2.20: Structure of the aliphatic PTMO mono ammonium ionenes.[92]

Ikeda et al. prepared aliphatic ammonium PTMO ionenes by polymerizing tetrahydrofuran and terminating with N,N-dimethylamino trimethyl silane.[92] Then, the anion was exchanged by sodium bromide or sodium chloride to introduce Br^- and Cl^- counterions, respectively (Figure 2.20). The ionenes had only one ammonium cation in each repeating unit that caused the ionic segments to weakly aggregate in comparison to diammonium cations in each repeating unit, and thus exhibited a short rubbery plateau region.[93] These results showed how the type of counterion could change the mechanical properties and the morphology of ionenes. Br^- counterions aggregated more tightly and stably relative to Cl- counterions, inhibited room-temperature crystallization in the soft

segment, and also promoted strain-induced crystallization, all of which increased the ultimate tensile stress and produced a flatter rubbery plateau region (Figure 2.21).

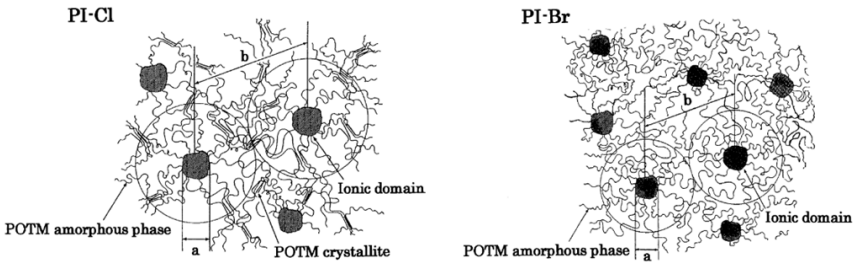

Figure 2.21: Schematic of the effect of counterions on the morphology of aliphatic ammonium PTMO ionenes at room temperature (PI-Cl: PTMO ionenes containing Cl^- counterions, and PI-Br: PTMO ionenes containing Br^- counterions).[92]

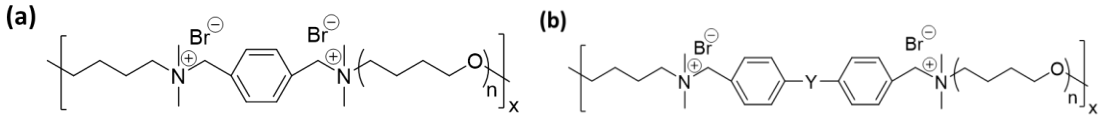

Figure 2.22: (a) Structure of the aromatic PTMO ammonium ionenes using dimethylamino terminated PTMO and 1,4-dibromo-*p*-xylene.[94] (b) structure of aromatic PTMO ammonium ionenes containing a variable spacer group between benzyl groups.[11]

Feng et al. prepared an aromatic ammonium PTMO ionene containing Br^- counterions by reacting dimethylamino terminated PTMO with 1,4-dibromo-*p*-xylene (Figure 2.22a); the ionenes displayed no PTMO crystallization at room temperature when the M_n was < 3,400 g/mol.[11,94] Transmission electron microscopy (TEM) revealed cylindrical ionic domains and increasing the PTMO molecular weight from 1,800 g/mol to 6,600 g/mol decreased the volume fraction of the ionic segments leading to randomly distributed ionic domains with weaker phase separation and increased d-spacing. Ikeda et al. also studied segmented pyridinium-based PTMO ionenes in which reducing the PTMO molecular weight caused PTMO chain extension because of stronger Coulombic interaction energies

per unit volume (when PTMO M_n < ~5,000 g/mol).[95,96] Moreover, the increase of the PTMO molecular weight from 3,400 g/mol to 10,000 g/mol decreased the tensile strength (from 45 MPa to 30 MPa), strain at break (between ca. 900-1200%), and rubbery plateau modulus due to the induced lower portion of hard segments.[11] Aromatic PTMO ionenes with an aliphatic ether spacer group between dibenzyl halide, Y in Figure 2.22b, showed a lower stress at a given elongation compared to the non-spacer group (No Y) due to three potential reasons: poor phase separation due to weaker ionic association; a higher degree of hard-soft segment mixing, and/or interactions between two benzyl halide due to the flexible ether linkage. Generally, the incorporation of the spacer group decreased the rubbery plateau modulus due to the weaker overall association of the ionenes. Furthermore, regardless of the presence of spacer group, ionenes containing Cl^- counterions showed a higher stress at a given elongation and a lower strain at break than ionenes containing Br^- counterions due to the smaller size and greater electronegativity of Cl^-, which promotes better packing and Coulombic interactions and, thus, provides a stronger ionic association in the aromatic PTMO ionenes.

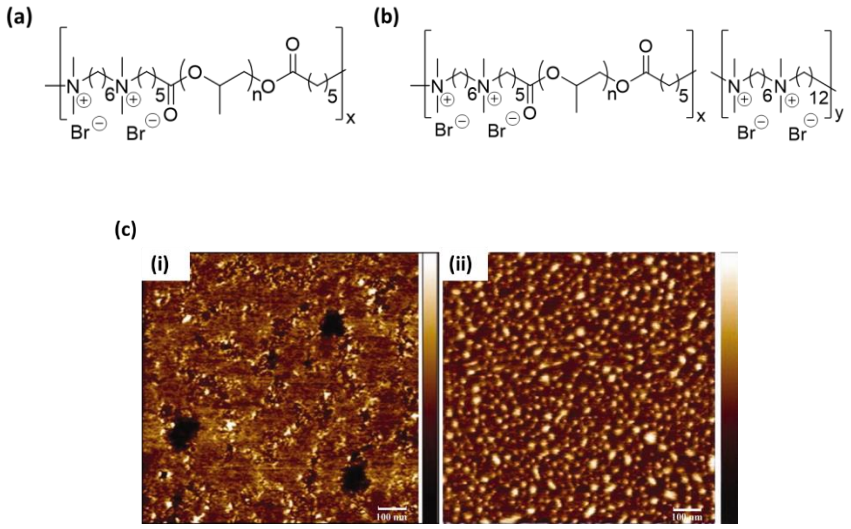

Figure 2.23: Structure of the aliphatic ammonium PPG ionenes having (a) bromine end-capped PPG with one hard segment, and (b) copolymerized with two hard segments.[17]. (c) microphase separation of segmented ionenes having 1k PPG (i) and 4k PPG (ii) revealed by atomic force microscopy.[17]

Unlike PTMO that crystallizes at ambient temperature, the amorphous PPG does not crystallize even at high molecular weight. Tamami et al. studied the effect of the PPG soft segment molecular weight on the characteristics of aliphatic ammonium ionenes with Br^- counterions (Figure 2.23a).[17] The higher concentration of hard segments reduced the thermal stability, decreasing the onset of degradation temperature from ca. 250 °C to 210 °C. The higher charge density also increased the rubbery plateau modulus, potentially due to higher hard segment content that reduces chain mobility. The authors also prepared copolymers to study the effect of charge density by supplementing the hard segment with a 1,12-dibromododecane comonomer (Figure 2.23b). Decreasing the soft segment molecular weight reduced the viscous flow temperature due to fewer chain entanglements as well as microphase separation (Figure 2.23c), but increased the rubbery plateau modulus and stress during elongation due to the high charge density. Interestingly, when the PPG

soft segment molecular weight was kept constant at 1,000 g/mol and the charge density was altered via copolymerization, an increase in the hard segment content from 12 wt% to 33 wt% caused the rubbery plateau modulus to increase two orders of magnitude. Based on this research, design strategies to modify the charge density of ionenes through soft segment molecular weight and copolymerization are conceived to alter the mechanical properties and microphase separation of segmented ionene elastomers. Hall and coworkers showed that the decrease of PPG content from 70% to 29% in aliphatic ammonium PPG copolymer ionenes increased the microphase separation and local ionic aggregation via molecular dynamics simulations using a coarse-grained model.[97] Moreover, the microphase separation increased with decreasing temperature.

The 7,7,8,8-tetracyano-quinodimethane (TCNQ) salt, which is a strong electron acceptor, has been used for conducting polymers due to its high electrical conductivity.[98] It has been shown that carrier electrons move through the TCNQ moiety and polycations arrange the TCNQ salt.[99] Ionenes with $TCNQ^-$ counterions showed higher electrical conductivity than the ionomers, and the aliphatic ammonium ionenes had a higher resistivity than aromatic ammonium ionenes.[100,101] Incorporating the rigid ring structure (i.e., pyridinium) in the backbone of ionenes reduced the Coulombic repulsion between counterions, and thus increased the electrical conductivity.[99] The authors also studied a series of aromatic compounds, but found that the structural differences among the aromatic compounds in the ionenes backbone did not show any significant difference in the electrical conductivity of the ionenes with $TCNQ^-$ counterions.[100] However, heterocyclic (DABCO) or heterocyclic aromatic (pyridinium) ammonium ionenes showed rigidity and a large distance between

the quaternized nitrogen atoms that enabled $TCNQ^-$ counterions to have a high electrical conductivity.[98] Based on their result, it is noteworthy that an even number of methylene groups between DABCO made polymer chain to be straight whereas an odd number of methylene units caused the polymer to be bent; thus, an even number of methylene groups increased the electrical conductivity. Pyridinium-based ionenes were not affected by the number of methylene groups between bipyridine because the bipyridine ring is bulkier than DABCO ring.

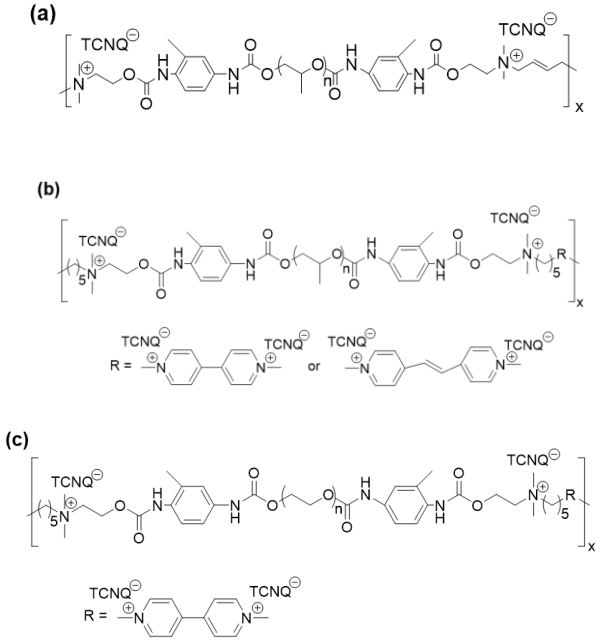

Figure 2.24: (a) Synthesis of the aromatic ammonium PPG ionenes containing $TCNQ^-$ counterions.[90] and the structure of the bipyridine incorporated aromatic ammonium (b) PPG ionenes,[88] and (c) PEG ionenes[102] with $TCNQ^-$ counterions.

Although the ionene elastomer is known to have a lower conductivity, it has received great attention due to its useful chemical and physical properties. The Rembaum group reported a conducting elastomer using the aromatic ammonium PPG ionenes with $TCNQ^-$ counterions (Figure 2.24a)[90] wherein the resistivity was inversely proportional to the

charge density and directly proportional to the distance between $TCNQ^-$ counterions. An increase in the molecular weight of the PPG soft segment decreased the charge density and the electrical conductivity. Furthermore, Watanabe et al. incorporated the heterocyclic aromatic bipyridine into the aromatic ammonium PPG ionenes with $TCNQ^-$ counterions (Figure 2.24b) and it effectively decreased the resistivity by optimizing the spacing between ionic sites.[88] Takizawa et al. synthesized bipyridine-based aromatic ammonium PEG ionenes with $TCNQ^-$ counterions as shown in Figure 2.24c.[102] The growth of the spherulites due to the incorporation of PEG prevented the formation of a conduction path, but the resistivity significantly decreased at temperatures above the T_m of PEG.

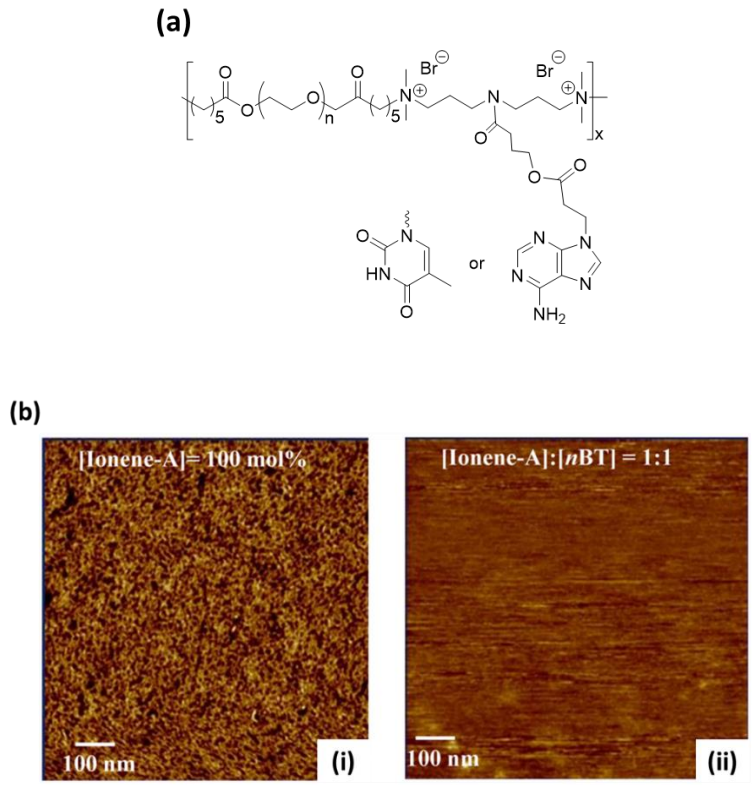

Figure 2.25: (a) Structure of the aliphatic ammonium PEG ionenes containing nucleobases as a pendent group with Br^- counterions and (b) microphase separation of Ionene-A (i) and Ionene-A with nBT (ii) revealed by atomic force microscopy.[105]

Burmistr et al. studied the synthesis, thermal properties, and ionic conductivity of aliphatic ammonium PEG ionenes with Cl^- counterions.[103] Increasing the PEG soft segment molecular weight decreased the T_g, transitioned the polymer from amorphous to semi-crystalline, improved microphase separation, and decreased the ionic conductivity due to the reduction of free carriers of charge. The synthesis of aliphatic ammonium PEG ionenes with various pendant functional groups were reported by Dimitrov and Berlinova.[104] The incorporation of zwitterionic and perfluorooctyl functional groups into aliphatic ammonium PEG ionenes decreased the crystallinity and the zwitterionic groups possessed the lowest T_m. Tamami et al. designed and synthesized aliphatic ammonium PEG ionenes

containing the adenine and thymine nucleobases as a pendant group with Br^- counterions (Figure 2.25a) to study the effect of hydrogen bonding between nucleobases and also with guest molecules (n-butyl adenine or n-butyl thymine) on thermal and morphological properties of ionenes.[105] The hydrogen bonds did not affect the T_g of the PEG soft segment and induced shorter Bragg spacing. Moreover, introducing guest molecules disrupted original morphology and decreased the phase contrast revealed by AFM as shown in Figure 2.25b.

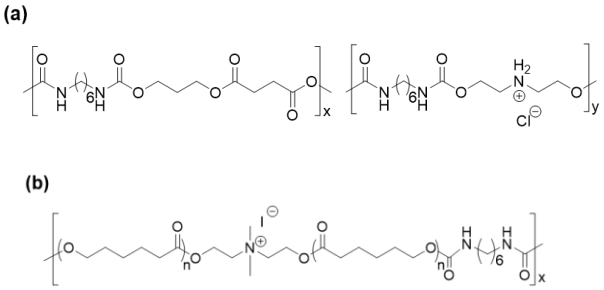

Figure 2.26: Structure of aliphatic ammonium (a) poly(butylene succinate) (PBS) urethane ionenes containing Cl^- counterions[106] and (b) poly(caprolactone) (PCL) urethane ionenes containing I^- counterions.[107]

Wu et al. reported aliphatic ammonium poly(butylene succinate) (PBS) urethane ionenes containing Cl^- counterions (Figure 2.26a) to study the effect of the urethane ionic hard segment on the properties of the ionenes.[106] The incorporation of the urethane ionic segment decreased the degree of crystallinity of the PBS soft segment without changing the crystal structure, while the crystallization rate was increased because the ionic aggregates promoted urethane alignment. Moreover, the urethane ionic segment increased the hydrophilicity, but did not change the tensile strength and elongation at break which were ca. 40 MPa and ca. 530%, respectively. Also, Nakayama et al. prepared aliphatic poly(caprolactone) (PCL) urethane ammonium ionenes containing I^- counterions (Figure

2.26b).[107] The ionenes were synthesized by mixing hydroxyl-end functionalized PCL, which was polymerized from ε-Caprolactone initiated by N-methyldiethanolamine, and HMDI, and the tertiary amine was quaternized with iodomethane to compare the difference between the urethane polymer and the urethane ammonium ionenes. Modifying the tertiary amine to quaternary ammonium to form ionenes did not change the tensile strength (ca. 30 MPa) but increased the elongation at break (ca. 2,300%) due to the presence of ionic groups. This observation, in contrast to that seen by Wu et al., could be attributed to the difference in counterion.[106] In addition, the urethane ionenes showed slower biodegradation than uncharged urethane polymers, but the highest molecular weight of PCL (M_n = 13,000 g/mol) did not show slow biodegradation compare to uncharged polymer due to the relatively low charge density.

2.4.1.2 Heterocyclic Ammonium Ionenes

2.4.1.2.1 DABCO-based Ionenes (Heterocyclic Ammonium Ionenes)

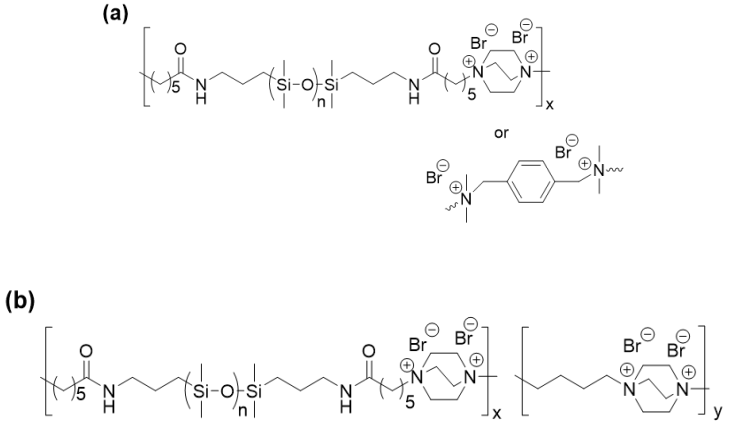

Figure 2.27: Structure of (a) DABCO-based PDMS ionenes and aromatic ammonium PDMS ionenes, and (b) DABCO-based PDMS ionenes with chain extended DABCO.[13]

Das et al. reported DABCO-based copolymer ionenes with Br^- counterions, DABCO/butane hard segments, and poly(dimethylsiloxane) (PDMS) soft segments (Figure 2.27).[13] TGA revealed that the DABCO-based ionenes showed a much higher char yield compared to the xylene-based ionenes due to the bicyclic structure that caused enhanced crosslinking upon exposure to elevated temperature. However, the copolymer ionenes with DABCO/butane-based hard segments showed the lower char yield. The ionenes with chain extended DABCO, which has the highest wt% of hard segments, showed the highest rubbery plateau modulus, which decreased with an increasing molecular weight of PDMS. The xylene-based ionenes exhibited a lower rubbery plateau modulus than DABCO-based ionenes. AFM showed microphase separation in all ionenes, wherein hard segments formed thread-like domains and dispersed in the PDMS soft segment, and X-ray scattering studies revealed that the hard segments formed cylindrical domains and were oriented in a stretch direction.

2.4.1.2.2 Imidazolium-based Ionenes (Heterocyclic Aromatic Ammonium Ionenes)

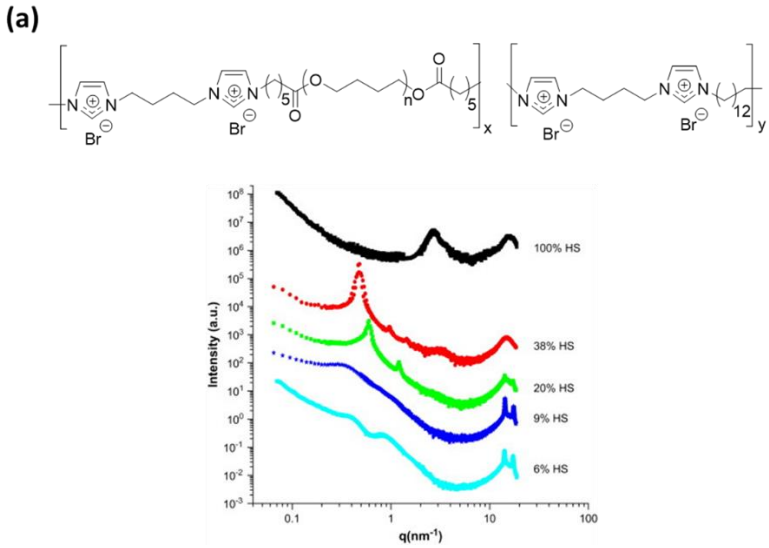

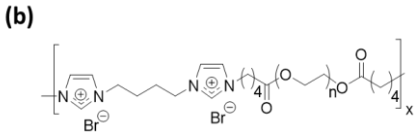

Figure 2.28: (a) Synthesis of copolymerized imidazolium-based PTMO ionenes copolymers and multi-angle X-ray scattering intensity.[8] (b) imidazolium-based PEG ionenes.[22]

Williams et al. introduced the first copolymer imidazolium-based PTMO ionenes (Figure 2.28a) with bisimidazolium/dodecane hard segments and PTMO soft segments.[8] The increase of hard segments reduced the PTMO crystallinity and showed clearer microphase separation (i.e., at 20 wt% and 38 wt% hard segment multiple scattering peaks at scattering vectors from 0.2 to 2 nm^{-1} were observed). Other literature accounts used imidazolium-based PTMO ionenes to prepare nonwoven fibers using electrospinning.[108] Three different PTMO soft segment molecular weights were used to vary the hard segment content. The tensile strength increased with an increasing molecular weight of PTMO, which disagrees with other literature that reported a decrease in tensile strength as a function of increasing the soft segment molecular weight.[11,17] The authors observed strain-induced crystallization of PTMO at the higher PTMO molecular weights, which could have accounted for the contradictory trends in tensile performance. Others prepared an imidazolium-based PEG ionenes (Figure 2.28b), which exhibited an outstanding thermal stability (for ionenes) with the onset of degradation occurring at 260 °C.[22]

2.4.1.2.3 Pyridium-based Ionenes

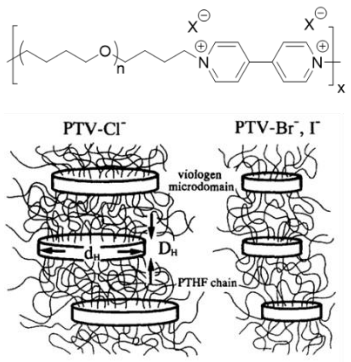

Figure 2.29: Structure of the pyridinium-based PTMO ionenes and schematic of the effect of counterions on the morphology (PTV-Cl^- : pyridinium-based PTMO ionenes containing Cl^- counterions, and PTV-Br^-, I^- : pyridinium-based PTMO ionenes containing Br^- and I^- counterions, respectively).[91]

Viologen units have been used as an ionic hard segment in elastomeric segmented ionenes due to their unique structure and properties. The pyridinium-based ionenes display comparable mechanical properties but improved thermal properties compared to aromatic ammonium ionenes.[21] Hashimoto et al. generated pyridinium-based PTMO ionenes, which showed stress-induced crystallization of the PTMO after 300% strain and an increase in the tensile strength at break Cl^- to Br^- and I^- ($Cl^-<Br^-<I^-$) counterions.[91] This result corroborates findings from previous literature that Br^- counterions have a more significant effect than Cl^- counterions on the tensile performance of aliphatic PTMO ammonium ionenes.[92] The pyridinium-based ionenes, with all counterions, showed a rubbery plateau region until 150 °C; however, the ionenes containing Cl^- counterions showed the highest T_m and T_g and the lowest crystallization temperature (T_c) compared to Br^- and I^-. Moreover, the tan δ peak intensity increased in the order of $Cl^-<Br^-<I^-$, corroborating the above results; furthermore, the ionene with the Cl^- counterion had the widest tan δ peak because the crystallites constrained the motion of the amorphous PTMO soft segments. Overall, the

pyridinium-based PTMO ionenes with Cl^- counterions showed the highest degree of microphase separation and a schematic of the morphology depicting the lamellar morphology with the disk-like aggregation of the ionic segments based on the SAXS analysis is shown in Figure 2.29.[91] This pyridinium-based PTMO ionenes swelled in room temperature water because the ionic aggregates created physical crosslink points, the polymers absorbed 53.1%, 43.2% and 8.8% water for the Cl^-, Br^- and I^- counterion, respectively.[109] The tensile strength decreased with increasing water content, but the elongation at break did not change substantially. They also showed the photochromic reaction as ionenes containing Cl^- counterions exhibited a color change from colorless to green. A tensile strength relaxation also occurred by light irradiation due to the photoreduction of the viologen group causing changes in the ammonium cation of viologen group into the radical cation and resulting in a decrease in the ionic charge. Meanwhile, ionenes containing Br^- counterions needed poly(N-vinyl-2-pyrrolidone) as an accelerator for the photo-induced reaction, which did not negatively affect the elastic properties of the ionene, to show the color changed and tensile strength relaxation.[110]

Feng et al. determined that the PTMO soft segment in the pyridinium-based PTMO ionenes showed stress-induced crystallization when the PTMO molecular weight was 1,300 g/mol.[21] Also, the tensile strength increased with an increase in the PTMO molecular weight from 1,300 g/mol to 1,700 g/mol and then decreased with an increase in the PTMO molecular weight from 1,700 g/mol to 2,500 g/mol. These results corroborate the results discussed in the imidazolium-based ionenes section.[108] The tendency toward stress-induced

crystallization of PTMO with the increase in the PTMO molecular weight may not be affected by the hard segment or ionic composition.

The pyridinium-based PTMO ionenes using 4,4'-bipyridine hard segments with $CF_3SO_3^-$ counterions showed an unusual 'jump' in the storage modulus at around 50 °C (after melting of PTMO soft segment) due to the conformational, or repacking, changes in the ionic hard segments.[21] In contrast, incorporating methylene groups between hard segments did not cause a modulus 'jump' but showed a weakened ionic association. Furthermore, $CF_3SO_3^-$ counterions in pyridinium ionenes showed weaker ionic aggregation than Cl^-, Br^- and I^- counterions.[91] Ikeda et al. prepared pyridinium-based PTMO ionenes containing Cl^- counterions and 2,2'-bipyridine hard segments.[96] The molecular weight of PTMO was ca. 10,000 g/mol and showed a tensile strength of 34 MPa and an elongation at break of 540%. By comparison, an aromatic ammonium PTMO ionene (also with a 10,000 g/mol PTMO soft segment but with a dibenzyl hard segment and Br^- counterions) showed similar tensile strength and a much higher elongation at break (ca. 900%).[11] This is likely due to the difference in the hard segment moiety or counterions since previous work determined that Br^- counterions improved the tensile performance.[11,91]

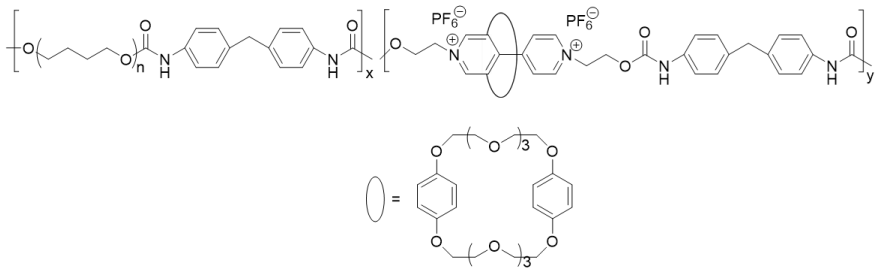

Figure 2.30: Structure of the copolymerized pyridinium-based PTMO ionenes with rotaxane moiety at the hard segment.[111]

Loveday et al. designed a rotaxane moiety, bis(*p*-phenylene)-30-crown-10, to complex with the hard segment in pyridinium-based PTMO ionenes as shown in Figure 2.30.[111] The presence of the rotaxane moiety enhanced the thermal stability and increased the elastic modulus compared to non-rotaxane analogs. SAXS showed no difference in d-spacing as a function of change in the molecular weight of PTMO. However, Br^- counterions promoted better phase separation and packing (smaller d-spacing and increased peak sharpness) compared to bulky PF_6^- counterions due to the smaller and more electron-dense Br^- counterions.

2.5 Conclusion

Ionenes have been developed into a variety of diverse and complicated structures, with an ever expanding library of monomers or prepolymers, since their introduction to the literature in 1933. Most reported ionenes are cationic ionenes, which presents an opportunity to develop and investigate the complementary anionic ionenes. Ionenes can also be divided into the categories of segmented and non-segmented ionenes, in a similar fashion to polyurethanes and polyureas. Segmented ionenes have robust thermoplastic elastomer characteristics, but non-segmented ionenes have seen action in a diverse set of applications over the past 10 years. There is still ample room for further investigation to understand the performance of non-segmented ionenes in reported and new applications. Nevertheless, they are a promising candidate for CO_2 separation membranes and within various biomedical fields due to their high charge density and the interaction between the counterions and the charged polymer backbone. Non-segmented ionenes have been deployed in polymer networks by incorporating crosslinkers and encapsulating ILs for

membrane applications. They have recently been studied as hydrogels for biomedical applications. The use of different counterions, different monomeric isomers, and secondary bonds (i.e., hydrogen bonds) results in the production of ionene hydrogels with a range of properties. On the other hand, segmented ionenes have not been fully optimized for other applications. They have numerous advantages including the combination of elasticity, strong mechanical stability, and tunable thermal properties. The majority of reported segmented ionenes include ammonium cations (including heterocyclic DABCO-based ionenes, and heterocyclic aromatic imidazolium and pyridinium-based ionenes), presenting opportunities for different types of ionenes, such as segmented phosphonium-based ionenes. Furthermore, the elastic properties and ionene morphology vary with the structural characteristics, including the soft segment molecular weight, the overall ionene molecular weight, counterion composition, presence of aromatic, heterocyclic or heterocyclic aromatic components, and functional pendant groups. In other words, synthesizing novel segmented ionenes presents a near-infinite research space. The current trends reveal that segmented ionenes have potential for electrochemical and biomedical applications due to their robust and high mechanical, thermal, conductive, and elastic properties that can be designed by various factors. In this work, we highlight the many structural variations in segmented and non-segmented ionenes, and, as often as possible, correlate those structural variations to functional characteristics and desirable properties that were observed.

2.6 Acknowledgements

The authors wish to thank the Army Research Office (W911NF-18-1-0412) and NASA (80NSSC18K1508) for financial support.

2.7 References

1. Williams, S. R. & Long, T. E. Recent advances in the synthesis and structure–property relationships of ammonium ionenes. *Prog. Polym. Sci.* **34**, 762–782 (2009).

2. Williams, S. R., Long, T. E., Ward, T. C., Turner, S. R. & Roman, M. Influence of Electrostatic Interactions and Hydrogen Bonding on the Thermal and Mechanical Properties of Step-Growth Polymers Influence of Electrostatic Interactions and Hydrogen Bonding on the Thermal and Mechanical Properties of Step-Growth Polymers. *Dissertation* (2008).

3. Bara, J. E. & O'Harra, K. E. Recent Advances in the Design of Ionenes: Toward Convergence with High-Performance Polymers. *Macromol. Chem. Phys.* **220**, 1900078 (2019).

4. Gibbs, C. F., Littmann, E. R. & Marvel, C. S. Quaternary Ammonium Salts from Halogenated Alkyl Dimethylamines. II. The Polymerization of Gamma-Halogenopropyldimethylamines. *J. Am. Chem. Soc.* **55**, 753–757 (1933).

5. Rembaum, A., Baumgartner, W. & Eisenberg, A. Aliphatic ionenes. *J. Polym. Sci. Part B Polym. Lett.* **6**, 159–171 (1968).

6. Daly, W. H. & Hölle, H. J. Polyarylsulfonimides. *J. Polym. Sci. Part B Polym. Lett.* **10**, 519–525 (1972).

7. Shi, Q. *et al.* Improvement in LiFePO4–Li battery performance via poly(perfluoroalkylsulfonyl)imide (PFSI) based ionene composite binder. *J. Mater. Chem. A* **1**, 15016 (2013).

8. Williams, S. R., Salas-de la Cruz, D., Winey, K. I. & Long, T. E. Ionene segmented block copolymers containing imidazolium cations: Structure–property relationships as a function of hard segment content. *Polymer (Guildf).* **51**, 1252–1257 (2010).

9. Das, S. *et al.* Structure–property relationships and melt rheology of segmented, non-chain extended polyureas: Effect of soft segment molecular weight. *Polymer (Guildf).* **48**, 290–301 (2007).

10. Kohjiya, S., Ohtsuki, T. & Yamashita, S. Polyelectrolyte Behavior of an Ionene Containing Poly(oxytetramethylene) Units. *Makromol. Chemie, Rapid Commun.* **2**, 417–420 (1981).

11. Feng, D., Venkateshwaran, L. N., Wilkes, G. L., Leir, C. M. & Stark, J. E. Structure-property behavior of elastomeric segmented PTMO–ionene polymers. II. *J. Appl. Polym. Sci.* **38**, 1549–1565 (1989).

12. Wang, M. Z., Li, D. S., Luo, X. L. & Ma, D. Z. Crystallization and melting behavior of the soft and hard segments in poly(ester-ether)s. II. Ethylene oxide-

butylene terephthalate segmented copolymers. *J. Polym. Sci. Part B Polym. Phys.* **37**, 2928–2940 (1999).

13. Das, S. *et al.* Synthesis and Characterization of Novel Segmented Polyionenes Based on Polydimethylsiloxane Soft Segments. *J. Macromol. Sci. Part A* **47**, 215–224 (2010).

14. Rutkowska, M. Polyester polyurethane ionomers. *J. Appl. Polym. Sci.* **31**, 1469–1482 (1986).

15. Rembaum, A. & Noguchi, H. Reactions of N,N,N',N'-Tetramethyl-α,ι-diaminoalkanes with α,ι-Dihaloalkanes. II. x-y Reactions. *Macromolecules* **5**, 261–269 (1972).

16. Zelikin, A. N., Akritskaya, N. I. & Izumrudov, V. A. Modified Aliphatic Ionenes. Influence of Charge Density and Length of the Chains on Complex Formation with Poly(methacrylic acid). *Macromol. Chem. Phys.* **202**, 3018–3026 (2001).

17. Tamami, M., Williams, S. R., Park, J. K., Moore, R. B. & Long, T. E. Poly(propylene glycol)-based ammonium ionenes as segmented ion-containing block copolymers. *J. Polym. Sci. Part A Polym. Chem.* **48**, 4159–4167 (2010).

18. Bachl, J., Bertran, O., Mayr, J., Alemán, C. & Díaz Díaz, D. Aromatic ionene topology and counterion-tuned gelation of acidic aqueous solutions. *Soft Matter* **13**, 3031–3041 (2017).

19. Suzuki, K., Yamaguchi, M., Hotta, S., Tanabe, N. & Yanagida, S. A new alkyl-imidazole polymer prepared as an inonic polymer electrolyte by in situ polymerization of dye sensitized solar cells. *J. Photochem. Photobiol. A Chem.* **164**, 81–85 (2004).

20. Hemp, S. T. *et al.* Comparing Ammonium and Phosphonium Polymerized Ionic Liquids: Thermal Analysis, Conductivity, and Morphology. *Macromol. Chem. Phys.* **214**, 2099–2107 (2013).

21. Feng, D., Wilkes, G. L., Lee, B. & McGrath, J. E. Structure-property behaviour of segmented poly (tetramethylene oxide)-based bipyridinium ionene elastomers. *Polymer (Guildf).* **33**, 526–535 (1992).

22. Thankamony, R. L. *et al.* Preparation and characterization of imidazolium-PEO-based Ionene/PVDF(HFP)/LiTFSI as a novel Gel polymer electrolyte. *Macromol. Res.* **23**, 38–44 (2015).

23. Matsumi, N., Sugai, K., Miyake, M. & Ohno, H. Polymerized Ionic Liquids via Hydroboration Polymerization as Single Ion Conductive Polymer Electrolytes. *Macromolecules* **39**, 6924–6927 (2006).

24. Druchok, M., Vlachy, V. & Dill, K. A. Explicit-water molecular dynamics study of a short-chain 3,3 ionene in solutions with sodium halides. *J. Chem. Phys.* **130**, 134903 (2009).

25. Rodič, P., Bratuša, M., Lukšič, M., Vlachy, V. & Hribar-Lee, B. Influence of the hydrophobic groups and the nature of counterions on ion-binding in aliphatic ionene solutions. *Colloids Surfaces A Physicochem. Eng. Asp.* **424**, 18–25 (2013).

26. Lukšič, M., Hribar-Lee, B., Buchner, R. & Vlachy, V. Modelling fast mode dielectric relaxation of counterions in aqueous solutions of ionene bromides and fluorides. *Phys. Chem. Chem. Phys.* **11**, 10053 (2009).

27. Lukšič, M., Buchner, R., Hribar-Lee, B. & Vlachy, V. Dielectric Relaxation Spectroscopy of Aliphatic Ionene Bromides and Fluorides in Water: The Role of the Polyion's Charge Density and the Nature of the Counterions. *Macromolecules* **42**, 4337–4342 (2009).

28. Tamami, M., Salas-de la Cruz, D., Winey, K. I. & Long, T. E. Structure-Property Relationships of Water-Soluble Ammonium-Ionene Copolymers. *Macromol. Chem. Phys.* **213**, 965–972 (2012).

29. Meyer, W. H., Rietz, R. R., Schaefer, D. & Kremer, F. Dielectric and electric relaxation in ionene-glasses. *Electrochim. Acta* **37**, 1491–1494 (1992).

30. Haskins, N. J. & Mitchell, R. Thermal degradation of some benzyltrialkylammonium salts using pyrolysis–gas chromatography–mass spectrometry. *Analyst* **116**, 901–903 (1991).

31. Charlier, P., Jérome, R., Teyssié, P. & Proud'Homme, R. E. Thermal stability of modified telechelic polystyrenes. *J. Polym. Sci. Part A Polym. Chem.* **31**, 129–134 (1993).

32. Tsutsui, T., Tanaka, R. & Tanaka, T. Mechanical relaxations in some ionene polymers. I. Effect of Ion concentration. *J. Polym. Sci. Polym. Phys. Ed.* **14**, 2259–2271 (1976).

33. Kammakakam, I., O'Harra, K. E., Dennis, G. P., Jackson, E. M. & Bara, J. E. Self-healing imidazolium-based ionene-polyamide membranes: an experimental study on physical and gas transport properties. *Polym. Int.* **68**, 1123–1129 (2019).

34. Mittenthal, M. S. *et al.* Ionic Polyimides: Hybrid Polymer Architectures and Composites with Ionic Liquids for Advanced Gas Separation Membranes. *Ind. Eng. Chem. Res.* **56**, 5055–5069 (2017).

35. Kammakakam, I. *et al.* An imidazolium-based ionene blended with crosslinked PEO as a novel polymer membrane for selective CO2 separation. *Macromol. Res.* **22**, 907–916 (2014).

36. Li, P. & Coleman, M. R. Synthesis of room temperature ionic liquids based random copolyimides for gas separation applications. *Eur. Polym. J.* **49**, 482–491 (2013).

37. Li, P., Zhao, Q., Anderson, J. L., Varanasi, S. & Coleman, M. R. Synthesis of copolyimides based on room temperature ionic liquid diamines. *J. Polym. Sci. Part*

A Polym. Chem. **48**, 4036–4046 (2010).

38. O'Harra, K. *et al.* Synthesis and Performance of 6FDA-Based Polyimide-Ionenes and Composites with Ionic Liquids as Gas Separation Membranes. *Membranes (Basel).* **9**, 79 (2019).

39. Hemp, S. T., Zhang, M., Tamami, M. & Long, T. E. Phosphonium ionenes from well-defined step-growth polymerization: thermal and melt rheological properties. *Polym. Chem.* **4**, 3582–3590 (2013).

40. Bradaric, C. J., Downard, A., Kennedy, C., Robertson, A. J. & Zhou, Y. Industrial preparation of phosphonium ionic liquids. *Green Chem.* **5**, 143–152 (2003).

41. Yang, X. & Smith, R. C. Phosphonium-based polyelectrolyte networks with high thermal stability, high alkaline stability, and high surface areas. *J. Polym. Sci. Part A Polym. Chem.* **57**, 598–604 (2019).

42. Williams, S. R., Barta, Z., Ramirez, S. M. & Long, T. E. Synthesis of 12,12-Ammonium Ionenes with Functionality for Chain Extension and Cross-Linking via UV Irradiation. *Macromol. Chem. Phys.* **210**, 555–564 (2009).

43. Jeon, Y. M. & Gong, M. S. Preparation of water-resistant humidity sensor using photocurable reactive oligomers containing lonene unit and their properties. *Polym.* **33**, 19–25 (2009).

44. Gong, M.-S. Anchoring of self-curable ionene-containing polyesters to electrode surface by UV irradiation and their humidity-sensitive properties. *Sensors Actuators B Chem.* **148**, 559–568 (2010).

45. Zelikin, A. N., Litmanovich, A. A., Paraschuk, V. V., Sybatchin, A. V. & Izumrudov, V. A. Conformational Changes of Aliphatic Ionenes in Water-Salt Solutions as a Factor Controlling Stability of Their Complexes with Calf Thymus DNA. *Macromolecules* **36**, 2066–2071 (2003).

46. Narita, T., Ohtakeyama, R., Nishino, M., Gong, J. P. & Osada, Y. Effects of charge density and hydrophobicity of ionene polymer on cell binding and viability. *Colloid Polym. Sci.* **278**, 884–887 (2000).

47. Zelikin, A. N., Putnam, D., Shastri, P., Langer, R. & Izumrudov, V. A. Aliphatic Ionenes as Gene Delivery Agents: Elucidation of Structure−Function Relationship through Modification of Charge Density and Polymer Length. *Bioconjug. Chem.* **13**, 548–553 (2002).

48. Izumrudov, V. A. & Zhiryakova, M. V. Stability of DNA-containing interpolyelectrolyte complexes in water-salt solutions. *Macromol. Chem. Phys.* **200**, 2533–2540 (1999).

49. Izumrudov, V. A., Zhiryakova, M. V & Kudaibergenov, S. E. Controllable stability of DNA-containing polyelectrolyte complexes in water-salt solutions. *Biopolymers* **52**, 94–108 (1999).

50. Zelikin, A. N. & Izumrudov, V. A. Polyelectrolyte Complexes Formed by Calf Thymus DNA and Aliphatic Ionenes: Unexpected Change in Stability upon Variation of Chain Length of Ionenes of Different Charge Density. *Macromol. Biosci.* **2**, 78–81 (2002).

51. Wahlund, P.-O., Izumrudov, V. A., Gustavsson, P.-E., Larsson, P.-O. & Galaev, I. Y. Phase Separations in Water-Salt Solutions of Polyelectrolyte Complexes Formed by RNA and Polycations: Comparison with DNA Complexes. *Macromol. Biosci.* **3**, 404–411 (2003).

52. El-Hamshary, H., El-Newehy, M. H., Moydeen Abdulhameed, M., El-Faham, A. & Elsherbiny, A. S. Evaluation of clay-ionene nanocomposite carriers for controlled drug delivery: Synthesis, in vitro drug release, and kinetics. *Mater. Chem. Phys.* **225**, 122–132 (2019).

53. Tomlinson, E., Brown, M. R. W. & Davis, S. S. Effect of colloidal association on the measured activity of alkylbenzyldimethylammonium chlorides against Pseudomonas aeruginosa. *J. Med. Chem.* **20**, 1277–1282 (1977).

54. Liu, X., Zhang, H., Tian, Z., Sen, A. & Allcock, H. R. Preparation of quaternized organic–inorganic hybrid brush polyphosphazene-co-poly[2-(dimethylamino)ethyl methacrylate] electrospun fibers and their antibacterial properties. *Polym. Chem.* **3**, 2082 (2012).

55. Ding, B.-P., Wu, F., Chen, S.-C., Wang, Y.-Z. & Zeng, J.-B. Synthesis and characterization of a polyurethane ionene/zinc chloride complex with antibacterial properties. *RSC Adv.* **5**, 12423–12433 (2015).

56. Cakmak, I., Ulukanli, Z., Tuzcu, M., Karabuga, S. & Genctav, K. Synthesis and characterization of novel antimicrobial cationic polyelectrolytes. *Eur. Polym. J.* **40**, 2373–2379 (2004).

57. Venkataraman, S. *et al.* Identi fication of Structural Attributes Contributing to the Potency and Selectivity of Antimicrobial Polyionenes: Amides Are Better Than Esters. *Biomacromolecules* **20**, 2737–2742 (2019).

58. Geng, Z. & Finn, M. G. Thiabicyclononane-Based Antimicrobial Polycations. *J. Am. Chem. Soc.* **139**, 15401–15406 (2017).

59. Strassburg, A. *et al.* Cross-Linking of a Hydrophilic, Antimicrobial Polycation toward a Fast-Swelling, Antimicrobial Superabsorber and Interpenetrating Hydrogel Networks with Long Lasting Antimicrobial Properties. *ACS Appl. Mater. Interfaces* **9**, 36573–36582 (2017).

60. Lakouraj, M. M., Soleimani, M. & Hasantabar, V. Synthesis and physical properties of interpenetrating network of poly (Acrylamide-Co-2, 4-Ionene) hydrogels. *World Appl. Sci. J.* **21**, 250–259 (2013).

61. Liu, S. *et al.* Biomaterials Highly potent antimicrobial polyionenes with rapid

killing kinetics , skin biocompatibility and in vivo bactericidal activity. *Biomaterials* **127**, 36–48 (2017).

62. Berginc, M., Opara Krašovec, U., Jankovec, M. & Topič, M. The effect of temperature on the performance of dye-sensitized solar cells based on a propyl-methyl-imidazolium iodide electrolyte. *Sol. Energy Mater. Sol. Cells* **91**, 821–828 (2007).

63. Abate, A. *et al.* A polyfluoroalkyl imidazolium ionic liquid as iodide ion source in dye sensitized solar cells. *Org. Electron.* **13**, 2474–2478 (2012).

64. Fei, Z. *et al.* A Supercooled Imidazolium Iodide Ionic Liquid as a Low-Viscosity Electrolyte for Dye-Sensitized Solar Cells. *Inorg. Chem.* **45**, 10407–10409 (2006).

65. Li, F. *et al.* Novel quasi-solid electrolyte for dye-sensitized solar cells. *J. Power Sources* **165**, 911–915 (2007).

66. Ng, H. M., Ramesh, S. & Ramesh, K. Efficiency improvement by incorporating 1-methyl-3-propylimidazolium iodide ionic liquid in gel polymer electrolytes for dye-sensitized solar cells. *Electrochim. Acta* **175**, 169–175 (2015).

67. Shi, Q. *et al.* Single ion solid-state composite electrolytes with high electrochemical stability based on a poly(perfluoroalkylsulfonyl)-imide ionene polymer. *J. Mater. Chem. A* **2**, 15952–15957 (2014).

68. Terenteva, E. A., Arkhipova, V. V., Apyari, V. V., Volkov, P. A. & Dmitrienko, S. G. Simple and rapid method for screening of pyrophosphate using 6,6-ionene-stabilized gold and silver nanoparticles. *Sensors Actuators B Chem.* **241**, 390–397 (2017).

69. Terenteva, E. A., Apyari, V. V., Dmitrienko, S. G. & Zolotov, Y. A. Spectrophotometric determination of sulfates using silver nanoparticles stabilized with 6,6-ionene. *Moscow Univ. Chem. Bull.* **70**, 157–161 (2015).

70. Apyari, V. V., Ioutsi, A. N., Arkhipova, V. V., Dmitrienko, S. G. & Shapovalova, E. N. 6,6-ionene-stabilized gold nanoparticles: synthesis, characterization and prospects of use. *Adv. Nat. Sci. Nanosci. Nanotechnol.* **6**, 025002 (2015).

71. Arkhipova, V. V., Apyari, V. V. & Dmitrienko, S. G. A colorimetric probe based on desensitized ionene-stabilized gold nanoparticles for single-step test for sulfate ions. *Spectrochim. Acta Part A Mol. Biomol. Spectrosc.* **139**, 335–341 (2015).

72. Teli, M. D. & Nadathur, G. T. Adsorptive removal of acid yellow 17 (an anionic dye) from water by novel ionene chloride modified electrospun silica nanofibres. *J. Environ. Chem. Eng.* **6**, 7257–7272 (2018).

73. Dragan, E. S., Mayr, J., Häring, M., Cocarta, A. I. & Díaz, D. D. Spectroscopic Characterization of Azo Dyes Aggregation Induced by DABCO-Based Ionene Polymers and Dye Removal Efficiency as a Function of Ionene Structure. *ACS Appl. Mater. Interfaces* **8**, 30908–30919 (2016).

74. Pirogov, A. V., Krokhin, O. V., Platonov, M. M., Deryugina, Y. I. & Shpigun, O. A. Ion-chromatographic selectivity of polyelectrolyte sorbents based on some aliphatic and aromatic ionenes. *J. Chromatogr. A* **884**, 31–39 (2000).

75. Mansur, C. R. E. *et al.* Nanocomposites based on ionene-bentonite used to treat oily water. *J. Appl. Polym. Sci.* **123**, 218–226 (2012).

76. Saborío, M. G. *et al.* Cationic ionene as an n-dopant agent of poly(3,4-ethylenedioxythiophene). *Phys. Chem. Chem. Phys.* **20**, 9855–9864 (2018).

77. Sandoval, A. P., Feliu, J. M., Torresi, R. M. & Suárez-Herrera, M. F. Electrochemical properties of poly(3,4-ethylenedioxythiophene) grown on Pt(111) in imidazolium ionic liquids. *RSC Adv.* **4**, 3383–3391 (2014).

78. Kundu, S. K., Matsunaga, T., Yoshida, M. & Shibayama, M. Rheological Study on Rapid Recovery of Hydrogel Based on Oligomeric Electrolyte. *J. Phys. Chem. B* **112**, 11537–11541 (2008).

79. Le Bideau, J., Ducros, J.-B., Soudan, P. & Guyomard, D. Solid-State Electrode Materials with Ionic-Liquid Properties for Energy Storage: the Lithium Solid-State Ionic-Liquid Concept. *Adv. Funct. Mater.* **21**, 4073–4078 (2011).

80. Chen, B. *et al.* Highly Stretchable and Transparent Ionogels as Nonvolatile Conductors for Dielectric Elastomer Transducers. *ACS Appl. Mater. Interfaces* **6**, 7840–7845 (2014).

81. Yoshida, M. Ionic gelators: oligomeric and polymeric electrolytes as novel gel forming materials. *Chem. Rec.* **10**, 230–242 (2010).

82. Yoshida, M. *et al.* Oligomeric Electrolyte as a Multifunctional Gelator. *J. Am. Chem. Soc.* **129**, 11039–11041 (2007).

83. Kundu, S. K., Yoshida, M. & Shibayama, M. Effect of Salt Content on the Rheological Properties of Hydrogel Based on Oligomeric Electrolyte. *J. Phys. Chem. B* **114**, 1541–1547 (2010).

84. Koumura, N., Matsumoto, H., Kawanami, H., Tamaoki, N. & Yoshida, M. Tuning of solubility and gelation ability of oligomeric electrolyte by anion exchange. *Polym. J.* **42**, 759–765 (2010).

85. Misawa, Y., Koumura, N., Matsumoto, H., Tamaoki, N. & Yoshida, M. Hydrogels Based on Surfactant-Free Ionene Polymers with N,N′ -(p -Phenylene)dibenzamide Linkages. *Macromolecules* **41**, 8841–8846 (2008).

86. Bachl, J. *et al.* Synergistic Computational-Experimental Approach to Improve Ionene Polymer-Based Functional Hydrogels. *Adv. Funct. Mater.* **24**, 4893–4904 (2014).

87. Häring, M., Grijalvo, S., Haldar, D., Saldías, C. & Díaz, D. D. Polymer topology-controlled self-healing properties of polyelectrolyte hydrogels based on DABCO-

containing aromatic ionenes. *Eur. Polym. J.* **115**, 221–224 (2019).

88. Watanabe, M., Toneaki, N. & Shinohara, I. Preparation of Elastomeric Ionene Polymers Containing 4,4′-Bipyridinium or 1,2-Bis(4-pyridinium)ethylene Ring and the Conductivity of Their TCNQ Salts. *Polym. J.* **14**, 189–195 (1982).

89. Grassl, B. & Galin, J. C. Segmented Poly(tetramethylene oxide) Zwitterionomers and Their Homologous Ionenes. 1. Synthesis, Molecular Characterization, and Thermal Stability. *Macromolecules* **28**, 7035–7045 (1995).

90. Somoano, R., Yen, S. P. S. & Rembaum, A. VI. Electronic conductivity of elastomeric ionenes. *J. Polym. Sci. Part B Polym. Lett.* **8**, 467–479 (1970).

91. Hashimoto, T. *et al.* Structure and properties of poly(tetrahydrofuran) viologen ionene: effects of halide counter-anions. *Polymer (Guildf).* **35**, 2672–2678 (1994).

92. Ikeda, Y., Yamato, J., Murakami, T. & Kajiwara, K. Aliphatic poly(oxytetramethylene) ionenes: effect of counter-anion on the properties and morphology. *Polymer (Guildf).* **45**, 8367–8375 (2004).

93. Ikeda, Y. *et al.* One-pot synthesis and characterization of aliphatic poly(oxytetramethylene) ionene. *Polymer (Guildf).* **43**, 3483–3488 (2002).

94. Feng, D., Wilkes, G. L., Leir, C. M. & Stark, J. E. Morphological Investigation of Polytetba-Methyleneoxide-Dibbomoxylene Segmented Ionene Polymebs by Tbansmission Electbon Micboscopy and Small-Angle X-Ray Scattebing. *J. Macromol. Sci. Part A - Chem.* **26**, 1151–1181 (1989).

95. Feng, D. & Wilkes, G. L. Chain extension in unoriented ion-containing polymers - does it occur? *Macromolecules* **24**, 6788–6790 (1991).

96. Ikeda, Y., Murakami, T., Yuguchi, Y. & Kajiwara, K. Synthesis and Characterization of Poly(oxytetramethylene) Ionene with 2,2‘-Bipyridinium Units. *Macromolecules* **31**, 1246–1253 (1998).

97. Vijayaraghavan, P., Brown, J. R. & Hall, L. M. Modeling the Effect of Polymer Composition on Ionic Aggregation in Poly(propylene glycol)-Based Ionenes. *Macromol. Chem. Phys.* **217**, 930–939 (2016).

98. Kamiya, T., Goto, K. & Shinohara, I. Electric conductivity of TCNQ salts of ionene polymers containing triethylenediammonium or 4,4′-bipyridilium ring. *J. Polym. Sci. Polym. Chem. Ed.* **17**, 561–569 (1979).

99. Kamiya, T., Tsuji, S., Ogatsu, K. & Shinohara, I. Effect of Polycations Containing Aromatic Heterocyclic Compounds on the Conductivity of Their TCNQ Salts. *Polym. J.* **11**, 219–226 (1979).

100. Hochberg, G. C. Electrically conductive TCNQ complexes of aromatic ionenes. *Polym. Int.* **38**, 119–124 (1995).

101. Ciesielski, W., Pęcherz, J. & Kryszewski, M. Electric properties of TCNQ complex salts of ionenes containing aromatic rings in the main chain. *Acta Polym.* **33**, 318–321 (1982).

102. Takizawa, Y., Aiga, H., Watanabe, M. & Shinohara, I. Thermoswitching property in TCNQ salts of ionenes containing poly(ethylene oxide) segments. *J. Polym. Sci. Polym. Chem. Ed.* **21**, 3145–3153 (1983).

103. Burmistr, M. V. *et al.* Structure, thermal properties and ionic conductivity of polymeric quaternary ammonium salts (polyionenes) containing ethylene oxide and aliphatic chain fragments. *Solid State Ionics* **176**, 1787–1792 (2005).

104. Dimitrov, I. V. & Berlinova, I. V. Synthesis of Poly(ethylene oxide)s Bearing Functional Groups along the Chain. *Macromol. Rapid Commun.* **24**, 551–555 (2003).

105. Tamami, M. *et al.* Poly(ethylene glycol)-based ammonium ionenes containing nucleobases. *Polymer (Guildf).* **54**, 1588–1595 (2013).

106. Wu, F., Huang, C. L., Zeng, J. B., Li, S. L. & Wang, Y. Z. Synthesis and characterization of segmented poly(butylene succinate) urethane ionenes containing secondary amine cation. *Polymer (Guildf).* **55**, 4358–4368 (2014).

107. Nakayama, Y. *et al.* Synthesis and Properties of Poly(ε-carprolactone)-based Poly(ester-urethane)s Having Quaternary Ammonium Groups. *J. Japan Inst. Energy* **93**, 916–920 (2014).

108. Schreiner, C., Bridge, A. T., Hunley, M. T., Long, T. E. & Green, M. D. Segmented imidazolium ionenes: Solution rheology, thermomechanical properties, and electrospinning. *Polymer (Guildf).* **114**, 257–265 (2017).

109. Kohjiya, S., Hashimoto, T. & Yamashita, S. Hydrophilic elastomer containing poly(tetrahydrofuran) segments and viologen units. *J. Appl. Polym. Sci.* **44**, 555–559 (1992).

110. Hashimoto, T., Kohjiya, S., Yamashita, S. & Irie, M. Photochromic and photomechanical ionene elastomer containing poly(tetrahydrofuran) segments and viologen units. *J. Polym. Sci. Part A Polym. Chem.* **29**, 651–655 (1991).

111. Loveday, D., Wilkes, G. L., Bheda, M. C., Shen, Y. X. & Gibson, H. W. Structure-Property Relationships in Segmented Polyviologen Ionene Rotaxanes. *J. Macromol. Sci. Part A* **32**, 1–27 (1995).

CHAPTER 3

SYNTHESIS AND CHARACTERIZATION OF POLY(ETHYLENE GLYCOL)-BASED SEGMENTED IONENES BLOCK COPOLYMER WITH ALIPHATIC OR DABCO HARD SEGMENTS

Reproduced with permission from: Lee, J.; Taghavimehr, M.; Montazami, R.; Green, M. D. *Polymer*, 242, 124543, 2022. Copyright 2023. Elsevier

3.1 Abstract

A series of poly(ethylene glycol) (PEG)-based segmented block copolymers were synthesized with two structurally different hard segments, linear and heterocyclic aliphatic amines. Ionenes were synthesized via a modified Menshutkin reaction with three different weight fractions of hard domains (amine rich segment) and soft domains (PEG oligomers). TGA results show that both aliphatic and DABCO-based ionenes were thermally stable up to 250 °C. DSC and XRD data indicate that increasing the weight fraction of the soft segment from 25 wt% to 50 wt% triggered better chain packing of the PEG soft segment for both hard segments. Also, the DABCO-based ionenes displayed the highest PEG crystallite purity at 50 wt% of soft segment. The segmented ionenes exhibited high strain elongation percentages at elevated temperatures (i.e., above the PEG melting temperature). The mechanical properties of ionenes changed by varying the nature and the weight fractions of soft and hard domains. DMA analysis concluded that DABCO-based ionenes possess superior elastomeric behavior by having a wider rubbery plateau and higher

rubbery plateau storage modulus compared to aliphatic analogs at all weight fractions potentially due to better microphase separation and ionic aggregation. DMA and AFM confirmed that the 25 wt% soft segment ionenes had a relatively higher degree of microphase separation among the other weight fractions.

3.2 Introduction

Ionenes are ion-containing polymers that have charges in the polymer backbone, whereas traditional ionomers have charges on the pendant site of the polymer backbone. The ammonium ionenes were synthesized for the first time in 1933 via a step-growth polymerization.[1] Ionenes have been developed into elastomers, hydrogels, nanofibers, or have been incorporated into crosslinked networks and thermosets for diverse applications over the last 90 years.[2] The advantage of ionenes over ionomers is presenting an equal distribution of ionic groups within a polymer backbone, which provides unique strategies to design and understand the behavior of the polymer.[2] Ionenes can be described either as cationic or anionic ionenes by possessing positive or negative charges in their backbone, respectively; cationic ionenes have been widely studied while anionic ionenes are less prevalent in the literature due to the challenging synthesis protocols involved.[3]

Ionenes can be further divided into two categories: segmented and non-segmented ionenes. Segmented ionenes have alternating hard and soft segments along the backbone and typically the chain comprising the soft domain is oligomeric or would have a significantly higher molecular weight than the polymer segment making up the hard domain. This configuration produces polymers with exceptional mechanical and thermal properties as well as microphase separated morphologies (typically disordered

bicontinuous networks, but the lamellar-type morphology has also been observed).[4] Segmented ionenes behave like an elastomer by having a low glass transition temperature (T_g) rubbery soft segments and physically crosslinked (i.e., the presence of ionic aggregates) hard segments, similar to synthetic rubbers and elastomeric polyurethanes (PU).[5] However, segmented ionenes have garnered attention relative to PU for their facile, less toxic, and environmentally friendly synthesis process, which embodies principles of green chemistry.[6]

Non-segmented ionenes have been used in various applications[7–11]; however, the high charge density of non-segmented ionenes compared to segmented ionenes limited their use in applications such as wearable and flexible electronic devices. In fact, the presence of spacers between the charged segments provides a variety of mechanical properties for segmented ionene. However, there are limited analyses of the properties of segmented ionenes on the influence of type, structure, and content of soft/hard segments, which are needed to tune the mechanical properties for a diverse set of applications.

Segmented ionenes synthesized via the Menshutkin reaction using halide and tertiary compounds have gained attention as an attractive material due to the facile one-pot reaction, and thus offer endless possibilities for designing materials. Several oligomeric monomers for the soft segments, including poly(tetramethylene oxide) (PTMO)[12], poly(ethylene glycol) (PEG)[13], and poly(propylene glycol) (PPG)[14], have been synthesized into various segmented ionenes. The properties such as elasticity, crystallinity, and microphase separation highly rely on the chemistry and molecular weight of the soft segment,

counterion type, chemistry of the hard segment, and the ratio between the soft and hard segments.

PEG has been used as the soft segment in segmented ionene copolymers due to its high availability, biocompatibility, and low cytotoxicity.[15] Ding et al. synthesized PEG-based segmented ionenes, and studied the dependance of antibacterial properties of the segmented ionene on the counterion type. It was demonstrated that the antibacterial capability of the PEG-based segmented ionenes increased gradually with the increase in the concentration of a zinc chloride counterion.[16] PEG can better crystallize compared to other soft segments commonly used (e.g., PTMO or PPG), which gives some unique properties and thus widens the potential application of ionenes. The incorporation of the PEG soft segments can control the electrochemical behavior of ionenes.[17] At temperatures below the melting temperature ($T<T_m$) the presence of spherulites promoted long-term electrochemical stability by obstructing the conduction paths. However, at $T>T_m$ ionic conductivity was promoted due to the enhanced chain mobility.

1,4-diazabicyclo[2.2.2]octane (DABCO) was first introduced into ionene synthesis by Salamone and Snider in 1970.[18] DABCO-containing polymers have shown excellent antimicrobial activities and DABCO-imidazolium copolymers exhibited enhanced biocompatibility.[19] Zhang et al. synthesized DABCO-containing ionomers, which displayed better phase separation and stronger ionic interactions when compared to singly charged ammonium cation.[20] Several DABCO-based non-segmented ionenes have been reported. Misawa et al. introduced DABCO-based polyamide non-segmented ionenes to form a hydrogel resulting from the physical crosslinking due to the hydrogen bonding

between polyamide ionenes.[21] Díaz and coworkers synthesized non-segmented ionenes using different structural isomers of phenylenediamine-based dihalides with DABCO to form hydrogels that have both hydrogen bonding between amide bonds and electrostatic interactions.[22–24] However, there are few studies using DABCO in segmented ionenes that characterize the elastomeric properties. The Long group prepared segmented ionenes using DABCO as the hard segment and varied the molecular weight of PDMS as the soft segment to study the effect of oligomer segment length (at two molecular weight of 2000 and 3000 g/mol) on ionene properties.[25] It was revealed that the mechanical properties are dependent on both the presence of the chain extender and the content of DABCO hard segments. However, there is still a gap in the literature identifying the influence that the various content and type of soft and hard segments have on the mechanical and thermomechanical properties of segmented ionenes through a direct comparison.

The viscoelastic behavior of the segmented ionenes can be controlled by changing the ion density, and soft segment composition and molecular weight. The regular ion placement along the backbone results in patterned microphase segregation between soft and hard domains that control the polymer microstructure. Increasing the molecular weight of PDMS soft segments in DABCO-based PDMS ionenes led to shortening the breadth and lowering the modulus of the rubbery plateau owing to the relatively reduced contents of hard segments and a weakening of the ionic association of the hard domains.[25] Williams et al. revealed that increasing hard segment content up to 38 wt% in imidazolium-based ionenes increased the toughness of the polymer, but the sample was too brittle with 100 wt% of hard segment.[4] While decreasing the hard segment content from 38 wt% to 20 wt%

doubled the value of the storage modulus of the glassy region due to higher crystallinity of soft segment. Moreover, the counterion selection shows a profound impact on the viscoelastic behavior as well as thermal properties of ionenes by having different size and basicity. Abdulahad et al. revealed that exchanging Br^- counterion to BF_4^- or Tf_2N^- counterions reduced the T_g significantly and increased the thermal stability of ionenes due to the increased size of the counterions and reduced anion basicity.[26]

Using different composition of segments in block copolymers incurs phase separation, and thus affects the viscoelastic properties of the copolymer. Generally, a higher molecular weight soft segment provides more significant phase separation, where 4,000 g/mol PPG showed more significant microphase separation as compared to 1,000 g/mol PPG.[27] The utilization of heterocyclic or linear aliphatic ammonium diamines as the hard segment is expected to alter the mechanical properties resulting from the ionic interaction's strength due to the nature of ionic domains.

In this study, we synthesized PEG-based segmented ionenes with two structurally different, linear or heterocyclic aliphatic diamine, hard segments via Menshutkin reaction. Both linear aliphatic and DABCO-based ionenes were synthesized with three different weight fractions, 25, 50, and 75 wt% of soft segment and counterparts of hard segments. Their thermal and mechanical properties as well as elastomeric behavior were analyzed through differential scanning calorimetry (DSC), x-ray diffraction (XRD), thermogravimetric analysis (TGA), dynamic mechanical analysis (DMA), and tensile analysis, while the morphologies were probed using atomic force microscopy (AFM).

3.3 Experimental

3.3.1 Materials

Poly(ethylene glycol) (PEG) 2,000, chloroform-d, and dimethyl sulfoxide-d were supplied from Alfa Aesar. *N,N,N',N'*-tetramethyl-1,6-hexanediamine (99%), triethylamine (≥99.5%), 6-bromohexanoyl chloride (97%), 1,4-diazabicyclo[2.2.2]octane (DABCO) (≥99%), and dimethyl sulfoxide (≥99.9%) were supplied from Sigma Aldrich. Dichloromethane (DCM) and methanol (MeOH) were supplied from VWR Chemicals. 1,12-dibromodedecane (>98%) was obtained from TCI America. All materials were used as received except 1,12-dibromododecane, which was recrystallized in isopropyl alcohol.

3.3.2 Synthesis of Bromine End-capped PEG2000

PEG2k (7g, 1eq) was dissolved in DCM (50 ml), and triethylamine (0.7893 g, 2.2 eq) was added in a round bottom flask. 6-bromohexanoyl chloride (1.6653 g, 2.2 eq) was added drop-wise at 0 °C and slowly heated to room temperature, and stirred for 1 day. Then the salt was filtered, and the organic phase was washed with the saturated sodium bicarbonate solution. The organic phase solution was dried under vacuum at 40 °C for 1 day, and yellowish product was obtained.

3.3.3 Synthesis of Aliphatic PEGXX/DD-ionenes

Three types of ionenes having different wt% of PEG soft segment, 25, 50, and 75 wt%, were synthesized with PEG2k dibromide, 1,12-dibromododecane, and *N,N,N',N'*-tetramethyl-1,6-hexanediamine. The concentration of all series of ionenes was 2 mol/L, and the molar ratio of PEG2k dibromide, a soft segment, to the sum of 1,12-dibromododecane and *N,N,N',N'*-tetramethyl-1,6-hexanediamine, which are hard

segments, was equal to 1. For example, the aliphatic PEG75/DD-ionenes, which has 75 wt% of PEG soft segment, PEG2k dibromide (1.5 g), 1,12-dibromododecane (0.256 g), and *N,N,N',N'*-tetramethyl-1,6-hexanediamine (0.244 g) were added with MeOH and stirred at 75 °C for 3 days with the condenser connected. The synthesized ionenes polymers were dried at 60 °C in the oven for 3 days followed by drying under vacuum at room temperature for 1 day.

3.3.4 Synthesis of DABCO-based PEGXX/DD-ionenes

The calculation of adding the amount of three components, PEG2k dibromide, 1,12-dibromododecane, and DABCO, was identical with the aliphatic PEG/DD-ionenes synthesis. For example, DABCO-based PEG50/DD-ionenes, which has 50 wt% of PEG soft segment, PEG2k dibromide (1 g), 1,12-dibromododecane (0.7097 g), and DABCO (0.2904 g) were added in DMSO (2 mol/L) and stirred at 75 °C for 3 days. The synthesized ionenes polymers were dried at room temperature for 1 day to prevent the defect of film and dried at 60 °C in the oven for 3 days followed by drying under vacuum at room temperature for one day.

3.3.5 Characterizations

^{1}H NMR spectroscopic analyses were performed on Bruker Avance III 500 MHz NMR using DMSO-d and chloroform-d for DABCO-based ionenes and aliphatic ionenes, respectively. Differential scanning calorimetry (DSC) was performed on TA instrument Q2000. Purge gas was ultra high purity (UHP) nitrogen with gas flow of 25 mL/min. The sample was heated from 40 °C to 160 °C, cooled down to -80 °C, and then heated up to

160 °C. The heating and cooling rate were 10 °C/min and isothermal for 10 min at each ramp. Thermogravimetric analysis (TGA) was conducted on TA instrument TGA 5500 in UHP nitrogen atmosphere with a sample purge of 25 mL/min and balance purge of 10 mL/min. The sample was heated (20 °C/min) to 120 °C, isothermal for 10 min, cooled down (20 °C/min) to 40 °C, isothermal for 10 min, and heated up (10 °C/min) again up to 600 °C. X-ray diffraction (XRD) was performed on PANalytical X'Pert PRO MRD with nickel-filtered Cu Kα radiation source (λ = 1.54 Å), divergence slit 1/4º, anti-scatter slits 1/2º, 45 kV/40 mA, and 2θ = 3-60º at room temperature with 1cm × 1cm sample area. A tensile test was performed on Instron E3000 with a 5 mm/min extension rate at room temperature and 60 ºC. The thickness of all dog-bone-shaped samples was ca. 1 mm for tensile analysis. Atomic force microscopy (AFM) was conducted on Bruker MultiMode 8 with 0.6-0.7 setpoint amplitude (moderate force imaging) using an NCHV-A probe for tapping mode at room temperature. Dynamic mechanical analysis (DMA) was conducted on a Mettler Toledo Polymer-1 analyzer in tension mode in a temperature range of -80 to 200 ˚C at a heating rate of 3 ˚C/min, a frequency of 1 Hz, and under 0.1% strain. Because of the hygroscopic nature of PEG segments, all samples were dried thoroughly under vacuum overnight prior to DMA testing to eliminate the effect of moisture on test results.

3.4 Results and Discussion

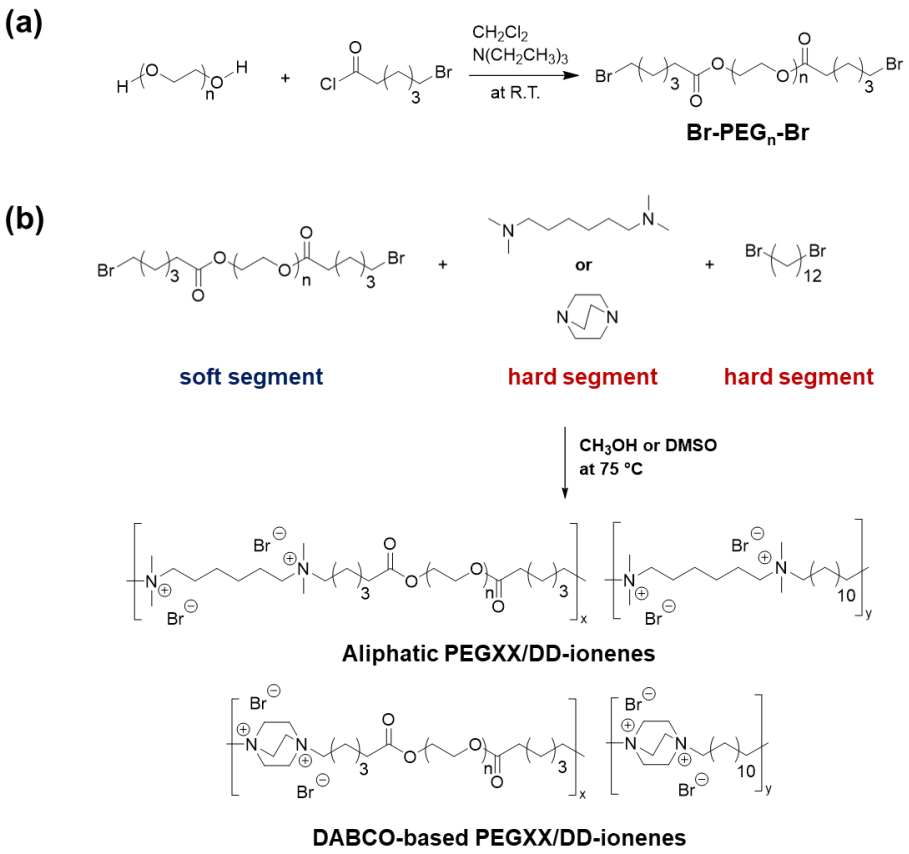

Scheme 3.1: The synthesis of (a) Br-PEG$_n$-Br and (b) aliphatic PEGXX/DD-ionenes or DABCO-based PEGXX/DD-ionenes. XX refers to 25, 50, or 75, which corresponds to the overall weight fraction of the PEG soft segment.

PEG-2k dibromide oligomers (Br-PEG$_n$-Br) suitable for the segmented ionene synthesis were prepared by reacting PEG-2k with a slight excess of 6-bromohexanoyl chloride in the presence of triethylamine to ensure all PEG react and difunctional bromine-capped monomers are obtained (Scheme 3.1a). The presence of the bromoalkyl functional group in PEG oligomers was analyzed by ^{1}H NMR spectroscopy, as shown in Figure 3.1. The presence of *f* and *h* peaks along with an *f* to *a* ratio of 0.93:1 confirmed the successful synthesis of Br-PEG$_n$-Br.

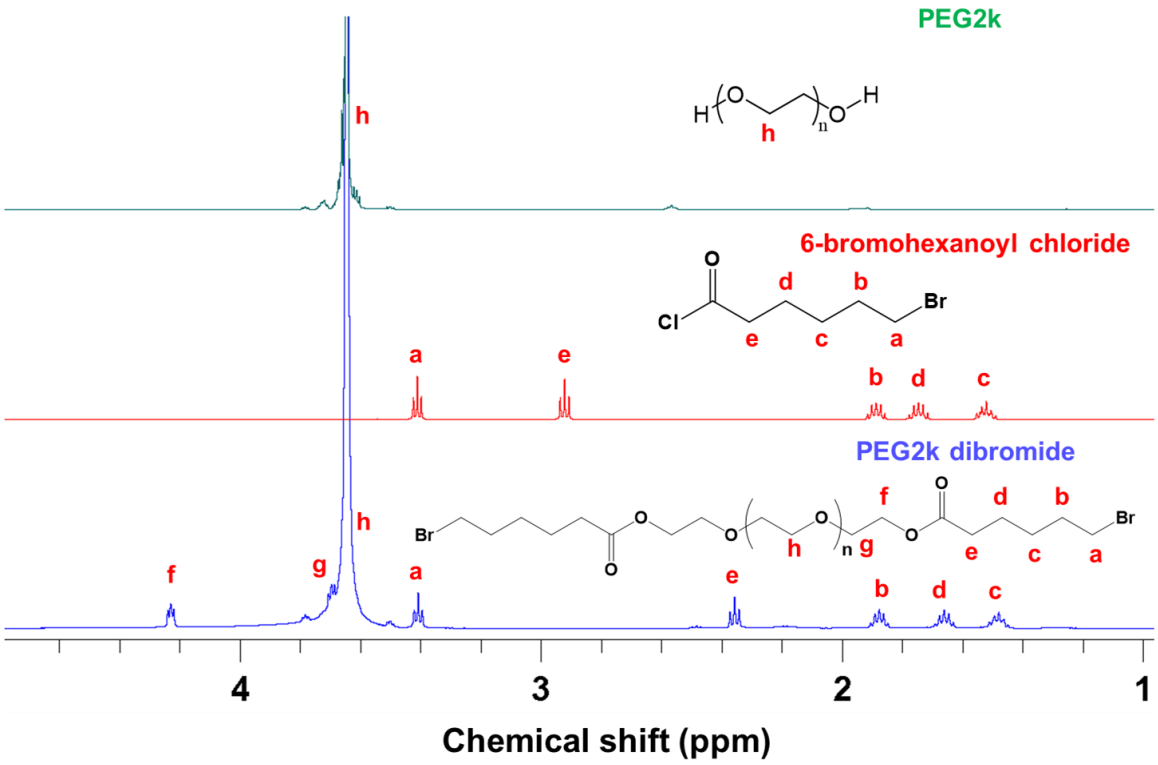

Figure 3.1: ^{1}H NMR spectra of (top) PEG-2k, (middle) 6-bromohexanoyl chloride, and (bottom) Br-PEG$_n$-Br with labeled peaks corresponding to their respective protons.

Segmented ionenes containing PEG-2k copolymerized with *N,N,N',N'*-tetramethyl-1,6-hexanediamine (linear aliphatic hard segment) or DABCO (heterocyclic aliphatic hard segment) and 1,12-dibromododecane were successfully synthesized (Scheme 3.1b) and confirmed by ^{1}H NMR spectroscopy as shown in Figure 3.2 and Figure A1. The molar ratio between the sum of Br-PEG$_n$-Br and 1,12-dibromododecane to *N,N,N',N'*-tetramethyl-1,6-hexanediamine or DABCO was kept at a 1:1 stoichiometry and reacted for 3 days to obtain a high molecular weight ionene polymer. The resonance at 2.2 and 2.6 ppm in the ^{1}H NMR spectrum attributed to methylene protons of *N,N,N',N'*-tetramethyl-1,6-hexanediamine and DABCO, respectively, shifted to 3.5 and 3.9 ppm, respectively, as

the tertiary amine became quaternized. The peaks also broaden after polymerization (an indication of the long relaxation times of the polymers and relatively high molecular weights), confirming the quaternization of the tertiary amines and the synthesis of segmented ionene block copolymers.

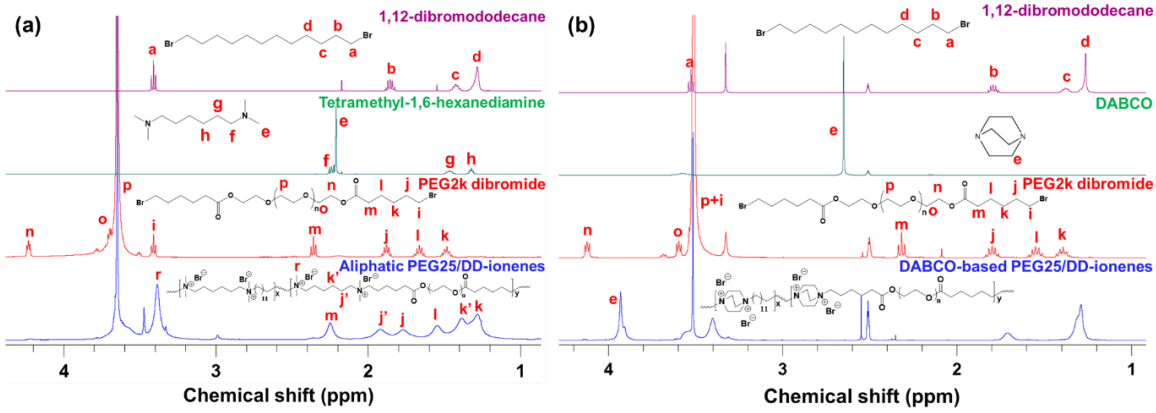

Figure 3.2: ^{1}H NMR spectra of 1,12-dibromododecane, tetramethyl-1,6,-hexanediamine or DABCO, Br-PEG$_n$-Br, and (a) aliphatic PEG25/DD-ionenes and (b) DABCO-based PEG25/DD-ionenes from the top to bottom with labeled peaks corresponding to their respective alkyl hydrogens.

The photographic images (Figure A2) of both aliphatic and DABCO-based PEGXX/DD-ionenes showed that all ionenes polymer formed good elastomeric films. Our previous work revealed that aliphatic PEGXX/DD-ionenes did not make mechanically robust films when the weight fraction of the soft segment exceeded 50 wt% with reaction times of 1 day;[28] however, herein, increasing the reaction time and monomer concentration in the polymerization increased, we assume, the degree of polymerization. Thus, robust polymer films were obtained even with 75 wt% of the PEG soft segment, which qualitatively indicated that high molecular weight segmented ionenes were achieved. By increasing the weight fraction of PEG soft segment in aliphatic ionenes, films became opaque at room temperature; however, the film became transparent when heated above ca.

60 °C. Ding et al. showed that crystallization resulted from the PEG soft segment, although hard segments affect the chain mobility and thus affect the soft segment's ability to crystallize.[16] Also, Saralegi et al. showed that increasing the molecular weight of the soft segment led to an increase in the degree of crystallization of soft segments.[29] In the current work, we demonstrated that increasing the weight fraction of soft segments can have a similar effect as increasing the molecular weight of the soft segment. Two strategies for casting films were tested to control the degree of crystallinity, because the crystallinity affects the quality of the films. First, we pre-dried at room temperature for 1 day before elevating the temperature to 60 °C, and second, we skipped the pre-dry and dried at 60 °C. Generally pre-drying at room temperature prevents film defect formation due to the slow evaporation of solvents compared to drying directly at elevated temperature. Unlike DABCO-based ionenes, aliphatic ionenes, especially with over 50 wt% of PEG soft segments, including aliphatic PEG50/DD-ionenes and PEG75/DD-ionenes, formed robust samples with flat surfaces when dried directly at elevated 60 °C without pre-drying at room temperature for one day. Drying aliphatic PEG50 and 75/DD-ionenes at room temperature after synthesis produced a rough and non-uniform film and did not change to a good film even after drying them at 60 °C. This is due to the low boiling point of MeOH and a high degree of crystallinity of PEG, which hinders the formation of a flat and uniform film at room temperature; however, drying directly at elevated temperature eliminates the effect of PEG crystallites and improve the quality of the films. Dimethyl sulfoxide (DMSO) was chosen as the polymerization solvent for the DABCO-based ionenes due to the low solubility of DABCO in MeOH, and reactions between 1,12-dibromododecane and

DABCO showed better yield in DMSO compared to a mixture of DMF and MeOH.[18] This allows samples to form a robust film even after pre-drying at room temperature for 1 day before elevating the temperature to 60 °C due to the high boiling point of DMSO, and thus prevents film defects. All DABCO-based PEGXX/DD-ionenes made yellow-brown films as a final product.

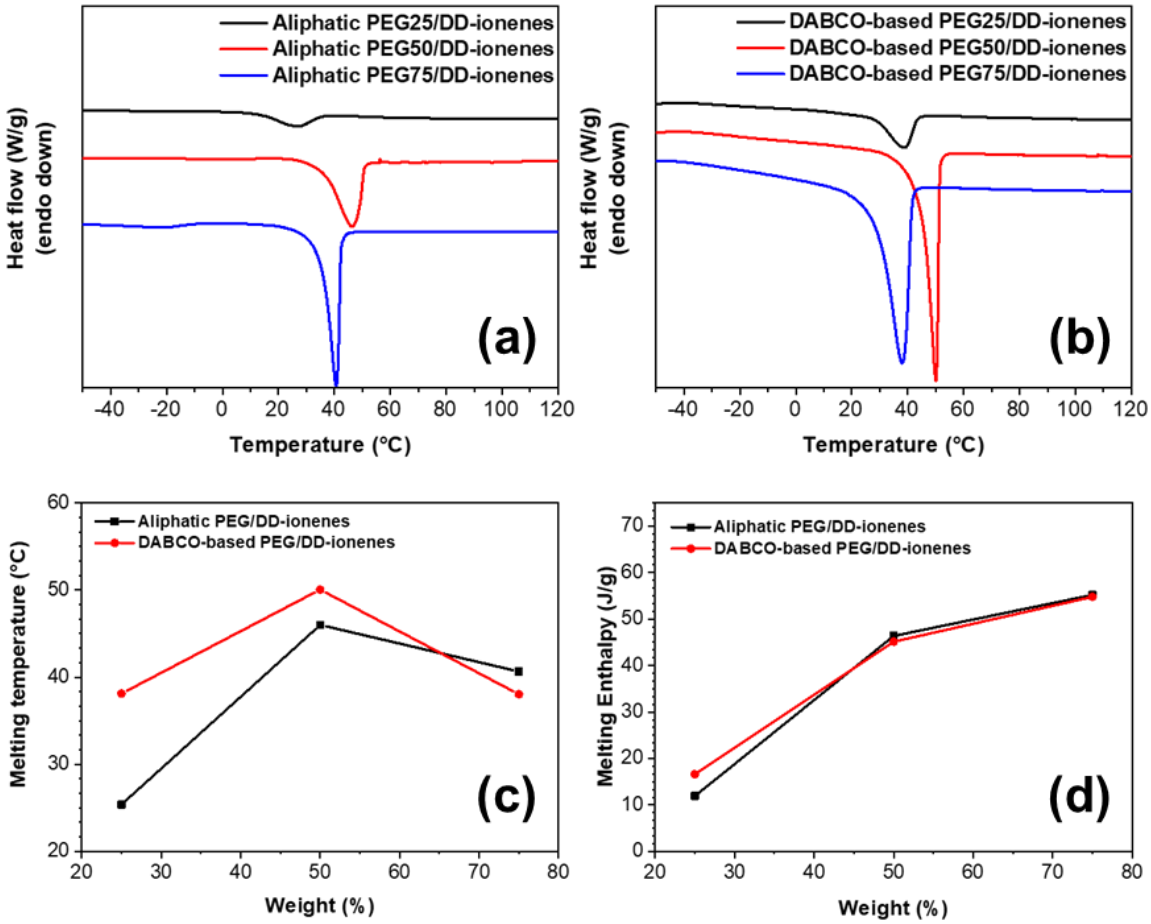

Figure 3.3: DSC results of (a) aliphatic PEGXX/DD-ionenes and (b) DABCO-based PEGXX/DD-ionenes. DSC also determined (c) melting temperature and (d) melting enthalpy of aliphatic PEGXX/DD-ionenes and DABCO-based PEGXX/DD-ionenes. The weight (%) on x axis refers to the weight fraction of PEG soft segments.

Both aliphatic and DABCO-based PEGXX/DD-ionenes showed an increase in melting temperature in the order 25 < 75 < 50 wt% of soft segments revealed by DSC analysis as shown in Figure 3.3a-c. Ionenes possessing the heterocyclic aliphatic hard segment (DABCO) had a significantly higher melting temperature than their linear aliphatic analogous with 25 wt% of soft segments. However, the melting temperature was similar when the weight fraction of the soft segment reached 50 wt%, showing that the effect of hard segments on melting temperature was debilitated at higher contents of soft segments. The melting enthalpy suggested that changing the type of hard segments, DABCO or linear aliphatic hexanediamine, would have a similar trend in the change of the degree of crystallization of the PEG soft segment with the increase in the content of the soft segment, as shown in Figure 3.3d. Both 50 wt% aliphatic and DABCO-based ionenes showed the highest melting temperature among series; however, the melting temperature decrease when soft segment weight fraction increases to 75 wt% regardless of the type of hard segment. This suggests that the tendency of the phase separation reduced with the 75 wt% of soft segments, which may induce a phase mixing and decrease the melting temperature regardless of the type of hard segments, and it will be further discussed below. The DABCO-based ionenes had narrower melting peaks compared to aliphatic ionenes less than or equal to 50 wt% of soft segments (Table A1), which suggests that DABCO hard segment contributes to forming a higher purity of crystallites compared to linear aliphatic hard segment. However, the melting peak for the DABCO-based ionenes broadens when PEG soft segments reached 75 wt%. The increase of melting temperature, which increased as melting enthalpy increased, also suggested that increasing the weight fraction of the soft

segment magnifies the purity of crystallites and induces better chain packing; however, the change in melting enthalpy was not proportional to the increment of weight fraction of soft segments.[28] In fact, the data indicates that a low fraction of additional soft segments crystallized when the soft segment weight fraction exceeded 50 wt%, likely due to phase mixing as seen previously. DSC data confirmed that the melting temperature of ionenes, the crystallinity of soft segment, and purity of crystallites could be tuned by changing the weight fraction of soft and hard segments and the type of hard segments.

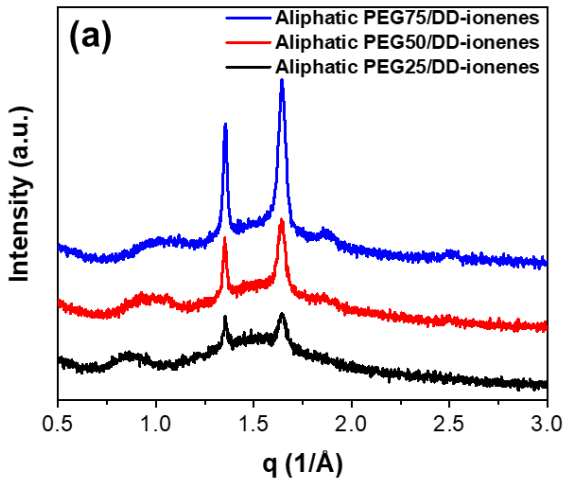
(a)
Aliphatic PEG75/DD-ionenes
Aliphatic PEG50/DD-ionenes
Aliphatic PEG25/DD-ionenes
Intensity (a.u.)
0.5
1.0
1.5
2.0
2.5
3.0
q (1/Å)

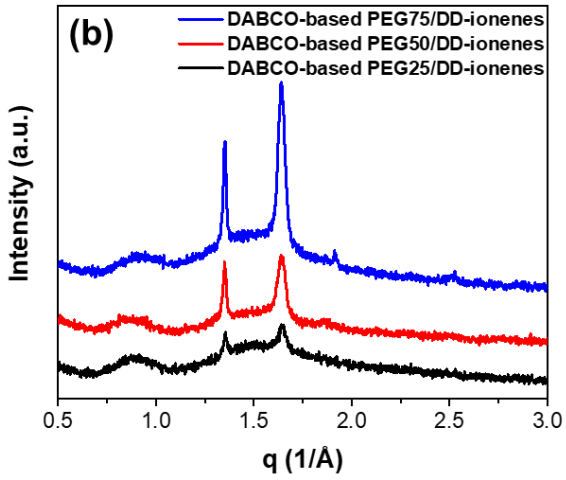
(b)
DABCO-based PEG75/DD-ionenes
DABCO-based PEG50/DD-ionenes
DABCO-based PEG25/DD-ionenes
Intensity (a.u.)
0.5
1.0
1.5
2.0
2.5
3.0
q (1/Å)

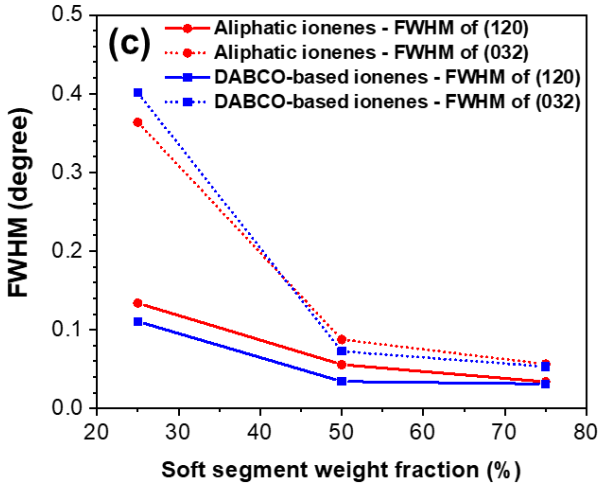
(c)
Aliphatic ionenes - FWHM of (120)
Aliphatic ionenes - FWHM of (032)
DABCO-based ionenes - FWHM of (120)
DABCO-based ionenes - FWHM of (032)
FWHM (degree)
0.0
0.1
0.2
0.3
0.4
0.5
20
30
40
50
60
70
80
Soft segment weight fraction (%)

Figure 3.4: Overlayed XRD diffraction of (a) aliphatic PEGXX/DD-ionenes and (b) DABCO-based PEGXX/DD-ionenes, and (c) full width half maximum of diffraction peaks of PEG (120) and (032) crystal planes.

The degree of crystallinity and the purity of crystallites were confirmed with XRD where both semi-crystalline aliphatic and DABCO-based PEG75/DD-ionenes had the highest intensity of two prominent peaks for the PEG soft segment (at $2\theta = 19.2^{\circ}$ and 23.4°, at $q = 1.35$ and 1.64) and they decreased with decreasing weight fraction of soft segment as shown in Figure 3.4a-b. The values of the full width at half maximum (FWHM) of PEG (120) and (032) crystal planes decreased as the weight fraction of the PEG soft segment increased for both aliphatic and DABCO-based ionenes, as shown in Figure 3.4c. However, DABCO-based ionenes had lower FWHM values than aliphatic ionenes up to 50 wt% of soft segments, which confirmed that DABCO induced higher purity of crystallites of PEG soft segments compared to linear aliphatic hard segments with the increase of contents of soft segments, which was consistent with DSC data. However, the FWHM value reduced when the content of the soft segments increased to 75 wt%. In addition, the significant decrease of the FWHM value from 25 wt% to 50 wt% of soft segments in both aliphatic and DABCO-based ionenes showed that increasing the content of the soft segment up to 50 wt% provided better configurational freedom, and hence increased the degree of crystallization. Moreover, the slight decrease of FWHM from 50 wt% to 75 wt% of soft segments was observed since the degree of crystallinity increased at a smaller rate than the contents of soft segments due to the lowered phase purity with 75 wt% of soft segments regardless of the type of hard segments.

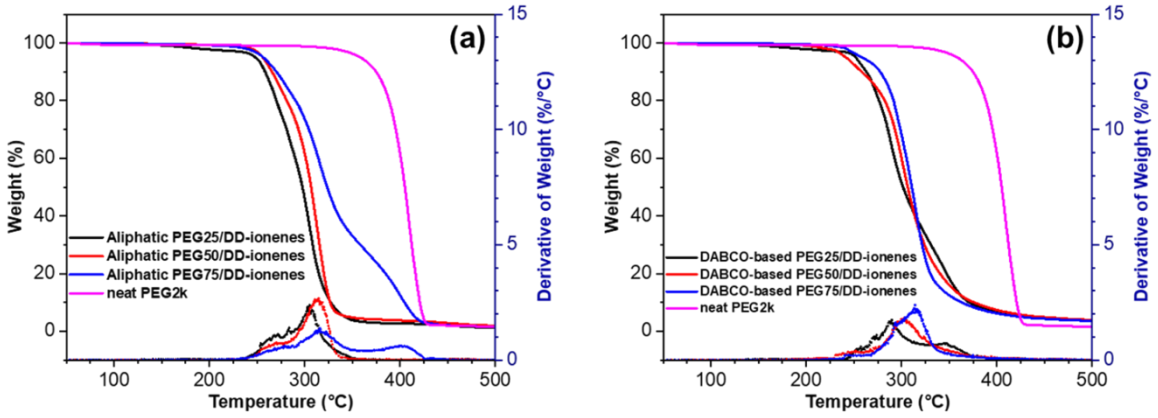

Figure 3.5: Overlayed TGA curves (solid lines) and derivative weight loss curves (dashed lines) for (a) aliphatic PEGXX/DD-ionenes and (b) DABCO-based PEGXX/DD-ionenes compared to neat PEG2k.

The thermal stability of the ionenes was measured using TGA under a nitrogen atmosphere. All PEG-based ionenes, regardless of whether they possessed linear aliphatic or DABCO hard segments, displayed high thermal stability up to ~250 °C, as shown in Figure 3.5. The onset of degradation of the neat PEG-2k was ca. 350 °C; however, both aliphatic and DABCO-based ionenes degraded earlier than neat PEG-2k due to the several possible degradation pathways of ionenes. Ionenes typically degrade at elevated temperatures due to the nucleophilic substitution and/or Hoffman elimination reaction, during which a basic counterion attacks the α-carbon and produces tertiary amine and saturated alkane or it abstracts a β-hydrogen generating a tertiary amine and unsaturated alkene, respectively[2,20] Quaternization of amines enhances the thermal stability because tertiary amine typically volatilize at 170 °C, whereas quaternary ammoniums are stable up to ca. 220 °C.[30] We have introduced the aliphatic PEG-based ionenes previously that showed two clear two steps of degradation at which hard segments degrade followed by

soft segments.[28] Here, both aliphatic and DABCO-based ionenes showed a two-step degradation. The initial degradation of the hard segment is slower and is followed by a more rapid degradation of the soft segment. Wang and Hsieh revealed that the degree of phase separation gives enormous effect on the thermal stability and more phase mixing favored the thermal stability under nitrogen atmosphere.[31] Both aliphatic and DABCO-based PEG75/DD-ionenes showed higher stability at lower temperature compared to lower soft segment contents. However, DABCO-based PEG75/DD-ionenes degraded at lower temperature compared to aliphatic PEG75/DD-ionenes, which suggest that the aliphatic PEG75/DD-ionenes was more phase mixed. DABCO-containing copolymers have been known to have more complex thermal degradation.[20] Moreover, DABCO-based ionenes showed char residues, which was not shown with aliphatic ionenes owing to the possible crosslinking of bicyclic amine, DABCO, upon exposure to elevated temperatures.[25]

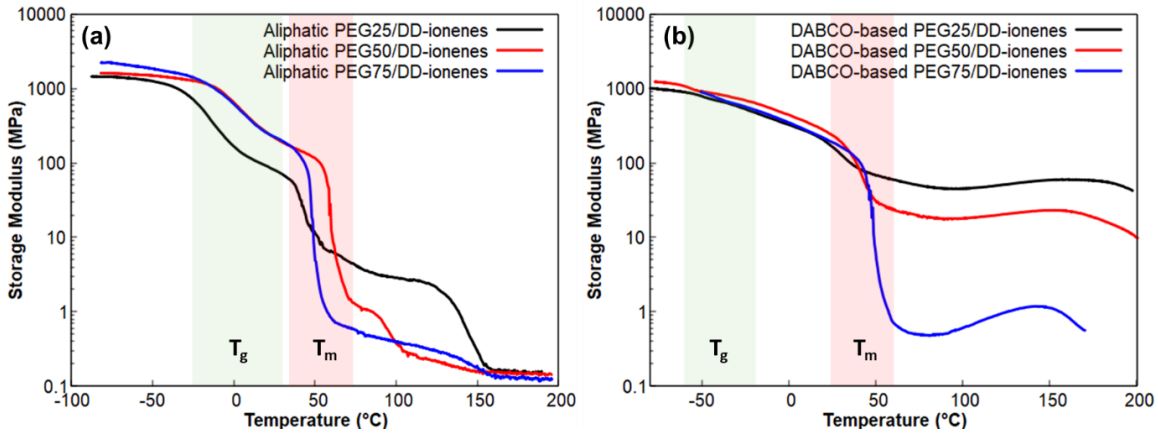

Figure 3.6: Overlayed DMA results of (a) aliphatic and (b) DABCO-based PEGXX/DD-ionenes. Green and red shaded regions refer to T_g of soft segment and melting temperature of PEG crystallites, respectively.

The viscoelastic properties of the PEG-based ionenes were analyzed using DMA. As shown in Figure 3.6a, the storage modulus of the glassy plateau increased by lowering the

charge density (weight fraction of hard segments) for the linear aliphatic ionenes. A higher glassy storage modulus in the temperature range of -80 to -25 °C was obtained for ionenes with 50 and 75 wt% of soft segments compared to 25 wt% for the ionenes with linear aliphatic hard segments. We attribute this behavior to the presence of more crystalline domains, where the higher soft segment fraction increases the storage modulus before the soft segment T_g and melting temperature. Whereas the DABCO ionenes (Figure 3.6b) had glassy storage modulus values that were approximately the same for all soft segment contents.

The T_g values of aliphatic PEG ionenes were higher than pure PEG, indicating restrictions on chain mobility of the PEG soft segment. The T_g values of aliphatic PEG ionenes highly depend on the weight fraction of soft segments. Asensio et al. showed that the difference of final T_g of elastomeric polymer from pure soft segment indicates the degree of mixing of soft and hard segments; specifically, a smaller difference designates better phase segregation.[32] According to Figure A3, aliphatic PEG25/DD-ionenes showed the least increase of T_g, suggesting it has the least amount of soft-hard segment mixing among the samples tested. While aliphatic PEG50/DD-ionenes and PEG75/DD-ionenes are more phase mixed, which caused the increase in T_g. In fact, lowering the soft segment fraction from 75 wt% to 25 wt% induced more substantial microphase separation and increased ionic aggregate connectivity and size, and this was previously seen in our study of similar linear aliphatic segmented ionenes.[28] DABCO-based ionenes possessed a lower soft segment T_g compared to aliphatic ionenes, which revealed that DABCO induced better phase separation of the soft and hard segment at all weight fractions.

The second feature occurred due to the melting of crystallites in the PEG soft segment. Figure 3.6 shows that PEG50/DD-ionenes have the highest melting temperature among other weight fractions (especially for the aliphatic sample). Although the melting occurred at a lower temperature for PEG25/DD-ionenes, the drop in storage modulus was less significant compared to PEG50 and PEG75/DD-ionenes due to the higher weight fraction of hard segments in the PEG25/DD-ionenes structure for both aliphatic and DABCO ionenes (a higher physical crosslinking effect). Also, a longer rubbery plateau of PEG25/DD-ionenes was observed, which is related to the increase in concentration of ionic associations in the structure (still more physical crosslinks) that confirms a wide window of application of this sample. The ionic aggregates from hard segments act as non-covalent physical crosslinks by attractive electrostatic forces and induce elastomeric behavior.[33]

DABCO-based PEG25/DD-ionenes and PEG50/DD-ionenes showed ca. one-hundred-fold increase in rubbery plateau storage modulus when compared to the aliphatic analogs; this effect comes from stronger physical crosslinks in DABCO hard segments. Zhang et al. observed a similar phenomenon wherein DABCO containing copolymers provided stronger ionic interactions and greater microphase separation compared to singly charged ammonium.[20]

The dissociation of the ionic aggregates of DABCO-based ionenes occurred at a higher temperature compared to aliphatic analogs since DABCO has a higher positive charge density and better proximity of charged sites compare to the aliphatic analogs. DABCO-based ionenes have been shown to have better chain packing, even than aromatic ammonium ionenes, which had a lower rubbery plateau modulus indicated by DMA data.[25]

Moreover, there is a big temperature difference between the flow region of aliphatic ionenes which depicts weaker ionic interactions in PEG75/DD-ionenes, whereas PEG25/DD-ionenes flowed at high temperature (~ 140 °C) in which ionic dissociation occurs, indicating that aliphatic PEG25/DD-ionenes have better elastomeric behavior than aliphatic PEG50 and PEG75/DD-ionenes. A meaningfully lower storage modulus (ca. 0.7 MPa) at ca. 60 °C occurred for both aliphatic and DABCO-based PEG75/DD-ionenes compared to 25 and 50 wt% of soft segment. After the significant drop of the storage modulus of DABCO-based PEG75/DD-ionenes after melting the PEG crystallites, the E' increased. This "jump" in E' has been observed for other ionenes before. The "jump" temperature occurred at higher temperatures with increasing the hard segment fractions. This behavior has only happened in DABCO-based ionenes, which reveals the role of DABCO in increasing the storage modulus at elevated temperatures. As reported previously, the conformational changes of ionic segments in the system could repack the heterocyclic aliphatic (i.e., "hard") domains.[34]

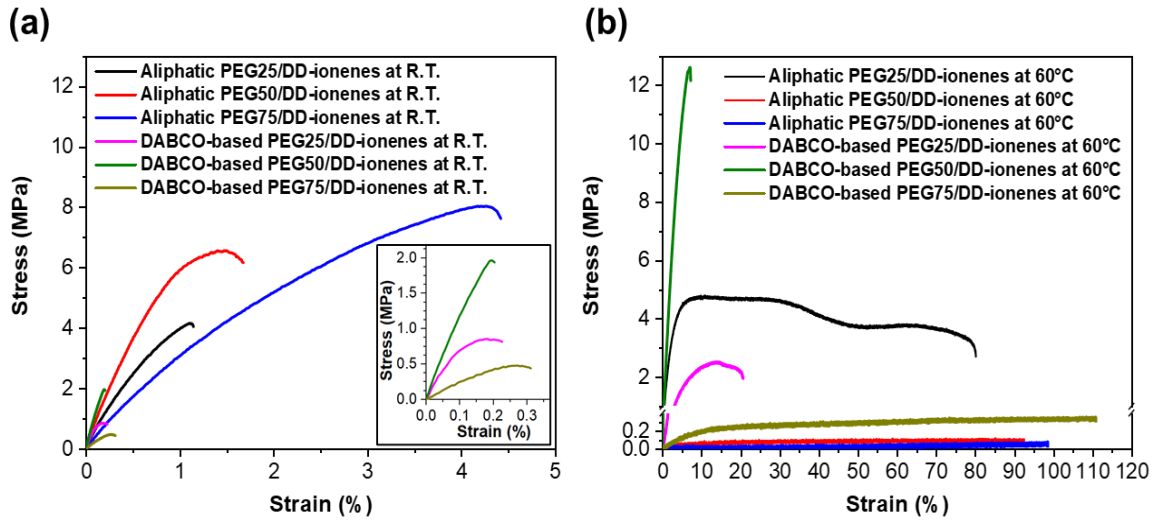

Figure 3.7: Tensile analysis of aliphatic PEGXX/DD-ionenes and DABCO-based PEGXX/DD-ionenes at (a) room temperature and (b) elevated temperature (60 °C).

Tensile testing was performed at room temperature and at 60 °C with both the linear aliphatic and DABCO-based PEGXX/DD-ionenes, as shown in Figure 3.7. The temperature of 60 °C was chosen based on the melting temperature of the PEG soft segments in both aliphatic and DABCO-based ionenes, which avoids the effect that PEG crystallites have on the tensile analysis. All linear aliphatic and DABCO-based ionenes exhibited a lower elongation at room temperature relative to 60 ˚C (Table A2). At room temperature, the DABCO-based ionenes had a shorter elongation than aliphatic ionenes due to the nature of the rigid heterocyclic structure of DABCO and the fact that they have a higher storage modulus as shown by the DMA results. In fact, the linear aliphatic ionenes were relatively more flexible than DABCO-based ionenes when samples were kept at ambient temperature for several days due to the hygroscopic nature of PEG soft segments and relatively low melting temperature of PEG crystallites; however, all samples were kept under vacuum until performing the tensile test to avoid the water absorption. Both aliphatic and DABCO-based PEG50/DD-ionenes showed the highest Young's modulus when compared to PEG25 and 75/DD-ionenes at room temperature due to higher melting temperature. The elongation at break for the aliphatic ionenes decreased with increasing hard segment content at room temperature. Although all ionenes were not stretchy at room temperature, they showed elastomeric properties at temperatures above the PEG melting temperature. Aliphatic ionenes elongated dramatically at all weight fractions. In contrast, DABCO-based ionenes show decent elastomeric properties with the highest weight fraction of soft segments (75 wt%), which showed that the DABCO ionenes tolerated a

higher strain compared to linear aliphatic hard segment. It needs to be noted that the aliphatic PEG50/DD-ionenes and PEG75/DD-ionenes and DABCO-based PEG75/DD-ionenes reached over 90% of strain, but did not break (they could not be elongated any longer due to the height limitation of the instrument equipped with a heating chamber). The tensile strength of linear aliphatic ionenes decreased at 60 °C with the increase of the weight fraction of the soft segment compared to at room temperature, and there was a dramatic decrease in the tensile strength when the soft segment content increased to 50 wt%. This reveals that higher contents of PEG soft segment (i.e., >50 wt%) make ionene films remarkably soft due to the decrease of the ionic aggregation, which was consistent with DMA data that the rubbery plateau of aliphatic PEG 50/DD-ionenes and 75/DD-ionenes was significantly lowered at 60 °C compared to aliphatic PEG25/DD-ionenes. The DABCO-based PEG50/DD-ionenes showed the lowest elongation at 60 °C due to the high melting temperature as DSC showed the highest and narrow melting temperature among all series, and the testing temperature was not high enough for crystalline to be fully melted. By comparing between aliphatic PEG75/DD-ionenes and DABCO-based PEG75/DD-ionenes at 60 °C, DABCO provided higher modulus and better elastomeric properties than linear aliphatic hard segment. This indicates that crystallites of PEG in the soft segments affect the elongation of ionenes enormously. The tensile strength of ionenes was more dependent on the melting temperature of crystallites than the degree of crystallinity and hard segment content, and the elongation at break and ultimate tensile strength are expected to be controlled by modifying the temperature. Among all series of ionenes, aliphatic

PEG25/DD-ionenes showed the best tensile performance in terms of a persistent toughness and elongation at elevated temperatures.

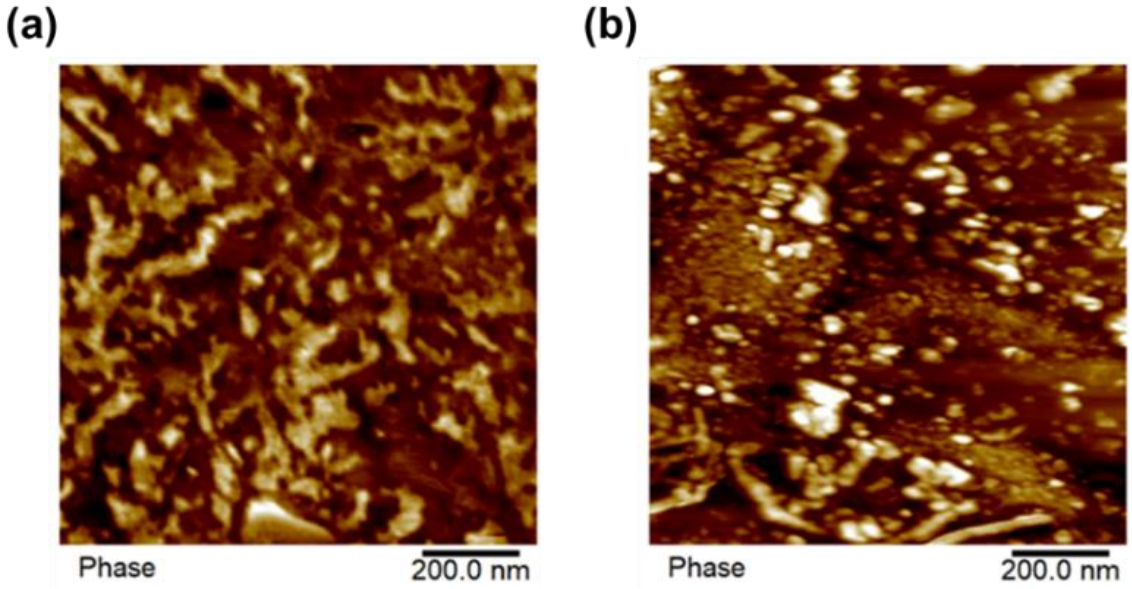

Figure 3.8: Microphase separation of (a) aliphatic PEG25/DD-ionenes and (b) DABCO-based PEG25/DD-ionenes at room temperature revealed by atomic force microscopy.

The morphology of the aliphatic and DABCO-based ionenes were analyzed by using AFM at room temperature, as shown in Figure 3.8. Since all of the aliphatic and DABCO-based ionenes crystallize at room temperature and the degree of crystallinity increases with the increase of weight fraction of soft segment, the aliphatic and DABCO-based PEG25/DD-ionenes, which have the lowest and similar degree of crystallization revealed from DSC and XRD, were selected for the AFM analysis. The brighter and darker regions corresponding to the hard and soft segments, respectively. Both aliphatic and DABCO-based PEG25/DD-ionenes showed significant microphase separation. Interestingly, DABCO-based PEG25/DD-ionenes formed more isolated hard domains whereas the linear aliphatic hard domains were more likely interconnected, at least on the film surfaces. Van

Bogart et al. revealed that more interconnected hard segment domains have better tensile strength in which a larger total surface area of hard domains effectively diminish crack growth through the soft segment domain.[35]

Overall, we observed that the content and nature of the soft and hard segments affect the elastomeric behavior, crystal purity, melting transition, and degree of phase separation. the increase of ionic connectivity by lowering the soft segment content improved the elastomeric behavior of the segmented ionenes as shown in the DMA results and tensile testing. The DABCO hard segments exhibit better ionic aggregation compared to the linear aliphatic hard segment, which also induced a higher purity soft segment crystallite. The higher purity crystallite may be attributed to less restriction of chain configuration by the DABCO hard segments that comes from the smaller soft-hard segment interface. Wang and Cooper showed that segmented copolymers with a high degree of phase separation have relatively purer soft and hard segment domains and limit segment interaction at the interfaces.[36] The crystallites of the PEG soft segment play a key role in the mechanical properties of segmented ionenes, and thus the crystal melting temperature has a huge impact on elastomeric behavior, tensile strength, and extensibility. Increasing the soft segment weight fraction to 75 wt% induced phase mixing and linear aliphatic hard segments were more phase mixed than DABCO hard segments. The difference in phase mixing between hard segment type could be due to the change in charge proximity; for example, DABCO has two methylenes between two ammonium cations, which could cause the hard segments to be less phase mixed. However, the 75 wt% of soft segments could not provide comparable viscoelastic properties relative to other hard segment weight fractions.

Forthcoming publications will discuss the influence of the molecular weight of soft segments, counterion selection, and type of soft segment in greater detail.

3.5 Conclusions

We presented the successful synthesis and characterization of a series of PEG-based segmented ionene copolymers with two structurally different hard segments, linear and heterocyclic aliphatic diamines. Segmented ionenes were prepared via Menshutkin reaction having three different weight fractions between soft and hard domains. TGA showed that both DABCO-based and aliphatic PEG ionenes thermally stable up to ~ 250 °C, as expected. DSC and XRD revealed that DABCO-based ionenes possess higher purity PEG crystallites compared to aliphatic ionenes, especially for DABCO-based PEG50/DD-ionenes that had the highest melting temperature and lowest FWHM among all samples. In addition, increasing the weight fraction of soft segment up to 75 wt% triggered soft-hard mixing in both linear aliphatic and DABCO hard segments. The linear aliphatic hard segment exhibited a greater degree of phase mixing than the DABCO hard segment based on the results of DMA and TGA. Uniaxial tensile analysis showed that ionenes elongated substantially after PEG crystallites melt at elevated temperature, and modulus decreases significantly with over 50 wt% of soft segments and was highly dependent on the melting temperature of the crystallites. DMA showed that DABCO-based ionenes showed markedly better phase separation compared to aliphatic ionenes in all weight fractions. The value and breadth of the rubbery plateau moduli, as well as softening temperature, was tuned by the nature and content of ionic hard segments. Also, the modulus at glassy state was dependent on the content of crystallites in the PEG soft segment. The evidence of chain

repacking of DABCO hard segments in DABCO-based ionenes was observed. Both aliphatic and DABCO-based PEG25/DD-ionenes showed superior phase separation among the various soft segment weight fractions, and AFM confirmed the presence of microphase separated morphologies. We propose a morphological difference between linear aliphatic and DABCO hard segments, where the former showed interconnected hard domains whereas the latter showed isolated hard domains. These findings highlight the effect of the type of hard segment and the content of the soft and hard domain on the thermomechanical properties of microphase separated ionene elastomers.

3.6 Acknowledgements

The authors wish to thank the Army Research Office (W911NF-18-1-0412) and NASA (80NSSC18K1508) for financial support.

3.7 References

1. Gibbs, C. F., Littmann, E. R. & Marvel, C. S. Quaternary Ammonium Salts from Halogenated Alkyl Dimethylamines. II. The Polymerization of Gamma-Halogenopropyldimethylamines. *J. Am. Chem. Soc.* **55**, 753–757 (1933).
2. Lee, J. S., Hocken, A. & Green, M. D. Advances in the molecular design of ionenes for a diverse range of applications. *Mol. Syst. Des. Eng.* **6**, 334–354 (2021).
3. Bara, J. E. & O'Harra, K. E. Recent Advances in the Design of Ionenes: Toward Convergence with High-Performance Polymers. *Macromol. Chem. Phys.* **220**, 1900078 (2019).
4. Williams, S. R., Salas-de la Cruz, D., Winey, K. I. & Long, T. E. Ionene segmented block copolymers containing imidazolium cations: Structure–property relationships as a function of hard segment content. *Polymer (Guildf).* **51**, 1252–1257 (2010).
5. Hashimoto, T. *et al.* Structure and properties of poly(tetrahydrofuran) viologen ionene: effects of halide counter-anions. *Polymer (Guildf).* **35**, 2672–2678 (1994).
6. Dubé, M. A. & Salehpour, S. Applying the Principles of Green Chemistry to Polymer Production Technology. *Macromol. React. Eng.* **8**, 7–28 (2014).

7. Kammakakam, I., O'Harra, K. E., Dennis, G. P., Jackson, E. M. & Bara, J. E. Self-healing imidazolium-based ionene-polyamide membranes: an experimental study on physical and gas transport properties. *Polym. Int.* **68**, 1123–1129 (2019).

8. Strassburg, A. *et al.* Cross-Linking of a Hydrophilic, Antimicrobial Polycation toward a Fast-Swelling, Antimicrobial Superabsorber and Interpenetrating Hydrogel Networks with Long Lasting Antimicrobial Properties. *ACS Appl. Mater. Interfaces* **9**, 36573–36582 (2017).

9. Yoshida, M. *et al.* Oligomeric Electrolyte as a Multifunctional Gelator. *J. Am. Chem. Soc.* **129**, 11039–11041 (2007).

10. Suzuki, K., Yamaguchi, M., Hotta, S., Tanabe, N. & Yanagida, S. A new alkyl-imidazole polymer prepared as an inonic polymer electrolyte by in situ polymerization of dye sensitized solar cells. *J. Photochem. Photobiol. A Chem.* **164**, 81–85 (2004).

11. Terenteva, E. A., Apyari, V. V., Dmitrienko, S. G. & Zolotov, Y. A. Spectrophotometric determination of sulfates using silver nanoparticles stabilized with 6,6-ionene. *Moscow Univ. Chem. Bull.* **70**, 157–161 (2015).

12. Feng, D., Wilkes, G. L., Leir, C. M. & Stark, J. E. Morphological Investigation of Polytetba-Methyleneoxide-Dibbomoxylene Segmented Ionene Polymebs by Tbansmission Electbon Micboscopy and Small-Angle X-Ray Scattebing. *J. Macromol. Sci. Part A - Chem.* **26**, 1151–1181 (1989).

13. Burmistr, M. V. *et al.* Structure, thermal properties and ionic conductivity of polymeric quaternary ammonium salts (polyionenes) containing ethylene oxide and aliphatic chain fragments. *Solid State Ionics* **176**, 1787–1792 (2005).

14. Somoano, R., Yen, S. P. S. & Rembaum, A. VI. Electronic conductivity of elastomeric ionenes. *J. Polym. Sci. Part B Polym. Lett.* **8**, 467–479 (1970).

15. Petersen, H. *et al.* Polyethylenimine- graft -Poly(ethylene glycol) Copolymers: Influence of Copolymer Block Structure on DNA Complexation and Biological Activities as Gene Delivery System. *Bioconjug. Chem.* **13**, 845–854 (2002).

16. Ding, B.-P., Wu, F., Chen, S.-C., Wang, Y.-Z. & Zeng, J.-B. Synthesis and characterization of a polyurethane ionene/zinc chloride complex with antibacterial properties. *RSC Adv.* **5**, 12423–12433 (2015).

17. Shi, Q. *et al.* Single ion solid-state composite electrolytes with high electrochemical stability based on a poly(perfluoroalkylsulfonyl)-imide ionene polymer. *J. Mater. Chem. A* **2**, 15952–15957 (2014).

18. Salamone, J. C. & Snider, B. Quaternary ammonium polymers from 1,4-diaza[2.2.2]bicyclooctane. *J. Polym. Sci. Part A-1 Polym. Chem.* **8**, 3495–3501 (1970).

19. Yuan, Y., Liang, S., Li, J., Zhang, S. & Zhang, Y. Copolymers with both soft and

rigid cationic rings as highly selective antimicrobials to combat antibiotic resistant microbes and biofilms. *J. Mater. Chem. B* **7**, 5620–5625 (2019).

20. Zhang, K., Drummey, K. J., Moon, N. G., Chiang, W. D. & Long, T. E. Styrenic DABCO salt-containing monomers for the synthesis of novel charged polymers. *Polym. Chem.* **7**, 3370–3374 (2016).

21. Misawa, Y., Koumura, N., Matsumoto, H., Tamaoki, N. & Yoshida, M. Hydrogels Based on Surfactant-Free Ionene Polymers with N,N′ -(p -Phenylene)dibenzamide Linkages. *Macromolecules* **41**, 8841–8846 (2008).

22. Bachl, J. *et al.* Synergistic Computational-Experimental Approach to Improve Ionene Polymer-Based Functional Hydrogels. *Adv. Funct. Mater.* **24**, 4893–4904 (2014).

23. Häring, M., Grijalvo, S., Haldar, D., Saldías, C. & Díaz, D. D. Polymer topology-controlled self-healing properties of polyelectrolyte hydrogels based on DABCO-containing aromatic ionenes. *Eur. Polym. J.* **115**, 221–224 (2019).

24. Dragan, E. S., Mayr, J., Häring, M., Cocarta, A. I. & Díaz, D. D. Spectroscopic Characterization of Azo Dyes Aggregation Induced by DABCO-Based Ionene Polymers and Dye Removal Efficiency as a Function of Ionene Structure. *ACS Appl. Mater. Interfaces* **8**, 30908–30919 (2016).

25. Das, S. *et al.* Synthesis and Characterization of Novel Segmented Polyionenes Based on Polydimethylsiloxane Soft Segments. *J. Macromol. Sci. Part A* **47**, 215–224 (2010).

26. Abdulahad, A. I., Jangu, C., Hemp, S. T. & Long, T. E. Influence of Counterion on Thermal, Viscoelastic, and Ion Conductive Properties of Phosphonium Ionenes. *Macromol. Symp.* **342**, 56–66 (2014).

27. Tamami, M., Williams, S. R., Park, J. K., Moore, R. B. & Long, T. E. Poly(propylene glycol)-based ammonium ionenes as segmented ion-containing block copolymers. *J. Polym. Sci. Part A Polym. Chem.* **48**, 4159–4167 (2010).

28. Liesen, N. T. *et al.* The influence of spacer composition on thermomechanical properties, crystallinity, and morphology in ionene segmented copolymers. *Soft Matter* **17**, 5508–5523 (2021).

29. Saralegi, A. *et al.* Thermoplastic polyurethanes from renewable resources: effect of soft segment chemical structure and molecular weight on morphology and final properties. *Polym. Int.* **62**, 106–115 (2013).

30. Charlier, P., Jérome, R., Teyssié, P. & Proud'Homme, R. E. Thermal stability of modified telechelic polystyrenes. *J. Polym. Sci. Part A Polym. Chem.* **31**, 129–134 (1993).

31. Wang, T.-L. & Hsieh, T.-H. Effect of polyol structure and molecular weight on the thermal stability of segmented poly(urethaneureas). *Polym. Degrad. Stab.* **55**, 95–

102 (1997).

32. Asensio, M., Costa, V., Nohales, A., Bianchi, O. & Gómez, C. M. Tunable Structure and Properties of Segmented Thermoplastic Polyurethanes as a Function of Flexible Segment. *Polymers (Basel).* **11**, 1910 (2019).

33. Wu, F., Huang, C. L., Zeng, J. B., Li, S. L. & Wang, Y. Z. Synthesis and characterization of segmented poly(butylene succinate) urethane ionenes containing secondary amine cation. *Polymer (Guildf).* **55**, 4358–4368 (2014).

34. Feng, D., Wilkes, G. L., Lee, B. & McGrath, J. E. Structure-property behaviour of segmented poly (tetramethylene oxide)-based bipyridinium ionene elastomers. *Polymer (Guildf).* **33**, 526–535 (1992).

35. Van Bogart, J. W. C., Gibson, P. E. & Cooper, S. L. Structure-property relationships in polycaprolactone-polyurethanes. *J. Polym. Sci. Polym. Phys. Ed.* **21**, 65–95 (1983).

36. Wang, C. B. & Cooper, S. L. Morphology and properties of segmented polyether polyurethaneureas. *Macromolecules* **16**, 775–786 (1983).

CHAPTER 4

SYNTHESIS AND CHARACTERIZATION OF POLY(TETRAMETHYLENE OXIDE)-BASED SEGMENTED IONENES BLOCK COPOLYMER WITH ALIPHATIC OR DABCO HARD SEGMENTS

Reproduced with permission from: Lee, J.; Taghavimehr, M.; Montazami, R.; Green, M. D. *Polymer*, 270, 125772, 2023. Copyright 2023. Elsevier

4.1 Abstract

In this study, the effects of the contents of the soft and hard segments as well as the type of hard segments (linear aliphatic and DABCO) on the properties of PTMO-based segmented ionenes were investigated. DSC revealed that soft segment weight fractions up to 75 wt% induced heterogeneous crystallization while the melting temperature decreased due to the lower degree of crystallization. DMA showed the formation of a higher degree of ionic aggregates in both linear aliphatic and DABCO-based PTMO ionenes with 25 wt% of soft segment resulting from strong Coulombic interactions between hard segments. DABCO-based ionenes showed a higher degree of phase separation compared to linear aliphatic analogs and displayed a long-range ordered lamellar structure. In contrast, linear aliphatic ionenes showed the formation of random ionic domains, which was confirmed by SAXS and AFM. TGA showed that the PTMO-based ionenes were thermally stable up to 250 °C and suggested that the DABCO hard segment has a weaker protective effect against the degradation of the PTMO soft segment at elevated temperatures compared to the linear

aliphatic hard segment. Uniaxial tensile tests exhibited stress-induced crystallization of PTMO-based ionenes, high elongation at break with linear aliphatic hard segment compared to the DABCO hard segment, and the opposite trend of Young's modulus and ultimate tensile strength by changing the type of the hard segment.

4.2 Introduction

Ammonium ionenes contain quaternary nitrogen atoms in their backbone chain. Gibbs et al. were the first to synthesize ammonium ionenes via step-growth polymerization in 1933,[1] and Rembaum et al. first adopted the name "ionenes" for polymers containing ionic groups synthesized based on the Menshutkin reaction in 1968.[2] Ionenes have been prepared via the Menshutkin reaction, a reaction of tertiary amine with a halide, and the polymerization typically proceeds via an S_N2 mechanism.[3] Bromine is the most widely used halogen since it is a weak base and an excellent leaving group. Generally, there are two types of ionenes: non-segmented[4,5] and segmented ionenes.[6–9] Segmented ionenes have relatively soft and hard segments along the backbone and the soft segments are relatively long oligomeric monomers whereas hard segments are usually short-length monomers.[10] Segmented ionenes show elastomeric behavior similar to polyurethane (PU) elastomers, but segmented ionenes possess non-covalent physical crosslinks caused by ionic interaction or aggregation.[11] Several oligomeric monomers for the soft segment, including poly(tetramethylene oxide) (PTMO)[12], poly(ethylene glycol) (PEG)[9], polydimethylsiloxane (PDMS)[13], and poly(propylene glycol) (PPG)[14], have been reported for synthesizing segmented ionenes. The PTMO soft segment has been utilized in various

segmented ionenes more compared to other soft segments with a different type of hard segments, and Kohjiya et al. introduced the first aliphatic ammonium PTMO ionene.[15]

The elastomeric behavior results from the ionic aggregation of hard segments, and this behavior depends on the type of hard segments. Ikeda et al. synthesized the mono ammonium ionenes containing only one ammonium cation in each repeating unit with PTMO soft segments and showed a short rubbery plateau due to the weaker ionic aggregation compared to segmented ionenes with two ammonium cations in each repeating unit.[16,17] Williams et al. introduced the first imidazolium-based PTMO ionene with bisimidazolium/dodecane hard segments and 2000 g mol^{-1} PTMO soft segments.[18] The imidazolium-based ionenes did not show an extended rubbery plateau with 20 wt% and 38 wt% of the hard segment revealed by dynamic mechanical analysis (DMA). However, they clearly showed the microphase separation, which arose from the incompatibility of the PTMO soft segment and the ionic domains of the hard segment, revealed by X-ray scattering. The high degree of microphase separation results in the high strength of the segmented ionenes necessary to enhance physical properties.[19] Feng et al. revealed that aromatic ammonium PTMO ionenes with an aliphatic ether spacer group between dibenzyl halide showed a lower strength at a given elongation compared to the non-spacer group due to the poor phase separation.[12] The PTMO-based ionene with 2,2'-bipyridine hard segment (pyridinium-based PTMO ionenes) exhibited high tensile strength up to 34 MPa and 540% elongation at break at room temperature and showed a microphase separated structure consisting of three phases: i) PTMO amorphous matrix, ii) PTMO crystalline domain, and iii) ionic hard domain.[20] Moreover, the high degree of phase separation

promotes stress-induced crystallization (or strain-induced crystallization) of the PTMO soft segment. The stress-induced crystallization forms crystals to be oriented, resulting in anisotropy in the material's mechanical response determined by the deformation in the amorphous phase at the rapid growth of the crystalline phase.[21] Hashimoto et al. synthesized pyridinium-based PTMO ionenes, which showed stress-induced crystallization of PTMO soft segment after 300% strain regardless of the type of counterions, Cl^-, Br^-, and I^-.[22] Imidazolium-based PTMO ionenes have been prepared into nonwoven fibers using electrospinning, and the stress-induced crystallization was observed with the higher molecular weight of PTMO soft segments.[23]

The morphological features of segmented ionenes also can be tuned by changing the molecular weight of the soft segment and the type of the hard segment and counterion. Grassl et al. observed a change in morphology from lamellae to hexagonally-packed cylinders by increasing the molecular weight of the PTMO soft segment using aliphatic ammonium hard segments, as revealed by small-angle X-ray scattering (SAXS).[24] Furthermore, the rigid structure of the viologen hard segment showed a disc-like aggregation of hard domains instead of spherical aggregation that has been considered for segmented ionenes.[22] Ikeda et al. revealed that both Cl^- and Br^- counterions did not show any ordered morphology, such as lamellae, with mono ammonium PTMO ionenes; however, the Cl^- counterion induced a bigger size of the ionic hard domain and longer distance between hard domains compared to the Br^- counterion.[17] Moreover, the mechanical and thermal properties of ionenes can be tuned by introducing different type of counterion. Hunley et al. showed that increasing the size of counterion ($Cl^- < BF_4^- < Tf_2N^-$)

decreased the T_g of ionomers.[25] Abdulahad et al. revealed that exchanging Br^- counterion to BF_4^- or TF_2N^- counterions reduced the T_g significantly and increased thermal stability of phosphonium non-segmented ionenes due to the increased size of the counterions and reduced anion basicity.[26]

Segmented ionenes have not been studied and used in many applications; however, they are hypothesized to be useful for thermoplastic elastomers and in flexible and wearable electronic devices. Segmented ionenes have been compared with PU because they mechanically resemble segmented PU. However, segmented PU are prepared using toxic isocyanates, whereas segmented ionenes can be environmentally friendly, synthesized in a single step process, and generally possess quaternary ammoniums with counterions that enable a diverse set of applications. Due to the lack of in-depth studies that define the properties of PTMO-based segmented ionenes through direct comparisons of chemical structure or content of soft/hard segments, studies that establish fundamental structure-property relationships for PTMO-based segmented ionenes are needed.

In the present study, we report the synthesis of a series of PTMO-based segmented ionenes with one structural difference as not seen elsewhere: the ionenes possess either linear aliphatic or 1,4-diazabicyclo[2.2.2]octane (DABCO) hard segments. Both linear aliphatic and DABCO-based ionenes have Br^- counterions and four different soft segment contents. The thermal and mechanical properties of these segmented ionenes were analyzed by differential scanning calorimetry (DSC), thermogravimetric analysis (TGA), DMA, and uniaxial tensile analysis. The morphologies were probed with X-ray diffraction (XRD), SAXS, and atomic force microscopy (AFM).

4.3 Experimental

4.3.1 Materials

Poly(tetrahydrofuran) (PTMO) 2,000 g/mol, *N,N,N',N'*-tetramethyl-1,6-hexanediamine (99%), triethylamine (≥99.5%), 6-bromohexanoyl chloride (97%), 1,4-diazabicyclo[2.2.2]octane (DABCO) (≥99%), and dimethyl sulfoxide (DMSO) (≥99.9%) were purchased from Sigma Aldrich. Chloroform-*d*, and dimethyl sulfoxide-d_6 were purchased from Alfa Aesar. Dichloromethane (DCM), dimethylformamide (DMF), and methanol (MeOH) were purchased from VWR Chemicals. 1,12-dibromodedecane was obtained from TCI America. All materials were used as received except 1,12-dibromododecane (≥98%), which was recrystallized in isopropyl alcohol.

4.3.2 Synthesis of Bromine end-capped PTMO2k (Br-PTMO$_n$-Br)

Br-PTMO$_n$-Br was prepared as described in detail elsewhere.[6] PTMO-2k (7g, 1eq) was dissolved in DCM (50 ml), and triethylamine (0.7893 g, 2.2 eq) was added in a round bottom flask. 6-bromohexanoyl chloride (1.6653 g, 2.2 eq) was added dropwise at 0 °C (ice bath) and slowly heated to room temperature and stirred for 1 d. Then the salt was filtered four times, and the organic phase was washed with a saturated sodium bicarbonate solution five times. The organic phase solution was dried in the vacuum oven at 40 °C for 1 d.

4.3.3 Synthesis of aliphatic PTMO93-ionenes and DABCO-based PTMO95-ionenes

Aliphatic and DABCO-based PTMO-ionenes are synthesized with Br-PTMO$_n$-Br and *N,N,N',N'*-tetramethyl-1,6-hexanediamine or DABCO in MeOH or DMF, respectively,

and stirred at 75 °C for 3 d. The molar ratio of Br-PTMO$_n$-Br to *N,N,N',N'*-tetramethyl-1,6-hexanediamine or DABCO was equal to one. The synthesized ionenes were dried at room temperature for 1 d followed by drying at 60 °C for 1 d, and at room temperature under vacuum for 1 d.

4.3.4 Synthesis of aliphatic and DABCO-based PTMOXX/DD-ionenes

Three different weight fractions of PTMO soft segment, 25, 50, and 75 wt%, and counterparts of hard segments were synthesized with Br-PTMO$_n$-Br, 1,12-dibromododecane, and *N,N,N',N'*-tetramethyl-1,6-hexanediamine or DABCO. The molar ratio of Br-PTMO$_n$-Br to the sum of 1,12-dibromododecane and *N,N,N',N'*-tetramethyl-1,6-hexanediamine or DABCO was equal to one, as shown in Table 4.1. For example, the aliphatic PTMO50/DD-ionenes, which has 50 wt% of PTMO soft segment and 50 wt% of hard segments, Br-PTMO$_n$-Br (1 g), 1,12-dibromododecane (0.608 g), and *N,N,N',N'*-tetramethyl-1,6-hexanediamine (0.392 g) was added in MeOH and stirred at 75 °C for 3 d with the condenser connected. The concentration of all series of linear aliphatic ionenes was 2 mol/L. The synthesized ionenes were dried at room temperature for 1 d, followed by drying at 60 °C for 1 d and at room temperature under vacuum for 1 d. The mixture of DMF and DMSO solvents was used for DABCO-based ionenes and stirred at 75 °C for 5 d. The synthesized ionenes were dried at 80 °C under vacuum for 1 d. Then, DABCO-based ionenes were re-casted by dissolving in DMSO. They were dried at room temperature for 4 d to prevent the defect of film, followed by drying at 80 °C in the oven for 2 d and an additional 1 d at room temperature under vacuum. The nomenclature of synthesized segmented ionenes is shown below (Scheme 4.1) to provide information on

the type of hard segment and contents of the soft segments. Samples were transported directly from the oven to the equipment used for characterization below to avoid water uptake from the ambient air.

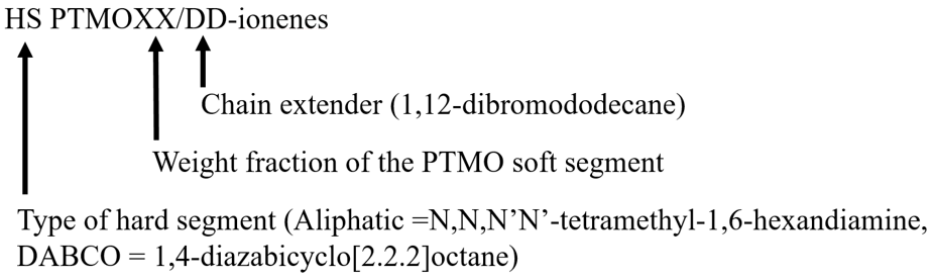

Scheme 4.1: The nomenclature of synthesized segmented ionenes.

4.3.5 Characterizations

^{1}H NMR spectroscopic analyses were performed on Bruker Avance III 500 MHz NMR. Chloroform-*d* and DMSO-d_6 were used for linear aliphatic and DABCO-based ionenes, respectively. DSC was performed on a TA Instruments Q2000. The sample was heated from 40 °C to 160 °C, cooled down to -80 °C, and then heated up to 160 °C. The purge gas was ultra-high purity (UHP) nitrogen with a gas flow rate of 25 mL/min. The heating and cooling rate were both 10 °C/min, and the sample was held isothermally for 10 min before each ramp. The second heating cycle was used for DSC analysis. TGA was conducted on TA Instruments TGA 5500 in a UHP nitrogen atmosphere with a sample purge rate of 25 mL/min and a balance purge rate of 10 mL/min. The sample was heated (20 °C/min) to 120 °C, cooled down (20 °C/min) to 40 °C, and heated up (10 °C/min) again to 600 °C with an isothermal pause for 10 min before each temperature ramp. XRD was performed on a PANalytical X'Pert PRO MRD with nickel-filtered Cu Kα radiation source (λ = 1.54 Å), divergence slit 1/4º, anti-scatter slits 1/2º, 45 kV/40 mA, and 2θ = 3-60º at room

temperature. Tensile tests were performed on an Instron E3343 with a 20 mm/min extension rate. All samples were prepared using a dog-bone-shaped die (ASTM D1708). AFM was conducted on a Bruker MultiMode 8 using an ACSTA probe at room temperature. DMA was conducted on a Mettler Toledo Polymer-1 analyzer in tension mode in a temperature range of -80 to 200 ˚C at a heating rate of 3 ˚C/min, a frequency of 1 Hz, and under 0.1% strain. The DMA measurements were done under dried nitrogen. SAXS was conducted using a CuKα radiation (λ = 0.154 nm) source. Before the test, calibration of the sample-to-detector distance and beam centering was performed. The sample to detector distance was 2.54 m, and two-dimensional diffraction patterns were collected using a multivariate detector. Then, the patterns were converted to a one-dimensional figure. All X-ray scattering measurements were done at ambient temperature.

Table 4.1: Compositions of linear aliphatic and DABCO-based PTMO-ionenes. DD and AM refer to 1,12-dibromododecane and *N,N,N'N'*-tetramethyl-1,6-hexandiamine or DABCO, respectively.

Sample	Molar ratio PTMO/DD/AM	Soft segment, wt%	Hard segment, wt%	
			DD	AM
Aliphatic PTMO25/DD-ionenes	1.0/13.7/14.7	25	53	22
Aliphatic PTMO50/DD-ionenes	1.0/4.4/5.4	50	30.4	19.6
Aliphatic PTMO75/DD-ionenes	1.0/1.2/2.2	75	12.8	12.2
Aliphatic PTMO93-ionenes	1.0/0/1.0	93	0	7
DABCO-based PTMO25/DD-ionenes	1.0/15.8/16.8	25	55	20
DABCO-based PTMO50/DD-ionenes	1.0/5.1/6.1	50	35.5	14.5
DABCO-based PTMO75/DD-ionenes	1.0/1.5/2.5	75	15.9	9.1
DABCO-based PTMO95-ionenes	1.0/0/1.0	95	0	5

4.4 Results and Discussion

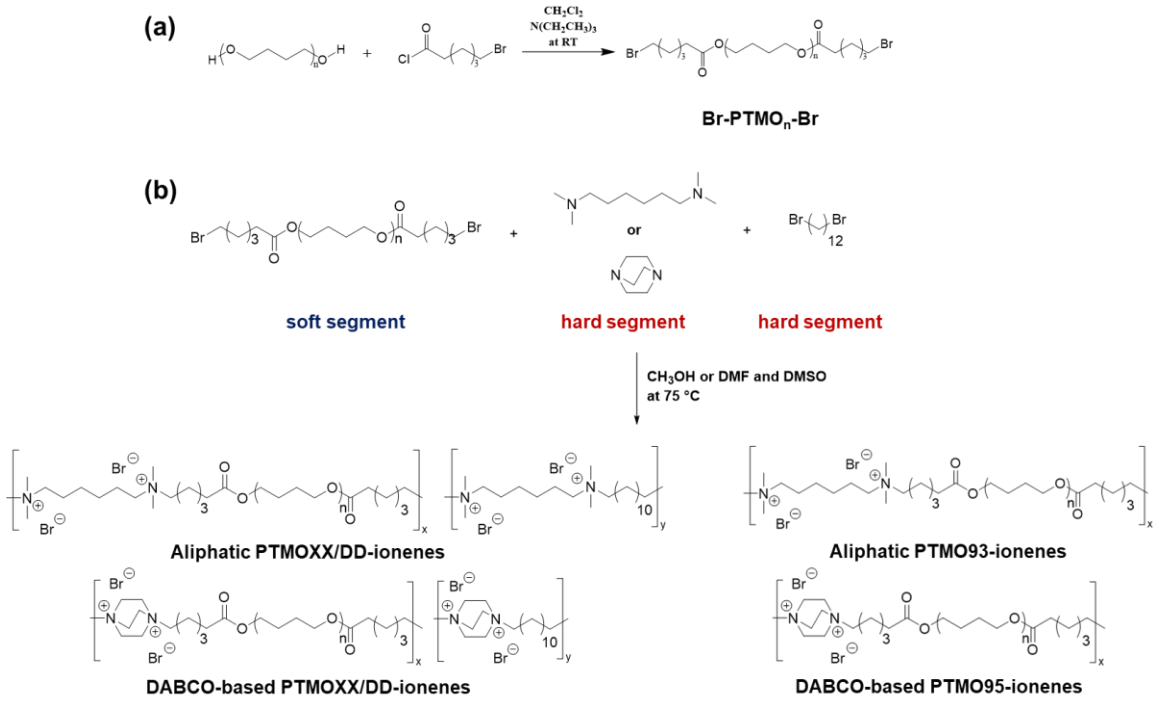

Scheme 4.2: The synthesis of (a) Br-PTMO$_n$-Br and (b) linear aliphatic PTMOXX/DD-ionenes or DABCO-based PTMOXX/DD-ionenes. XX refers to 25, 50, or 75, which corresponds to the overall weight fraction of the PTMO soft segment.

The desired linear aliphatic or DABCO-based PTMO-ionenes were synthesized via the Menshutkin reaction, as shown in Scheme 4.2. The Br-PTMO$_n$-Br was used as a soft segment, which is responsible for providing the material flexibility and softness. Two different hard segments, either a combination of 1,12-dibromododecane and *N,N,N',N'*-tetramethyl-1,6-hexanediamine (linear aliphatic ammonium) or a combination of 1,12-dibromododecane and DABCO (heterocyclic aliphatic ammonium) were used, which are responsible for the material stiffness and mechanical behavior. Br-PTMO$_n$-Br was prepared by reacting PTMO-2k with a slight excess of 6-bromohexanoyl chloride in the presence of triethylamine to obtain the difunctional bromide end-capped monomer. The

presence of the bromoalkyl functional group in PTMO oligomers was analyzed by ^{1}H NMR spectroscopy (the presence of the *n*, *o*, and *m* peaks and the ratio 0.97 of *p* to *m* confirmed the synthesis of Br-PTMO$_n$-Br, and more details can be found in Figure B1)

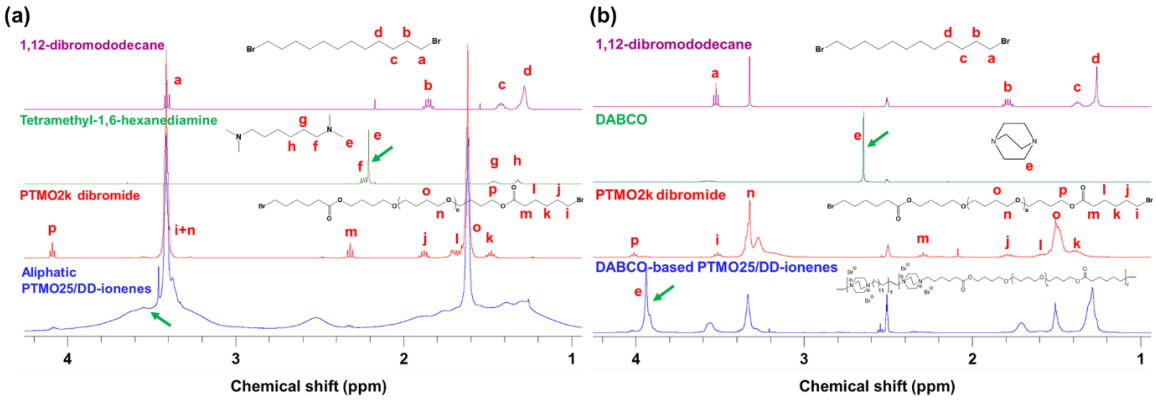

Figure 4.1: ^{1}H NMR spectra of 1,12-dibromododecane, tetramethyl-1,6-hexanediamine or DABCO, Br-PTMO$_n$-Br, and (a) linear aliphatic PTMO25/DD-ionenes in $CDCl_3$ and (b) DABCO-based PTMO25/DD-ionenes in DMSO-d_6 with labeled peaks corresponding to the respectively labeled protons.

PTMO-based segmented ionenes with two different hard segments were successfully synthesized and confirmed by ^{1}H NMR spectroscopy (Figure 4.1 and Figure B2). The peaks from all samples were broadened after polymerization, which indicates a relatively higher molecular weight of the polymer and was seen in our previous study of PEG-based ionenes.[27] The shift of resonance at 2.2 and 2.6 ppm in the ^{1}H NMR spectrum attributed to methylene protons of *N,N,N',N'*-tetramethyl-1,6-hexandiamine and DABCO, respectively, to 3.5 and 3.9 ppm, respectively, confirmed the quaternarization of the tertiary amines (green arrows). Because of differences in solubility, the linear aliphatic PTMO ionenes (Figure 1a) were analyzed in deuterated chloroform whereas the DABCO-based PTMO ionenes (Figure 1b) were analyzed in deuterated DMSO. The differing polymer-solvent interactions are responsible for the shifts in peak locations when comparing the two spectra.

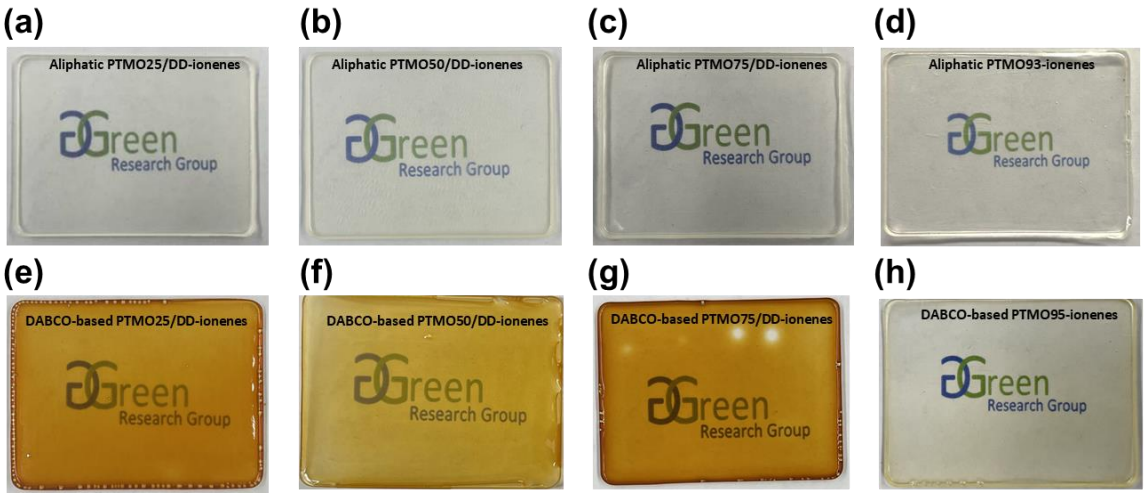

Figure 4.2: Photographic images of linear aliphatic PTMO (a) 25/DD-ionenes, (b) 50/DD-ionenes, (c) 75/DD-ionenes, and (d) 93-ionenes, and DABCO-based PTMO (e) 25/DD-ionenes, (f) 50/DD-ionenes, (g) 75/DD-ionenes, and (h) 95-ionenes.

All PTMO-based ionenes with linear aliphatic and DABCO hard segments made robust films regardless of the contents of soft/hard segments, as shown in Figure 4.2. Generally, the estimation of the molecular weight of ionenes is challenging if an appropriate GPC column is not available due to the possible ionic interactions with the column as well as the complicated solution conformation of ionenes.[28] The absolute molecular weight of ionenes can be achieved with SEC that is coupled with multi-angle laser light scattering, but again this is dependent on the assumption of athermal solution conditions.[3] In present work, the synthesis reaction time and solvent concentration were controlled precisely, and it is presumed that segmented ionenes reached relatively high molecular weight by forming a decent elastomer. All samples were transparent, and DABCO-based PTMOXX/DD-ionenes created yellow-brown films as a final product, and DABCO-based PTMO95-ionenes had a faint yellow color. The mixture of DMF and DMSO was chosen as a polymerization solvent for the DABCO-based PTMOXX/DD-ionenes to achieve a higher

molecular weight of segmented ionenes. The DABCO-based PTMOXX/DD-ionenes dissolve well in DMSO but are less soluble in DMF, whereas the monomers dissolve well in DMF. However, DABCO-based PTMO95-ionenes synthesized without 1,12-dibromododecane hard segment dissolved well in DMF. Therefore, we suspect the use of DMSO and, to a lesser extent, DMF was responsible for the color in the DABCO-based PTMOXX/DD-ionenes. Linear aliphatic and DABCO-based PTMOXX/DD-ionenes were re-casted in MeOH and DMSO, respectively, in a Teflon mold, and all samples had ~0.5 mm thickness.

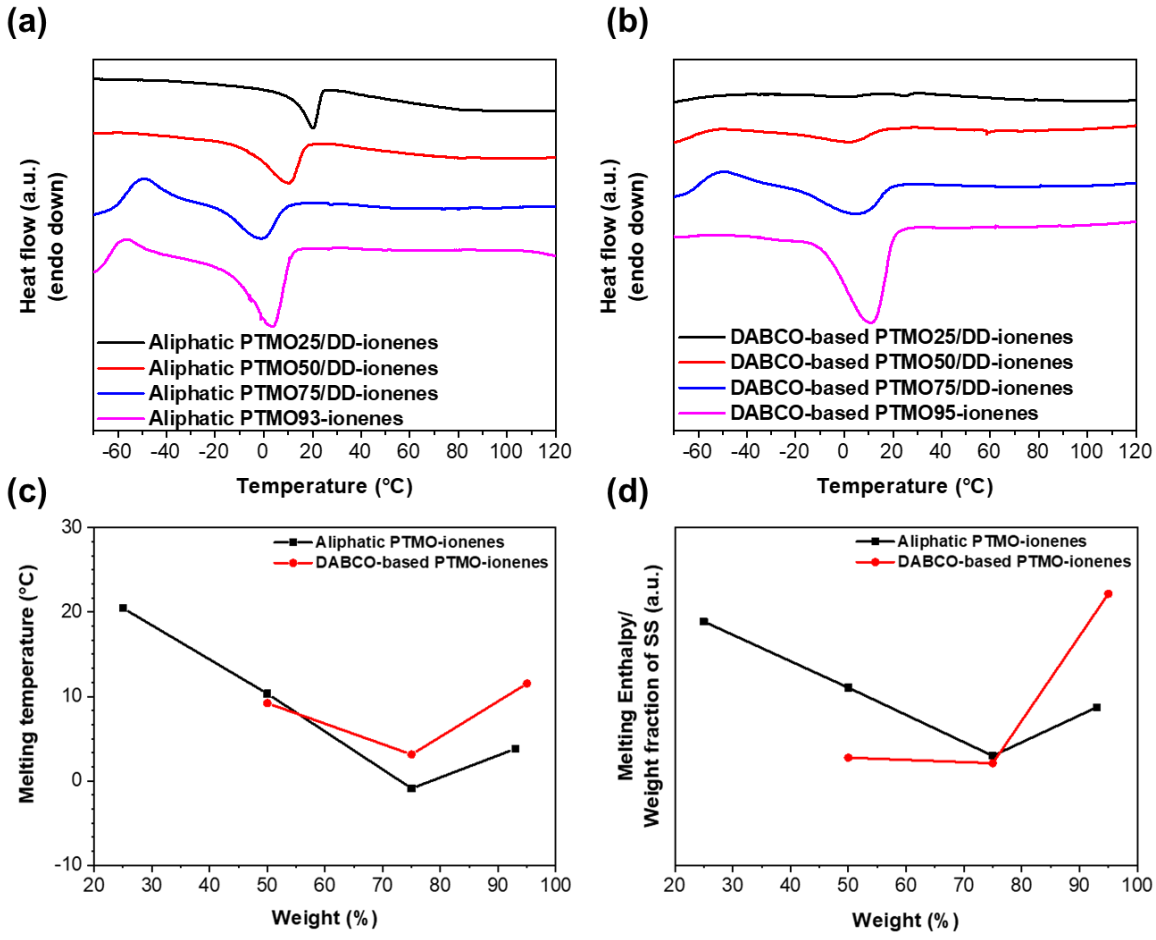

Figure 4.3: DSC results of (a) linear aliphatic and (b) DABCO-based PTMO ionenes. DSC also determined (c) melting temperature, and (d) degree of crystallization by dividing

the value of melting enthalpy by the weight fraction of PTMO soft segment of linear aliphatic and DABCO-based PTMO ionenes. The weight (%) on the x-axis corresponds to the weight fraction of PTMO soft segments.

Thermal transitions of linear aliphatic or DABCO-based PTMO ionenes were studied by using DSC, as shown in Figure 4.3. All samples except DABCO-based 25/DD-ionenes, which had a negligible melting temperature, displayed a melting temperature lower than room temperature. Linear aliphatic and DABCO-based PTMO50/DD-ionenes and 75/DD-ionenes showed similar melting temperatures, which indicates a negligible effect of the structure of hard segment type on melting temperature of PTMOXX/DD-ionenes. The decrease of melting temperature with increasing the soft segment fractions up to 75 wt% was observed in both linear aliphatic and DABCO-based ionenes. This is possibly attributed to a decrease in the degree of crystallization of the PTMO soft segment. However, a further increase of the content of the soft segment over 75 wt% resulted in the increase of the melting temperature in which DABCO-based PTMO 95-ionene showed the highest melting temperature among DABCO-based PTMO ionenes. The heterocyclic aliphatic ammonium without dodecane hard segment provided better configurational freedom of PTMO soft segments to be crystallized than the linear aliphatic ammonium, and thus increased the melting temperature. The linear aliphatic PTMO93-ionene also showed an increase in the degree of crystallization by increasing the content of the soft segment from 75 wt% to 93 wt%; however, it was not significant compared to the DABCO hard segment. This revealed that alternating soft/hard segments might crystallize better than randomly distributed soft/hard segments regardless of the type of structure of hard segment, and the heterocyclic aliphatic structure (i.e., DABCO) induced better chain packing than linear aliphatic hard segment. Moreover, the incorporation of relatively long aliphatic

hydrocarbons present in 1,12-dibromododecane and *N,N,N',N'*-tetramethyl-1,6-hexanediamine hard segments possibly restricted chain mobility of PTMO-based ionenes. In fact, the absence of the dodecane hard segment induced a higher degree of crystallization of the PTMO soft segment of the DABCO-based PTMO95-ionene compared to the linear aliphatic PTMO93-ionene as shown in Figure 4.3d. The melting peaks for both the linear aliphatic and DABCO-based PTMOXX/DD-ionenes broaden with an increasing content of the soft segment. It is suspected that increasing the PTMO soft segment content caused a heterogeneous size distribution of spherulites with both linear aliphatic and DABCO hard segments when dodecane was present. Ultimately, this caused loose chain packing and decreased the degree of crystallinity (Table B1). However, further increase in the content of the soft segment without the presence of dodecane hard segments (i.e., 93% samples) resulted in a more homogeneous size distribution of crystallites and caused the increase in the degree of crystallinity. The presence of the cold crystallization was observed with ionenes containing higher contents of PTMO soft segments, as indicated by an exotherm attributed to the rearrangement of the PTMO soft segment from a disordered state to a loose chain packing. For example, over 50 wt% and 25 wt% of the soft segment for PTMO-based ionenes with linear aliphatic and DABCO hard segments, respectively, showed the cold crystallization although it was not observed with DABCO-based PTMO95-ionenes.

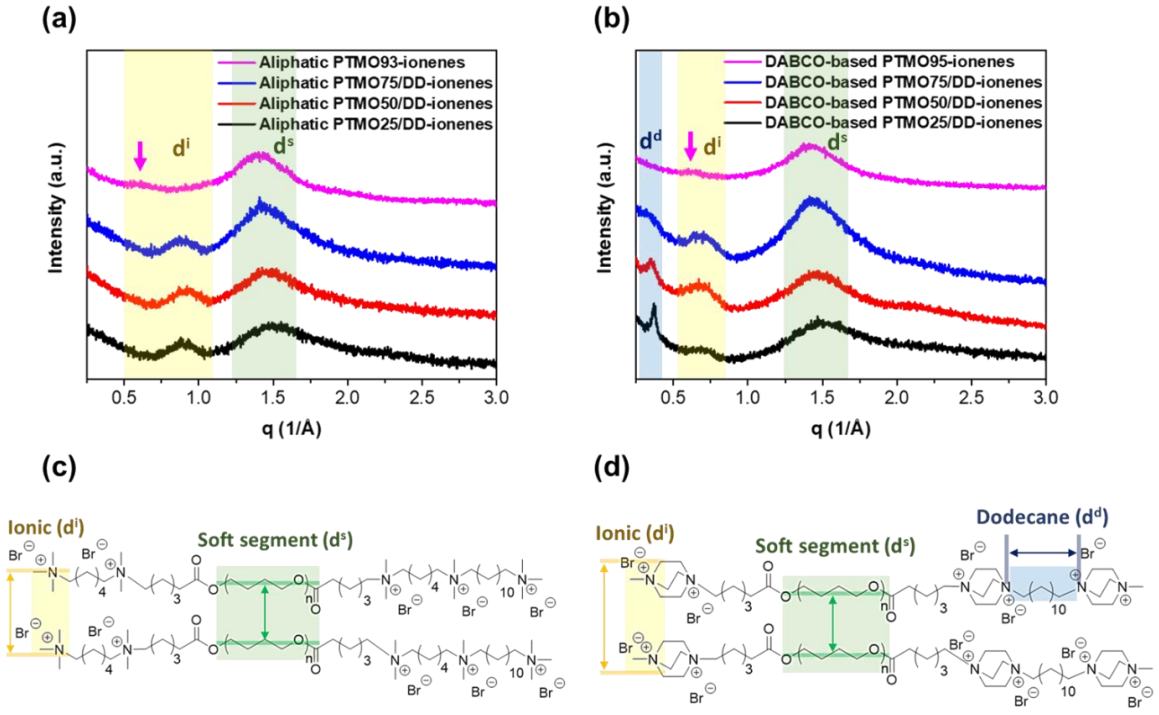

Figure 4.4: Overlayed XRD diffraction of (a) linear aliphatic PTMO ionenes and (b) DABCO-based PTMO ionenes. Schematic of characteristic length scale of (c) linear aliphatic PTMO ionenes and (d) DABCO-based PTMO ionenes, where $d^x = 2\pi/q^x$ and x is PTMO soft segment (s), ionic (i), or dodecane (d).

The local structure within the ionenes was confirmed with XRD. Because PTMO crystallites have a melting temperature below room temperature all of the PTMO-based ionenes were amorphous at room temperature, as shown in Figure 4.4. Our previous study of similar PEG-based segmented ionenes showed two prominent peaks for the PEG soft segment, which had a melting temperature higher than room temperature, but this also created a brittle material at room temperature.[27] However, PTMO soft segments undergo less crystallization compared to PEG soft segments and show flexible features at room temperature. The Br-PTMO$_n$-Br monomer showed two prominent sharp peaks (q = 1.47 and 1.78 Å^{-1}) from the PTMO crystallites (Figure B3) at room temperature; however, the PTMO soft segment of PTMO-based ionenes showed a broad amorphous halo. Two or

three distinct peaks were observed for linear aliphatic versus DABCO-based PTMO-ionenes, respectively. The peaks below 0.5 $Å^{-1}$ were referred to as dodecane peaks (q^d), the peaks at 0.5–1 $Å^{-1}$ were referred to as ion-to-ion peaks (q^i), and peaks at 1–2 $Å^{-1}$ were attributed to PTMO-to-PTMO peaks (q^s). The idealized schematic of contributions to q_d, q_i, and q_s are shown in Figure 4.4c and 4.4d. The PTMO-based ionenes with soft segment fractions from 25-75 wt% showed two broad peaks (ca. q = 0.91 $Å^{-1}$ (d^i = 0.69 nm) and q = 1.46 $Å^{-1}$ (d^s = 0.43 nm) for linear aliphatic ionenes, and ca. q = 0.68 $Å^{-1}$ (d^i = 0.92 nm) and q = 1.46 $Å^{-1}$ (d^s = 0.43 nm) for DABCO-based ionenes) as shown in Table 4.2. The highest soft segment fractions showed slightly different behavior with peaks at ca. 0.62 $Å^{-1}$ (d^i = 1.01 nm) and 1.41 $Å^{-1}$ (d^s = 0.44 nm) for both linear aliphatic PTMO93 and DABCO-based PTMO95-ionenes. The linear aliphatic PTMO ionenes with soft segment fractions from 25-75 wt% showed a higher value of d^i compared to DABCO-based ionenes possibly due to the rigid heterocyclic structure of DABCO. DABCO-based PTMOXX/DD-ionenes showed an additional peak at ca. q = 0.37 $Å^{-1}$ (d^d = 1.69 nm), presenting the periodicity between DABCO units when the dodecane hard segments were introduced. A similar observation was made by Williams and coworkers for an imidazolium-based ionene wherein the periodicity between imidazolium ions resulted in a similar peak.[18] In fact, DABCO-based PTMO95-ionenes exhibited no diffraction peak in this region due to the absence of dodecane hard segments (spacer), however; the peak became narrower with increasing dodecane fractions. Linear aliphatic PTMOXX/DD-ionenes did not show d^d due to two possible reasons: i) linear aliphatic-dodecane chains are more randomly distributed compared to DABCO-dodecane chains, or ii) linear aliphatic hard segment has a lower

electron density contrast compared to DABCO hard segment. A combination of the two is probable since the DABCO ion has less conformational freedom; therefore, a more uniform periodicity of groups with a higher electron density relative to the polymer matrix would produce the scattering peak observed. Salas de la Cruz et al. observed similar effects in the scattering profiles of polyelectrolytes with varying electron density differences.[29] The d-spacing in the amorphous halo from the PTMO soft segments, d^s, were similar regardless of the type of hard segment and the presence of the spacer.

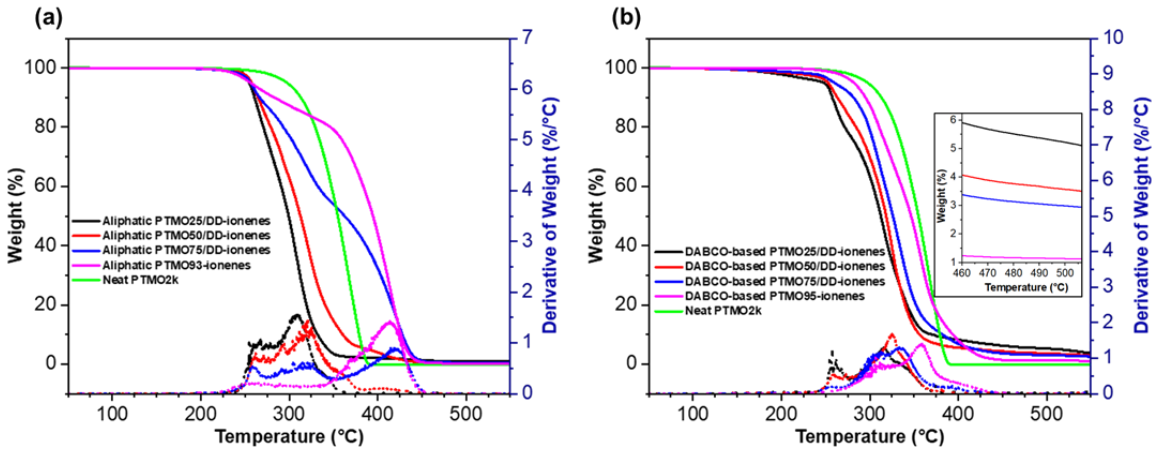

Figure 4.5: Overlayed TGA curves (solid lines) and derivative weight loss curves (dashed lines) for (a) linear aliphatic PTMO ionenes and (b) DABCO-based PTMO ionenes.

The thermal stability of PTMO-based ionenes was studied using TGA under a nitrogen atmosphere, as shown in Figure 4.5. The thermal stability depends on the content of the soft segment, mutual interaction between degradation of soft/hard segment, and degree of phase separation.[30–32] Linear aliphatic and DABCO-based PTMO-ionenes showed thermal stability ($T_{d5\%}$) up to ca. 250 °C, and DABCO-based PTMO-ionenes showed a clear gradual increase of thermal stability from 247 °C to 281 °C by increasing the content of the soft segment from 25-95 wt% (Table 4.2). Whereas, linear aliphatic PTMO-ionenes

showed slightly higher thermal stability with higher content of soft segment compared to 25 wt%; however, it was not significant. The PTMO-based ionenes possessing higher amounts of DABCO hard segments showed higher char residue at ca. 500 ºC compared to linear aliphatic ionenes, as shown in Figure 4.5b. This was shown with similar PEG-based ionenes that may be attributed to the crosslinking of DABCO hard segment and revealed that char formation in DABCO-based ionenes is not affected by the type of soft segment.[27] Ionenes and other molecules containing quaternary ammoniums have similar degradation pathways including nucleophilic substitution and/or Hoffman elimination reaction, which, in the case of ionenes, are dependent on the counterion present in the hard segment. The two-step weight loss of all ionenes is clearly shown in the derivative of the weight curve. The first weight loss corresponded to the hard segment, and the value of the derivative of weight increased with decreasing the soft segment content. The linear aliphatic ionenes with over 50 wt% of PTMO soft segment clearly showed a different degradation trend than DABCO-based ionenes analogs against neat PTMO2k. In fact, the linear aliphatic ionenes exceeded the degradation temperature of neat PTMO2k with over 50 wt% of PTMO soft segment at elevated temperatures (ca. 400 °C). This suggests that DABCO has a weaker protective effect against the degradation of PTMO soft segments compared to the linear aliphatic hard segment.

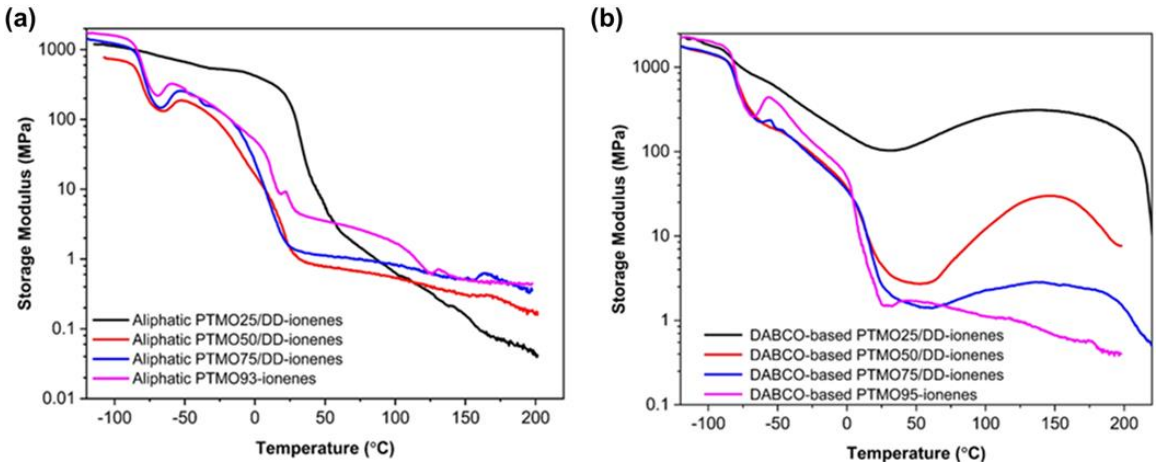

Figure 4.6: Overlayed DMA results of (a) linear aliphatic PTMO ionenes and (b) DABCO-based PTMO ionenes.

The viscoelastic properties of PTMO-based ionenes were analyzed using DMA. The first transition is attributed to the segmental motions of PTMO soft segments, and as can be seen in Figure 4.6, the T_g value is ca. -70 °C for all samples regardless of the hard segment type and this value is within the range of the T_g of pure PTMO. This revealed the presence of phase separation in the PTMO-based ionenes regardless of the type of hard segments. At the end of the glass transition region, a cold crystallization occurred in linear aliphatic and DABCO-based ionenes for soft segments over 25 wt% and 50 wt%, respectively, which was observed with the DSC data. However, the inconsistency between DSC and DMA results of the weight fraction at which the cold crystallization appears is likely due to the different thermal history of PTMO-based ionenes. The presence of higher amounts of crystallites in the samples by reducing the spacer content was reflected in an increase of the glassy modulus.

The third transition describes the melting temperature of PTMO crystallites that caused a significant decrease in storage modulus. The DABCO-based PTMO25/DD-ionene

showed the most negligible loss of storage modulus among all PTMO-based ionenes due to the absence of crystallization and the presence of ionic domains. The rubbery plateau was observed for DABCO-based PTMOXX/DD-ionenes, and the DABCO-based PTMO25/DD-ionene showed the broadest plateau as well as the highest rubbery plateau storage modulus among the samples due to the high charge density and ionic aggregation. The physical cross-linking effect was notable in DABCO-based PTMO25/DD-ionene compared to its linear aliphatic counterpart, according to a higher value of its plateau modulus (i.e., 100 MPa). This also suggested that DABCO-based PTMO25/DD-ionene had a higher degree of microphase separation. In fact, Feng et al. speculated that the more aliphatic character of hard segments promotes poorer phase separation than aromatic hard segment structures.[12] Furthermore, DABCO hard segments have shown better chain packing than aromatic hard segments resulting in a higher rubbery plateau.[13] It is worth mentioning that an overshoot occurred in the storage modulus of DABCO-based PTMO50/DD-ionenes after the melting of crystallites. This can be due to the chain packing of hard segments after rearrangement of the structure that changed the conformation of ionic domains.

The fourth transition occurred following ion dissociation and the onset of viscous flow in the PTMO-based ionenes. The linear aliphatic PTMO ionenes showed a weak fourth transition due to the weak ionic aggregation at temperatures between 125-175 ˚C compared to DABCO-based ionenes, which flowed at higher temperatures between 150-220 °C. The DABCO-based PTMO25/DD-ionene showed the highest ion dissociation temperature (~215 °C) due to the highest content of hard segment and the nature of higher positive

charge density and better proximity of charged sites, which appeared as a significant increase in tan delta curve (Figure B4) due to the softening of higher fraction of DABCO hard segments.

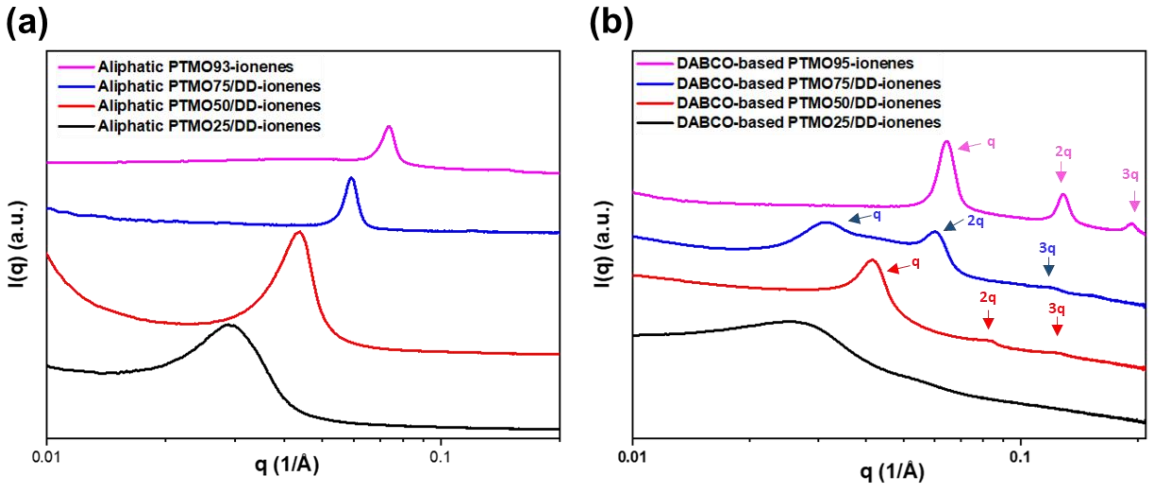

Figure 4.7: SAXS intensity as a function of scattering vector (q) of (a) linear aliphatic PTMO ionenes and (b) DABCO-based PTMO ionenes.

SAXS experiments can be used to investigate the microstructure of segmented block polymers based on the electron density difference between the different domains.[12] The covalent bond between the soft and hard segments prevents macrophase separation, but, still, due to different chemical components the two blocks formed segregated structures. Therefore, periodic microphase separation happens in the nanometer scale (1-100 nm). The Bragg spacing (d, or interdomain spacing) can be calculated using the value of the scattering vector (q) according to the following equation, where q1 is the value of the scattering vector at the maximum of the first peak ($d= 2\pi/q1$).

Table 4.2: Characteristic dimensions of the soft and hard domains, and thermal stability as determined by XRD, SAXS, and TGA. Superscripts d (dodecane), i (ionic), and s (soft segment) correspond to blue, yellow, and green shades in the XRD data, respectively, shown in Figure 4.

Sample	SAXS		XRD					TGA
	q1	d	d^d	d^i	$FWHM^i$	d^s	$FWHM^s$	$T_{d5\%}$

	(nm^{-1})	(nm)	(nm)	(nm)	(°)	(nm)	(°)	(°C)
Aliphatic PTMO25/DD-ionenes	0.29	21.66	-	0.69	2.88	0.43	7.92	254
Aliphatic PTMO50/DD-ionenes	0.43	14.61	-	0.68	3.02	0.43	6.53	257
Aliphatic PTMO75/DD-ionenes	0.59	10.65	-	0.71	2.72	0.43	6.05	256
Aliphatic PTMO93-ionenes	0.73	8.6	-	0.99	1.91	0.45	5.69	256
DABCO-based PTMO25/DD-ionenes	0.25	25.13	1.69	0.91	2.28	0.42	8.63	247
DABCO-based PTMO50/DD-ionenes	0.41	15.32	1.79	0.92	3.61	0.43	6.18	252
DABCO-based PTMO75/DD-ionenes	0.31	20.26	1.96	0.92	3.38	0.43	6.08	259
DABCO-based PTMO95-ionenes	0.64	9.8	-	1.01	2.31	0.44	5.40	281

The higher fraction of ionic hard segments increases the strength of Coulombic interactions and results in PTMO chain stretching between the ionic hard segments.[33] The decrease of q values as the content of the hard segment increases indicated an increase in the spacing of hard domains (an increase of microdomain spacing) by stretching the PTMO chains (Figure 4.7). Indeed, the largest d-spacing values (interdomain spacing) were observed for linear aliphatic and DABCO-based PTMO25/DD-ionenes at 21.66 nm and 25.31 nm, respectively (Table 4.2). Moreover, both PTMO-based ionenes with 25 wt% of soft segment showed the broadest peak among other fractions, resulting from the existence of a distribution of spacings attributed to the possible different degrees of the ordering. The polymers synthesized without any dibromododecane (i.e., linear aliphatic PTMO93 and DABCO-based PTMO95-ionenes) decreased the d-spacing to 8.6 nm (single broad peak) and 9.8 nm (lamellar morphology) for linear aliphatic PTMO93 and DABCO-based PTMO95-ionenes, respectively.

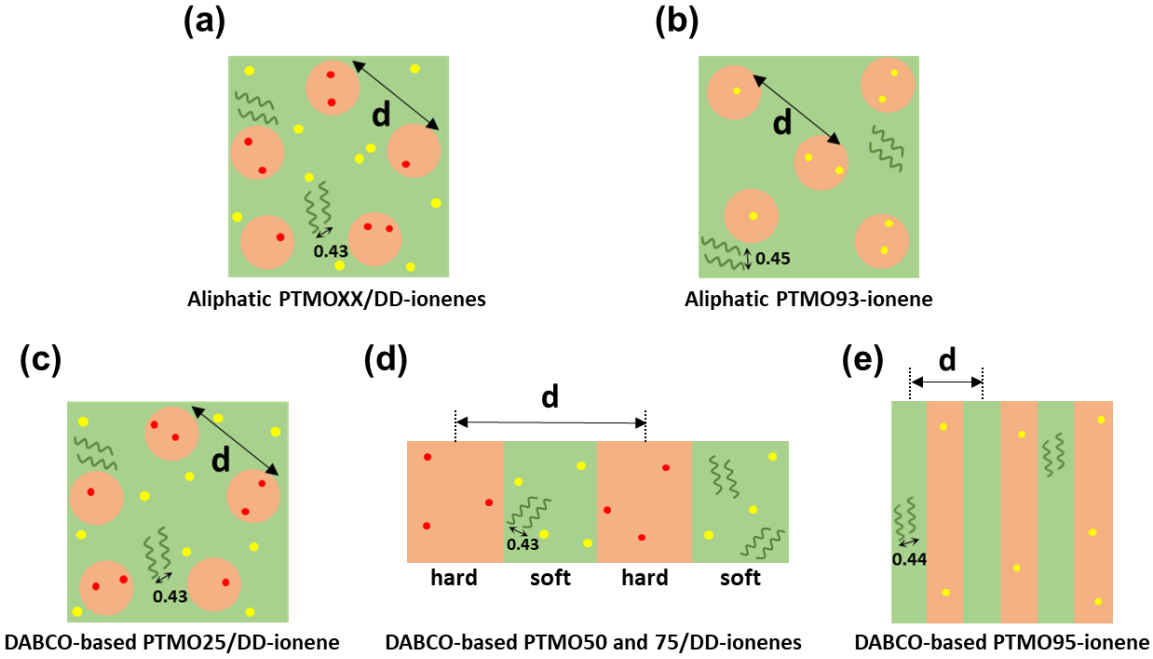

Figure 4.8: Schematic of the proposed morphology of (a) linear aliphatic PTMOXX/DD-ionenes, (b) linear aliphatic PTMO93-ionene, (c) DABCO-based PTMO25/DD-ionene, (d) DABCO-based PTMO50 and 75/DD-ionenes, and (e) DABCO-based PTMO95-ionene according to X-ray scattering results. Orange and Green colors represent the hard and soft domains, respectively. Circular red and yellow dots represent ion aggregates connected with and without dodecane, respectively.

The observation of a single and broad X-ray scattering peak is attributed to a spherical aggregation of ionic segments and a poorly ordered structure in the SAXS profiles of the linear aliphatic PTMO ionenes. In contrast, a sharp primary scattering peak accompanied by multiple scattering peaks for the DABCO-based ionenes indicates the existence of an ordered structure. Differing morphologies between DABCO-based and linear aliphatic ionenes could be due to the architectural difference of hard segments. Interestingly, the position of scattering maximums for DABCO-based PTMO ionenes with over 25 wt% of soft segment appeared at the ratio of 1:2:3 (i.e., q:2q:3q in Figure 7b) that represents the

formation of microphase separated lamellar structure. The intensity of the second-order peak decreases significantly in the case of DABCO-based PTMO50/DD-ionenes, suggesting a combination of lamellar structure and spherical ionic aggregates, while a fairly high intensity for the second and third-order peaks of DABCO-based PTMO95-ionenes showed an ordered lamellar structure. Disc-like aggregates are regarded as a lamellar type of structure and have been observed in block polymer systems.[34] Hashimoto et al. observed a disc-like lamellar structure using SAXS in a viologen hard segment and a PTMO soft segment.[22] This presents the possibility that DABCO-based PTMO75/DD-ionenes formed ordered lamellar structure with disc-like ionic aggregation. The proposed morphology of all PTMO-based ionenes based on X-ray scattering results are shown in Figure 4.8.

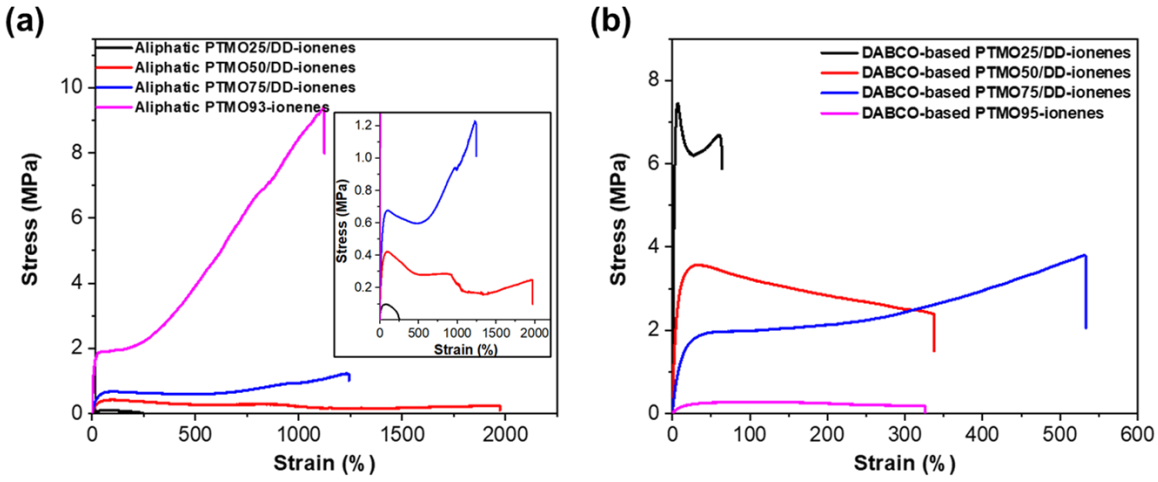

Figure 4.9: Tensile tests of (a) linear aliphatic PTMO ionenes and (b) DABCO-based PTMO ionenes at room temperature. The stress-strain curves shown are representative examples of replicate experiments.

Uniaxial tensile tests were performed at room temperature with both linear aliphatic and DABCO-based ionenes, as shown in Figure 4.9. PTMO-based ionenes with a linear aliphatic hard segment showed higher elongation than DABCO analogs (Table 4.3). The linear aliphatic PTMO50/DD-ionene showed the most promising elongation, ca. 2,070%,

among all the PTMO-based ionenes; however, increasing the content of the soft segment over 50 wt% decreased the elongation due to the stress-induced crystallization. It revealed that the stress-induced crystallization occurs effectively with over 50 wt% of PTMO soft segment, which caused an upturn in the stress-strain curve and provided high stress at break. This effect was significant for the linear aliphatic hard segment compared to the DABCO hard segment. The linear aliphatic PTMO93-ionene, PTMO75/DD-ionene, and DABCO-based PTMO75/DD-ionene displayed significant stress-induced crystallization of PTMO soft segment beginning at strains of ca. 100%, 500%, and 200%, respectively. Feng et al. showed a higher level of stress-induced crystallization with longer PTMO soft segments with pyridinium hard segments.[33] Schreiner et al. observed stress-induced crystallization of the PTMO soft segment at the PTMO molecular weight of 1,000 and 2,000 g mol^{-1}, but a PTMO molecular weight of 650 g mol^{-1} did not show the stress-induced crystallization with imidazolium hard segment.[3] In this work, the 25 and 50 wt% of PTMO (molecular weight 2000 g mol^{-1}) soft segment may not provide long enough soft segment to induce stress-induced crystallization.

Table 4.3: Tensile stress-strain data for linear aliphatic and DABCO-based PTMO ionenes at room temperature.

Sample	Young's Modulus (MPa)	Ultimate tensile strength (MPa)	Tensile strain at break (%)	Toughness (MPa)
Aliphatic PTMO25/DD-ionenes	0.444 ± 0.070	0.098 ± 0.005	261.34 ± 22.64	0.169 ± 0.015
Aliphatic PTMO50/DD-ionenes	1.249 ± 0.128	0.392 ± 0.082	2070.45 ± 137.98	5.302 ± 0.464
Aliphatic PTMO75/DD-ionenes	2.042 ± 0.202	1.539 ± 0.403	1414.58 ± 150.59	11.841 ± 2.566
Aliphatic PTMO93-ionenes	12.507 ± 1.160	8.901 ± 0.808	1140.8 ± 196.52	53.653 ± 11.408
DABCO-based PTMO25/DD-ionenes	231.469 ± 8.856	7.828 ± 0.477	63.051 ± 6.265	4.28 ± 0.278
DABCO-based PTMO50/DD-ionenes	43.065 ± 12.874	4.637 ± 2.462	335.66 ± 109.63	11.806 ± 4.299
DABCO-based PTMO75/DD-ionenes	10.157 ± 0.935	3.717 ± 1.028	509.411 ± 179.69	13.218 ± 6.246
DABCO-based PTMO95-ionenes	1.059 ± 0.078	0.287 ± 0.025	308.438 ± 50.42	0.743 ± 0.031

DABCO-based PTMOXX/DD-ionenes showed higher toughness compared to the corresponding linear aliphatic ionenes. The shorter hard segment chains extend first and cause a rapid stress increase.[35] The relatively short-chain and rigid heterocyclic structure of the DABCO hard segment induced a higher Young's modulus compared to the linear aliphatic hard segment. Young's modulus and ultimate tensile strength increased with decreasing soft segment content for DABCO-based ionenes due to the higher hard segment content, hence promoting better ionic aggregation. However, PTMO-based ionenes with linear aliphatic hard segments showed the opposite trend with increasing the hard segment content. This is possibly due to morphological differences, which will be further discussed below. The linear aliphatic PTMO93-ionene showed prominent stress-induced crystallization with high mechanical strength due to the high content of the soft segment, amorphous structure, and less degree of crystallization compared to the DABCO-based PTMO95-ionene, as shown by the DSC and XRD results (Figures 4.3 and 4.4 above). Register et al. suggested that the highly cohesive ionic aggregates do not rupture, induce the polymer chains to break, and thus fairly recover the original length, whereas weakly cohesive aggregates relax the stressed entanglements by ion hopping or pulling the ionic groups out of the aggregates.[36] It is noteworthy that DABCO-based ionenes snapped back to approximately their unstressed length after the break compared to the linear aliphatic ionenes, which implied that DABCO-based ionenes possessed higher cohesive ionic aggregates compared to linear aliphatic ionenes.

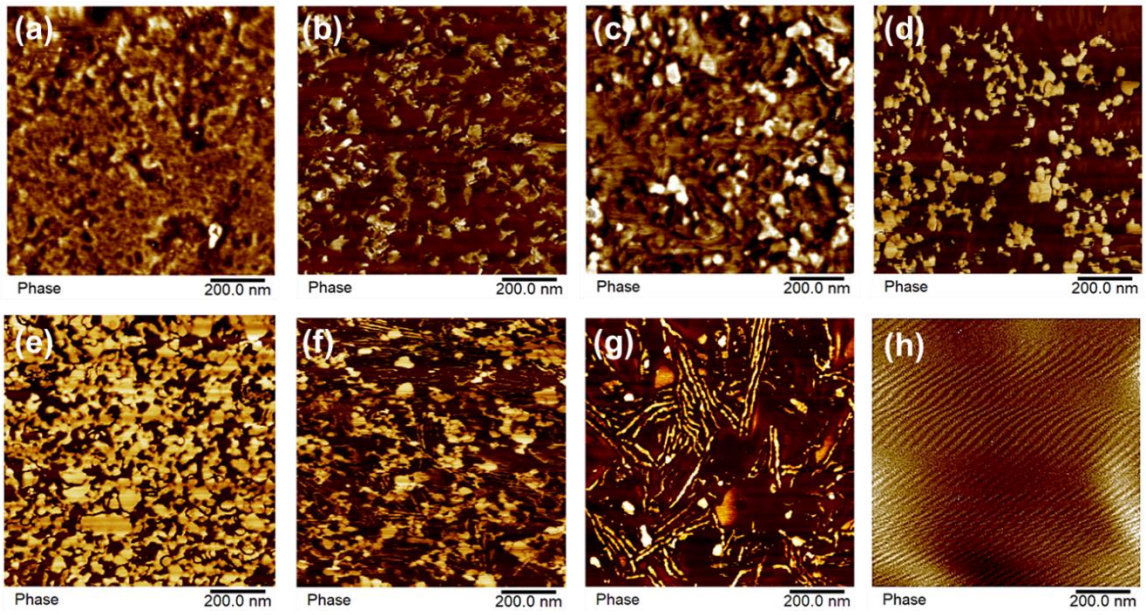

Figure 4.10: Microphase separation of linear aliphatic (a) PTMO25/DD-ionenes, (b) PTMO50/DD-ionenes, (c) PTMO75/DD-ionenes, and (d) PTMO93-ionenes, and DABCO-based (e) PTMO25/DD-ionenes, (f) PTMO50/DD-ionenes, (g) PTMO75/DD-ionenes, and (h) PTMO95-ionenes at room temperature revealed by atomic force microscopy.

The morphology of the linear aliphatic and DABCO-based PTMO ionenes was analyzed by using AFM at room temperature, as shown in Figure 4.10. The darker and brighter regions corresponded to the soft and ionic hard segments, respectively. DABCO-based ionenes with over 25 wt% of soft segments showed a relatively ordered lamellar structure compared to counterparts of linear aliphatic ionenes, which corroborated the SAXS results. All PTMO-based ionenes showed significant microphase separation regardless of the type of the hard segment. The linear aliphatic ionenes showed more interconnected hard domains with increasing soft segment content, whereas DABCO-based ionene hard segments were more isolated, at least on the film surface, as the soft segment content increased. Van Bogart et al. observed that changing the hard segment from rigid aromatic to more flexible aliphatic resulted in more interconnected morphology.[37] The opposite

trend of morphology between linear aliphatic PTMO-ionenes and DABCO-based ionenes confirmed the trend of tensile test results (Table 4.3) that linear aliphatic ionenes had lower Young's modulus and ultimate tensile strength with decreasing the soft segment content. As previously shown in SAXS results, DABCO-based PTMO50/DD-ionenes, PTMO75/DD-ionenes, and PTMO95-ionenes showed lamellar morphology, and it was more significant with increasing the content of the soft segment.

4.5 Conclusion

PTMO-based segmented ionenes with two structurally different hard segments and four different soft/hard segment contents were successfully synthesized via the Menshutkin reaction for the first time. All PTMO-based ionenes were thermally stable up to 250 °C. According to DSC results, the melting temperature gradually decreased with increasing the content of soft segments up to 75 wt% due to the decrease of the degree of crystallization. All PTMO-based ionenes displayed microphase separation regardless of the type of hard segments. DABCO-based PTMO ionenes induced a higher degree of phase separation compared to linear aliphatic analogs. Higher content of hard segment showed a better elastomeric behavior by having a higher rubbery plateau storage modulus and wider rubber plateau due to the strong ionic aggregation. XRD and SAXS revealed the spherical ionic aggregation in the linear aliphatic ionenes, whereas DABCO-based ionenes over 25 wt% of the soft segment exhibited an ordered lamellar structure, which was confirmed by AFM. The uniaxial tensile tests showed that the stress-induced crystallization occurred with higher contents of PTMO soft segment over 50 wt%, which prevents further elongation.

PTMO-based ionenes with the linear aliphatic hard segment showed a better elongation compared to DABCO-based ionenes at room temperature.

4.6 Acknowledgments

The authors wish to thank the Army Research Office (W911NF-18-1-0412 and W911NF-15-1-0353) and NASA (80NSSC18K1508) for financial support.

4.7 References

1. Gibbs, C. F., Littmann, E. R. & Marvel, C. S. Quaternary Ammonium Salts from Halogenated Alkyl Dimethylamines. II. The Polymerization of Gamma-Halogenopropyldimethylamines. *J. Am. Chem. Soc.* **55**, 753–757 (1933).
2. Rembaum, A., Baumgartner, W. & Eisenberg, A. Aliphatic ionenes. *J. Polym. Sci. Part B Polym. Lett.* **6**, 159–171 (1968).
3. Williams, S. R. & Long, T. E. Recent advances in the synthesis and structure–property relationships of ammonium ionenes. *Prog. Polym. Sci.* **34**, 762–782 (2009).
4. Kammakakam, I., O'Harra, K. E., Dennis, G. P., Jackson, E. M. & Bara, J. E. Self-healing imidazolium-based ionene-polyamide membranes: an experimental study on physical and gas transport properties. *Polym. Int.* **68**, 1123–1129 (2019).
5. Bara, J. E. & O'Harra, K. E. Recent Advances in the Design of Ionenes: Toward Convergence with High-Performance Polymers. *Macromol. Chem. Phys.* **220**, 1900078 (2019).
6. Liesen, N. T. *et al.* The influence of spacer composition on thermomechanical properties, crystallinity, and morphology in ionene segmented copolymers. *Soft Matter* **17**, 5508–5523 (2021).
7. Thankamony, R. L. *et al.* Preparation and characterization of imidazolium-PEO-based Ionene/PVDF(HFP)/LiTFSI as a novel Gel polymer electrolyte. *Macromol. Res.* **23**, 38–44 (2015).
8. Nakayama, Y. *et al.* Synthesis and Properties of Poly(ε-carprolactone)-based Poly(ester-urethane)s Having Quaternary Ammonium Groups. *J. Japan Inst. Energy* **93**, 916–920 (2014).
9. Tamami, M. *et al.* Poly(ethylene glycol)-based ammonium ionenes containing nucleobases. *Polymer (Guildf).* **54**, 1588–1595 (2013).
10. Lee, J. S., Hocken, A. & Green, M. D. Advances in the molecular design of ionenes

for a diverse range of applications. *Mol. Syst. Des. Eng.* **6**, 334–354 (2021).

11. Wu, F., Huang, C. L., Zeng, J. B., Li, S. L. & Wang, Y. Z. Synthesis and characterization of segmented poly(butylene succinate) urethane ionenes containing secondary amine cation. *Polymer (Guildf).* **55**, 4358–4368 (2014).

12. Feng, D., Venkateshwaran, L. N., Wilkes, G. L., Leir, C. M. & Stark, J. E. Structure-property behavior of elastomeric segmented PTMO–ionene polymers. II. *J. Appl. Polym. Sci.* **38**, 1549–1565 (1989).

13. Das, S. *et al.* Synthesis and Characterization of Novel Segmented Polyionenes Based on Polydimethylsiloxane Soft Segments. *J. Macromol. Sci. Part A* **47**, 215–224 (2010).

14. Somoano, R., Yen, S. P. S. & Rembaum, A. VI. Electronic conductivity of elastomeric ionenes. *J. Polym. Sci. Part B Polym. Lett.* **8**, 467–479 (1970).

15. Kohjiya, S., Ohtsuki, T. & Yamashita, S. Polyelectrolyte Behavior of an Ionene Containing Poly(oxytetramethylene) Units. *Makromol. Chemie, Rapid Commun.* **2**, 417–420 (1981).

16. Ikeda, Y. *et al.* One-pot synthesis and characterization of aliphatic poly(oxytetramethylene) ionene. *Polymer (Guildf).* **43**, 3483–3488 (2002).

17. Ikeda, Y., Yamato, J., Murakami, T. & Kajiwara, K. Aliphatic poly(oxytetramethylene) ionenes: effect of counter-anion on the properties and morphology. *Polymer (Guildf).* **45**, 8367–8375 (2004).

18. Williams, S. R., Salas-de la Cruz, D., Winey, K. I. & Long, T. E. Ionene segmented block copolymers containing imidazolium cations: Structure–property relationships as a function of hard segment content. *Polymer (Guildf).* **51**, 1252–1257 (2010).

19. Huang, Y., Pan, P., Shan, G. & Bao, Y. Polylactide-b-poly(ethylene-co-butylene)-b-polylactide thermoplastic elastomers: role of polylactide crystallization and stereocomplexation on microphase separation, mechanical and shape memory properties. *RSC Adv.* **4**, 47965–47976 (2014).

20. Ikeda, Y., Murakami, T., Yuguchi, Y. & Kajiwara, K. Synthesis and Characterization of Poly(oxytetramethylene) Ionene with 2,2‘-Bipyridinium Units. *Macromolecules* **31**, 1246–1253 (1998).

21. Rao, I. J. & Rajagopal, K. R. A study of strain-induced crystallization of polymers. *Int. J. Solids Struct.* **38**, 1149–1167 (2001).

22. Hashimoto, T. *et al.* Structure and properties of poly(tetrahydrofuran) viologen ionene: effects of halide counter-anions. *Polymer (Guildf).* **35**, 2672–2678 (1994).

23. Schreiner, C., Bridge, A. T., Hunley, M. T., Long, T. E. & Green, M. D. Segmented imidazolium ionenes: Solution rheology, thermomechanical properties, and electrospinning. *Polymer (Guildf).* **114**, 257–265 (2017).

24. Grassl, B., Mathis, A., Rawiso, M. & Galin, J.-C. Segmented Poly(tetramethylene oxide) Zwitterionomers and Their Homologous Ionenes. 3. Structural Study through SAXS and SANS Measurements. *Macromolecules* **30**, 2075–2084 (1997).

25. Hunley, M. T., England, J. P. & Long, T. E. Influence of Counteranion on the Thermal and Solution Behavior of Poly(2-(dimethylamino)ethyl methacrylate)-Based Polyelectrolytes. *Macromolecules* **43**, 9998–10005 (2010).

26. Abdulahad, A. I., Jangu, C., Hemp, S. T. & Long, T. E. Influence of Counterion on Thermal, Viscoelastic, and Ion Conductive Properties of Phosphonium Ionenes. *Macromol. Symp.* **342**, 56–66 (2014).

27. Lee, J. S., Taghavimehr, M., Montazami, R. & Green, M. D. Synthesis and characterization of Poly(ethylene glycol)-based segmented ionenes block copolymer with aliphatic or DABCO hard segments. *Polymer (Guildf).* **242**, 124543 (2022).

28. Matsumi, N., Sugai, K., Miyake, M. & Ohno, H. Polymerized Ionic Liquids via Hydroboration Polymerization as Single Ion Conductive Polymer Electrolytes. *Macromolecules* **39**, 6924–6927 (2006).

29. la Cruz, D. S. *et al.* Correlating backbone-to-backbone distance to ionic conductivity in amorphous polymerized ionic liquids. *J. Polym. Sci. Part B Polym. Phys.* **50**, 338–346 (2012).

30. Cakić, S. M., Ristić, I. S., Marinović Cincović, M. & Špírková, M. The effects of the structure and molecular weight of the macrodiol on the properties polyurethane anionic adhesives. *Int. J. Adhes. Adhes.* **41**, 132–139 (2013).

31. Princi, E. *et al.* On The Micro-Phase Separation in Waterborne Polyurethanes. *Macromol. Chem. Phys.* **210**, 879–889 (2009).

32. Cakić, S. M. *et al.* The waterborne polyurethane dispersions based on polycarbonate diol: Effect of ionic content. *Mater. Chem. Phys.* **138**, 277–285 (2013).

33. Feng, D., Wilkes, G. L., Lee, B. & McGrath, J. E. Structure-property behaviour of segmented poly (tetramethylene oxide)-based bipyridinium ionene elastomers. *Polymer (Guildf).* **33**, 526–535 (1992).

34. Arcos Hernandez, M. *et al.* Thermoresponsive Glycopolymers Based on Enzymatically Synthesized Oligo-β-Mannosyl Ethyl Methacrylates and N -Isopropylacrylamide. *Biomacromolecules* **22**, 2338–2351 (2021).

35. Smith, T. L. Strength of Elastomers. A Perspective. *Polym. Eng. Sci.* **17**, 129–143 (1977).

36. Register, R. A. *et al.* X-Ray Analysis of Ionomers. *ACS Symp. Ser.* **395**, 420–438 (1989).

37. Van Bogart, J. W. C., Gibson, P. E. & Cooper, S. L. Structure-property relationships

in polycaprolactone-polyurethanes. *J. Polym. Sci. Polym. Phys. Ed.* **21**, 65–95 (1983).

CHAPTER 5

EFFECT OF COUNTER-ANION SPECIES ON THE PROPERTIES AND MORPHOLOGY OF PEG OR PTMO-BASED SEGMENTED IONENES WITH ALIPHATIC OR DABCO HARD SEGMENT

To be published as: Lee, J.; Beyer, F. L.; Grim, B.; Green, M. D.

5.1 Abstract

Segmented ionenes with a direct comparison between the pairs of the type of soft and hard segment and counterions were investigated with PEG- and PTMO-based ionenes possessing two structurally different hard segments and three different counter-anion species. Counter-anion metathesis of the bromine counterion ionenes with tetrafluoroborate (BF_4) and bis(trifluoromethanesulfonyl)imide (TFSI) counter-anions was conducted. DSC and DMA revealed the increment of the glass transition temperature of the hard segment and enhanced ionic aggregation with decreasing the size of the counterion. TGA showed the increase in thermal stability with increasing the basicity of counter-anion in which Br^- counterion revealed the lowest thermal stability among counterions. DABCO hard segment and PTMO soft segment tailored a better degree of microphase separation compared to linear aliphatic hard segment and PEG soft segment, respectively, regardless of the type of counterions, confirmed by DMA and SAXS. DABCO-based PTMO ionenes suggested that increasing the size of the counterion induces higher chain repacking and degree of crystallization. The uniaxial tensile test supported the reduction of mechanical properties by increasing the size of the counterion due to the weaker ionic aggregation in agreement with DMA analysis. However, the morphological

differences between Br^- and BF_4^- in DABCO-based PTMO-ionenes arouse the increase of mechanical and viscoelastic properties with BF_4^- counterion.

5.2 Introduction

Ionenes are a class of ion-containing polymers that are synthesized via the Menshutkin reaction, which involves the reaction of tertiary diamines with dihalide through step-growth polymerization.[1] The discovery of ionenes was first reported in 1933 by Gibbs and co-workers.[2] Ionenes have recently gained significant attention due to their ability to regulate the charge density over ionomers, which shows unequal distributions of ionic groups within polymer chains, making their behavior challenging to predict.[3] Ionenes can be classified as cationic or anionic, depending on whether they possess positive or negative charges in their backbone, respectively. Furthermore, ionenes can be categorized as segmented ionenes[4–6] or non-segmented ionenes[7–9] based on their structure feature.

Segmented ionenes are characterized by alternating soft and hard segments along the backbone, which are formed by the polymerization of oligomeric spacers. The oligomeric spacers possess low glass transition temperature (T_g) between charge sites, resulting in excellent mechanical properties of segmented ionenes, which behave mechanically similarly to segmented polyurethane.[10] In contrast, non-segmented ionenes are typically brittle materials with poor mechanical properties, owing to their high charge density.[3] The nomenclature of non-segmented ionenes denotes the number of methylene units between diamine (x) and dihalide (y) monomers, i.e., x,y-ionenes.[11] Both segmented ionenes and non-segmented ionenes have been reported with various charged organic species, such as ammonium, phosphonium, and imidazolium.[12] Segmented ionenes also have been studied

with several oligomeric monomers, including poly(ethylene glycol) (PEG)[13], poly(tetramethylene oxide) (PTMO)[14], and polydimethylsiloxane (PDMS)[15].

The mechanical and thermal properties, as well as morphology, of ionenes, can be tailored by various factors, including the type and content of the soft and hard segments. Tamami et al. reported that poly(propylene glycol) (PPG)-based ionenes with aliphatic ammonium hard segment and Br^- counterion exhibited enhanced thermal stability with decreasing hard segment concentration, and increasing hard segment content led to higher rubbery plateau modulus due to increased physical crosslinks between ionene chains.[4] Vijayaraghavan et al. demonstrated through molecular dynamics simulations that decreasing PPG soft segment content increased the degree of microphase separation and local ionic aggregation.[16] Das et al. synthesized PDMS-based ionenes with DABCO hard segment and Br^- counterion and showed that the highest rubbery plateau modulus was achieved with the highest hard segment content, attained through decreasing the molecular weight of PDMS.[15] Additionally, the hard domains formed cylindrically packed regions consisting of packing of the hard segment and counterion pairs, attributed to incompatibility with the PDMS soft segment.

The type of counterion also greatly influences the properties of ionenes. In addition to molecular weight and chemical structure, the type of counterion has a significant impact on T_g. Hunley et al. showed that the ion exchange of Cl^- for larger counterions such as BF_4, PF_6, and TFSI, reduced T_g, while PF_6 counterion increased T_g due to hydrogen bonding interactions between the anion and cation.[17] Moreover, reducing the basicity of the anion increased the thermal stability of non-segmented ionenes, making them more resistant to

degradation through reverse Menshutkin reaction and Hofmann elimination mechanisms.[18] Long and co-workers synthesized non-segmented ionenes, 6,12-ionene and 12,12-ionene, with counter-anions of varying size.[19] The T_g increased with increasing the charge density and decreasing the size of the counterion (Br > BF_4 > TfO > TFSI) due to weaker ionic aggregation, and thermal stability increased from Br to TFSI. However, the structure-property relationship of segmented ionenes with different counterions has not been widely studied compared to non-segmented ionenes. Hashimoto et al. reported pyridinium-based PTMO segmented ionenes with different counter-anions (Cl, Br, and I). Ionenes with Cl^- counterion showed the highest T_g and degree of microphase separation than ionenes with Br and I, but all counterions exhibited an ordered lamellar morphology resulting from the rigid chemical structure of the viologen units.[20] Nevertheless, a further investigation involving a direct comparison of the chemical structure or type of soft/hard moiety with various counter-anions is necessary to fully understand and establish the properties and structure-property relationship of elastomeric segmented ionenes.

In the present study, we report on the synthesis of novel segmented ionenes with PEG or PTMO soft segments and two structurally different linear aliphatic or DABCO hard segments along with various counterions for the first time. Three different segmented ionenes, namely aliphatic PEG25/DD-ionenes, aliphatic PTMO25/DD-ionenes, and DABCO-based PTMO25/DD-ionenes, all with 25 wt% of soft segment and three different counter-anions comprising Br, BF_4, and TFSI. The thermal and mechanical properties of these segmented ionenes were characterized using differential scanning calorimetry (DSC), dynamic mechanical analysis (DMA), thermogravimetric analysis (TGA), and uniaxial

tensile analysis. Moreover, the probe of morphologies of these ionenes was conducted using X-ray diffraction (XRD), atomic force microscopy (AFM), and small-angle X-ray scattering (SAXS).

5.3 Experimental

5.3.1 Materials

Poly(ethylene glycol) (PEG) 2,000 g/mol, poly(tetrahydrofuran) (PTMO) 2,000 g/mol, *N,N,N',N'*-tetramethyl-1,6-hexanediamine (99%), 1,4-diazabicyclo[2.2.2]octane (DABCO) (≥99%), triethylamine (≥99.5%), 6-bromohexanoyl chloride (97%), dimethyl sulfoxide (≥99.9%), sodium tetrafluoroborate (98%), and dimethyl sulfoxide-d_6 were purchased from Sigma Aldrich. Chloroform-*d* was purchased from Alfa Aesar. 1,12-dibromododecane (>98%) and lithium bis(trifluoromethanesulfonyl)imide (>98%) were purchased from TCI America. Dichloromethane (DCM), dimethylformamide (DMF), isopropyl alcohol (IPA), and methanol (MeOH) were purchased from VWR Chemicals. Spectra/Por® 7 regenerated cellulose 1kD was purchased from Spectrum Laboratories. All materials were used as received except 1,12-dibromododecane, which was recrystallized in isopropyl alcohol.

5.3.2 Synthesis of PEG- or PTMO-based segmented ionenes with bromine counterion

Details of the synthesis of bromine end-capped PEG (Br-PEG$_n$-Br) or PTMO (Br-PTMO$_n$-Br) have been published elsewhere and will not be reiterated here.[21] Linear aliphatic PEG25/DD or PTMO25/DD-ionenes and DABCO-based PTMO25/DD-ionenes were synthesized in accordance with our previous work.[22,23] The resultant aliphatic PEG or PTMO25/DD-ionenes for anion exchange were dried at 60 °C for 2 d under vacuum,

and DABDO-based PTMO25/DD-ionenes for anion exchange was dried at 80 °C for 1 d and under vacuum at 80 °C for 1 d. Aliphatic PEG25/DD-ionenes and PTMO25/DD-ionenes with bromine counterion were dried under room temperature for 1 d, followed by drying at 60 °C for 1 d and at room temperature under vacuum for 1 d. DABCO-based PTMO25/DD-ionenes with bromine counterion were re-casted by dissolving in DMSO, followed by drying at room temperature for 4 d, drying at 80 °C for 2 d, and at room temperature under vacuum for 1 d.

5.3.3 Counteranion Metathesis

All aliphatic PEG25/DD-ionenes, aliphatic PTMO25/DD-ionenes, and DABCO-based PTMO25/DD-ionenes were counteranion exchanged to tetrafluoroborate (BF_4^-) bis(trifluoromethanesulfonyl)imide ($TFSI^-$) utilizing similar counteranion metathesis reaction. The excess sodium tetrafluoroborate or lithium bis(trifluoromethanesulfonyl)imide was dissolved in DI water (10 eq). All ionenes (1eq of *N,N,N',N'*-tetramethyl-1,6-hexanediamine or DABCO in ionenes) were dissolved in DI water. The dissolved ionene solution was added dropwise to the salt solution and yielded a precipitate. The solution was stirred for 24 hr at room temperature. The precipitate was washed with DI water three times and stirred in water for 24 hr at room temperature except for DABCO-based PTM25/DD-ionenes anion exchanged with $TFSI^-$. The precipitate was collected and dried at 60 °C under vacuum for 2 day. DABCO-based PTMO25/DD-ionenes anion exchanged with $TFSI^-$ was dried at 60 °C under vacuum for 1 day, dissolved in methanol, and dialyzed against methanol for 3 d. Then, rotovapped and dried at 60 °C

under vacuum for 2 day. All ionenes were dissolved in DMF and dried directly at 60 °C for 5 d followed by drying in vacuo at 60 °C and room temperature for 1 d each.

5.3.4 Characterizations

^{1}H NMR spectroscopic analyses were performed on Bruker Avance III 500 MHz NMR, and DMSO-d_6 was used for all ionene samples. DSC was performed on a TA instruments Q20. First, samples were heated from 40 °C to 160 °C, cooled down to -120 °C, and then heated up to 160 °C. The heating and cooling rates were both 10 °C/min, and samples were held isothermally for 10 min before each ramp. The DSC was cooled using liquid nitrogen filled into the internal reservoir of the manually operated quench cooling accessory. Argon was used as a purging gas with a gas flow rate of 50 mL/min. TGA was conducted on TA instruments TGA 5500. The sample was heated to 120 °C in 20 °C/min, cooled down to 40 °C in 20 °C/min, and heated up again to 600 °C in 10 °C/min. The samples were held isothermally for 10 min before each heating or cooling ramp. Ultra-high purity (UHP) nitrogen was used as a purging gas with a gas flow rate of 25 mL/min. XRD was performed on PANalytical X'Pert PRO MRD with nickel-filtered Cu Kα radiation source (λ = 1.54 Å), divergence slit 1/4º, anti-scatter slits 1/2º, 45 kV/40 mA, and 2θ = 3-60º at room temperature. A tensile test was conducted on Instron E3343 with a 20 mm/min of extension rate at room temperature. All samples were prepared with three dog-bone-shaped films using a die, ASTM D1708. AFM was conducted on Bruker MultiMode 8 using NCHV-A or ACSTA probe for tapping mode at room temperature. DMA was performed on a TA instruments Discovery HR-2 hybrid rheometer with a tension mode in a temperature range of -100 to 230 ˚C at a heating rate of 3 ˚C/min, a frequency of 1 Hz, and under 0.1% strain.

UHP nitrogen was used as a purging gas with a gas flow rate of 10 mL/min. SAXS was performed using a Xenocs "Xeuss X3-HR" camera and a Rigaku 007HF rotating anode X-ray generator. The generator was operated at 40 kV and 30 mA, and is equipped with a copper anode. After collimation with a focusing optic, the output is an intense beam of CuKα photons with wavelength (λ) 1.542 Å. This beam is further optimized by two slit apertures roughly 1.5 m apart. Two-dimensional (2-D) scattering data was measured using a Pilatus3R 300k hybrid photon counting detector positioned at sample-to-detector distances of 1800, 900, 370, and 150 mm. This configuration allows collection of SAXS data spanning an angular range of $0.004 \leq q \leq 1.8$ Å-1, where q is the magnitude of the scattering vector, the value of q is $4\pi \cdot \sin(\theta)/\lambda$, and 2θ is the scattering angle. Samples that were viscous liquids at room temperature were encapsulated in Scotch-brand Magic™ tape. All data were corrected for background scattering, placed on an absolute scale, and azimuthally averaged for analysis using Wavemetrics Igor Pro v8 and procedures available for download from Argonne National Laboratory.[24,25]

5.4 Results and Discussions

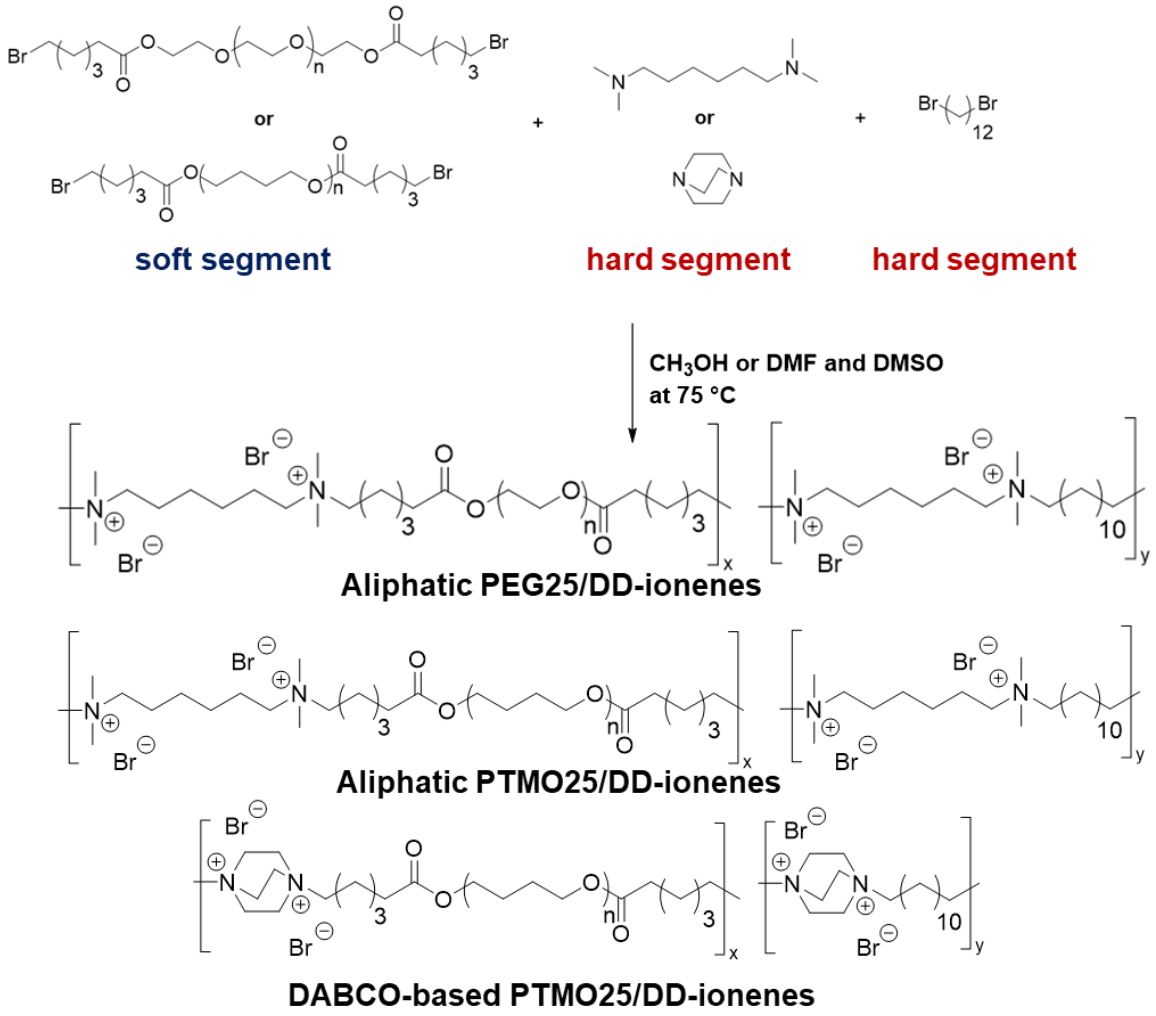

Scheme 5.1: The synthesis of aliphatic PEG25/DD-ionenes, PTMO25/DD-ionenes or DABCO-based PTMO25/DD-ionenes.

The linear aliphatic PEG25/DD-ionenes, PTMO25/DD-ionenes, and DABCO-based PTMO25/DD-ionenes were synthesized through the Menshutkin reaction depicted in Scheme 5.1. Methanol was employed as the polymerization solvent for linear aliphatic PEG25/DD-ionenes and PTMO25/DD-ionenes, while a mixture of DMF and DMSO was used for DABCO-based PTMO25/DD-ionenes to attain a higher molecular weight of segmented ionenes.[22] Previous research on segmented ionenes has demonstrated that a 25 wt% soft segment content exhibits better degrees of phase separation and ionic aggregation

than other soft segment contents, such as 50 and 75 wt%, regardless of the type of hard segment, whether linear aliphatic or DABCO.[22,23] Furthermore, PTMO soft segments resulted in a higher degree of ionic aggregation in both linear aliphatic and DABCO-based PTMO ionenes with a 25 wt% soft segment, as compared to PEG-based ionenes. Therefore, this study utilized 25 wt% PEG or PTMO soft segments with linear aliphatic or DABCO hard segments, as well as three different counter-anions, to further explore the effect of counterion on the properties of segmented ionenes.

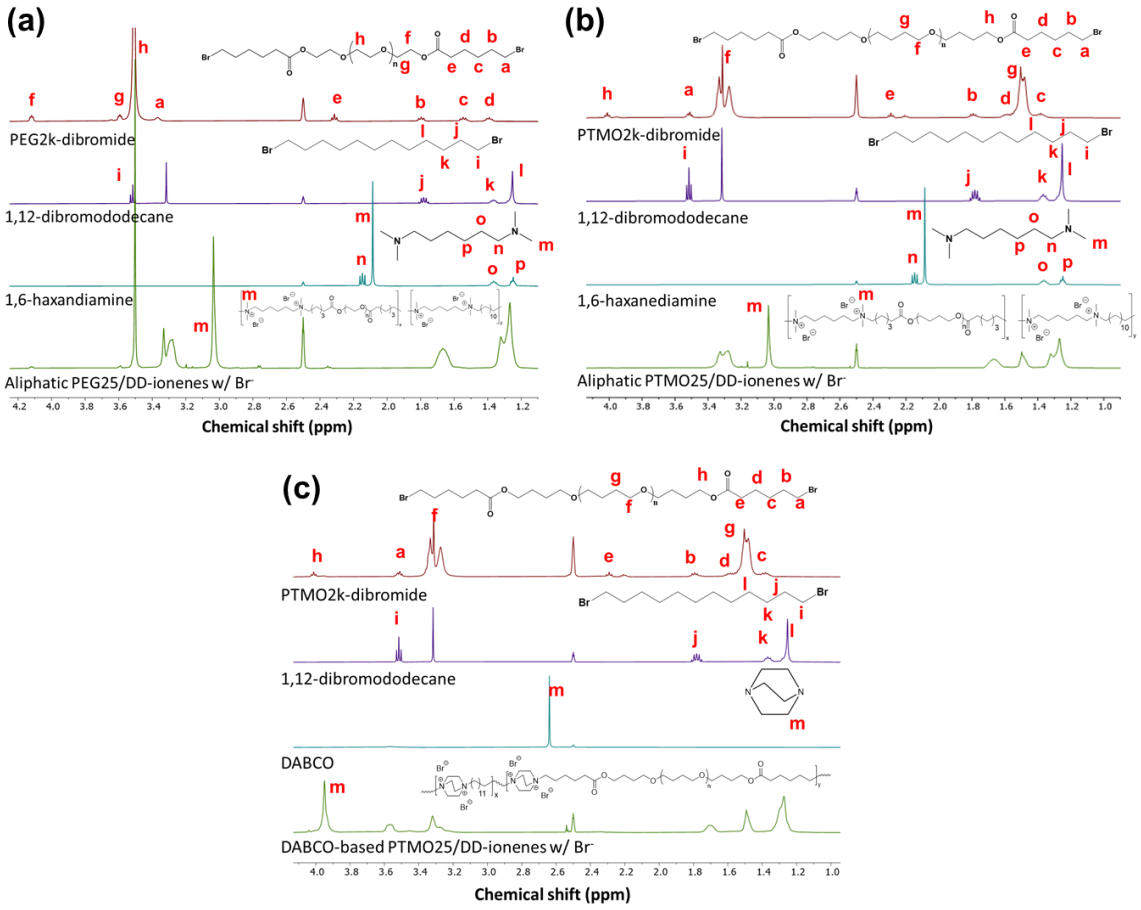

Figure 5.1: ^{1}H NMR spectra of Br-PTMO$_n$-Br or Br-PEG$_n$-Br, 1,12-dibromododecane, tetramethyl-1,6-haxanediamine or DABCO, and (a) aliphatic PEG25/DD-ionenes, (b) aliphatic PTMO25/DD-ionenes, and (c) DABCO-based PMTO25/DD-ionenes from the

top and bottom with labeled peaks corresponding to the respectively labeled protons. DMSO-d_6 was used for all samples.

PEG- or PTMO-based segmented ionenes were successfully synthesized with 25 wt% of a soft segment and two different hard segments, as confirmed by the ^{1}H NMR spectrum presented in Figure 5.1. The observed broadening of the peaks in all samples after polymerization is indicative of the relatively higher molecular weight of the polymer. Moreover, the absence and shift of the resonance at 2.0 and 2.6 ppm in the ^{1}H NMR spectrum, attributed to the methylene protons of *N*,*N*,*N*′,*N*′-tetramethyl-1,6-hexanediamine and DABCO, respectively, to 3.0 and 3.9 ppm, respectively, confirmed the quaternarization of the tertiary amines. Notably, all samples were analyzed in deuterated DMSO.

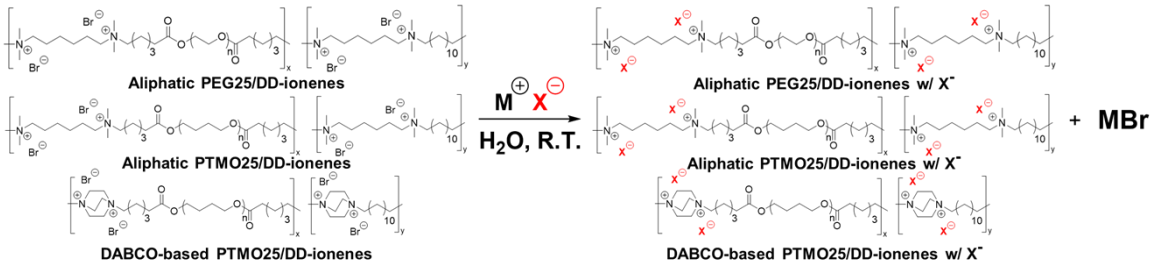

Scheme 5.2: Anion exchange of aliphatic PEG25/DD-ionenes, PTMO25/DD-ionenes, or DABCO-based PTMO25/DD-ionenes. MX refers to $NaBF_4$ and LiTFSI.

Counter-anion exchange of bromide with tetrafluoroborate (BF_4) and bis(trifluoromethane)sulfonimide (TFSI) anions was performed on synthesized linear aliphatic PEG25/DD-ionenes, PTMO25/DD-ionenes, and DABCO-based PTMO25/DD-ionenes, as shown in Scheme 5.2. Although the counter-anion exchange has been known to be done instantly, the samples were left stirring for 24 hours to ensure full exchange, followed by washing with DI water for an additional 24 hours since the short washing time was not sufficient to remove all residual $NaBF_4$ or LiTFSI, which was confirmed by XRD

showing multiple crystal peaks from residual $NaBF_4$ and LiTFSI. In particular, DABCO-based PTMO25/DD-ionene with $TFSI^-$ counterion was additionally purified using a dialysis bag for three days to fully remove the residual TFSI, as washing with DI water for 24 hours did not fully remove it. The resulting anion-exchanged ionenes were characterized using ^1H NMR spectroscopy (Figure C1-3). The anion metathesis from bromine to bulkier fluorinated counterions induced an upfield chemical shift of the methylene protons adjacent to quaternized cations.[18] The larger BF_4^- or $TFSI^-$ counterions compared to Br^- showed an upfield chemical shift to 2.98 ppm and 3.8 ppm, respectively, attributed to the methylene protons of *N,N,N′,N′*-tetramethyl-1,6-hexanediamine and DABCO. However, $TFSI^-$ counterion did not result in a more pronounced upfield shift than BF_4^-. Interestingly, the distinct separated peaks of the methylene protons of *N,N,N′,N′*-tetramethyl-1,6-hexanediamine and DABCO were observed with PTMO-based ionenes having $TFSI^-$ counterion. The integration ratio of the corresponding methylene protons of *N,N,N′,N′*-tetramethyl-1,6-hexanediamine and DABCO conjugated with Br^- and $TFSI^-$ counterions was 0.05 and 0.1, respectively. This suggests that Br counterions were not fully exchanged and remained with $TFSI^-$ counterions in PTMO-based ionenes and ionenes with DABCO hard segment showed relatively lower anion exchange than linear aliphatic hard segment. The prolonging of the anion metathesis time did not affect the degree of conversion.

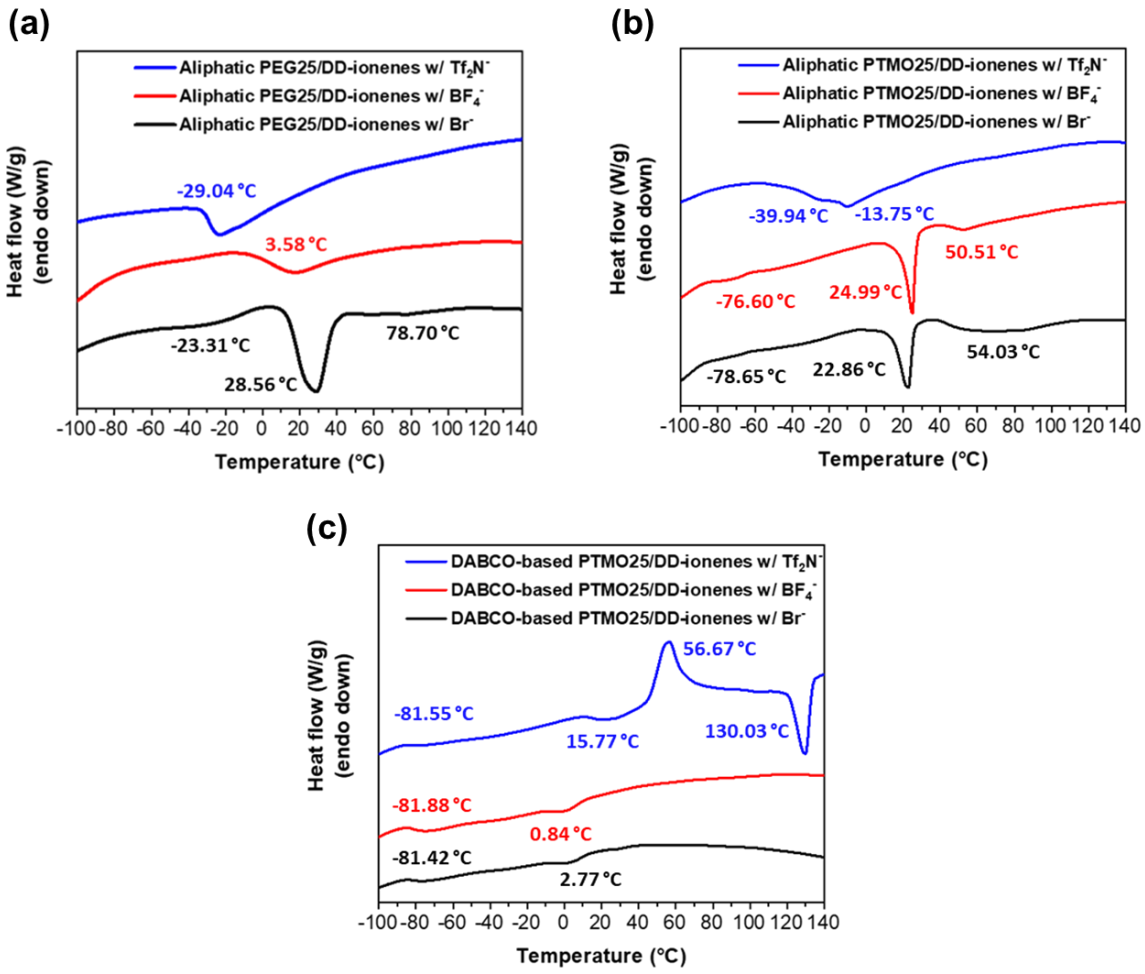

Figure 5.2: Overlayed DSC results of (a) aliphatic PEG25/DD-ionenes, (b) PTMO25/DD-ionenes, and (c) DABCO-based PTMO25/DD-ionenes with different counterion species.

The thermal transitions of linear aliphatic PEG25/DD-ionenes, PTMO25/DD-ionenes, and DABCO-based PTMO25/DD-ionenes with associated counter-anion species were investigated using DSC, as demonstrated in Figure 5.2 obtained from the second heating run, while the first heating run was utilized to erase thermal history. The PEG-based ionenes with linear aliphatic hard segment and Br^- counterion exhibited glass transition temperature (T_g) of soft and hard segments at ca. -23 °C and 78 °C, respectively, as well as a melting temperature (T_m) of ca. 28 °C, as presented in Table 5.1. However, exchanging

the counterion to BF_4 and TFSI induced the absence of a melting temperature and a sole T_g. This observation suggests that larger counterions caused phase mixing and amorphous morphology of PEG-based ionenes with a linear aliphatic hard segment.

Table 5.1: Characteristic dimension of ionenes as determined from DSC and TGA analysis. The values not detected from DSC were marked with a dash line. $T_{g,ss}$ and $T_{g,hs}$ refer to the glass transition of soft and hard segments, respectively.

Sample	DSC					TGA
	$T_{g,ss}$ (°C)	$T_{g,hs}$ (°C)	T_{cc} (°C)	T_m (°C)	ΔH_m (cal/g)	$T_{d5\%}$ (°C)
Aliphatic PEG25/DD-ionenes w/ Br^-	-23.31	78.70	-	28.56	19.65	254
Aliphatic PEG25/DD-ionenes w/ BF_4^-	3.58		-	-	-	301
Aliphatic PEG25/DD-ionenes w/ $TFSI^-$	-29.04		-	-	-	348
Aliphatic PTMO25/DD-ionenes w/ Br^-	-78.65	54.03	-	22.86	7.13	255
Aliphatic PTMO25/DD-ionenes w/ BF_4^-	-76.60	50.51	-	24.99	9.70	311
Aliphatic PTMO25/DD-ionenes w/ $TFSI^-$	-39.94	-13.75	-	-	-	266
DABCO-based PTMO25/DD-ionenes w/ Br^-	-81.42	-	-	2.77	1.65	258
DABCO-based PTMO25/DD-ionenes w/ BF_4^-	-81.88	-	-	0.84	1.93	290
DABCO-based PTMO25/DD-ionenes w/ $TFSI^-$	-81.55	15.77	56.67	130.03	10.18	274

In contrast, the PTMO-based ionenes with a linear aliphatic hard segment demonstrated a better degree of phase separation compared to their PEG-based counterparts. This effect can be attributed to the relatively higher polarity of PTMO compared to PEG.[21] PTMO-based ionenes with BF_4^- and $TFSI^-$ counterions displayed T_g of soft and hard segments, and BF_4^- counterion showed a distinct low T_g of PTMO soft segment at ca. -76 °C, which did not appear with PEG-based ionene analog. However, exchanging the counterion to TFSI resulted in an increased T_g of PTMO soft segment, indicating that the ionenes became relatively phase mixed compared to Br^- counterion but remained better phase separated than PEG-based ionene analog. The T_g of the hard segment decreased ($Br^- > BF_4^- > TFSI^-$) as the size of associated counterions increased ($Br^- < BF_4^- < TFSI^-$) due to facilitated long-range segmental motions attributed to the weaker ionic aggregation. Hunley et al. demonstrated that weaker interactions between cation and anion led to reductions in T_g by

the presence of bulkier fluorinated counterions.[17] Additionally, Cui et al. suggested that larger counterions not only lead to fewer and weaker physical cross-links, resulting in a decrease in T_g but also act as plasticizers, further lowering the T_g.[26] BF_4^- counterion exhibited a higher and narrower melting point than Br- counterion in linear aliphatic PTMO ionenes, implying that PTMO with BF_4^- counterion is more stable on heating and perhaps possesses a better organized and uniform structure of PTMO crystallites and a higher degree of crystallization than PTMO with Br^- counterion.

Comparatively, the DABCO hard segment demonstrated a better degree of phase separation than the linear aliphatic hard segment with all counter-anion species. All Br^-, BF_4^-, and $TFSI^-$ counterions showed a clear T_g of PTMO soft segment ca. 81°C. The melting temperature was observed with DABCO-based ionenes with Br^- and BF_4^- counterions, however; it was not significant due to the low degree of crystallization. Ionenes with TFSI counterion revealed cold crystallization temperature (T_{cc}) and melting temperature above T_g of the hard segment. The cold crystallization is attributed to the transition of the amorphous phase to an ordered crystalline phase upon heating, indicating slow kinetics of organization. Large TFSI counterions are relatively loosely bound to the polymer chain causing polymer chains with more free volumes and enhanced mobility.[27] The comparatively larger $TFSI^-$ counterion accompanied by the bulkier DABCO in comparison to other counterions along with a linear aliphatic hard segment, induced polymer chains to be loosely bound to the counter-anions, resulting in higher free volumes and enhanced chain mobility of hard segments and hence exhibited a high degree of crystallization above room temperature. The T_g of the hard segment was not clearly

observed with Br^- or BF_4^- counterions in DABCO-based ionenes in DSC and more details will be further discussed together with the DMA data below.

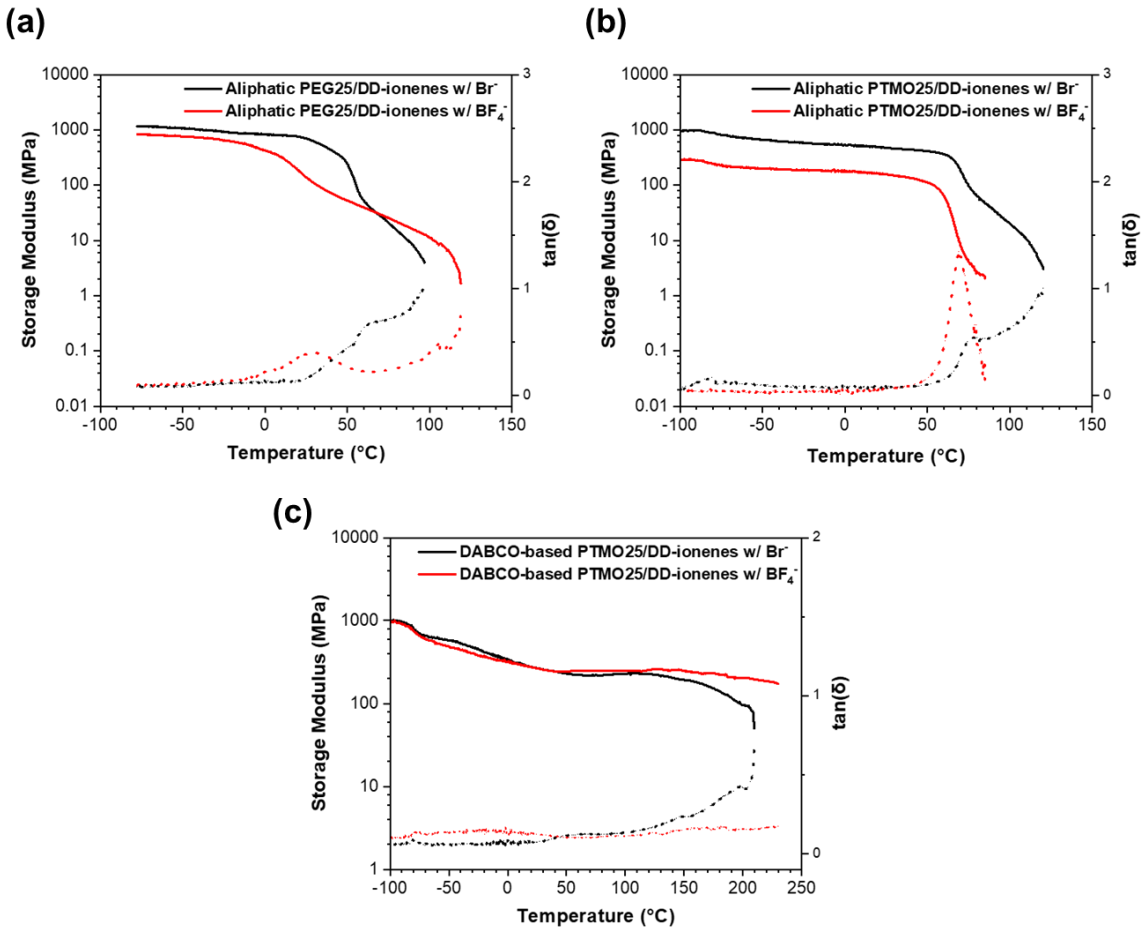

Figure 5.3: Overlayed DMA curves (solid lines) and tan delta (dotted lines) of (a) aliphatic PEG25/DD-ionenes, (b) PTMO25/DD-ionenes, and (c) DABCO-based PTMO25/DD-ionenes with different counterion species.

The viscoelastic properties of ionenes with different counter-anions were studied using DMA under an inert dry nitrogen atmosphere. Ionenes with Br^- and BF_4^- counterions were performed DMA regardless of the type of soft and hard segment. Linear aliphatic PEG25/DD-ionenes and PTMO25/DD-ionenes with $TFSI^-$ counterions became a gooey

liquid state (Figure C4) and DABCO-based PTMO25/DD-ionenes with TFSI counterion was too brittle to perform DMA. The temperature dispersions of storage modulus (*G'*) and corresponding tan delta of ionene films are shown in Figure 5.3. The T_g and T_m values and trends were corresponding to the values from DSC results, as listed in Table 5.2, however, some of the values were not exactly the same as the values from DSC likely due to the different thermal histories of ionenes, transitions occurred in a broad range of temperature, and as two techniques measure different polymer properties in which chain segmental motion is dependent on frequency in DMA, commonly seen in the literature.[28]

Table 5.2: Characteristic dimension of the six samples as determined from DMA analysis. The values not detected from DMA were marked with a dash line.

Sample	$T_{g,ss}$ (°C)	$T_{g,hs}$ (°C)	$T_{m,\ onset}$ (°C)	T_{flow} (°C)
Aliphatic PEG25/DD-ionenes w/ Br^-	-21.12	52.38	27.45	105.51
Aliphatic PEG25/DD-ionenes w/ BF_4^-	7.73		-	118.92
Aliphatic PTMO25/DD-ionenes w/ Br^-	-79.05	68.51	-	119.46
Aliphatic PTMO25/DD-ionenes w/ BF_4^-	-76.89	61.43	-	87.47
DABCO-based PTMO25/DD-ionenes w/ Br^-	-81.13	148.53	4.31	208.71
DABCO-based PTMO25/DD-ionenes w/ BF_4^-	-82.52	122.97	-2.92	≥230

The glass transition of the amorphous PEG phase, the melting of the PEG crystalline phase, and the dissociation of ionic aggregates were observed during the heating from -80 °C with linear aliphatic PEG25/DD-ionenes having Br^- counterion. However, the glass transition of the PEG phase was less clear compared to PTMO-based ionenes, which was consistent with the result obtained by the DSC analysis due to a higher degree of crystallization of PEG. The exchange of counterion to BF_4^- demonstrated one T_g value without T_m, which confirmed that larger counterion induced linear aliphatic PEG25/DD-ionenes to be phase-mixed and have amorphous morphology. Both PEG-based ionenes became remarkably soft after the melting of PEG crystallites and a rubbery plateau was not

presented. It is worth mentioning that BF_4^- counterion showed a slower decline in the storage modulus in a long range of temperature after T_g and higher temperature of dissociation of ionic aggregates compared to Br^- counterion. This suggests that linear aliphatic PEG-based ionenes BF_4^- possessed a higher density of chain entanglement due to phase-mixing compared to Br^- counterion ionene, which was better phase-separated, and thus induced a slower decline of *G'* and higher T_{flow}.

Linear aliphatic PTMO25/DD-ionenes with Br^- or BF_4^- counterions clearly showed both T_g of the PTMO soft segment and hard segments. This showed that PTMO soft segments induced a better degree of phase separation compared to ionenes with PEG soft segment, and PTMO-based ionenes with larger BF_4^- counterion still induced phase to be separated unlike PEG-based ionenes analog. The melting temperature of the PTMO crystallite was not clearly observed with DMA, which was expected to be detected in a range of ca. 23-25 °C for both ionenes with Br^- and BF_4^- counterions based on DSC results, and maintained high *G'* up to the T_g of hard segments. This suggests that the melting of PTMO crystallites did not affect the loss of storage modulus significantly due to the low degree of crystallization and a higher degree of ionic aggregation compared to PEG-based ionenes. The T_g of hard segments decreased with increasing the size of counterions in agreement with DSC findings. Linear aliphatic PTMO-based ionenes with Br^- or BF_4^- counterions did not present a rubbery plateau, and Br^- counterion showed higher ion dissociation temperature than BF_4^- owing to the stronger ionic aggregation.

Clear evidence of phase separation was observed with DABCO-based PTMO-ionenes by showing a distinct low T_g of the PTMO soft segment and the values was slightly lower

than linear aliphatic PTMO-based ionenes analogs. Hence, this supports that DABCO hard segment enhanced a better degree of phase separation compared to the linear aliphatic hard segment regardless of the size of counterions. The T_g of the hard segment, which was not detected with DSC results, was determined with DMA, and it decreased with increasing the size of the counterions. DABCO-based PTMO ionenes with Br^- counterion revealed the highest T_g of hard segment among ionene samples due to strong ionic aggregation. Moreover, DABCO-based ionenes revealed rubbery plateaus regardless of the type of counterions, indicative of the presence of physical crosslinks, supporting that the DABCO hard segment induced a better degree of phase separation and ionic aggregation. Interestingly, ionenes with BF_4^- counterion showed higher rubbery plateau storage modulus and wider rubbery plateau between 43-144 °C in contrast to ionenes with Br^- counterion, where the rubbery plateau was observed between 58-148 °C. This indicates that ionic physical crosslinks are stable even at high temperatures for both counterions owing to the synergetic effect of the DABCO hard segment and PTMO soft segment. T_g of hard segment with ionenes having BF_4^- counterion was lower than the ionenes with Br^- counterion, however; the *G'* slightly increased at T_g of hard segment possibly due to the chain packing of DABCO hard segment, and thus induced an extended rubbery plateau. This also supports the finding from DSC that further increase of the size of counterion to $TFSI^-$ presented a cold crystallization as bulky DABCO hard segment and larger $TFSI^-$ counterion offered higher free volume, increased the chain mobility, and thus induced chain packing. DABCO hard segment caused higher ion dissociation occurred at over 200 °C compared to linear aliphatic hard segment regardless of the size of counterion.

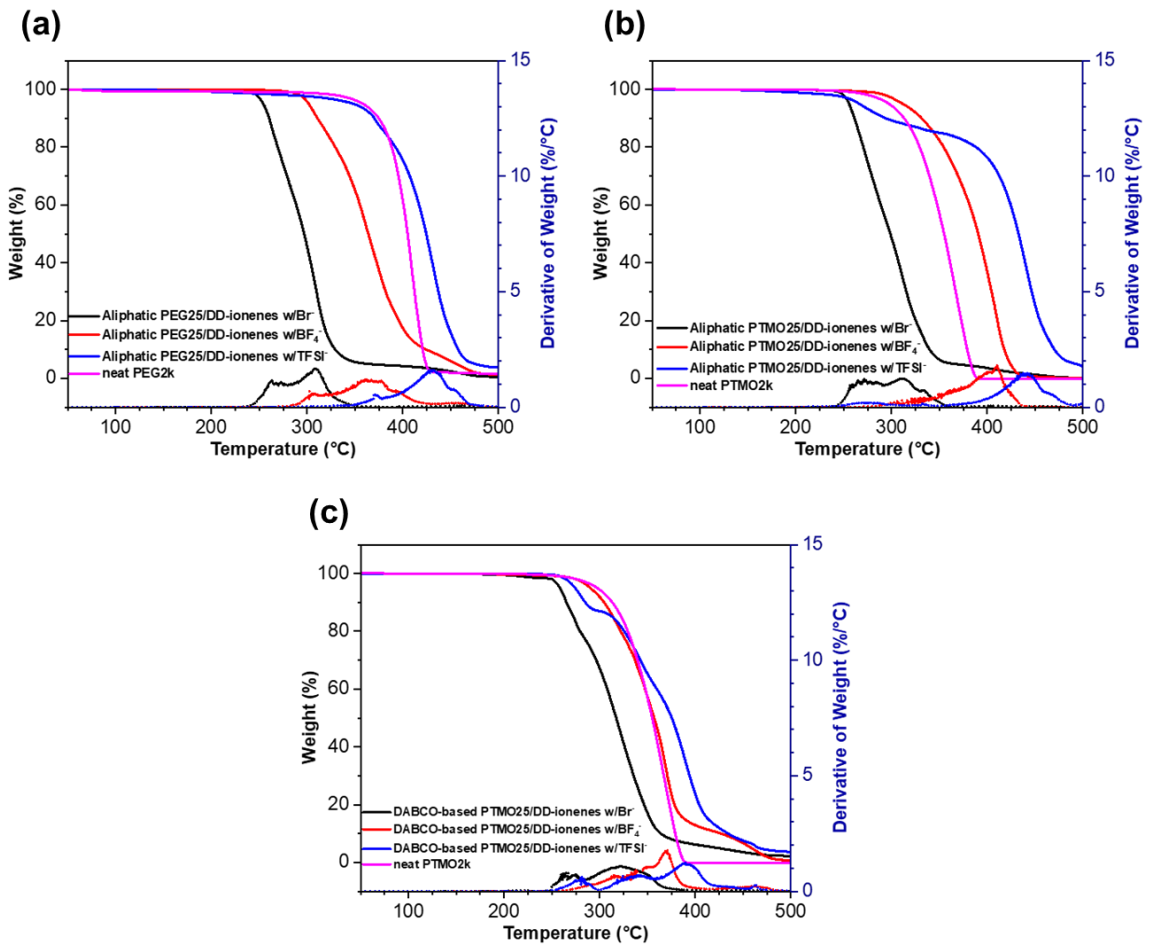

Figure 5.4: Overlayed TGA curves (solid lines) and derivative weight loss curves (dotted lines) for (a) aliphatic PEG25/DD-ionenes, (b) PTMO25/DD-ionenes, and (c) DABCO-based PTMO25/DD-ionenes with different counterion species.

The thermal stability of all samples was studied using TGA under a nitrogen atmosphere, as shown in Figure 5.4. Ionenes contain quaternary ammoniums that undergo nucleophilic substitutions and/or Hoffman elimination reactions dependent on the counterion present in the hard segment, in which the Hofmann elimination reaction depends upon the basicity of the associated counter-anions.[18,19,29] The weaker basic (more stable) counterions will degrade at elevated temperatures compared to stronger basic (less stable) counterions. Generally, the lower charge density, conjugated base with resonance structure, and

electron-withdrawing groups decrease the basicity. The onset degradation temperature of ionenes with Br^- counterions regardless of the type of soft and hard segment showed that Br^- exhibits the lowest thermal stability due to the increased anion basicity than other counter-anions, as shown in Table 5.1. The two-step weight loss of ionenes is clearly presented in the derivative of the weight curve except for PTMO-based ionenes with $TFSI^-$ counterions. The first and second weight loss corresponded to the hard and soft segment degradation, respectively. It was noted earlier that $TFSI^-$ counterions were not fully exchanged from Br^- counterions with PTMO-based ionenes regardless of the type of the hard segment hence presenting the three-step weight loss. The first-step weight loss was attributed to the degradation of the hard segment with Br^- counterions followed by the soft segment and hard segment with $TFSI^-$ counterions. Although the thermal stability of ionenes with $TFSI^-$ counterions with linear aliphatic and DABCO-based PTMO-ionenes was not significantly higher than ionenes with Br^- counterions, it was clearly seen that the derivative of the weight curve of the third step occurred at the elevated temperature. Our previous study suggested that DABCO has a weaker protective effect against the degradation of PTMO soft segments compared to linear aliphatic hard segments.[22] DABCO-based PTMO-ionenes showed a low degree of increase in degradation temperature at elevated temperatures (ca. 400 °C) with reducing the basicity of counter-anions compared to linear aliphatic analogs, which supported that DABCO induced a weaker protective effect against the degradation of PTMO soft segments.

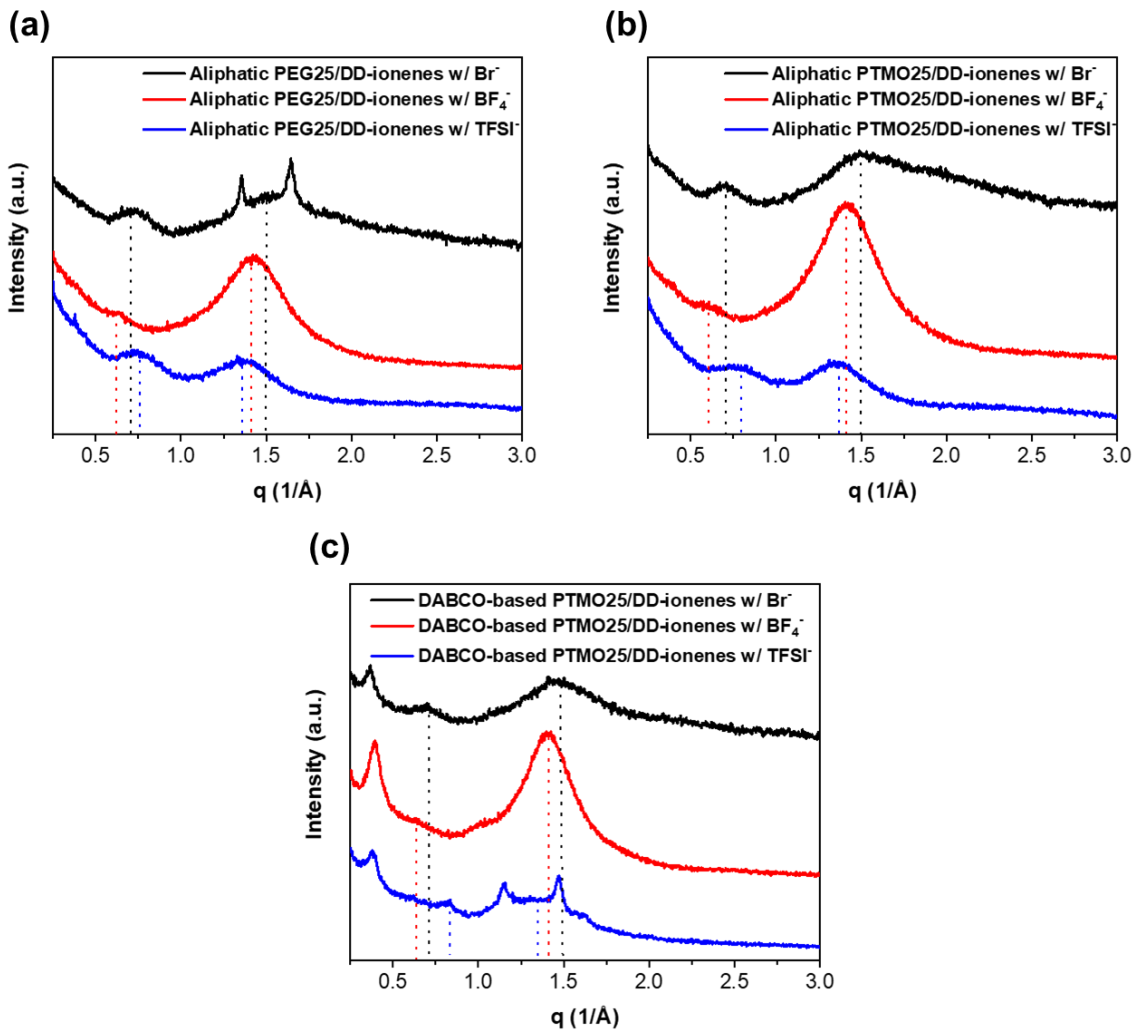

Figure 5.5: Overlayed XRD diffraction of (a) aliphatic PEG25/DD-ionenes, (b) PTMO25/DD-ionenes, and (c) DABCO-based PTMO25/DD-ionenes with different counterion species.

The local structure within ionenes was studied with XRD, as shown in Figure 5.5. Increasing the size of associated counter-anions resulted in amorphous morphology with linear aliphatic PEG-based ionenes in agreement with DSC findings. Linear aliphatic PEG-based ionenes and PTMO-based ionenes showed two peaks at $q_1 \approx 1.3$ to 1.5 $Å^{-1}$ and $q_2 \approx 0.6$ to 0.8 $Å^{-1}$ (Table 5.3). However, DABCO-based ionenes showed three peaks at $q_1 \approx 1.3$ to 1.5 $Å^{-1}$, $q_2 \approx 0.6$ to 0.8 $Å^{-1}$, and $q_3 \approx 0.37$ $Å^{-1}$. All ionenes irrespective of the type of

soft and hard segment showed q_1 that decreased with increasing the size of counter-anion from Br (1.5 $Å^{-1}$) to BF_4 (1.4 $Å^{-1}$) and TFSI (1.36 $Å^{-1}$). The peak q_1 having a correlation distance d_1, which increased with increasing the size of counter-anions from Br (0.42 nm) to BF_4 (0.45 nm) and TFSI (0.46 nm), corresponds to the amorphous halo of the soft segment and attributed to the distance PEG-to-PEG or PTMO-to-PTMO, as shown in Scheme 5.3. This suggests that the distance between soft segments increased with increasing the size of counterions, and it was not affected by the type of soft and hard segments.

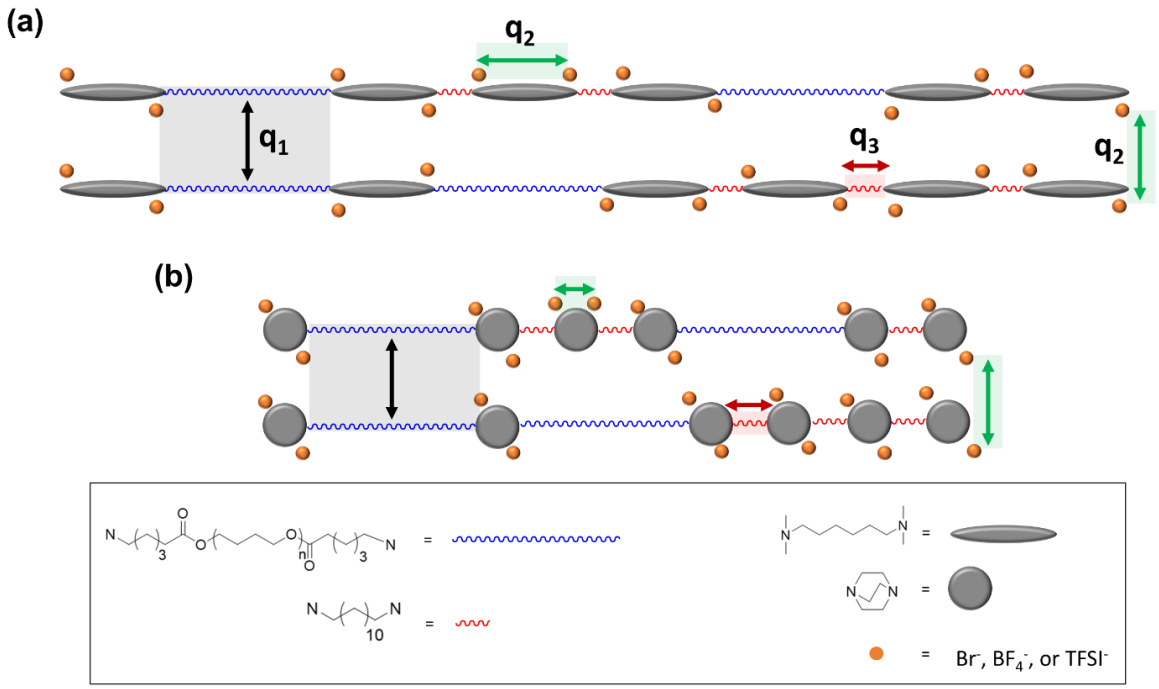

Scheme 5.3: Schematic of characteristic length scale of ionenes with (a) linear aliphatic and (b) DABCO hard segment, where $d_x = 2\pi/q_x$.

The peak q_2 correlates to the distance between ion-to-ion along the backbone or adjacent polymer chain. Although ionenes with BF_4^- counterion showed the increase in d-spacing to 1.05 nm ($q \approx 0.6$ $Å^{-1}$) from ionenes with Br^- counterion ($d \approx 0.9$ nm ($q \approx 0.7$ $Å^{-1}$)), the

peaks became nearly invisible suggesting that BF_4^- counterions are barely visible to X-rays possibly due to the low atomic number may not scatter X-rays strongly and thus making them difficult to detect. Interestingly, the further increase of the size of counterions to $TFSI^-$ slightly decreased the d-spacing to 0.81 nm ($q \approx 0.78$ $Å^{-1}$) and it was prominent with DABCO hard segment, which showed a d-spacing of 0.77 nm ($q \approx 0.82$ $Å^{-1}$). This support that the peak q_2 also resulted from the ion-to-ion along the backbone, and a closer distance between ammoniums in DABCO compared to linear aliphatic ammoniums induced a lower d-spacing between TFSI anions.

Additionally, DABCO-based ionenes showed a peak q_3 correlates to the distance between the ionic group along the backbone ($d \approx 1.7$ nm ($q \approx 0.37$ $Å^{-1}$)), especially 12 methylene units of dodecane hard segment, which was not affected by the size of counterions. Tamami et al. showed similar peaks with dodecane hard segments between ammoniums and proposed that the polymer chain is in the *all-trans* conformation (≈ 1.6 nm).[19] Our previous study suggested that DABCO ion has less conformational freedom; therefore, a more uniform periodicity of groups with a higher electron density relative to the polymer matrix would produce the scattering peak observed with DABCO-based ionenes compared to linear aliphatic ammonium.[22]

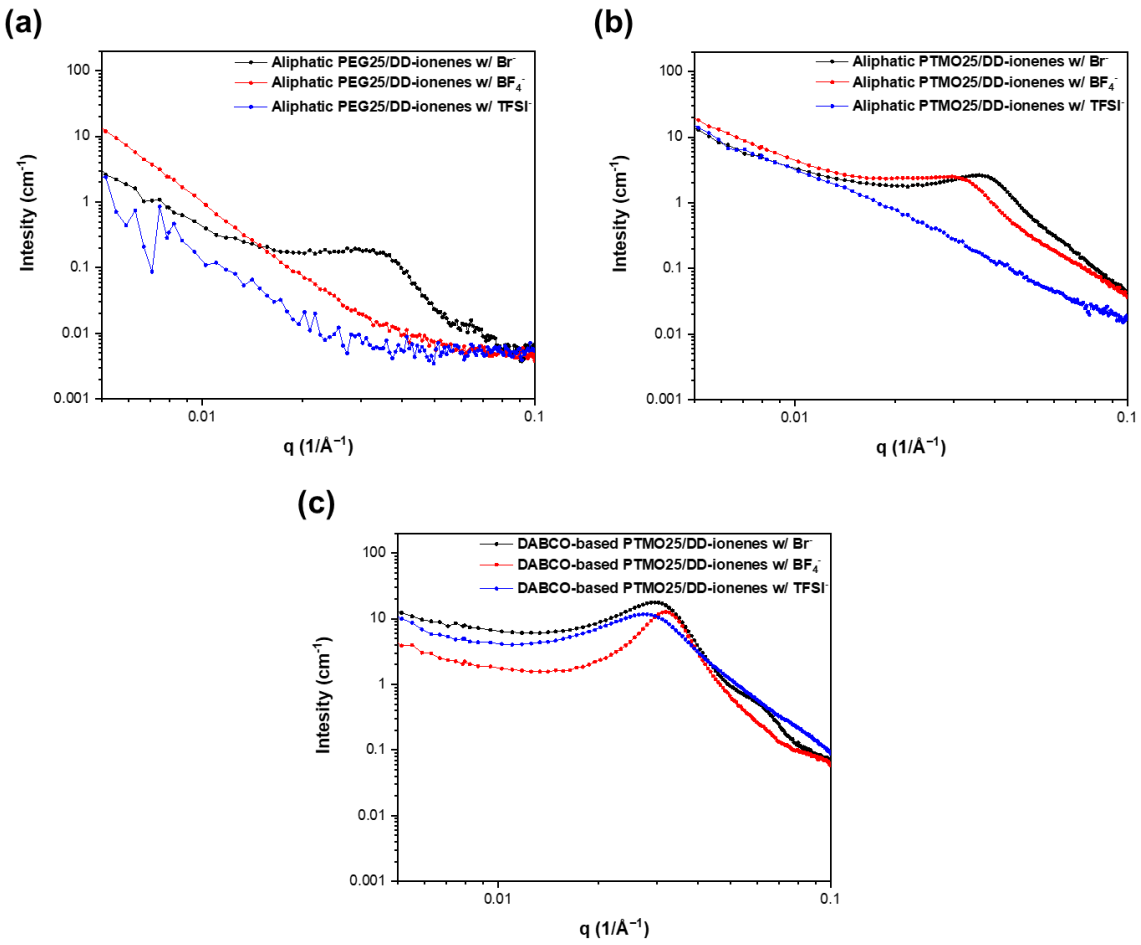

Figure 5.6: SAXS intensity as a function of scattering vector (q) (log-log scale) of (a) aliphatic PEG25/DD-ionenes, (b) PTMO25/DD-ionenes, and (c) DABCO-based PTMO25/DD-ionenes with different counterion species.

SAXS analysis was conducted to investigate the microstructure of ionenes with different counter-anion species based on the electron density difference between the different domains.[30] All ionenes with Br^- counterion showed single broad peaks irrespective of the type of soft and hard segment indicating the phase separation between soft and hard domains, as shown in Figure 5.6. However, increasing the size of the counterion to BF_4^- or $TFSI^-$ with linear aliphatic PEG-based ionenes resulted in the absence of the peak due to the phase mixing, which corroborated the DSC and DMA results. Linear aliphatic PTMO-

ionenes showed a better degree of phase separation with a larger counterion, BF_4^-, compared to PEG-based ionene analog, however, the further increase to $TFSI^-$ counterion still induced a higher degree of phase mixing. PTMO-ionenes with DABCO hard segment showed a superior degree of phase separation compared to linear aliphatic PEG and PTMO-ionenes regardless of the size of the counterion. It has been reported that DABCO hard segment induced a better degree of phase separation resulting from the higher positive charge density and better proximity of charged sites, and increasing the content of soft segment over 50 wt% with Br^- counterion even showed an ordered lamellar structure.[22] Since the ionenes we propose in this study have 25 wt% of the soft segment, DABCO-based PTMO-ionenes with Br^- did not present a clearly ordered structure. PEG- and PTMO-based ionenes with Br^- counterion showed an additional small peak at higher q, and it was prominent with DABCO-based PTMO ionenes ($q \approx 0.06$ $Å^{-1}$) with a peak at $q_4 \approx 0.03$ $Å^{-1}$ at the ratio of 1:2 (i.e., q:2q in Figure 5.6), indicating that smaller Br^- counterion induced more uniform size of hard domains than larger counterions.

Table 5.3: Characteristic dimensions of the soft and hard domains, as determined by XRD, SAXS.

Sample	SAXS		XRD		
	q_4 (nm^{-1})	d_4 (nm)	d_3 (nm)	d_2 (nm)	d_1 (nm)
Aliphatic PEG25/DD-ionenes w/ Br^-	0.36	17.45	-	0.90	0.42
Aliphatic PEG25/DD-ionenes w/ BF_4^-	-	-	-	1.01	0.45
Aliphatic PEG25/DD-ionenes w/ $TFSI^-$	-	-	-	0.84	0.46
Aliphatic PTMO25/DD-ionenes w/ Br^-	0.36	17.45	-	0.90	0.42
Aliphatic PTMO25/DD-ionenes w/ BF_4^-	0.32	19.63	-	1.05	0.45
Aliphatic PTMO25/DD-ionenes w/ $TFSI^-$	-	-	-	0.81	0.46
DABCO-based PTMO25/DD-ionenes w/ Br^-	0.30	20.94	1.70	0.90	0.42
DABCO-based PTMO25/DD-ionenes w/ BF_4^-	0.32	19.63	1.65	1.00	0.45
DABCO-based PTMO25/DD-ionenes w/ $TFSI^-$	0.28	22.43	1.70	0.77	0.47

Generally, a single and broad X-ray scattering represents a spherical aggregation of the ionic domain and a poorly ordered structure.[31] The presence of a peak is attributed to the different electron densities of the ionic aggregates and the surrounding matrix.[32] The linear aliphatic PEG or PTMO-ionenes showed similar spacing of hard domains (microdomain spacing) at $q_4 \approx 0.36$ nm^{-1} ($d \approx 17.45$ nm) due to the same content of soft segment, type of hard segment, and counterion species. The peak became narrower with BF_4^- counterion compared to Br^- counterion with DABCO-based PTMO-ionenes. This suggests that BF_4^- counterion has more uniform distance between hard segment domain than Br^- counterion analog.

Table 5.4: Tensile stress-strain data of segmented ionenes as determined from tensile test.

Sample	Young's Modulus (MPa)	Ultimate tensile strength (MPa)	Tensile strain at break (%)	Toughness (MPa)
Aliphatic PEG25/DD-ionenes w/ Br^-	1369.54 ± 180.87	11.58 ± 1.71	1.26 ± 0.12	0.07 ± 0.02
Aliphatic PEG25/DD-ionenes w/ BF_4^-	7.87 ± 2.11	0.22 ± 0.06	413.70 ± 137.98	0.26 ± 0.11
Aliphatic PTMO25/DD-ionenes w/ Br^-	583.46 ± 52.59	15.91 ± 1.63	152.36 ± 50.84	18.11 ± 4.69
Aliphatic PTMO25/DD-ionenes w/ $BF4^-$	54.13 ± 20.82	3.51 ± 1.51	216.788 ± 53.38	4.36 ± 0.61
DABCO-based PTMO25/DD-ionenes w/ Br^-	289.85 ± 48.55	11.86 ± 2.03	56.09 ± 4.12	5.12 ± 0.35
DABCO-based PTMO25/DD-ionenes w/ $BF4^-$	616.97 ± 28.39	23.47 ± 0.49	8.75 ± 1.20	1.46 ± 0.29

A uniaxial tensile test was performed at room temperature with ionenes with different counter-anions, as shown in Table 5.4. Since ionenes with $TFSI^-$ counterions did not form a film or were too brittle to perform a tensile test, ionenes with Br^- and BF_4^- were selected for the tensile test. Linear aliphatic PEG-based ionene with Br^- counterion was rigid but brittle at room temperature by showing the highest Young's modulus and the lowest elongation due to the PEG crystallites and T_m is higher than room temperature, as shown

in DSC and XRD results. However, ionenes became less stiff and strong but ductile with larger BF_4^- counterion by showing the decrease of Young's modulus and ultimate tensile strength with increasing the size of counter-anion regardless of the type of soft segment with a linear aliphatic hard segment. In fact, linear aliphatic PEG or PTMO-based ionenes with BF_4 counterions showed a lower *G'* than Br^- analogs. Linear aliphatic PTMO-ionenes with Br^- counterion showed the highest toughness among all samples by revealing decent elongation and ultimate tensile strength. However, ionenes with DABCO hard segment showed opposite trends. As mentioned above, DABCO-based ionenes become brittle when exchanging counterion to BF_4^- or $TFSI^-$, and the ionene with $TFSI^-$ was too brittle to perform a tensile test. DSC and XRD showed that DABCO-based PTMO-ionenes with $TFSI^-$ counterion showed PTMO crystallization at room temperature and even suspected chain packing of DABCO hard segment, which possibly made the film remarkably brittle. DABCO-based PTMO-ionene with BF_4^- was more brittle but rigid and strong under tensile stress compared to Br^- counterion analog. DMA showed similar *G'* at room temperature between BF_4^- and Br^- counterion, although Young's modulus was higher with ionene with BF_4^-counterion. It has been commonly seen that *G'* can be lower than Young's modulus since two modulus values are measured with different types of deformation. The storage modulus measured the ability to store energy elastically under deformation and responds to a small oscillatory deformation, while Young's modulus measures the resistance to deformation under tension, and responds to large deformation. Larger ionic aggregates induce non-homogeneous network formation and thus decrease mechanical properties.[33] DABCO-based PTMO-ionenes with BF_4^- counterion showed uniform distance between

hard domains (ion aggregates) from soft segments compared to ionenes with Br^- counterion, which possibly caused higher mechanical strength in the tensile test as well as high ion dissociation temperature observed in DMA.

Overall, the thermal and mechanical properties, as well as the morphology of segmented ionenes, were significantly influenced by the type of soft and hard segments and the type of counterion. The T_g of the hard segment decreased as the size of the counterion increased, while thermal stability increased due to the reduced basicity of the anion. The more polar PTMO soft segment induced a higher degree of phase separation than the less polar PEG soft segment and induced decent phase separation with a larger size of counterion, BF_4^-. However, with a further increase in the size of the counterion, TFSI, the PTMO soft segment did not provide enough driving force for phases to be separated, but showed a better degree of phase separation compared to PEG-based ionene analogs. The DABCO hard segment induced significant phase separation compared to the linear aliphatic hard segment, due to stronger ionic aggregation. DABCO-based PTMO ionenes maintained superior microphase separation, irrespective of the size of counterions, due to the synergistic effect of having PTMO and DABCO as soft and hard segments. The Br counter-anion typically caused greater ionic aggregation than larger counterions, regardless of the type of soft and hard segment, and displayed enhanced mechanical properties. However, incorporating the bulky DABCO hard segment with PTMO soft segment induced better mechanical and viscoelastic properties with BF_4^- counterion, owing to the possible chain packing of the DABCO hard segment, attributed to the increased free volume by the bulk DABCO and BF_4^- counterion. The more uniform dispersion of phases contribute to

enhancing mechanical performance.[34] This can be also owing to the morphological difference between Br^- and BF_4^- counterions, and BF_4^- counterion exhibited more uniform dispersion of ion aggregates.

5.5 Conclusions

PEG- and PTMO-based segmented ionenes with two structurally different hard segments were successfully synthesized and counter-anion metathesis (Br, BF_4, TFSI) was performed with corresponding ionenes for the first time. The thermal, mechanical, and morphological properties of a series of segmented ionenes were investigated. The glass transition temperature of the hard segment decreased with increasing the size of counterions except for linear aliphatic PEG-based ionenes, which showed amorphous and more phase mixed morphology with increasing the size of counterions. The more basic counter-anions led to increasing in thermal stability. All DABCO-based PTMO-ionenes exhibited superior microphase separation irrespective of the size of the counterion. The PTMO soft segment and DABCO hard segment induced a better degree of phase separation than the PEG soft segment and linear aliphatic hard segment, respectively. The bulk DABCO accompanied by a large counterion than Br- suggested to trigger chain packing of DABCO hard segment and enhance the degree of crystallization. Especially, DABCO-based PTMO ionenes with BF_4^- counterion showed uniform and homogenously dispersed ionic aggregation compared to Br^- counterion analog and induced higher mechanical and viscoelastic properties of segmented ionenes.

5.6 References

1. Rembaum, A., Baumgartner, W. & Eisenberg, A. Aliphatic ionenes. *J. Polym. Sci. Part B Polym. Lett.* **6**, 159–171 (1968).

2. Gibbs, C. F., Littmann, E. R. & Marvel, C. S. Quaternary Ammonium Salts from Halogenated Alkyl Dimethylamines. II. The Polymerization of Gamma-Halogenopropyldimethylamines. *J. Am. Chem. Soc.* **55**, 753–757 (1933).

3. Lee, J. S., Hocken, A. & Green, M. D. Advances in the molecular design of ionenes for a diverse range of applications. *Mol. Syst. Des. Eng.* **6**, 334–354 (2021).

4. Tamami, M., Williams, S. R., Park, J. K., Moore, R. B. & Long, T. E. Poly(propylene glycol)-based ammonium ionenes as segmented ion-containing block copolymers. *J. Polym. Sci. Part A Polym. Chem.* **48**, 4159–4167 (2010).

5. Williams, S. R., Salas-de la Cruz, D., Winey, K. I. & Long, T. E. Ionene segmented block copolymers containing imidazolium cations: Structure–property relationships as a function of hard segment content. *Polymer (Guildf).* **51**, 1252–1257 (2010).

6. Wu, F., Huang, C. L., Zeng, J. B., Li, S. L. & Wang, Y. Z. Synthesis and characterization of segmented poly(butylene succinate) urethane ionenes containing secondary amine cation. *Polymer (Guildf).* **55**, 4358–4368 (2014).

7. Williams, S. R., Barta, Z., Ramirez, S. M. & Long, T. E. Synthesis of 12,12-Ammonium Ionenes with Functionality for Chain Extension and Cross-Linking via UV Irradiation. *Macromol. Chem. Phys.* **210**, 555–564 (2009).

8. Williams, S. R. *et al.* Synthesis and Characterization of Well-Defined 12,12-Ammonium Ionenes: Evaluating Mechanical Properties as a Function of Molecular Weight. *Macromolecules* **41**, 5216–5222 (2008).

9. Kammakakam, I., O'Harra, K. E., Dennis, G. P., Jackson, E. M. & Bara, J. E. Self-healing imidazolium-based ionene-polyamide membranes: an experimental study on physical and gas transport properties. *Polym. Int.* **68**, 1123–1129 (2019).

10. Williams, S. R. & Long, T. E. Recent advances in the synthesis and structure–property relationships of ammonium ionenes. *Prog. Polym. Sci.* **34**, 762–782 (2009).

11. Rembaum, A. & Noguchi, H. Reactions of N,N,N',N'-Tetramethyl-α,ι-diaminoalkanes with α,ι-Dihaloalkanes. II. x-y Reactions. *Macromolecules* **5**, 261–269 (1972).

12. Bara, J. E. & O'Harra, K. E. Recent Advances in the Design of Ionenes: Toward Convergence with High-Performance Polymers. *Macromol. Chem. Phys.* **220**, 1900078 (2019).

13. Tamami, M. *et al.* Poly(ethylene glycol)-based ammonium ionenes containing nucleobases. *Polymer (Guildf).* **54**, 1588–1595 (2013).

14. Schreiner, C., Bridge, A. T., Hunley, M. T., Long, T. E. & Green, M. D. Segmented imidazolium ionenes: Solution rheology, thermomechanical properties, and electrospinning. *Polymer (Guildf).* **114**, 257–265 (2017).

15. Das, S. *et al.* Synthesis and Characterization of Novel Segmented Polyionenes Based on Polydimethylsiloxane Soft Segments. *J. Macromol. Sci. Part A* **47**, 215–224 (2010).

16. Vijayaraghavan, P., Brown, J. R. & Hall, L. M. Modeling the Effect of Polymer Composition on Ionic Aggregation in Poly(propylene glycol)-Based Ionenes. *Macromol. Chem. Phys.* **217**, 930–939 (2016).

17. Hunley, M. T., England, J. P. & Long, T. E. Influence of Counteranion on the Thermal and Solution Behavior of Poly(2-(dimethylamino)ethyl methacrylate)-Based Polyelectrolytes. *Macromolecules* **43**, 9998–10005 (2010).

18. Abdulahad, A. I., Jangu, C., Hemp, S. T. & Long, T. E. Influence of Counterion on Thermal, Viscoelastic, and Ion Conductive Properties of Phosphonium Ionenes. *Macromol. Symp.* **342**, 56–66 (2014).

19. Tamami, M., Salas-de la Cruz, D., Winey, K. I. & Long, T. E. Structure-Property Relationships of Water-Soluble Ammonium-Ionene Copolymers. *Macromol. Chem. Phys.* **213**, 965–972 (2012).

20. Hashimoto, T. *et al.* Structure and properties of poly(tetrahydrofuran) viologen ionene: effects of halide counter-anions. *Polymer (Guildf).* **35**, 2672–2678 (1994).

21. Liesen, N. T. *et al.* The influence of spacer composition on thermomechanical properties, crystallinity, and morphology in ionene segmented copolymers. *Soft Matter* **17**, 5508–5523 (2021).

22. Lee, J. S., Taghavimehr, M., Montazami, R. & Green, M. D. Synthesis and characterization of poly(tetramethylene oxide)-based segmented ionenes block copolymer with aliphatic or DABCO hard segments. *Polymer (Guildf).* **270**, 125772 (2023).

23. Lee, J. S., Taghavimehr, M., Montazami, R. & Green, M. D. Synthesis and characterization of Poly(ethylene glycol)-based segmented ionenes block copolymer with aliphatic or DABCO hard segments. *Polymer (Guildf).* **242**, 124543 (2022).

24. Ilavsky, J. & Jemian, P. R. Irena : tool suite for modeling and analysis of small-angle scattering. *J. Appl. Crystallogr.* **42**, 347–353 (2009).

25. Ilavsky, J. Nika : software for two-dimensional data reduction. *J. Appl. Crystallogr.* **45**, 324–328 (2012).

26. Cui, J. *et al.* Novel imidazolium-based poly(ionic liquid)s with different counterions for self-healing. *J. Mater. Chem. A* **5**, 25220–25229 (2017).

27. Guo, P., Zhang, H., Liu, X. & Sun, J. Counteranion-Mediated Intrinsic Healing of Poly(ionic liquid) Copolymers. *ACS Appl. Mater. Interfaces* **10**, 2105–2113 (2018).

28. Zhang, K., Fahs, G. B., Drummey, K. J., Moore, R. B. & Long, T. E. Doubly-Charged Ionomers with Enhanced Microphase-Separation. *Macromolecules* **49**, 6965–6972 (2016).

29. Green, M. D. *et al.* Alkyl-Substituted N-Vinylimidazolium Polymerized Ionic Liquids: Thermal Properties and Ionic Conductivities. *Macromol. Chem. Phys.* **212**, 2522–2528 (2011).

30. Feng, D., Venkateshwaran, L. N., Wilkes, G. L., Leir, C. M. & Stark, J. E. Structure-property behavior of elastomeric segmented PTMO–ionene polymers. II. *J. Appl. Polym. Sci.* **38**, 1549–1565 (1989).

31. Gouin, J. P., Williams, C. E. & Eisenberg, A. Microphase Structure of Block Ionomers. 1. Study of Molded Styrene-4-Vinylpyridinium ABA Blocks by SAXS and SANS. *Macromolecules* **22**, 4573–4578 (1989).

32. Wu, T., Beyer, F. L., Brown, R. H., Moore, R. B. & Long, T. E. Influence of Zwitterions on Thermomechanical Properties and Morphology of Acrylic Copolymers: Implications for Electroactive Applications. *Macromolecules* **44**, 8056–8063 (2011).

33. Topuz, F., Henke, A., Richtering, W. & Groll, J. Magnesium ions and alginate do form hydrogels: a rheological study. *Soft Matter* **8**, 4877 (2012).

34. Huang, D. *et al.* Functionalized Elastomeric Ionomers Used as Effective Toughening Agents for Poly(lactic acid): Enhancement in Interfacial Adhesion and Mechanical Performance. *ACS Sustain. Chem. Eng.* **8**, 573–585 (2020).

CHAPTER 6

SYNTHESIS AND CHARACTERIZATION OF RANDOM OR BLOCKY POLY(TETRAMETHYLENE OXIDE)-BASED SEGMENTED IONENES WITH A MIXTURE OF LINEAR ALIPHATIC AND DABCO HARD SEGMENTS

To be published as: Lee, J.; Beyer, F. L.; Green, M. D.

6.1 Abstract

The synthesis of mixing of two hard segment types in segmented ionenes was proposed for the first time. Ionenes with a randomly or blocky distribution of two hard segments were successfully synthesized and their properties were compared with the segmented ionenes having each hard segment type. DSC revealed the distinct low T_g of the soft segment, indicating the existence of microphase separation. In addition, mixing two hard segments affected the size distribution of spherulites. DMA confirmed the microphase separation of PTMO-based segmented ionenes, and the blocky arrangement of two hard segments showed a higher rubbery plateau modulus compared to randomly distributed analog due to the higher degree of microphase separation. However, randomly arranged hard segments induced higher entanglement, which induced extended rubbery plateau modulus at a higher temperature for ion aggregates to be dissociated. The mixing of two hard segments affected the mechanical properties of the segmented ionenes in which randomly arranged two hard segments revealed the highest elongation due to the fewer interchain interactions. In addition, the blocky arrangement of two hard segments more resembles the distinct properties of the ionenes with each hard segment type regarding the stiffness of extensibility of the ionenes. SAXS revealed that mixing two hard segments did

not influence the morphology of the segmented ionenes significantly, and all PTMO-based ionenes showed microphase-separated lamellar morphology.

6.2 Introduction

Ionenes are polymers that contain ionic groups in their backbone as opposed to pendant sites. Generally, ionenes have cationic groups in the polymer chain, and various cationic ionenes containing ammonium, pyridinium, imidazolium, and phosphonium groups have been reported.[1] Segmented ionenes possess oligomeric spacers between the hard segments, which often improved mechanical properties compared to non-segmented ionenes.[2] The ionic group tends to aggregate to form physical crosslinking and significantly modify the physical properties of segmented ionenes, which resemble conventional polyurethane elastomers.

Mixing two different soft segments in polyurethane, which also works like an elastomer similar to segmented ionenes, has been studied.[3] Ahn et al. synthesized polyurethane with two different soft segments, PTMO and poly(hexamethylene carbonate)diol (PHC), to understand the properties of polyurethane.[4] This random copolymer of polyurethane with two different soft segments induced enhanced phase mixing between hard and soft segments due to the more polar nature of PHC. However, Mirhosseini et al. revealed that mixing PTMO and poly(caprolactone) soft segments in thermoplastic polyurethane elastomers accelerated the microphase separation process compared to samples with one type of soft segment.[5] Mixing two different soft segments (Bi-soft segment) is a convenient way to adjust the performance of the elastomer, and the mechanism is primarily divided into two aspects: the influence of the characteristics of two soft segments on polymer; and

the interaction between the two soft segments and interactions with hard segment result in affecting the microphase structure.[6] Askari et al. mixed PTMO and poly(dimethylsiloxane) (PDMS) soft segments, and hydrophobicity, thermal stability, and fire resistance of elastomer were improved by introducing PDMS.[7] However, the elastomers mixing different hard segments were studied to a considerably lesser extent, although hard segments in segmented ionenes play a crucial role in the ionic aggregation and control the degree of phase separation result in influencing the properties of the segmented ionenes. Thus, synthesizing segmented ionenes by mixing two structurally different hard segments in one polymer chain to study the properties of the segmented ionenes will further provide the structure-property relationship of segmented ionenes.

Typically, block copolymers show superior properties than random copolymers in that block copolymers have characteristics of each of the homopolymers and a set of properties.[8] Kang et al. revealed that block copolymers showed more distinct phase separation than the random copolymer.[9] Cho et al. studied the influence of soft segment arrangement, block or random, on mechanical properties of polyurethane elastomers.[10] The random arrangement of two different molecular weights of PTMO soft segments showed higher elongation than block copolymers due to the fewer interchain interactions. However, there is still no studies have been performed mixing two different hard segmented, as well as the effect of blocky and random arrangement of two hard segments with segmented ionenes.

In the present study, we report the synthesis and characterization of block and random PTMO-based segmented ionenes having two different hard segments, linear aliphatic and

heterocyclic aliphatic (DABCO). Moreover, we are comparing the blocky and random copolymer of hear segments with each ionenes with one type of hard segment to investigate the effect of mixing two hard segments. The thermal and mechanical properties of these segmented ionenes were analyzed by differential scanning calorimetry (DSC), thermogravimetric analysis (TGA), dynamic mechanical analysis (DMA), and uniaxial tensile analysis. The local structure and morphology of the segmented ionenes were probed with X-ray diffraction (XRD) and SAXS.

6.3 Experimental

5.3.1 Materials

N,N,N',N'-tetramethyl-1,6-hexanediamine (99%), 1,4-diazabicyclo[2.2.2]octane (DABCO) (≥99%), poly(tetrahydrofuran) (PTMO) 2,000 g/mol, triethylamine (≥99.5%), 6-bromohexanoyl chloride (97%), and dimethyl sulfoxide-d_6 were purchased from Sigma Aldrich. Chloroform-*d* was purchased from Alfa Aesar. Dichloromethane (DCM), dimethylformamide (DMF), and methanol (MeOH) were purchased from VWR Chemicals. All materials were used as received.

5.3.2 Synthesis of aliphatic PTMO93-ionenes and DABCO-based PTMO95-ionenes

Details of synthesis of bromine end-capped PTMO (Br-PTMO$_n$-Br) have been published elsewhere and will not be reiterated here.[11] Aliphatic or DABCO-based PTMO-ionenes are synthesized with Br-PTMO$_n$-Br with N,N,N',N'-tetramethyl-1,6-hexanediamine or DABCO in MeOH or DMF, respectively, for 3 d under stirring at 75 °C. The molar ratio of Br-PTMO$_n$-Br and aliphatic or DABCO was equal to one. The concentration of all series

of ionenes were 1 mol/L. Then, ionenes solution were dried in a Teflon mold at room temperature for 1 d followed by drying at 60 °C for 2 d, and under vacuum at room temperature for 2 d.

5.3.3 Synthesis of aliphatic-DABCO PTMO94 Random-ionene

Aliphatic-DABCO PTMO94 random-ionene was synthesized by mixing Br-PTMO$_n$-Br, *N,N,N',N'*-tetramethyl-1,6-hexanediamine and DABCO in DMF for 3 d under stirring at 75 °C. The molar ratio of Br-PTMO$_n$-Br and sum of aliphatic and DABCO was equal to one. For example, Br-PTMO$_n$-Br (1.9329 g), *N,N,N',N'*-tetramethyl-1,6-hexanediamine (0.0682 g), and DABCO (0.0478 g) was added in DMF. Then, ionenes solution were dried in a Teflon mold at room temperature for 1 d followed by drying at 60 °C for 2 d, and under vacuum at room temperature for 2 d. The concentration of ionene were 1 mol/L.

5.3.4 Synthesis of aliphatic-DABCO PTMO94 Blocky-ionene

Aliphatic-DABCO PTMO94 Blocky-ionenes was synthesized by mixing two blocks of DABCO-PTMO and aliphatic-PTMO. DABCO-PTMO block was synthesized by mixing DABCO (1.05 eq) and Br-PTMO$_n$-Br (1 eq), and aliphatic-PTMO block was synthesized by mixing *N,N,N',N'*-tetramethyl-1,6-hexanediamine (1 eq) and Br-PTMO$_n$-Br (1.05 eq). Both blocks were synthesized in DMF for 3 d under stirring at 75 °C. The synthesized blocks were dried at 60 °C under vacuum for 2 d. Then two blocks were synthesized by dissolving in DMF and stirring at 75 °C for 3 d. Then, ionenes solution were dried in a Teflon mold at room temperature for 1 d followed by drying at 60 °C for 2 d, and under vacuum at room temperature for 2 d. The final weight of polymer was identical to the

aliphatic-DABCO based PTMO94 Random ionenes, and the concentration of ionene were 1 mol/L.

5.3.5 Characterizations

^{1}H NMR spectroscopic analyses were performed on Bruker Avance III 500 MHz NMR. DMSO-d_6 was used for all ionene samples. DSC was performed on a TA instruments Q20. All samples were heated from 40 °C to 160 °C, cooled down to -120 °C, and then heated up to 160 °C. The DSC was cooled using liquid nitrogen filled into the internal reservoir of the manually operated quench cooling accessory. The heating and cooling rate were both 10 °C/min, and samples were held isothermally for 10 min before each ramp. The purge gas was argon with a gas flow rate of 50 mL/min. TGA was conducted on TA instruments TGA 5500. The sample was heated to 120 °C (20 °C/min), cooled down to 40 °C (20 °C/min), and heated up again to 600 °C (10 °C/min). The samples were held isothermally for 10 min before each ramp. The purge gas was ultra-high purity (UHP) nitrogen with a gas flow rate of 25 mL/min. XRD was performed on PANalytical X'Pert PRO MRD with nickel-filtered Cu Kα radiation source (λ = 1.54 Å), divergence slit 1/4º, anti-scatter slits 1/2º, 45 kV/40 mA, and 2θ = 3-60º at room temperature. Tensile test was conducted on Instron E3343 with 20 mm/min of extension rate at room temperature. All samples were prepared with three dog-bone shaped films using a dog-bone-shaped die (ASTM D1708), and samples were stored under vacuum until performing a tensile test. DMA was performed on a TA instruments Discovery HR-2 hybrid rheometer with a tension mode in a temperature range of -100 to 230 ˚C at a heating rate of 3 ˚C/min, a frequency of 1 Hz, and under 0.1% strain. The purge gas was UHP nitrogen with as gas

flow rate of 10 mL/min. SAXS was performed using a Xenocs "Xeuss X3-HR" camera and a Rigaku 007HF rotating anode X-ray generator. The generator was operated at 40 kV and 30 mA, and is equipped with a copper anode. After collimation with a focusing optic, the output is an intense beam of CuKα photons with wavelength (λ) 1.542 Å. This beam is further optimized by two slit apertures roughly 1.5 m apart. Two-dimensional (2-D) scattering data was measured using a Pilatus3R 300k hybrid photon counting detector positioned at sample-to-detector distances of 1800, 900, 370, and 150 mm. This configuration allows collection of SAXS data spanning an angular range of $0.004 \leq q \leq 0.4$ Å-1, where q is the magnitude of the scattering vector, the value of q is $4\pi \cdot \sin(\theta)/\lambda$, and 2θ is the scattering angle. Samples that were viscous liquids at room temperature were encapsulated in Scotch-brand Magic™ tape. All data were corrected for background scattering, placed on an absolute scale, and azimuthally averaged for analysis using Wavemetrics Igor Pro v8 and procedures available for download from Argonne National Laboratory.[12,13]

6.4 Results and Discussion

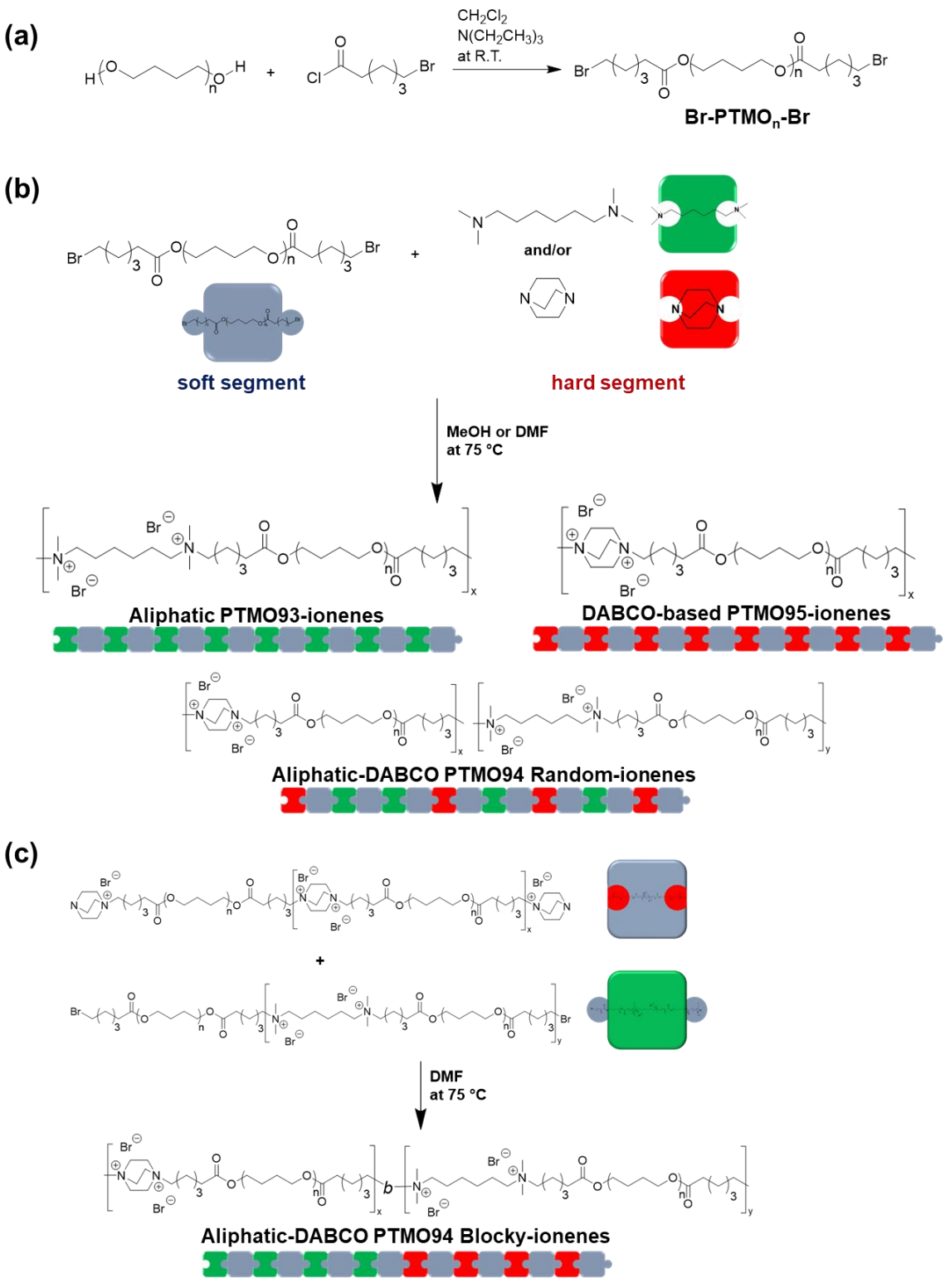
(a)
CH2Cl2
N(CH2CH3)3
at R.T.
Br-PTMOn-Br
(b)
and/or
soft segment
hard segment
MeOH or DMF
at 75 °C
Aliphatic PTMO93-ionenes
DABCO-based PTMO95-ionenes
Aliphatic-DABCO PTMO94 Random-ionenes
(c)
DMF
at 75 °C
Aliphatic-DABCO PTMO94 Blocky-ionenes

Scheme 6.1: The synthesis of (a) Br-PTMO$_n$-Br and (b) aliphatic PTMO93-ionenes or DABCO-based PTMO94-ionenes, or aliphatic-DABCO PTMO94 Random-ionenes, and (c) aliphatic-DABCO PTMO94 Blocky-ionenes.

The desired aliphatic or DABCO-based PTMO-ionenes and aliphatic-DABCO PTMO random or blocky-ionenes were synthesized via Menshutkin reaction as shown in Scheme 6.1. The balanced 1:1 stoichiometry is required to obtain high molecular weight polymers in step-growth polymerization.[14] Aliphatic PTMO93-ionenens, DABCO-based PTMO95-ionenes, and aliphatic-DABCO PTMO94 random-ionenes were synthesized in a one-pot under the 1:1 stoichiometry between the soft segment and the hard segments using MeOH or DMF. Aliphatic-DABCO PTMO94 Blocky-ionene was synthesized by mixing two blocks of pre-polymer, aliphatic-PTMO and DABCO-PTMO blocks, using DMF. All resultant polymers were transparent and formed robust films after drying solvents, as shown in Figure 6.1.

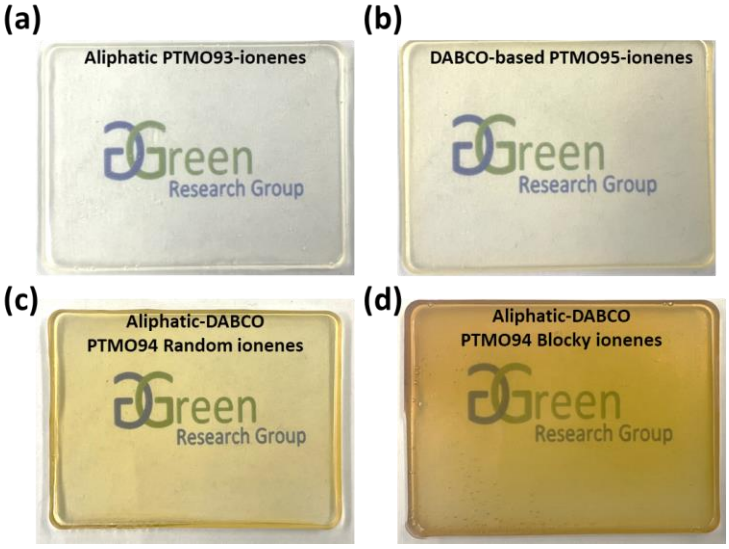

Figure 6.1: Photographic images of (a) aliphatic PTMO93-ionenes, (b) DABCO-based PTMO95-ionenes, (c) aliphatic-DABCO PTMO94 Random-ionenes, and (d) aliphatic-DABCO PTMO94 Blocky-ionene.

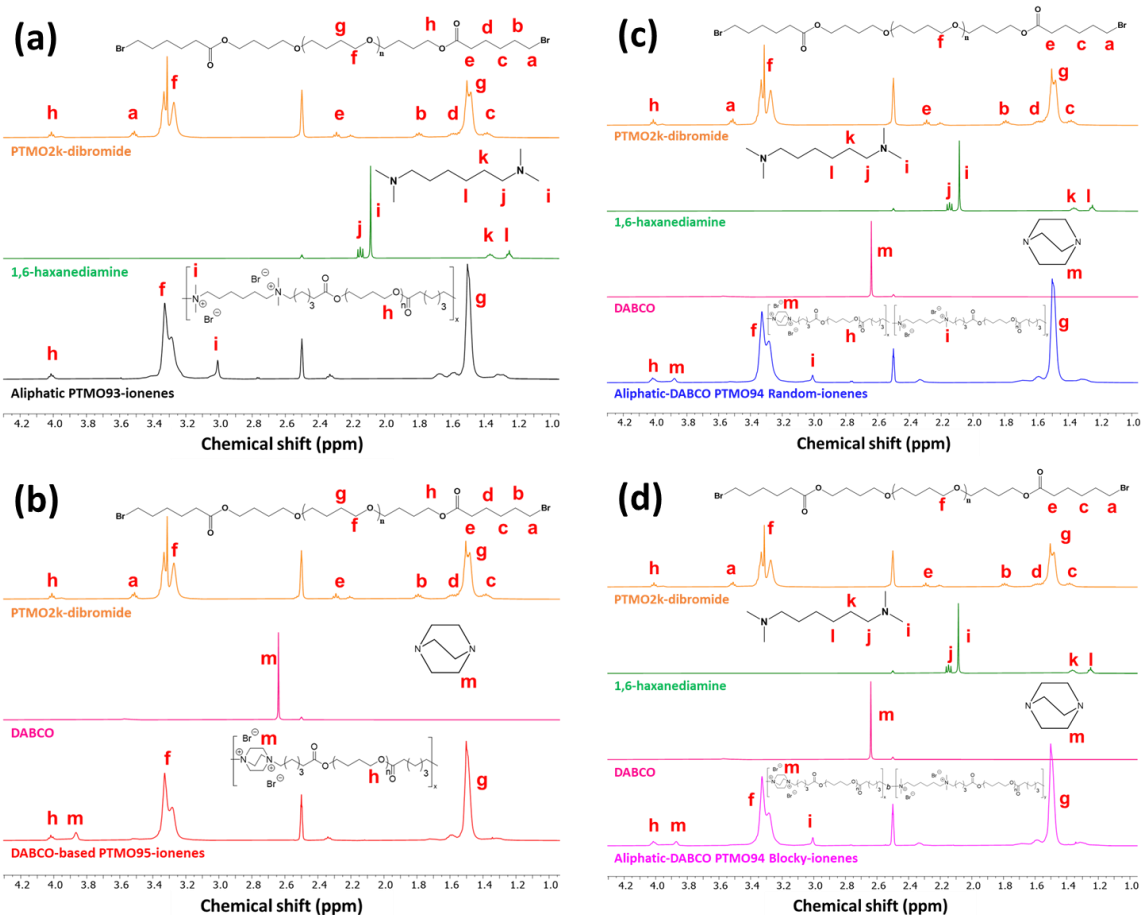

Figure 6.2: ^{1}H NMR spectra of Br-PTMO$_n$-Br, tetramethyl-1,6-haxanediamine and/or DABCO, and (a) aliphatic PTMO93-ionene, (b) DABCO-based PTMO95-ionene, (c) aliphatic-DABCO PMTO94 Random-ionene, and (d) aliphatic-DABCO PTMO94 Blocky ionene from the top and bottom with labeled peaks corresponding to the respectively labeled protons. DMSO-d_6 was used for all samples.

PTMO-based segmented ionenes were successfully synthesized and confirmed by the ^{1}H NMR spectrum (Figure 6.2). The peaks from all samples were broadened after polymerization which is an indication of the relatively higher molecular weight of the polymer. The resonance at 2.1 and 2.6 ppm in the ^{1}H NMR spectrum attributed to methylene protons of *N,N,N',N'*-tetramethyl-1,6-hexandiamine and DABCO monomers, respectively, shifted to 3.0 and 3.9 ppm, respectively, which confirmed the quaternarization

of the tertiary amines. Aliphatic-DABCO mixture ionenes showed two shifted peaks of *N,N,N',N'*-tetramethyl-1,6-hexandiamine and DABCO monomers and the integration ratio of the corresponding *m* and *i* peaks were identical for aliphatic-DABCO mixture ionenes, which indicated aliphatic-DABCO mixture ionenes were successfully synthesized and possess an equal molar ratio of each hard segments.

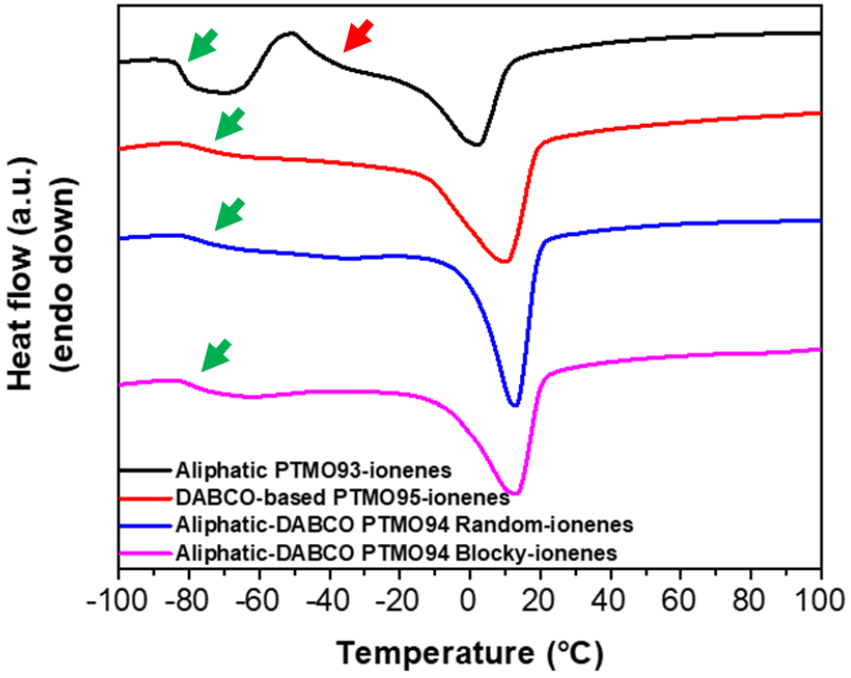

Figure 6.3: Overlayed DSC results of aliphatic PTMO93-ionenes, DABCO-based PTMO95-ionenes, aliphatic-DABCO PTMO94 Random-ionenes, and aliphatic-DABCO PTMO94 Blocky-ionenes from top to bottom. Green and red arrows represent glass transition of PTMO soft segment and cold crystallization, respectively.

Thermal transitions of PTMO-based ionenes were determined by using DSC as shown in Figure 6.3. DSC analysis revealed a single T_g for all ionenes at approximately -80 °C. This behavior was owing to the microphase separation of the PTMO soft segment from the ionic hard segments. Previous studies on PTMO-based ionenes presented the T_g of the hard segment by the presence of the chain extender, 1,12-dibromododecane, which resulted in

the prominent segmental motion of the 6,12-ionene structure of the hard segment. However, the PTMO-based ionenes we present here do not possess the chain extender and the content of hard segment was less than 10% for all samples, which did not present the T_g of hard segments. Aliphatic PTMO93-ionenes showed the lowest T_g of soft segments among other samples. The shift of T_g of the soft segment is often discussed in terms of the degree of microphase separation, and lower T_g of the soft segment typically represents the higher degree of microphase separation. However, a constraint on the motion of amorphous soft segment chains due to the crystallites of the soft segment can elevate T_g.[15] Hence, the increase of T_g with DABCO hard segments possibly results from the high degree of crystallinity. In fact, the value of dividing the melting enthalpy by the content of the hard segment, which represents the relative degree of crystallization of the PTMO soft segment, increased with ionenes with DABCO hard segments (Table 6.1). To avoid the effect of the degree of crystallites of the soft segment on T_g of the soft segment, a more rapid quenching process is required by dipping the pan in liquid nitrogen and performing in the prechilled DSC.

Table 6.1: Characteristic dimension of the four samples as determined from DSC, DMA and TGA analysis.

Sample	$T_{g,\,DSC}$ (°C)	$T_{g,\,DMA}$ (°C)	$T_{m,\,DSC}$ (°C)	ΔH_m (J/g)	ΔH/SS wt% (a.u.)	FWHM of T_m (°C)	$T_{d5\%}$
Aliphatic PTMO93-ionenes	-81.5	-76.3	2.6	28.5	0.31	15.54	264
DABCO-based PTMO95-ionenes	-77.0	-78.3	10.6	39.5	0.42	18.67	296
Aliphatic-DABCO PTMO94 Random-ionenes	-78.2	-78.3	13.2	39.1	0.42	11.42	283
Aliphatic DABCO PTMO94 Blocky-ionenes	-79.5	-78.6	13.3	38.3	0.41	16.11	277

The cold crystallization is often observed with the segmented ionenes due to the rearrangement of the PTMO soft segments. It is noteworthy that only aliphatic PTMO93-

ionenes did not show the PTMO crystallization peak upon cooling and the cold crystallization occurred upon heating. Our previous studies on PTMO-based ionenes suggested that the content of the soft segment over 50 wt% induced the cold crystallization of PTMO soft segment but not with ionenes with DABCO hard segment without 1,12-dibromododecane chain extender.[11] The mixture of aliphatic and DABCO hard segments did not present cold crystallization, indicating that the slow kinetics of PTMO crystallization by the linear aliphatic hard segment was suppressed due to the mixing of the DABCO hard segment.

DABCO-based PTMO95-ionenes showed a higher melting temperature of the PTMO crystallites compared to linear aliphatic hard segments. This revealed that DABCO hard segment provided better configurational freedom of the PTMO soft segment to be crystallized than the linear aliphatic hard segment, which was observed in our previous studies. The mixing of two hard segments regardless of the arrangement of two hard segments showed a similar melting temperature, which was higher than DABCO-based PTMO95-ionenes. The higher melting temperature of ionenes with mixed hard segments is attributed to the more stable crystallites on heating. Indeed, the relative degree of crystallization of PTMO of ionenes with mixed two hard segments was similar to DABCO-based PTMO95-ionenes, however, the FWHM values decreased. Aliphatic-DABCO PTMO94 Random-ionene revealed the lowest FWHM values among ionenes. This supports that mixing two hard segments affect the size distribution of spherulites and the random arrangement of hard segments provided a more homogenous size distribution of spherulites compared to the blocky arrangement of hard segments.

Table 6.2: Characteristic dimensions of the soft and hard domains, as determined by XRD, SAXS.

Sample	SAXS		XRD	
	q_3 (nm^{-1})	d_3 (nm)	d_2 (nm)	d_1 (nm)
Aliphatic PTMO93-ionenes	0.67	9.38	0.92	0.45
DABCO-based PTMO95-ionenes	0.62	10.13	0.92	0.45
Aliphatic-DABCO PTMO94 Random-ionenes	0.64	9.82	0.84	0.45
Aliphatic DABCO PTMO94 Blocky-ionenes	0.65	9.67	0.84	0.45

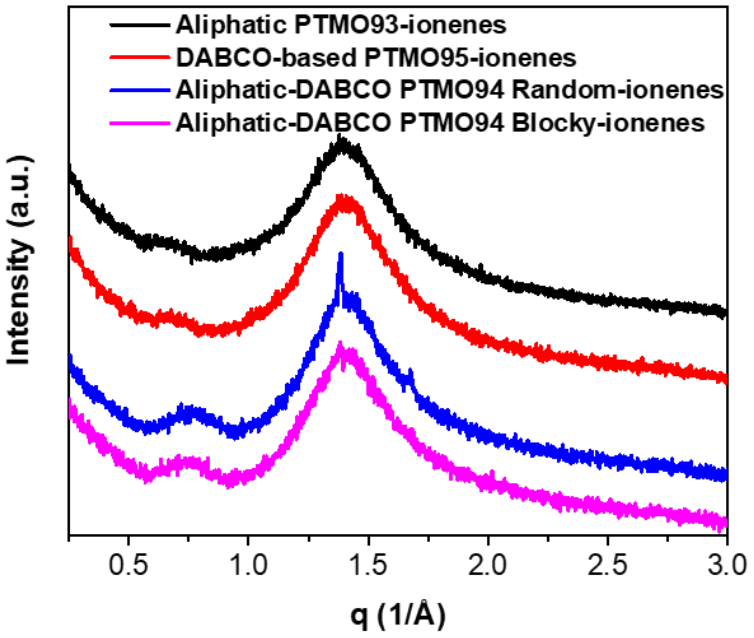

Figure 6.4: Overlayed XRD diffraction of aliphatic PTMO93-ionenes, DABCO-based PTMO95-ionenes, aliphatic-DABCO PTMO94 Random-ionenes, and aliphatic-DABCO PTMO94 Blocky-ionenes from top to bottom.

The morphology of ionenes was confirmed with XRD where all ionenes were amorphous at room temperature due to the lower melting temperature of PTMO crystallites as shown in Figure 6.4. However, aliphatic-DABCO PTMO94 Random-ionenes showed slight peaks of PTMO crystallites, which is owing to the high and narrow melting temperature in agreement with the DSC result. The PTMO dibromide monomer showed

two prominent sharp peaks (q = 1.47 and 1.78 $Å^{-1}$) from the PTMO crystallites.[11] The local structure within the ionenes was investigated with XRD. Two distinct peaks were observed for all ionenes. The peaks at 0.5-1 $Å^{-1}$ and 1-2 $Å^{-1}$ referred to as ion-to-ion peaks and PTMO-to-PTMO peaks, respectively. The peak q_1 having a correlation distance of $d_1 \approx$ 0.45 nm corresponds to the amorphous halo, and all ionenes showed a similar distance between PTMO-to-PTMO (Table 6.2). However, the Bragg distance between ion-to-ion decreased when mixing two hard segments to $d_2 \approx 0.84$ nm.

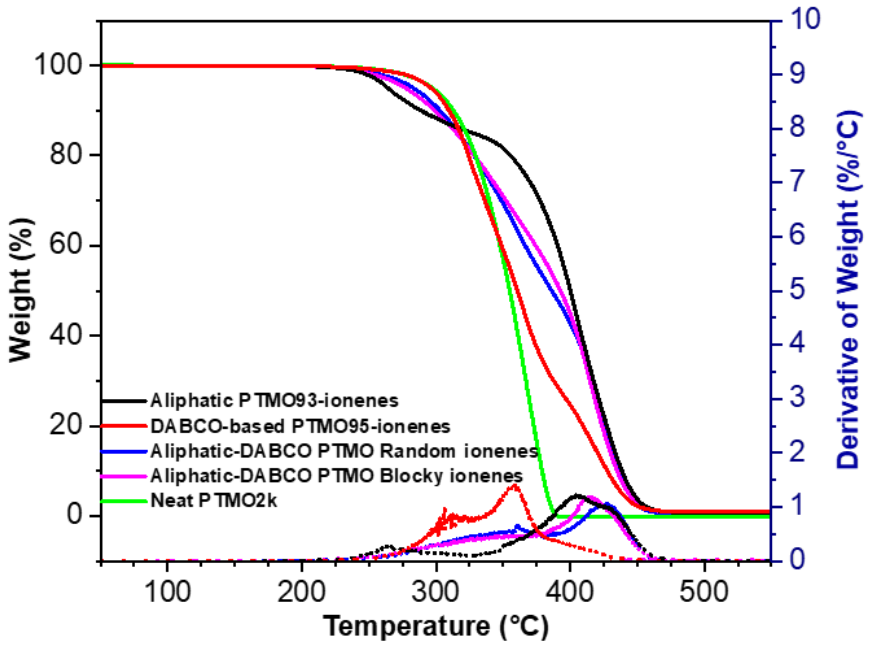

Figure 6.5: Overlayed TGA curves (solid lines) and derivative weight loss curves (dotted lines) for aliphatic PTMO93-ionenes, DABCO-based PTMO95-ionenes, aliphatic-DABCO PTMO94 Random-ionenes, and aliphatic-DABCO PTMO94 Blocky-ionenes.

The thermal stability of PTMO-based ionenes was studied using TGA under a nitrogen atmosphere as shown in Figure 6.5. Typically, segmented ionenes undergo degradation though the Hoffmann elimination depends on the basicity of the counterion, and Br counterion usually shows the Hoffmann elimination at approximately 250 °C. The

segmented ionenes degraded in two distinct steps. The first weight loss is attributed to the degradation of the hard segments, and the second weight loss corresponded to the degradation of the soft segments. The aliphatic PTMO93-ionene showed the lowest thermal stability ($T_{d5\%}$) and DABCO PTMO95-ionenes showed the highest thermal stability. This indicates that DABCO hard segment suppresses the Hoffmann elimination more significantly than the linear aliphatic hard segment. Mixing two hard segments showed the resemble thermal stability of linear aliphatic PTMO93-ionene and DABCO-based PTMO95-ionenes as expected. The temperature of 5% weight loss was between the temperature of linear aliphatic PTMO93-ionene and DABCO-based PTMO95-ionenes. Furthermore, the random arrangement of two hard segments showed higher thermal stability than the Blocky arrangement. Interestingly, DABCO-based PTMO95-ionene showed the second peak of the derivation of temperature at the lower temperature than aliphatic PTMO93-ionene, which indicates that the DABCO hard segment provided less protective effect on the degradation of the soft segments.

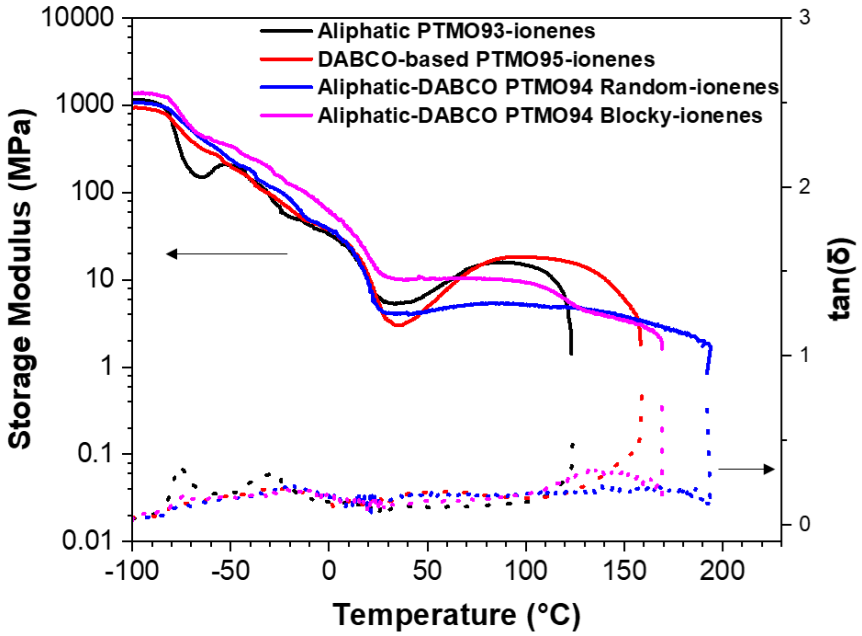

Figure 6.6: Overlayed DMA results of aliphatic PTMO93-ionenes, DABCO-based PTMO95-ionenes, aliphatic-DABCO PTMO94 Random-ionenes, and aliphatic-DABCO PTMO94 Blocky-ionenes.

The viscoelastic properties of PTMO-based ionenes were analyzed using DMA, as shown in Figure 6.6. The first transition is attributed to the segmental motions of the PTMO soft segment, and all samples showed T_g of the PTMO soft segment, which indicated the presence of the microphase separation. Aliphatic PTMO93-ionene showed the highest T_g of the soft segment among other segmented ionenes, and this support the discussion on DSC results that the lower T_g value of aliphatic PTMO93-ionene in DSC possibly resulted from the low degree of crystallization in the cooling process. In fact, the cooling rate of DMA was more rapid than DSC, which could suppress the degree of constraint on the motion of the amorphous PTMO chains, which are formed in the cooling process, in ionenes having DABCO hard segments. Hence, the change in the T_g values for PTMO soft segments described above with DSC results is not attributed to the degree of microphase

separation between ionic aggregates and PTMO soft segments. Furthermore, aliphatic PTMO93-ionene showed the upturn of storage modulus after T_g revealed the presence of cold crystallization of the PTMO soft segment in agreement with DSC analysis.

The second transition is attributed to the melting of PTMO crystallites, and aliphatic PTMO93-ionene showed a decrease of storage modulus at a lower temperature than other ionenes, which is consistent with the result obtained by DSC. All ionenes showed a significant reduction in storage modulus in the melting of PTMO crystallites.

The mixture of two hard segments revealed an extended rubbery plateau modulus than ionene with each hard segment, and aliphatic-DABCO PTMO94 Random ionene showed a wider rubbery plateau modulus than aliphatic-DABCO PTMO94Blocky-ionene. However, aliphatic-DABCO PTMO94 Blocky-ionene showed a higher rubbery plateau storage modulus than aliphatic-DABCO PTMO94 Random-ionene. This showed that the physical cross-linking effect is more notable in the blocky arrangement of hard segments compared to the random arrangement. This also suggests that the blocky arrangement of two hard segments had a higher degree of microphase separation. It is noteworthy that aliphatic PTMO93-ionene and DABCO-based PTMO95-ionenes showed an overshoot in the storage modulus after the melting of crystallites. This can be owing to the chain packing of the hard segment after rearrangement of the structure and changing the conformation of ionic domains.

The third transition occurred following ion dissociation. DABCO-based PTMO95-ionenes showed a higher temperature for the chains to completely disentangled than aliphatic PTMO93-ionenes, indicating that DABCO hard segment provided a higher

charge density and less mobility between physical cross-links. The mixture of two hard segments increased the ion dissociation temperature, and aliphatic-DABCO PTMO94 Random-ionene showed a higher ion dissociation temperature compared to aliphatic-DABCO PTMO94 Blocky-ionene. This showed that mixing two hard segments induced a higher percentage of entanglement and it became prominent with the random arrangement of the mixture of two hard segments.

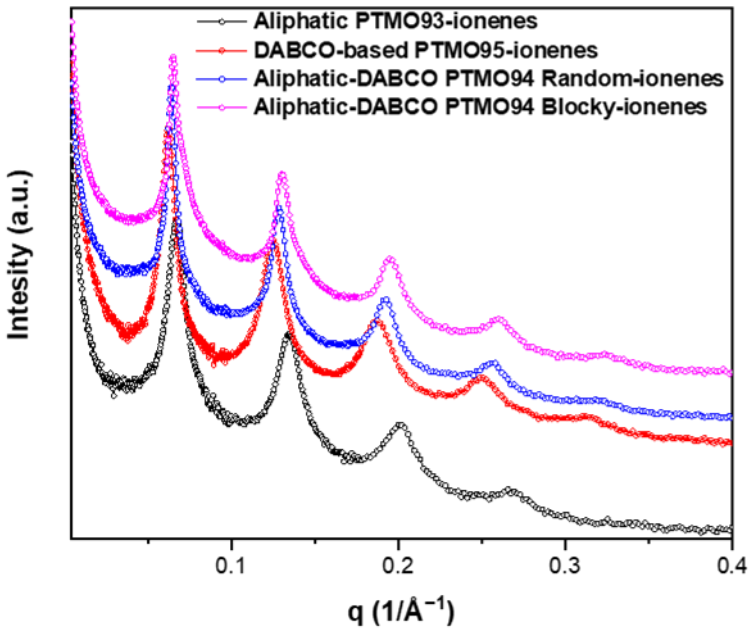

Figure 6.7: SAXS intensity as a function of scattering vector (q) (log-log scale) of aliphatic PTMO93-ionenes, DABCO-based PTMO95-ionenes, aliphatic-DABCO PTMO94 Random-ionenes, and aliphatic-DABCO PTMO94 Blocky-ionenes. Data are rescaled vertically.

SAXS showed that all ionenes exhibited a superior microphase separation. The first scattering peak at lower q represents the microdomain spacing. DABCO-based PTMO95-ionene showed a higher d-spacing value, 10.13 nm, compared to aliphatic PTMO93-ionene, 9.38 nm, as shown in Table 6.2. However, mixing two hard segments decreased

the d-spacing but was higher than aliphatic PTMO93-ionene. The SAXS profiles of all ionenes showed a sharp primary scattering peak accompanied by multiple scattering peaks indicating the existence of an ordered structure. The position of scattering maximums for all samples appeared at the ratio of 1:2:3:4 (i.e., q:2q:3q:4q in Figure 6.7) that represents the formation of microphase-separated lamellar structure. This also indicates that mixing two hard segments did not affect the morphology of the ionenes and showed lamellar structure.

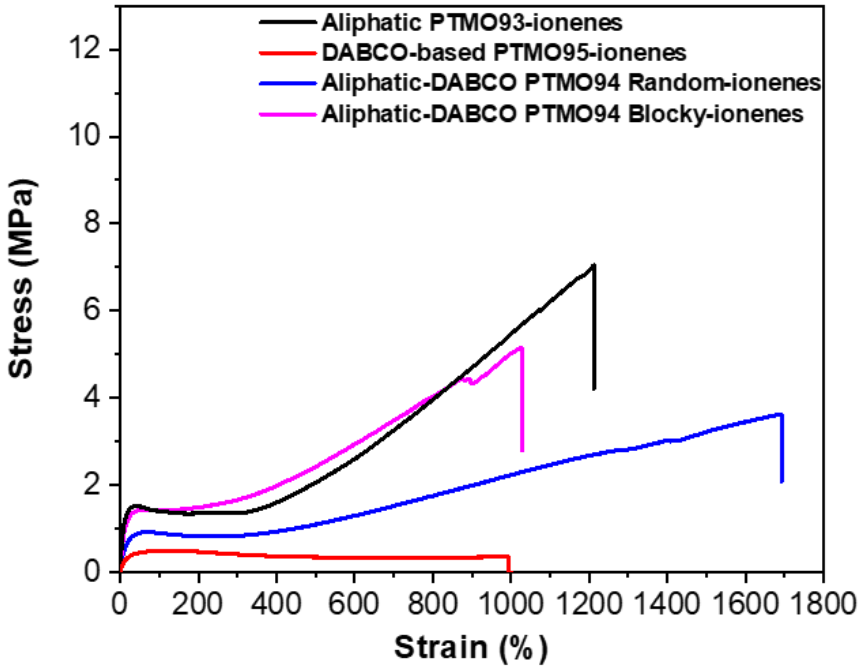

Figure 6.8: Tensile test of aliphatic PTMO93-ionenes, DABCO-based PTMO95-ionenes, aliphatic-DABCO PTMO94 Random-ionenes, and aliphatic-DABCO PTMO94 Blocky-ionenes. The stress-strain curves shown are representative examples of replicate experiments.

Mechanical properties of PTMO-based ionenes were investigated using tensile analysis. The tensile test was performed at room temperature as shown in Figure 6.8. The PTMO-based ionenes showed Young's modulus ranging from 1.4 to 8.3 MPa, an ultimate tensile

strength ranging from 0.5 to 6.1 MPa, and elongations at break ranging from 823% to 1465%, as listed in Table 6.3. The trends of Young's modulus followed the trends of the storage modulus in DMA results, which increased in the following order: DABCO-based PTMO95-ionene < aliphatic-DABCO PTMO94 Random-ionene < aliphatic PTMO93-ionene < aliphatic-DABCO PTMO94 Block-ionene, at room temperature. Our previous study showed that DABCO hard segment induced a higher Young's modulus compared to the linear aliphatic hard segment.[11] However, the results shown here contradict our previous results in that the linear aliphatic hard segment resulted in a stronger and more stretchy polymer compared to DABCO hard segment. This is possibly due to the absence of a chain extender, which provided the higher content of hard domain and larger ionic aggregation, thus shows a pronounced effect of enhanced charge density and ionic aggregation. Ionene with two hard segments showed the values of Young's modulus and ultimate tensile strength between the values of ionenes with each hard segment, and the blocky arrangement of hard segments formed a stronger and stiffer film than randomly arranged ionene. However, aliphatic-DABCO PTMO94 Random-ionene showed the highest elongation among PTMO-based ionenes, and even higher than blocky analog due to the fewer interchain interactions. Blocky arrangement of hard segments resembled the distinct mechanical properties resulting from each hard segment that led to lower elongation attributed to the DABCO hard segment, but higher Young's modulus attributed to the linear aliphatic hard segment. These results showed that mixing two hard segments can modify the stiffness and extensibility of the segmented ionenes.

Table 6.3: Tensile stress-strain data of four samples as determined from tensile test.

Sample	Young's Modulus (MPa)	Ultimate tensile strength (MPa)	Tensile strain at break (%)	Toughness (MPa)
Aliphatic PTMO93-ionenes	6.52 ± 4.62	6.12 ± 0.81	1293.68 ± 74.62	31.77 ± 5.89
DABCO-based PTMO95-ionenes	1.44 ± 0.11	0.48 ± 0.02	822.68 ± 278.43	3.19 ± 1.04
Aliphatic-DABCO PTMO94 Random-ionenes	4.88 ± 0.87	4.18 ± 1.49	1464.83 ± 199.49	32.37 ± 11.42
Aliphatic-DABCO PTMO94 Blocky-ionenes	8.28 ± 1.34	5.31 ± 1.28	1027.01 ± 117.54	30.21 ± 9.93

Moreover, the linear aliphatic hard segment cleared showed the stress-induced crystallization of PTMO chains under the elongation, which generated an upturn in the stress-strain curve and provided high stress at break, which was not shown with DABCO-based PTMO95-ionene. Nevertheless, the mixture of two hard segments also showed the stress-induced crystallization attributed to the linear aliphatic hard segment, and the blocky arrangement of the hard segment showed more comparable stress upon the stress-induced crystallization to aliphatic PTMO93-ionene than randomly arranged hard segments.

6.5 Conclusions

The mixing of two hard segments was successfully synthesized in segmented ionenes for the first time. The arrangement of two hard segments, randomly or blocky, was investigated on the properties and morphology of the segmented ionenes and compared with segmented ionenes possessing each hard segment type. All PTMO-based ionene regardless of the type of hard segment and whether it possesses a randomly or blocky arrangement of two hard segments showed superior microphase separation, which showed low distinct T_g of the PTMO soft segments. DMA confirmed the microphase separation.

Thermal stability and mechanical properties of the mixture of two hard segments resembled the trends of values of ionene with each hard segment type. DMA also suggested that the blocky arrangement of two hard segments provided higher charge density between ionic domain but showed lower entanglement compared to randomly distributed two hard segments, All PTMO-based ionene showed microphase-separated lamellar morphology revealed by SAXS, and the mixing of two hard segments did not affect the morphology of the segmented ionenes significantly.

6.6 References

1. Lee, J. S., Hocken, A. & Green, M. D. Advances in the molecular design of ionenes for a diverse range of applications. *Mol. Syst. Des. Eng.* **6**, 334–354 (2021).
2. Williams, S. R. & Long, T. E. Recent advances in the synthesis and structure–property relationships of ammonium ionenes. *Prog. Polym. Sci.* **34**, 762–782 (2009).
3. Yen, M. & Tsai, P. Study on polyethylene glycol/polydimethylsiloxane mixing soft-segment waterborne polyurethane from different mixing processes. *J. Appl. Polym. Sci.* **90**, 233–243 (2003).
4. Ahn, T. O., Jung, S.-U., Jeong, H. M. & Lee, S. W. The properties of polyurethanes with mixed chain extenders and mixed soft segments. *J. Appl. Polym. Sci.* **51**, 43–49 (1994).
5. Mirhosseini, M. M., Haddadi-Asl, V. & Jouibari, I. S. A simple and versatile method to tailor physicochemical properties of thermoplastic polyurethane elastomers by using novel mixed soft segments. *Mater. Res. Express* **6**, (2019).
6. Cui, Y., Wang, H., Pan, H., Yan, T. & Zong, C. The effect of mixed soft segment on the microstructure of thermoplastic polyurethane. *J. Appl. Polym. Sci.* **138**, 51346 (2021).
7. Askari, F., Barikani, M. & Barmar, M. Siloxane-based segmented poly(urethane-urea) elastomer: Synthesis and characterization. *J. Appl. Polym. Sci.* **130**, 1743–1751 (2013).
8. Kenney, J. F. Properties of block versus random copolymers. *Polym. Eng. Sci.* **8**, 216–226 (1968).

9. Kang, K. & Kim, D. Comparison of proton conducting polymer electrolyte membranes prepared from multi-block and random copolymers based on poly(arylene ether ketone). *J. Power Sources* **281**, 146–157 (2015).

10. Cho, J. W., Jung, Y. C., Chung, Y.-C. & Chun, B. C. Improved mechanical properties of shape-memory polyurethane block copolymers through the control of the soft-segment arrangement. *J. Appl. Polym. Sci.* **93**, 2410–2415 (2004).

11. Lee, J. S., Taghavimehr, M., Montazami, R. & Green, M. D. Synthesis and characterization of poly(tetramethylene oxide)-based segmented ionenes block copolymer with aliphatic or DABCO hard segments. *Polymer (Guildf).* **270**, 125772 (2023).

12. Ilavsky, J. & Jemian, P. R. Irena : tool suite for modeling and analysis of small-angle scattering. *J. Appl. Crystallogr.* **42**, 347–353 (2009).

13. Ilavsky, J. Nika : software for two-dimensional data reduction. *J. Appl. Crystallogr.* **45**, 324–328 (2012).

14. Tamami, M., Williams, S. R., Park, J. K., Moore, R. B. & Long, T. E. Poly(propylene glycol)-based ammonium ionenes as segmented ion-containing block copolymers. *J. Polym. Sci. Part A Polym. Chem.* **48**, 4159–4167 (2010).

15. Hashimoto, T. *et al.* Structure and properties of poly(tetrahydrofuran) viologen ionene: effects of halide counter-anions. *Polymer (Guildf).* **35**, 2672–2678 (1994).

CHAPTER 7

CONCLUSIONS AND FUTURE DIRECTIONS

7.1 Conclusions

In the pursuit of investigating the structure-property-function relationship of segmented ionenes, this dissertation work describes the synthesis and characterization of novel segmented ionenes with different types of soft and hard segments and counterion, and content of the soft/hard segments.

First, the segmented ionenes with two different soft segments, PEG and PTMO, structurally different hard segments, linear aliphatic ammonium and heterocyclic aliphatic ammonium, three different counter-anion species, bromine, tetrafluoroborate, and bis(trifluoromethanesulfonyl)imide, and three different weight fractions of soft and hard segments, 25/75, 50/50 and 75/25 wt%, were successfully synthesized for a direct comparison of each factor on the properties of segmented ionenes.

Linear aliphatic PEG-based segmented ionenes exhibited a lower degree of microphase separation compared to linear aliphatic PTMO-based segmented ionenes, owing to the less polar nature of the PEG soft segment. However, both DABCO-based PEG and PTMO ionenes demonstrated an enhanced degree of microphase separation due to the higher positive charge density and closer proximity of charged sites in the rigid DABCO structure. The mechanical properties of segmented ionenes were greatly influenced by the crystallites of the soft segment, as the melting temperature of the crystal had an impact on elastomeric behavior, tensile strength, and extensibility. The morphological difference between linear

aliphatic and DABCO hard segments was observed, with linear aliphatic displaying more interconnected hard domains, while the DABCO hard segment showed more isolated hard domains, regardless of the type of soft segment, thereby also affecting the mechanical properties of segmented ionenes.

The degree of crystallization of PEG and PTMO soft segments was observed to decrease with increasing content of the soft segment. PTMO-based ionenes were found to have a melting temperature of PTMO crystallites below room temperature and to form a robust elastomer compared to PEG-based ionenes, regardless of the content of the soft segments. Increasing the content of hard segments was observed to improve the elastomeric properties of segmented ionenes due to an increase in ionic aggregation, regardless of the type of soft segments (PEG or PTMO). When the weight fraction of the soft segment was increased up to 75 wt%, soft-hard mixing was triggered in both linear aliphatic and DABCO hard segments with PEG soft segment. However, PTMO soft segments showed a better degree of phase separation with both types of hard segments compared to their PEG-based analogs. Further increasing the weight fraction of the soft segment without the chain extender, 1,12-dibromododecane, resulted in an alternating arrangement of soft and hard segments and induced a microphase-separated lamellar morphology. Furthermore, PTMO soft segments induced stress-induced crystallization, unlike PEG soft segments, which occurred at higher contents of PTMO soft segments over 50 wt% and prevented further elongation.

The thermal, mechanical, and morphological properties of segmented ionenes were found to be significantly influenced by the type of counterion employed. A larger

counterion size was found to decrease the glass transition of the hard domain and promote weaker ionic aggregation. Thermal stability was found to be dependent on the basicity of the counter-anion, with lower basicity counter-ions inducing higher thermal stability irrespective of the type of soft and hard segments. The chain packing of hard segments was found to be influenced by the size of counterion in DABCO-based PTMO ionenes, but not observed in linear aliphatic hard segments with PEG or PTMO soft segments.

In addition, the mechanical and thermomechanical properties of segmented ionenes were found to be influenced by the combination of two types of hard segments and their arrangement within the polymer matrix. Random distribution of the two hard segments resulted in greater entanglement, while the blocky arrangement induced a higher degree of microphase separation compared to the randomly arranged analog. Despite the arrangement of the hard segments, the alternating soft and hard segments of the polymer structure still yielded a lamellar morphology.

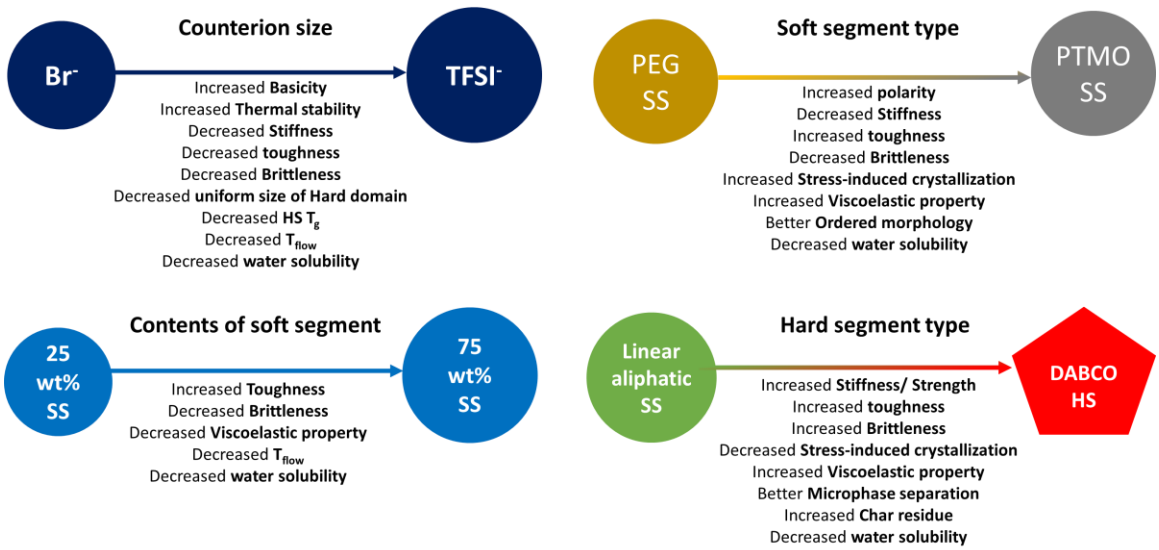

Figure 7.1: Schematic image of projected properties depending on the type of counterion, soft segment, hard segment, and contents of the soft segment.

The present study elucidates the anticipated characteristics of segmented ionenes based on various factors, such as the nature of the soft and hard segments, the type of counterions employed, and the soft segment content. The general overview of these properties is visually represented in Figure 7.1. Additionally, a comprehensive and intricate analysis of the projected properties of the ionenes investigated in this thesis is presented in Figure 7.2, revealing a multifaceted correlation among these properties.

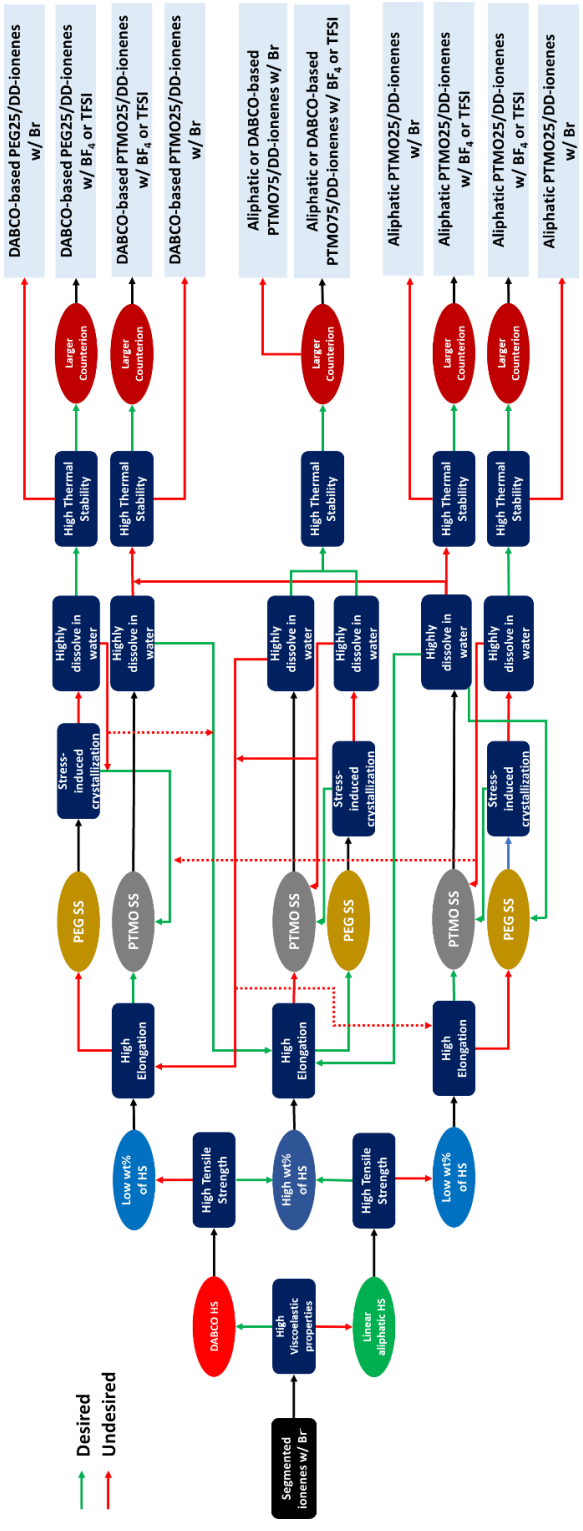

Figure 7.2: Schematic chart of ideal segmented ionenes depending on the anticipated performance and the intricate interplay among various factors.

7.2 Future Directions

The charge density of ionenes can be tuned not only by the content of soft/hard segments but also by the molecular weight of soft segments. Tamimi et al. revealed that increasing the molecular of the PPG soft segment resulted in the extension of the rubbery plateau modulus to higher temperature due to the enhanced entanglements.[1] However, a lower molecular weight of the PPG soft segment increased the rubbery plateau modulus owing to the stronger physical cross-linking by the lower molecular weight between ionic sites. Das et al. demonstrated the synthesis of PDMS-based segmented ionenes with different molecular weights of soft segments.[2] The increase in molecular weight of PDMS soft segments induced the weakening of the ionic association and led to the shortening of the rubbery plateau modulus and decreasing the ion dissociation temperature. Furthermore, Feng et al. described the synthesis of PTMO-based segmented ionenes with a different molecular weight of soft segments.[3] The increase of the molecular weight of the PTMO soft segment resulted in the decrease of rubbery storage modulus due to the weaker ionic aggregation.

In the realm of segmented ionenes, alterations in the molecular weight of the soft segment result in the adjustment of charge density, as the distance between charge sites is altered. It follows that any increase in the molecular weight of the soft segment would inevitably impact the content of the hard segment. As such, a mere modification of the soft segment's molecular weight cannot provide a comprehensive understanding of its exclusive effect on the properties of ionenes. Rather, a direct comparison between two segmented ionenes with varying molecular weights of the soft segment and the same hard segment

content is essential to grasp the true impact of molecular weight on ionene properties. Hence, further research on the modulation of the soft segment's molecular weight without affecting the hard segment's content is necessary to better comprehend the molecular weight's influence on the properties of segmented ionenes.

Segmented ionenes remain largely unexplored in practical applications, necessitating extensive research to investigate their performance in diverse fields such as biomedical devices and sorbents for carbon dioxide capture. Incorporation of hydrophobic soft segments, such as PDMS, and counterions such as BF_4, is suggested to facilitate the use of segmented ionenes in biological applications. Non-segmented ionenes have shown promising antimicrobial properties due to their strong electrostatic interaction with bacteria. However, segmented ionenes have even greater potential in biomedical applications due to their superior mechanical and elastomeric properties compared to non-segmented ionenes. In addition, segmented ionenes have been identified as strong candidates for carbon dioxide capture due to their ability to control charge density, which is higher than that of ionomers and thus acts as a driving force for capturing carbon dioxide. To fully understand the potential of segmented ionenes in carbon dioxide capture, investigation of a wider range of counter-anions, as well as the type of soft and hard segment, is recommended.

7.3 References

1. Tamami, M., Williams, S. R., Park, J. K., Moore, R. B. & Long, T. E. Poly(propylene glycol)-based ammonium ionenes as segmented ion-containing block copolymers. *J. Polym. Sci. Part A Polym. Chem.* **48**, 4159–4167 (2010).
2. Das, S. *et al.* Synthesis and Characterization of Novel Segmented Polyionenes Based on Polydimethylsiloxane Soft Segments. *J. Macromol. Sci. Part A* **47**, 215–224 (2010).

3. Feng, D., Venkateshwaran, L. N., Wilkes, G. L., Leir, C. M. & Stark, J. E. Structure-property behavior of elastomeric segmented PTMO–ionene polymers. II. *J. Appl. Polym. Sci.* **38**, 1549–1565 (1989).

REFERENCES

1. Williams, S. R. & Long, T. E. Recent advances in the synthesis and structure–property relationships of ammonium ionenes. *Prog. Polym. Sci.* **34**, 762–782 (2009).

2. Williams, S. R., Long, T. E., Ward, T. C., Turner, S. R. & Roman, M. Influence of Electrostatic Interactions and Hydrogen Bonding on the Thermal and Mechanical Properties of Step-Growth Polymers Influence of Electrostatic Interactions and Hydrogen Bonding on the Thermal and Mechanical Properties of Step-Growth Polymers. *Dissertation* (2008).

3. Bara, J. E. & O'Harra, K. E. Recent Advances in the Design of Ionenes: Toward Convergence with High-Performance Polymers. *Macromol. Chem. Phys.* **220**, 1900078 (2019).

4. Gibbs, C. F., Littmann, E. R. & Marvel, C. S. Quaternary Ammonium Salts from Halogenated Alkyl Dimethylamines. II. The Polymerization of Gamma-Halogenopropyldimethylamines. *J. Am. Chem. Soc.* **55**, 753–757 (1933).

5. Rembaum, A., Baumgartner, W. & Eisenberg, A. Aliphatic ionenes. *J. Polym. Sci. Part B Polym. Lett.* **6**, 159–171 (1968).

6. Daly, W. H. & Hölle, H. J. Polyarylsulfonimides. *J. Polym. Sci. Part B Polym. Lett.* **10**, 519–525 (1972).

7. Shi, Q. *et al.* Improvement in LiFePO4–Li battery performance via poly(perfluoroalkylsulfonyl)imide (PFSI) based ionene composite binder. *J. Mater. Chem. A* **1**, 15016 (2013).

8. Williams, S. R., Salas-de la Cruz, D., Winey, K. I. & Long, T. E. Ionene segmented block copolymers containing imidazolium cations: Structure–property relationships as a function of hard segment content. *Polymer (Guildf).* **51**, 1252–1257 (2010).

9. Das, S. *et al.* Structure–property relationships and melt rheology of segmented, non-chain extended polyureas: Effect of soft segment molecular weight. *Polymer (Guildf).* **48**, 290–301 (2007).

10. Kohjiya, S., Ohtsuki, T. & Yamashita, S. Polyelectrolyte Behavior of an Ionene Containing Poly(oxytetramethylene) Units. *Makromol. Chemie, Rapid Commun.* **2**, 417–420 (1981).

11. Feng, D., Venkateshwaran, L. N., Wilkes, G. L., Leir, C. M. & Stark, J. E. Structure-property behavior of elastomeric segmented PTMO–ionene polymers. II. *J. Appl. Polym. Sci.* **38**, 1549–1565 (1989).

12. Wang, M. Z., Li, D. S., Luo, X. L. & Ma, D. Z. Crystallization and melting behavior of the soft and hard segments in poly(ester-ether)s. II. Ethylene oxide-

butylene terephthalate segmented copolymers. *J. Polym. Sci. Part B Polym. Phys.* **37**, 2928–2940 (1999).

13. Das, S. *et al.* Synthesis and Characterization of Novel Segmented Polyionenes Based on Polydimethylsiloxane Soft Segments. *J. Macromol. Sci. Part A* **47**, 215–224 (2010).

14. Rutkowska, M. Polyester polyurethane ionomers. *J. Appl. Polym. Sci.* **31**, 1469–1482 (1986).

15. Rembaum, A. & Noguchi, H. Reactions of N,N,N',N'-Tetramethyl-α,ι-diaminoalkanes with α,ι-Dihaloalkanes. II. x-y Reactions. *Macromolecules* **5**, 261–269 (1972).

16. Zelikin, A. N., Akritskaya, N. I. & Izumrudov, V. A. Modified Aliphatic Ionenes. Influence of Charge Density and Length of the Chains on Complex Formation with Poly(methacrylic acid). *Macromol. Chem. Phys.* **202**, 3018–3026 (2001).

17. Tamami, M., Williams, S. R., Park, J. K., Moore, R. B. & Long, T. E. Poly(propylene glycol)-based ammonium ionenes as segmented ion-containing block copolymers. *J. Polym. Sci. Part A Polym. Chem.* **48**, 4159–4167 (2010).

18. Bachl, J., Bertran, O., Mayr, J., Alemán, C. & Díaz Díaz, D. Aromatic ionene topology and counterion-tuned gelation of acidic aqueous solutions. *Soft Matter* **13**, 3031–3041 (2017).

19. Suzuki, K., Yamaguchi, M., Hotta, S., Tanabe, N. & Yanagida, S. A new alkyl-imidazole polymer prepared as an inonic polymer electrolyte by in situ polymerization of dye sensitized solar cells. *J. Photochem. Photobiol. A Chem.* **164**, 81–85 (2004).

20. Hemp, S. T. *et al.* Comparing Ammonium and Phosphonium Polymerized Ionic Liquids: Thermal Analysis, Conductivity, and Morphology. *Macromol. Chem. Phys.* **214**, 2099–2107 (2013).

21. Feng, D., Wilkes, G. L., Lee, B. & McGrath, J. E. Structure-property behaviour of segmented poly (tetramethylene oxide)-based bipyridinium ionene elastomers. *Polymer (Guildf).* **33**, 526–535 (1992).

22. Thankamony, R. L. *et al.* Preparation and characterization of imidazolium-PEO-based Ionene/PVDF(HFP)/LiTFSI as a novel Gel polymer electrolyte. *Macromol. Res.* **23**, 38–44 (2015).

23. Matsumi, N., Sugai, K., Miyake, M. & Ohno, H. Polymerized Ionic Liquids via Hydroboration Polymerization as Single Ion Conductive Polymer Electrolytes. *Macromolecules* **39**, 6924–6927 (2006).

24. Druchok, M., Vlachy, V. & Dill, K. A. Explicit-water molecular dynamics study of a short-chain 3,3 ionene in solutions with sodium halides. *J. Chem. Phys.* **130**, 134903 (2009).

25. Rodič, P., Bratuša, M., Lukšič, M., Vlachy, V. & Hribar-Lee, B. Influence of the hydrophobic groups and the nature of counterions on ion-binding in aliphatic ionene solutions. *Colloids Surfaces A Physicochem. Eng. Asp.* **424**, 18–25 (2013).

26. Lukšič, M., Hribar-Lee, B., Buchner, R. & Vlachy, V. Modelling fast mode dielectric relaxation of counterions in aqueous solutions of ionene bromides and fluorides. *Phys. Chem. Chem. Phys.* **11**, 10053 (2009).

27. Lukšič, M., Buchner, R., Hribar-Lee, B. & Vlachy, V. Dielectric Relaxation Spectroscopy of Aliphatic Ionene Bromides and Fluorides in Water: The Role of the Polyion's Charge Density and the Nature of the Counterions. *Macromolecules* **42**, 4337–4342 (2009).

28. Tamami, M., Salas-de la Cruz, D., Winey, K. I. & Long, T. E. Structure-Property Relationships of Water-Soluble Ammonium-Ionene Copolymers. *Macromol. Chem. Phys.* **213**, 965–972 (2012).

29. Meyer, W. H., Rietz, R. R., Schaefer, D. & Kremer, F. Dielectric and electric relaxation in ionene-glasses. *Electrochim. Acta* **37**, 1491–1494 (1992).

30. Haskins, N. J. & Mitchell, R. Thermal degradation of some benzyltrialkylammonium salts using pyrolysis–gas chromatography–mass spectrometry. *Analyst* **116**, 901–903 (1991).

31. Charlier, P., Jérome, R., Teyssié, P. & Proud'Homme, R. E. Thermal stability of modified telechelic polystyrenes. *J. Polym. Sci. Part A Polym. Chem.* **31**, 129–134 (1993).

32. Tsutsui, T., Tanaka, R. & Tanaka, T. Mechanical relaxations in some ionene polymers. I. Effect of Ion concentration. *J. Polym. Sci. Polym. Phys. Ed.* **14**, 2259–2271 (1976).

33. Kammakakam, I., O'Harra, K. E., Dennis, G. P., Jackson, E. M. & Bara, J. E. Self-healing imidazolium-based ionene-polyamide membranes: an experimental study on physical and gas transport properties. *Polym. Int.* **68**, 1123–1129 (2019).

34. Mittenthal, M. S. *et al.* Ionic Polyimides: Hybrid Polymer Architectures and Composites with Ionic Liquids for Advanced Gas Separation Membranes. *Ind. Eng. Chem. Res.* **56**, 5055–5069 (2017).

35. Kammakakam, I. *et al.* An imidazolium-based ionene blended with crosslinked PEO as a novel polymer membrane for selective CO2 separation. *Macromol. Res.* **22**, 907–916 (2014).

36. Li, P. & Coleman, M. R. Synthesis of room temperature ionic liquids based random copolyimides for gas separation applications. *Eur. Polym. J.* **49**, 482–491 (2013).

37. Li, P., Zhao, Q., Anderson, J. L., Varanasi, S. & Coleman, M. R. Synthesis of copolyimides based on room temperature ionic liquid diamines. *J. Polym. Sci. Part*

A Polym. Chem. **48**, 4036–4046 (2010).

38. O'Harra, K. *et al.* Synthesis and Performance of 6FDA-Based Polyimide-Ionenes and Composites with Ionic Liquids as Gas Separation Membranes. *Membranes (Basel).* **9**, 79 (2019).

39. Hemp, S. T., Zhang, M., Tamami, M. & Long, T. E. Phosphonium ionenes from well-defined step-growth polymerization: thermal and melt rheological properties. *Polym. Chem.* **4**, 3582–3590 (2013).

40. Bradaric, C. J., Downard, A., Kennedy, C., Robertson, A. J. & Zhou, Y. Industrial preparation of phosphonium ionic liquids. *Green Chem.* **5**, 143–152 (2003).

41. Yang, X. & Smith, R. C. Phosphonium-based polyelectrolyte networks with high thermal stability, high alkaline stability, and high surface areas. *J. Polym. Sci. Part A Polym. Chem.* **57**, 598–604 (2019).

42. Williams, S. R., Barta, Z., Ramirez, S. M. & Long, T. E. Synthesis of 12,12-Ammonium Ionenes with Functionality for Chain Extension and Cross-Linking via UV Irradiation. *Macromol. Chem. Phys.* **210**, 555–564 (2009).

43. Jeon, Y. M. & Gong, M. S. Preparation of water-resistant humidity sensor using photocurable reactive oligomers containing lonene unit and their properties. *Polym.* **33**, 19–25 (2009).

44. Gong, M.-S. Anchoring of self-curable ionene-containing polyesters to electrode surface by UV irradiation and their humidity-sensitive properties. *Sensors Actuators B Chem.* **148**, 559–568 (2010).

45. Zelikin, A. N., Litmanovich, A. A., Paraschuk, V. V., Sybatchin, A. V. & Izumrudov, V. A. Conformational Changes of Aliphatic Ionenes in Water-Salt Solutions as a Factor Controlling Stability of Their Complexes with Calf Thymus DNA. *Macromolecules* **36**, 2066–2071 (2003).

46. Narita, T., Ohtakeyama, R., Nishino, M., Gong, J. P. & Osada, Y. Effects of charge density and hydrophobicity of ionene polymer on cell binding and viability. *Colloid Polym. Sci.* **278**, 884–887 (2000).

47. Zelikin, A. N., Putnam, D., Shastri, P., Langer, R. & Izumrudov, V. A. Aliphatic Ionenes as Gene Delivery Agents: Elucidation of Structure−Function Relationship through Modification of Charge Density and Polymer Length. *Bioconjug. Chem.* **13**, 548–553 (2002).

48. Izumrudov, V. A. & Zhiryakova, M. V. Stability of DNA-containing interpolyelectrolyte complexes in water-salt solutions. *Macromol. Chem. Phys.* **200**, 2533–2540 (1999).

49. Izumrudov, V. A., Zhiryakova, M. V & Kudaibergenov, S. E. Controllable stability of DNA-containing polyelectrolyte complexes in water-salt solutions. *Biopolymers* **52**, 94–108 (1999).

50. Zelikin, A. N. & Izumrudov, V. A. Polyelectrolyte Complexes Formed by Calf Thymus DNA and Aliphatic Ionenes: Unexpected Change in Stability upon Variation of Chain Length of Ionenes of Different Charge Density. *Macromol. Biosci.* **2**, 78–81 (2002).

51. Wahlund, P.-O., Izumrudov, V. A., Gustavsson, P.-E., Larsson, P.-O. & Galaev, I. Y. Phase Separations in Water-Salt Solutions of Polyelectrolyte Complexes Formed by RNA and Polycations: Comparison with DNA Complexes. *Macromol. Biosci.* **3**, 404–411 (2003).

52. El-Hamshary, H., El-Newehy, M. H., Moydeen Abdulhameed, M., El-Faham, A. & Elsherbiny, A. S. Evaluation of clay-ionene nanocomposite carriers for controlled drug delivery: Synthesis, in vitro drug release, and kinetics. *Mater. Chem. Phys.* **225**, 122–132 (2019).

53. Tomlinson, E., Brown, M. R. W. & Davis, S. S. Effect of colloidal association on the measured activity of alkylbenzyldimethylammonium chlorides against Pseudomonas aeruginosa. *J. Med. Chem.* **20**, 1277–1282 (1977).

54. Liu, X., Zhang, H., Tian, Z., Sen, A. & Allcock, H. R. Preparation of quaternized organic–inorganic hybrid brush polyphosphazene-co-poly[2-(dimethylamino)ethyl methacrylate] electrospun fibers and their antibacterial properties. *Polym. Chem.* **3**, 2082 (2012).

55. Ding, B.-P., Wu, F., Chen, S.-C., Wang, Y.-Z. & Zeng, J.-B. Synthesis and characterization of a polyurethane ionene/zinc chloride complex with antibacterial properties. *RSC Adv.* **5**, 12423–12433 (2015).

56. Cakmak, I., Ulukanli, Z., Tuzcu, M., Karabuga, S. & Genctav, K. Synthesis and characterization of novel antimicrobial cationic polyelectrolytes. *Eur. Polym. J.* **40**, 2373–2379 (2004).

57. Venkataraman, S. *et al.* Identi fication of Structural Attributes Contributing to the Potency and Selectivity of Antimicrobial Polyionenes: Amides Are Better Than Esters. *Biomacromolecules* **20**, 2737–2742 (2019).

58. Geng, Z. & Finn, M. G. Thiabicyclononane-Based Antimicrobial Polycations. *J. Am. Chem. Soc.* **139**, 15401–15406 (2017).

59. Strassburg, A. *et al.* Cross-Linking of a Hydrophilic, Antimicrobial Polycation toward a Fast-Swelling, Antimicrobial Superabsorber and Interpenetrating Hydrogel Networks with Long Lasting Antimicrobial Properties. *ACS Appl. Mater. Interfaces* **9**, 36573–36582 (2017).

60. Lakouraj, M. M., Soleimani, M. & Hasantabar, V. Synthesis and physical properties of interpenetrating network of poly (Acrylamide-Co-2, 4-Ionene) hydrogels. *World Appl. Sci. J.* **21**, 250–259 (2013).

61. Liu, S. *et al.* Biomaterials Highly potent antimicrobial polyionenes with rapid

killing kinetics , skin biocompatibility and in vivo bactericidal activity. *Biomaterials* **127**, 36–48 (2017).

62. Berginc, M., Opara Krašovec, U., Jankovec, M. & Topič, M. The effect of temperature on the performance of dye-sensitized solar cells based on a propyl-methyl-imidazolium iodide electrolyte. *Sol. Energy Mater. Sol. Cells* **91**, 821–828 (2007).

63. Abate, A. *et al.* A polyfluoroalkyl imidazolium ionic liquid as iodide ion source in dye sensitized solar cells. *Org. Electron.* **13**, 2474–2478 (2012).

64. Fei, Z. *et al.* A Supercooled Imidazolium Iodide Ionic Liquid as a Low-Viscosity Electrolyte for Dye-Sensitized Solar Cells. *Inorg. Chem.* **45**, 10407–10409 (2006).

65. Li, F. *et al.* Novel quasi-solid electrolyte for dye-sensitized solar cells. *J. Power Sources* **165**, 911–915 (2007).

66. Ng, H. M., Ramesh, S. & Ramesh, K. Efficiency improvement by incorporating 1-methyl-3-propylimidazolium iodide ionic liquid in gel polymer electrolytes for dye-sensitized solar cells. *Electrochim. Acta* **175**, 169–175 (2015).

67. Shi, Q. *et al.* Single ion solid-state composite electrolytes with high electrochemical stability based on a poly(perfluoroalkylsulfonyl)-imide ionene polymer. *J. Mater. Chem. A* **2**, 15952–15957 (2014).

68. Terenteva, E. A., Arkhipova, V. V., Apyari, V. V., Volkov, P. A. & Dmitrienko, S. G. Simple and rapid method for screening of pyrophosphate using 6,6-ionene-stabilized gold and silver nanoparticles. *Sensors Actuators B Chem.* **241**, 390–397 (2017).

69. Terenteva, E. A., Apyari, V. V., Dmitrienko, S. G. & Zolotov, Y. A. Spectrophotometric determination of sulfates using silver nanoparticles stabilized with 6,6-ionene. *Moscow Univ. Chem. Bull.* **70**, 157–161 (2015).

70. Apyari, V. V., Ioutsi, A. N., Arkhipova, V. V., Dmitrienko, S. G. & Shapovalova, E. N. 6,6-ionene-stabilized gold nanoparticles: synthesis, characterization and prospects of use. *Adv. Nat. Sci. Nanosci. Nanotechnol.* **6**, 025002 (2015).

71. Arkhipova, V. V., Apyari, V. V. & Dmitrienko, S. G. A colorimetric probe based on desensitized ionene-stabilized gold nanoparticles for single-step test for sulfate ions. *Spectrochim. Acta Part A Mol. Biomol. Spectrosc.* **139**, 335–341 (2015).

72. Teli, M. D. & Nadathur, G. T. Adsorptive removal of acid yellow 17 (an anionic dye) from water by novel ionene chloride modified electrospun silica nanofibres. *J. Environ. Chem. Eng.* **6**, 7257–7272 (2018).

73. Dragan, E. S., Mayr, J., Häring, M., Cocarta, A. I. & Díaz, D. D. Spectroscopic Characterization of Azo Dyes Aggregation Induced by DABCO-Based Ionene Polymers and Dye Removal Efficiency as a Function of Ionene Structure. *ACS Appl. Mater. Interfaces* **8**, 30908–30919 (2016).

74. Pirogov, A. V., Krokhin, O. V., Platonov, M. M., Deryugina, Y. I. & Shpigun, O. A. Ion-chromatographic selectivity of polyelectrolyte sorbents based on some aliphatic and aromatic ionenes. *J. Chromatogr. A* **884**, 31–39 (2000).

75. Mansur, C. R. E. *et al.* Nanocomposites based on ionene-bentonite used to treat oily water. *J. Appl. Polym. Sci.* **123**, 218–226 (2012).

76. Saborío, M. G. *et al.* Cationic ionene as an n-dopant agent of poly(3,4-ethylenedioxythiophene). *Phys. Chem. Chem. Phys.* **20**, 9855–9864 (2018).

77. Sandoval, A. P., Feliu, J. M., Torresi, R. M. & Suárez-Herrera, M. F. Electrochemical properties of poly(3,4-ethylenedioxythiophene) grown on Pt(111) in imidazolium ionic liquids. *RSC Adv.* **4**, 3383–3391 (2014).

78. Kundu, S. K., Matsunaga, T., Yoshida, M. & Shibayama, M. Rheological Study on Rapid Recovery of Hydrogel Based on Oligomeric Electrolyte. *J. Phys. Chem. B* **112**, 11537–11541 (2008).

79. Le Bideau, J., Ducros, J.-B., Soudan, P. & Guyomard, D. Solid-State Electrode Materials with Ionic-Liquid Properties for Energy Storage: the Lithium Solid-State Ionic-Liquid Concept. *Adv. Funct. Mater.* **21**, 4073–4078 (2011).

80. Chen, B. *et al.* Highly Stretchable and Transparent Ionogels as Nonvolatile Conductors for Dielectric Elastomer Transducers. *ACS Appl. Mater. Interfaces* **6**, 7840–7845 (2014).

81. Yoshida, M. Ionic gelators: oligomeric and polymeric electrolytes as novel gel forming materials. *Chem. Rec.* **10**, 230–242 (2010).

82. Yoshida, M. *et al.* Oligomeric Electrolyte as a Multifunctional Gelator. *J. Am. Chem. Soc.* **129**, 11039–11041 (2007).

83. Kundu, S. K., Yoshida, M. & Shibayama, M. Effect of Salt Content on the Rheological Properties of Hydrogel Based on Oligomeric Electrolyte. *J. Phys. Chem. B* **114**, 1541–1547 (2010).

84. Koumura, N., Matsumoto, H., Kawanami, H., Tamaoki, N. & Yoshida, M. Tuning of solubility and gelation ability of oligomeric electrolyte by anion exchange. *Polym. J.* **42**, 759–765 (2010).

85. Misawa, Y., Koumura, N., Matsumoto, H., Tamaoki, N. & Yoshida, M. Hydrogels Based on Surfactant-Free Ionene Polymers with N,N′ -(p -Phenylene)dibenzamide Linkages. *Macromolecules* **41**, 8841–8846 (2008).

86. Bachl, J. *et al.* Synergistic Computational-Experimental Approach to Improve Ionene Polymer-Based Functional Hydrogels. *Adv. Funct. Mater.* **24**, 4893–4904 (2014).

87. Häring, M., Grijalvo, S., Haldar, D., Saldías, C. & Díaz, D. D. Polymer topology-controlled self-healing properties of polyelectrolyte hydrogels based on DABCO-

containing aromatic ionenes. *Eur. Polym. J.* **115**, 221–224 (2019).

88. Watanabe, M., Toneaki, N. & Shinohara, I. Preparation of Elastomeric Ionene Polymers Containing 4,4′-Bipyridinium or 1,2-Bis(4-pyridinium)ethylene Ring and the Conductivity of Their TCNQ Salts. *Polym. J.* **14**, 189–195 (1982).

89. Grassl, B. & Galin, J. C. Segmented Poly(tetramethylene oxide) Zwitterionomers and Their Homologous Ionenes. 1. Synthesis, Molecular Characterization, and Thermal Stability. *Macromolecules* **28**, 7035–7045 (1995).

90. Somoano, R., Yen, S. P. S. & Rembaum, A. VI. Electronic conductivity of elastomeric ionenes. *J. Polym. Sci. Part B Polym. Lett.* **8**, 467–479 (1970).

91. Hashimoto, T. *et al.* Structure and properties of poly(tetrahydrofuran) viologen ionene: effects of halide counter-anions. *Polymer (Guildf).* **35**, 2672–2678 (1994).

92. Ikeda, Y., Yamato, J., Murakami, T. & Kajiwara, K. Aliphatic poly(oxytetramethylene) ionenes: effect of counter-anion on the properties and morphology. *Polymer (Guildf).* **45**, 8367–8375 (2004).

93. Ikeda, Y. *et al.* One-pot synthesis and characterization of aliphatic poly(oxytetramethylene) ionene. *Polymer (Guildf).* **43**, 3483–3488 (2002).

94. Feng, D., Wilkes, G. L., Leir, C. M. & Stark, J. E. Morphological Investigation of Polytetba-Methyleneoxide-Dibbomoxylene Segmented Ionene Polymebs by Tbansmission Electbon Micboscopy and Small-Angle X-Ray Scattebing. *J. Macromol. Sci. Part A - Chem.* **26**, 1151–1181 (1989).

95. Feng, D. & Wilkes, G. L. Chain extension in unoriented ion-containing polymers - does it occur? *Macromolecules* **24**, 6788–6790 (1991).

96. Ikeda, Y., Murakami, T., Yuguchi, Y. & Kajiwara, K. Synthesis and Characterization of Poly(oxytetramethylene) Ionene with 2,2‘-Bipyridinium Units. *Macromolecules* **31**, 1246–1253 (1998).

97. Vijayaraghavan, P., Brown, J. R. & Hall, L. M. Modeling the Effect of Polymer Composition on Ionic Aggregation in Poly(propylene glycol)-Based Ionenes. *Macromol. Chem. Phys.* **217**, 930–939 (2016).

98. Kamiya, T., Goto, K. & Shinohara, I. Electric conductivity of TCNQ salts of ionene polymers containing triethylenediammonium or 4,4′-bipyridilium ring. *J. Polym. Sci. Polym. Chem. Ed.* **17**, 561–569 (1979).

99. Kamiya, T., Tsuji, S., Ogatsu, K. & Shinohara, I. Effect of Polycations Containing Aromatic Heterocyclic Compounds on the Conductivity of Their TCNQ Salts. *Polym. J.* **11**, 219–226 (1979).

100. Hochberg, G. C. Electrically conductive TCNQ complexes of aromatic ionenes. *Polym. Int.* **38**, 119–124 (1995).

101. Ciesielski, W., Pęcherz, J. & Kryszewski, M. Electric properties of TCNQ complex salts of ionenes containing aromatic rings in the main chain. *Acta Polym.* **33**, 318–321 (1982).

102. Takizawa, Y., Aiga, H., Watanabe, M. & Shinohara, I. Thermoswitching property in TCNQ salts of ionenes containing poly(ethylene oxide) segments. *J. Polym. Sci. Polym. Chem. Ed.* **21**, 3145–3153 (1983).

103. Burmistr, M. V. *et al.* Structure, thermal properties and ionic conductivity of polymeric quaternary ammonium salts (polyionenes) containing ethylene oxide and aliphatic chain fragments. *Solid State Ionics* **176**, 1787–1792 (2005).

104. Dimitrov, I. V. & Berlinova, I. V. Synthesis of Poly(ethylene oxide)s Bearing Functional Groups along the Chain. *Macromol. Rapid Commun.* **24**, 551–555 (2003).

105. Tamami, M. *et al.* Poly(ethylene glycol)-based ammonium ionenes containing nucleobases. *Polymer (Guildf).* **54**, 1588–1595 (2013).

106. Wu, F., Huang, C. L., Zeng, J. B., Li, S. L. & Wang, Y. Z. Synthesis and characterization of segmented poly(butylene succinate) urethane ionenes containing secondary amine cation. *Polymer (Guildf).* **55**, 4358–4368 (2014).

107. Nakayama, Y. *et al.* Synthesis and Properties of Poly(ε-carprolactone)-based Poly(ester-urethane)s Having Quaternary Ammonium Groups. *J. Japan Inst. Energy* **93**, 916–920 (2014).

108. Schreiner, C., Bridge, A. T., Hunley, M. T., Long, T. E. & Green, M. D. Segmented imidazolium ionenes: Solution rheology, thermomechanical properties, and electrospinning. *Polymer (Guildf).* **114**, 257–265 (2017).

109. Kohjiya, S., Hashimoto, T. & Yamashita, S. Hydrophilic elastomer containing poly(tetrahydrofuran) segments and viologen units. *J. Appl. Polym. Sci.* **44**, 555–559 (1992).

110. Hashimoto, T., Kohjiya, S., Yamashita, S. & Irie, M. Photochromic and photomechanical ionene elastomer containing poly(tetrahydrofuran) segments and viologen units. *J. Polym. Sci. Part A Polym. Chem.* **29**, 651–655 (1991).

111. Loveday, D., Wilkes, G. L., Bheda, M. C., Shen, Y. X. & Gibson, H. W. Structure-Property Relationships in Segmented Polyviologen Ionene Rotaxanes. *J. Macromol. Sci. Part A* **32**, 1–27 (1995).

112. Lee, J. S., Hocken, A. & Green, M. D. Advances in the molecular design of ionenes for a diverse range of applications. *Mol. Syst. Des. Eng.* **6**, 334–354 (2021).

113. Dubé, M. A. & Salehpour, S. Applying the Principles of Green Chemistry to Polymer Production Technology. *Macromol. React. Eng.* **8**, 7–28 (2014).

114. Petersen, H. *et al.* Polyethylenimine- graft -Poly(ethylene glycol) Copolymers: Influence of Copolymer Block Structure on DNA Complexation and Biological Activities as Gene Delivery System. *Bioconjug. Chem.* **13**, 845–854 (2002).

115. Salamone, J. C. & Snider, B. Quaternary ammonium polymers from 1,4-diaza[2.2.2]bicyclooctane. *J. Polym. Sci. Part A-1 Polym. Chem.* **8**, 3495–3501 (1970).

116. Yuan, Y., Liang, S., Li, J., Zhang, S. & Zhang, Y. Copolymers with both soft and rigid cationic rings as highly selective antimicrobials to combat antibiotic resistant microbes and biofilms. *J. Mater. Chem. B* **7**, 5620–5625 (2019).

117. Zhang, K., Drummey, K. J., Moon, N. G., Chiang, W. D. & Long, T. E. Styrenic DABCO salt-containing monomers for the synthesis of novel charged polymers. *Polym. Chem.* **7**, 3370–3374 (2016).

118. Abdulahad, A. I., Jangu, C., Hemp, S. T. & Long, T. E. Influence of Counterion on Thermal, Viscoelastic, and Ion Conductive Properties of Phosphonium Ionenes. *Macromol. Symp.* **342**, 56–66 (2014).

119. Liesen, N. T. *et al.* The influence of spacer composition on thermomechanical properties, crystallinity, and morphology in ionene segmented copolymers. *Soft Matter* **17**, 5508–5523 (2021).

120. Saralegi, A. *et al.* Thermoplastic polyurethanes from renewable resources: effect of soft segment chemical structure and molecular weight on morphology and final properties. *Polym. Int.* **62**, 106–115 (2013).

121. Wang, T.-L. & Hsieh, T.-H. Effect of polyol structure and molecular weight on the thermal stability of segmented poly(urethaneureas). *Polym. Degrad. Stab.* **55**, 95–102 (1997).

122. Asensio, M., Costa, V., Nohales, A., Bianchi, O. & Gómez, C. M. Tunable Structure and Properties of Segmented Thermoplastic Polyurethanes as a Function of Flexible Segment. *Polymers (Basel).* **11**, 1910 (2019).

123. Van Bogart, J. W. C., Gibson, P. E. & Cooper, S. L. Structure-property relationships in polycaprolactone-polyurethanes. *J. Polym. Sci. Polym. Phys. Ed.* **21**, 65–95 (1983).

124. Wang, C. B. & Cooper, S. L. Morphology and properties of segmented polyether polyurethaneureas. *Macromolecules* **16**, 775–786 (1983).

125. Huang, Y., Pan, P., Shan, G. & Bao, Y. Polylactide-b-poly(ethylene-co-butylene)-b-polylactide thermoplastic elastomers: role of polylactide crystallization and stereocomplexation on microphase separation, mechanical and shape memory properties. *RSC Adv.* **4**, 47965–47976 (2014).

126. Rao, I. J. & Rajagopal, K. R. A study of strain-induced crystallization of polymers. *Int. J. Solids Struct.* **38**, 1149–1167 (2001).

127. Grassl, B., Mathis, A., Rawiso, M. & Galin, J.-C. Segmented Poly(tetramethylene oxide) Zwitterionomers and Their Homologous Ionenes. 3. Structural Study through SAXS and SANS Measurements. *Macromolecules* **30**, 2075–2084 (1997).

128. Hunley, M. T., England, J. P. & Long, T. E. Influence of Counteranion on the Thermal and Solution Behavior of Poly(2-(dimethylamino)ethyl methacrylate)-Based Polyelectrolytes. *Macromolecules* **43**, 9998–10005 (2010).

129. Lee, J. S., Taghavimehr, M., Montazami, R. & Green, M. D. Synthesis and characterization of Poly(ethylene glycol)-based segmented ionenes block copolymer with aliphatic or DABCO hard segments. *Polymer (Guildf).* **242**, 124543 (2022).

130. la Cruz, D. S. *et al.* Correlating backbone-to-backbone distance to ionic conductivity in amorphous polymerized ionic liquids. *J. Polym. Sci. Part B Polym. Phys.* **50**, 338–346 (2012).

131. Cakić, S. M., Ristić, I. S., Marinović Cincović, M. & Špírková, M. The effects of the structure and molecular weight of the macrodiol on the properties polyurethane anionic adhesives. *Int. J. Adhes. Adhes.* **41**, 132–139 (2013).

132. Princi, E. *et al.* On The Micro-Phase Separation in Waterborne Polyurethanes. *Macromol. Chem. Phys.* **210**, 879–889 (2009).

133. Cakić, S. M. *et al.* The waterborne polyurethane dispersions based on polycarbonate diol: Effect of ionic content. *Mater. Chem. Phys.* **138**, 277–285 (2013).

134. Arcos Hernandez, M. *et al.* Thermoresponsive Glycopolymers Based on Enzymatically Synthesized Oligo-β-Mannosyl Ethyl Methacrylates and N -Isopropylacrylamide. *Biomacromolecules* **22**, 2338–2351 (2021).

135. Smith, T. L. Strength of Elastomers. A Perspective. *Polym. Eng. Sci.* **17**, 129–143 (1977).

136. Register, R. A. *et al.* X-Ray Analysis of Ionomers. *ACS Symp. Ser.* **395**, 420–438 (1989).

137. Williams, S. R. *et al.* Synthesis and Characterization of Well-Defined 12,12-Ammonium Ionenes: Evaluating Mechanical Properties as a Function of Molecular Weight. *Macromolecules* **41**, 5216–5222 (2008).

138. Kammakakam, I., O'Harra, K. E., Dennis, G. P., Jackson, E. M. & Bara, J. E. Self-healing imidazolium-based ionene-polyamide membranes: an experimental study on physical and gas transport properties. *Polym. Int.* **68**, 1123–1129 (2019).

139. Lee, J. S., Taghavimehr, M., Montazami, R. & Green, M. D. Synthesis and characterization of poly(tetramethylene oxide)-based segmented ionenes block copolymer with aliphatic or DABCO hard segments. *Polymer (Guildf).* **270**, 125772 (2023).

140. Lee, J. S., Taghavimehr, M., Montazami, R. & Green, M. D. Synthesis and characterization of Poly(ethylene glycol)-based segmented ionenes block copolymer with aliphatic or DABCO hard segments. *Polymer (Guildf).* **242**, 124543 (2022).

141. Ilavsky, J. & Jemian, P. R. Irena : tool suite for modeling and analysis of small-angle scattering. *J. Appl. Crystallogr.* **42**, 347–353 (2009).

142. Ilavsky, J. Nika : software for two-dimensional data reduction. *J. Appl. Crystallogr.* **45**, 324–328 (2012).

143. Cui, J. *et al.* Novel imidazolium-based poly(ionic liquid)s with different counterions for self-healing. *J. Mater. Chem. A* **5**, 25220–25229 (2017).

144. Guo, P., Zhang, H., Liu, X. & Sun, J. Counteranion-Mediated Intrinsic Healing of Poly(ionic liquid) Copolymers. *ACS Appl. Mater. Interfaces* **10**, 2105–2113 (2018).

145. Grassl, B., Meurer, B., Scheer, M. & Galin, J. C. Segmented Poly(tetramethylene oxide) Zwitterionomers and Their Homologous Ionenes. 2. Phase Separation through DSC and Solid State 1 H-NMR Spectroscopy. *Macromolecules* **30**, 236–245 (1997).

146. Zhang, K., Fahs, G. B., Drummey, K. J., Moore, R. B. & Long, T. E. Doubly-Charged Ionomers with Enhanced Microphase-Separation. *Macromolecules* **49**, 6965–6972 (2016).

147. Green, M. D. *et al.* Alkyl-Substituted N-Vinylimidazolium Polymerized Ionic Liquids: Thermal Properties and Ionic Conductivities. *Macromol. Chem. Phys.* **212**, 2522–2528 (2011).

148. Gouin, J. P., Williams, C. E. & Eisenberg, A. Microphase Structure of Block Ionomers. 1. Study of Molded Styrene-4-Vinylpyridinium ABA Blocks by SAXS and SANS. *Macromolecules* **22**, 4573–4578 (1989).

149. Wu, T., Beyer, F. L., Brown, R. H., Moore, R. B. & Long, T. E. Influence of Zwitterions on Thermomechanical Properties and Morphology of Acrylic Copolymers: Implications for Electroactive Applications. *Macromolecules* **44**, 8056–8063 (2011).

150. Topuz, F., Henke, A., Richtering, W. & Groll, J. Magnesium ions and alginate do form hydrogels: a rheological study. *Soft Matter* **8**, 4877 (2012).

151. Huang, D. *et al.* Functionalized Elastomeric Ionomers Used as Effective Toughening Agents for Poly(lactic acid): Enhancement in Interfacial Adhesion and Mechanical Performance. *ACS Sustain. Chem. Eng.* **8**, 573–585 (2020).

152. Yen, M. & Tsai, P. Study on polyethylene glycol/polydimethylsiloxane mixing soft-segment waterborne polyurethane from different mixing processes. *J. Appl. Polym. Sci.* **90**, 233–243 (2003).

153. Ahn, T. O., Jung, S.-U., Jeong, H. M. & Lee, S. W. The properties of polyurethanes with mixed chain extenders and mixed soft segments. *J. Appl. Polym. Sci.* **51**, 43–49 (1994).

154. Mirhosseini, M. M., Haddadi-Asl, V. & Jouibari, I. S. A simple and versatile method to tailor physicochemical properties of thermoplastic polyurethane elastomers by using novel mixed soft segments. *Mater. Res. Express* **6**, (2019).

155. Cui, Y., Wang, H., Pan, H., Yan, T. & Zong, C. The effect of mixed soft segment on the microstructure of thermoplastic polyurethane. *J. Appl. Polym. Sci.* **138**, 51346 (2021).

156. Askari, F., Barikani, M. & Barmar, M. Siloxane-based segmented poly(urethane-urea) elastomer: Synthesis and characterization. *J. Appl. Polym. Sci.* **130**, 1743–1751 (2013).

157. Kenney, J. F. Properties of block versus random copolymers. *Polym. Eng. Sci.* **8**, 216–226 (1968).

158. Kang, K. & Kim, D. Comparison of proton conducting polymer electrolyte membranes prepared from multi-block and random copolymers based on poly(arylene ether ketone). *J. Power Sources* **281**, 146–157 (2015).

159. Cho, J. W., Jung, Y. C., Chung, Y.-C. & Chun, B. C. Improved mechanical properties of shape-memory polyurethane block copolymers through the control of the soft-segment arrangement. *J. Appl. Polym. Sci.* **93**, 2410–2415 (2004).

APPENDIX A

SUPPORTING INFORMATION FOR CHAPTER 3

Reproduced with permission from: Lee, J.; Taghavimehr, M.; Montazami, R.; Green, M. D. *Polymer*, 242, 124543, 2022. Copyright 2023. Elsevier

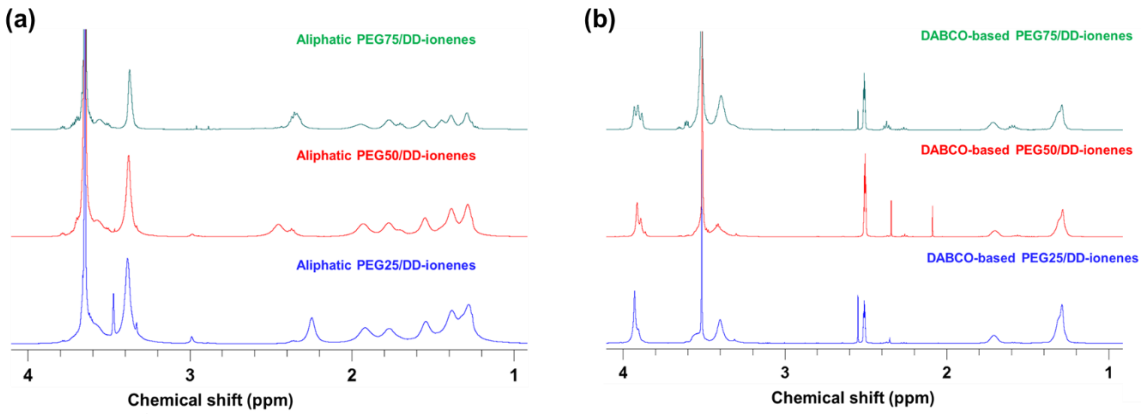

Figure A1: ^{1}H NMR spectra of (a)aliphatic PEGXX/DD-ionenes and (b) DABCO-based PEGXX/DD-ionenes with labeled peaks corresponding to their respective alkyl hydrogens. (top) 75 wt%, (middle) 50 wt%, and (bottom) 25 wt% of soft segments.

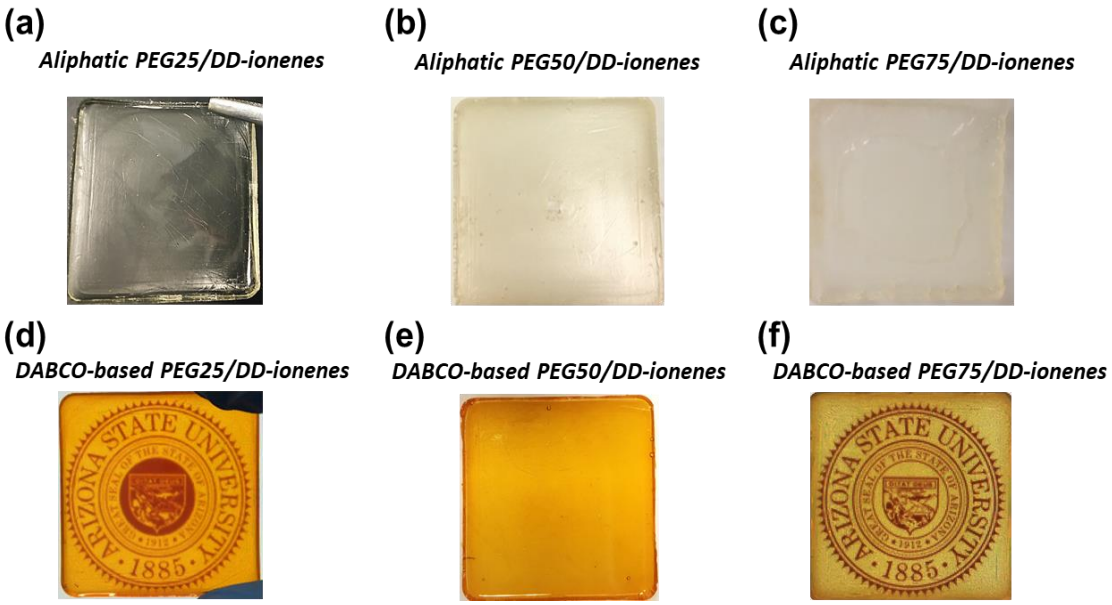

Figure A2: Photographic images of aliphatic (a) PEG25, (b) PEG50, and (c) PEG75/DD-ionenes and DABCO-based (d) PEG25, (e) PEG50, and (f) PEG75/DD-ionenes.

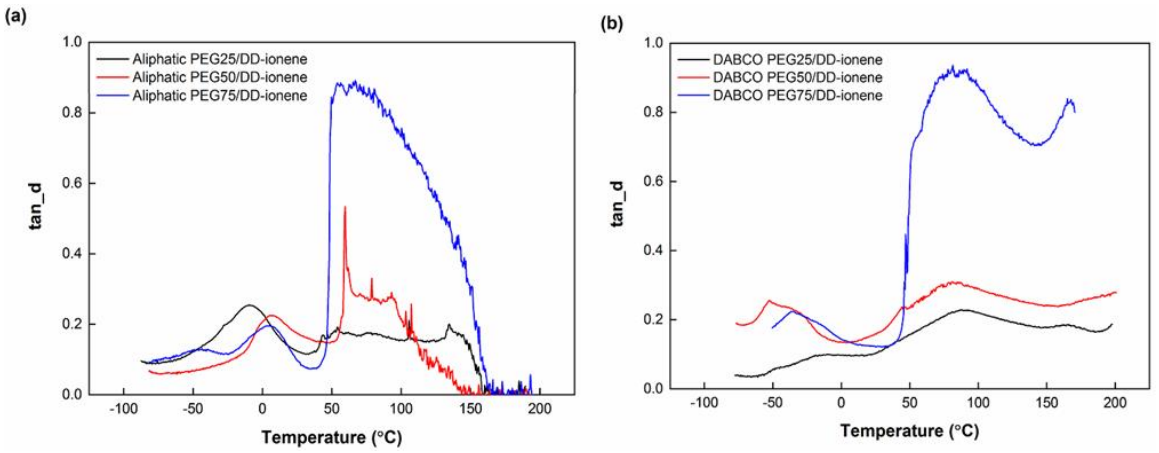

Figure A3: DMA temperature profile of tan delta of (a) Aliphatic and (b) DABCO-based PEGXX/DD-ionenes.

Table A1: Full width half maximum of melting temperature peaks of linear aliphatic and DABCO-based ionenes from differential scanning calorimetry.

	Linear aliphatic PEGXX/DD-ionenes			DABCO-based PEGXX/DD-ionenes		
Soft segment (wt%)	25	50	75	25	50	5
FWHM (°C)	13.167	9.224	4.185	9.441	3.861	7.636

Table A2: Tensile stress-strain data for aliphatic and DABCO-based PEGXX/DD-ionenes.

	Linear aliphatic PEGXX/DD-ionenes						DABCO-based PEGXX/DD-ionenes					
Temperature (°C)	R.T.			60			R.T.			60		
soft segment weight fraction (%)	25	50	75	25	50	75	25	50	75	25	50	75
Young's modulus (MPa)	431.08	643.53	220.13	86.86	0.72	0.59	708.98	1098.6	216.70	33.83	208.56	1.64
Ultimate tensile strength (MPa)	4.16	6.56	8.03	4.79	0.12	0.08	0.85	1.96	0.47	2.52	12.61	0.35
Tensile strain at break (%)	1.14	1.67	4.42	80.19	≥95.52	≥98.54	0.23	0.20	0.31	20.65	7.23	≥110.88
Toughness (MPa)	0.03	0.08	0.22	3.24	≥0.07	≥0.03	0.0014	0.0023	0.0009	0.39	0.57	≥0.31

APPENDIX B

SUPPORTING INFORMATION FOR CHAPTER 4

Reproduced with permission from: Lee, J.; Taghavimehr, M.; Montazami, R.; Green, M. D. *Polymer*, 270, 125772, 2023. Copyright 2023. Elsevier

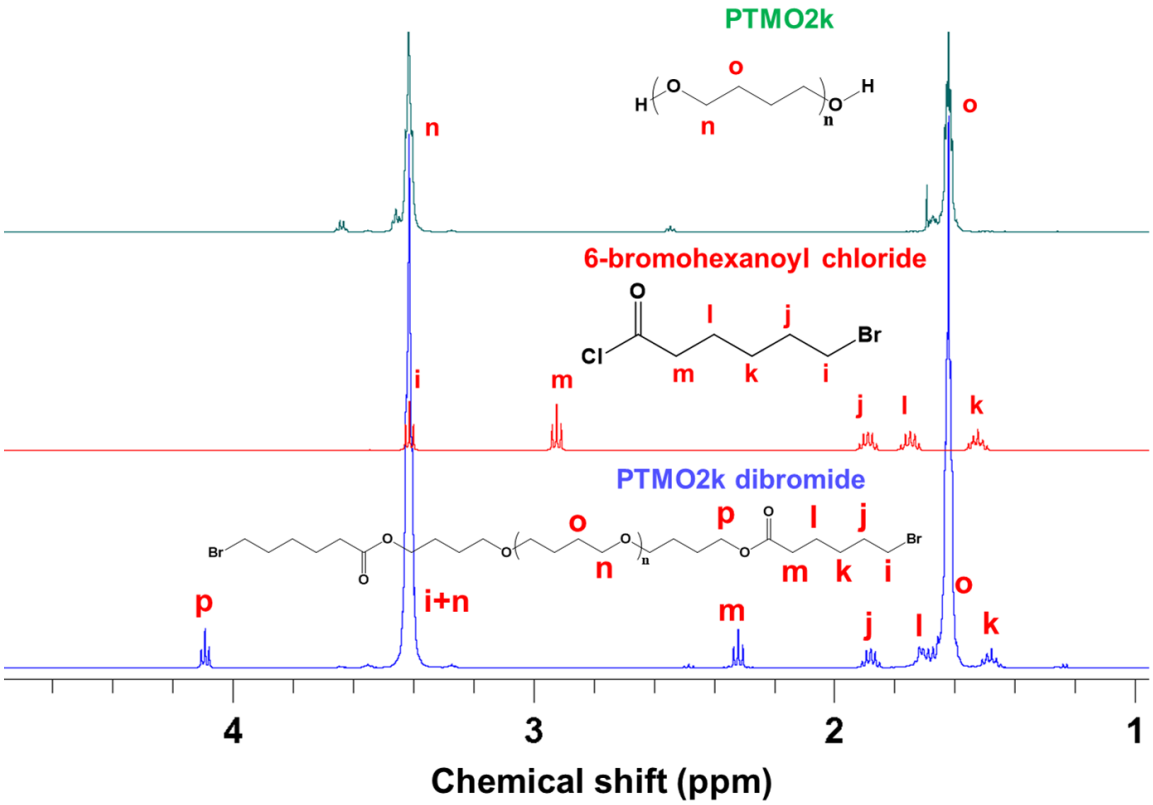

Figure B1: ^{1}H NMR spectra of (top) PTMO-2k, (middle) 6-bromohexanoyl chloride, and (bottom) Br-PTMO$_n$-Br with labeled peaks corresponding to their respective protons.

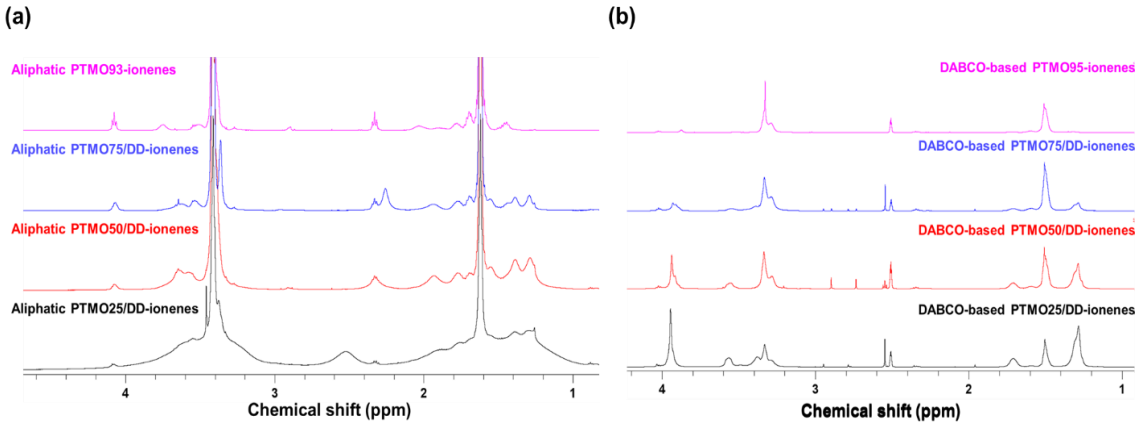

Figure B2: ^{1}H NMR spectra of (a)aliphatic PTMOXX/DD-ionenes and (b) DABCO-based PTMOXX/DD-ionenes with labeled peaks corresponding to their respective alkyl hydrogens. 93 wt% (or 95 wt% for DABCO-based) wt%, 75 wt%, 50 wt%, and 25 wt% of PTMO soft segments from top to bottom.

Table B1: Full width half maximum of melting temperature peaks of aliphatic and DABCO-based ionenes from differential scanning calorimetry.

	Aliphatic ionenes				DABCO-based ionenes			
Soft segment (wt%)	25	50	75	93	25	50	75	95
FWHM (°C)	6.854	14.525	17.206	14.943	-	20.710	24.725	17.310

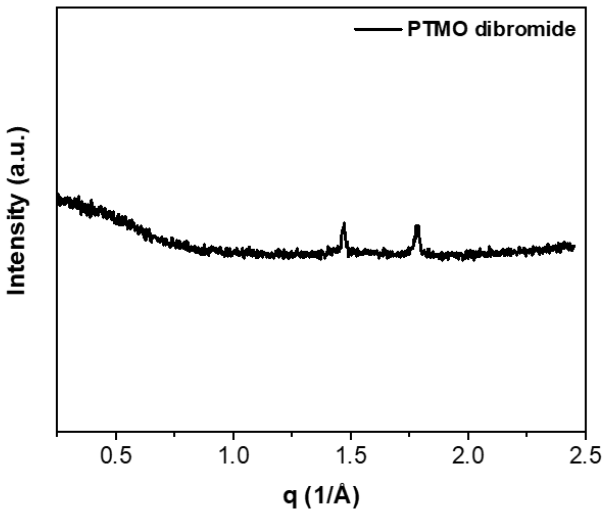

Figure B3: XRD diffraction of Br-PTMO$_n$-Br oligomer.

Table B2: Full width half maximum of d[d] peaks of DABCO-based ionenes from XRD.

	DABCO-based ionenes			
Soft segment (wt%)	25	50	75	95
FWHM (2theta)	1.69926	1.70455	1.98029	-

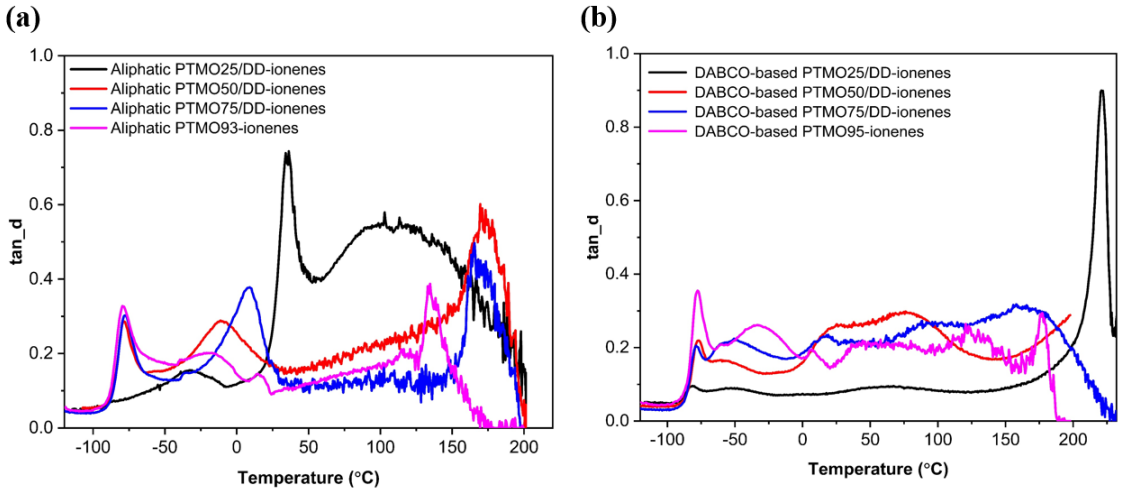

Figure B4: DMA temperature profile of tan delta of (a) aliphatic PTMO ionenes and (b) DABCO-based PTMO ionenes.

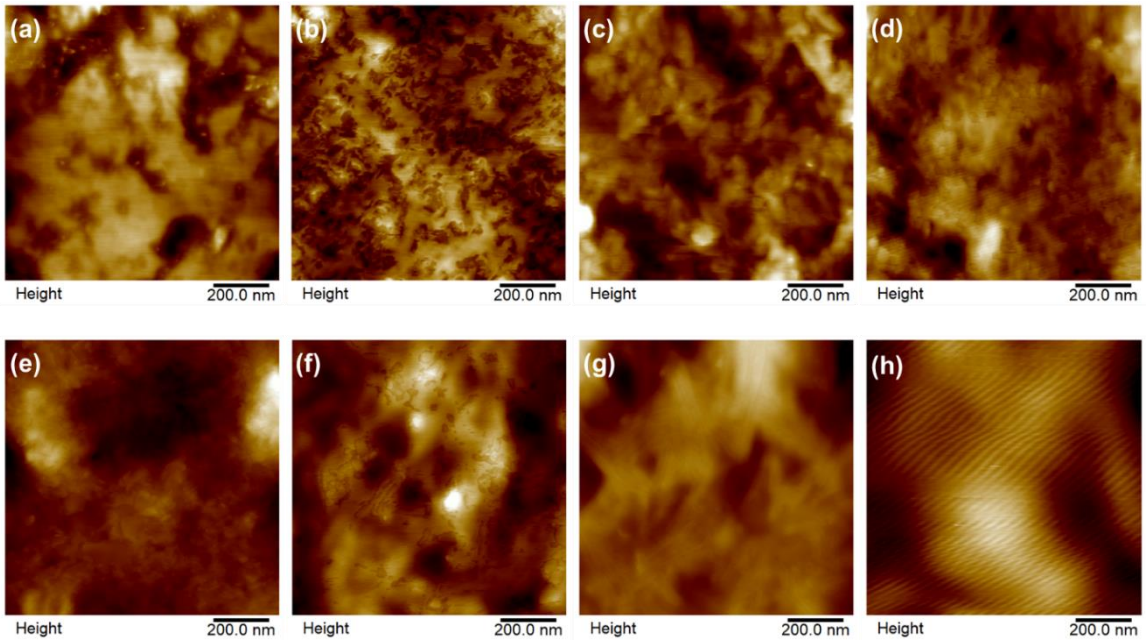

Figure B5: AFM height images of aliphatic (a) PTMO25/DD-ionenes, (b) PTMO50/DD-ionenes, (c) PTMO75/DD-ionenes, and (d) PTMO93-ionenes, and DABCO-based (e) PTMO25/DD-ionenes, (f) PTMO50/DD-ionenes, (g) PTMO75/DD-ionenes, and (h) PTMO95-ionenes at room temperature.

APPENDIX C

SUPPORTING INFORMATION FOR CHAPTER 5

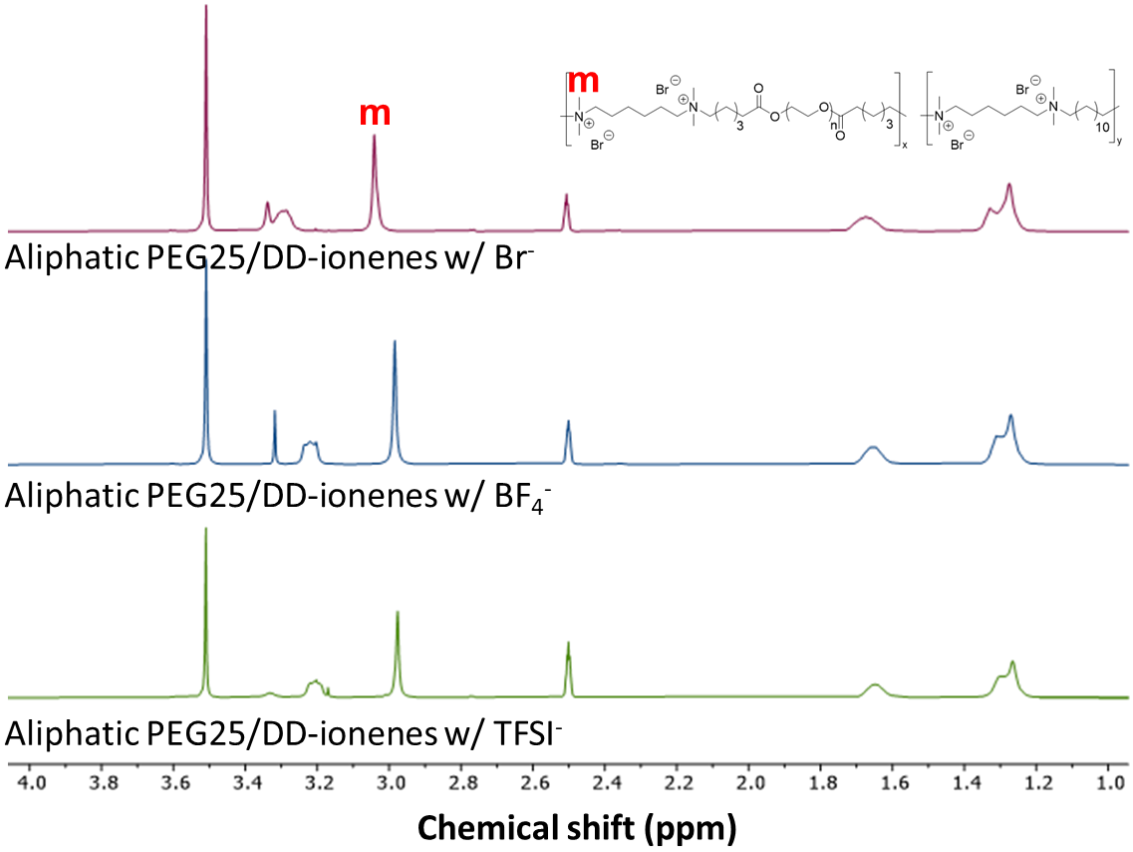

Figure C1: ^{1}H NMR spectra of aliphatic PEG25/DD-ionenes with different counterion species.

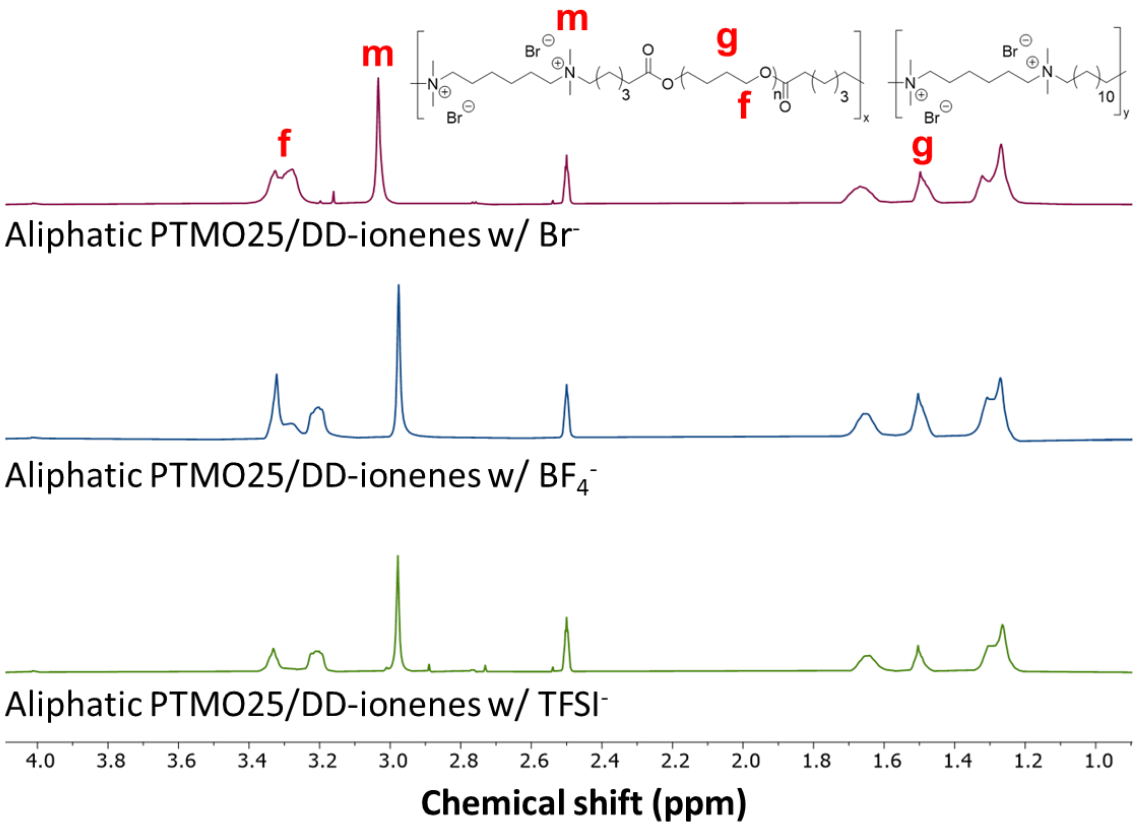

Figure C2: ^{1}H NMR spectra of aliphatic PTMO25/DD-ionenes with different counterion species.

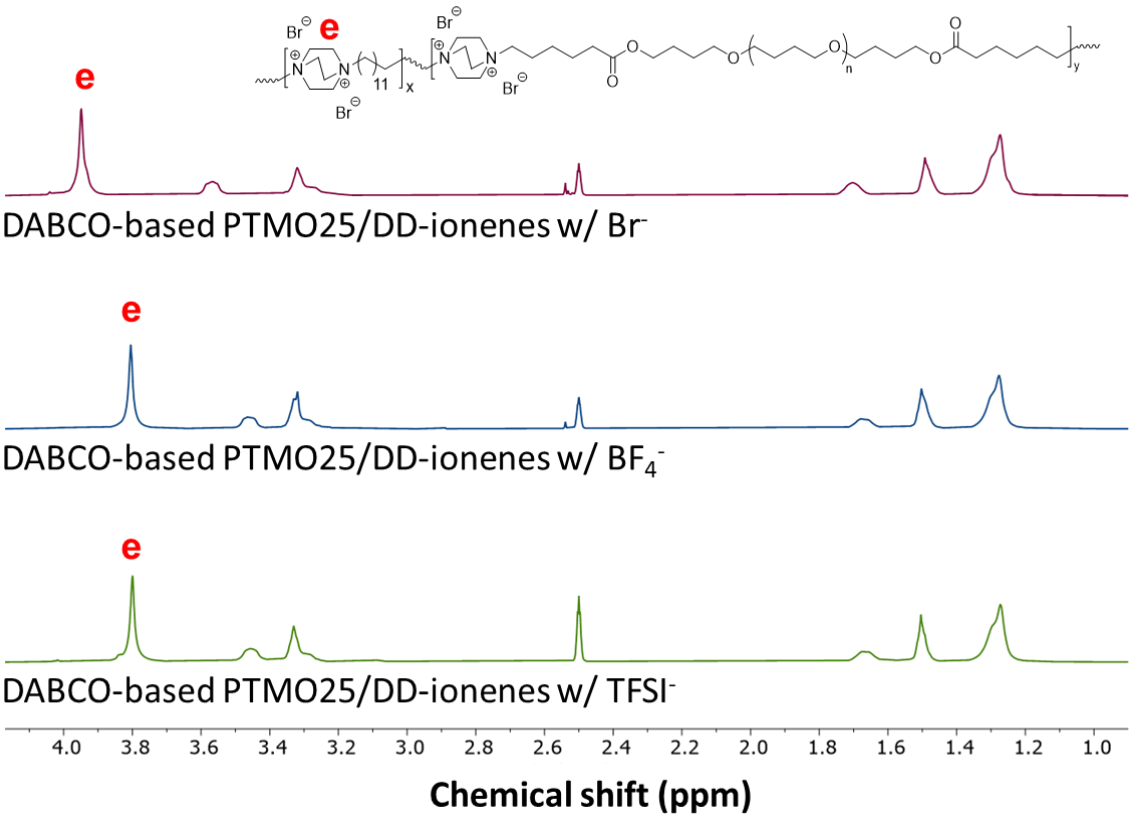

Figure C3: ^{1}H NMR spectra of DABCO-based PTMO25/DD-ionenes with different counterion species.

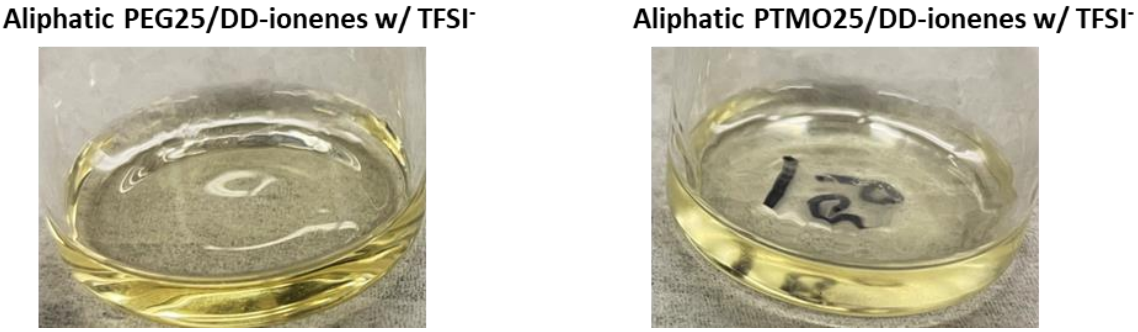

Figure C4: Photographic images of aliphatic PEG25/DD-ionenes or PTMO25/DD-ionenes with TFSI counter-anions.